Technische Universität München
TUM School of Engineering and Design

Adjoint Sensitivity Analysis for Non-parametric Shape Optimization with Geometric Nonlinearity and Elastoplasticity

Wenjia Wang

Vollständiger Abdruck der von der TUM School of Engineering and Design der Technischen Universität München zur Erlangung einer

Doktorin der Ingenieurwissenschaften (Dr.-Ing.)

genehmigten Dissertation.

Vorsitz: Prof. Dr.-Ing. habil. Fabian Duddeck

Prüfer der Dissertation:

1. Prof. Dr.-Ing. Kai-Uwe Bletzinger
2. Prof. Dr.-Ing. Axel Schumacher

Die Dissertation wurde am 13.03.2024 bei der Technischen Universität München eingereicht und durch die TUM School of Engineering and Design am 27.05.2024 angenommen.

Schriftenreihe des Lehrstuhls für Statik
TU München

Band 65

Wenjia Wang

ADJOINT SENSITIVITY ANALYSIS FOR NON-PARAMETRIC SHAPE OPTIMIZATION WITH GEOMETRIC NONLINEARITY AND ELASTOPLASTICITY

München 2024

Abstract

Gradient-based structural optimization has achieved great success in a wide range of industrial applications, in conjunction with linear finite element analysis. However, further applications in large-scale industrial problems with nonlinear behaviors, including geometric, material, and boundary condition nonlinearities, remain challenging tasks and face numerous hindrances. One of the fundamental difficulties lies in sensitivity analysis, i.e., evaluating derivatives of system responses with respect to design variables. Considering the characteristics of nonlinear finite element systems, much higher complexity and larger computational efforts are foreseeable, especially when node-based design variables are adopted. Obtaining sensitivities accurately and with high efficiency is hence of significant importance.

This thesis investigates several issues related to obtaining efficient and accurate sensitivity analysis for two types of nonlinear structural systems: geometric nonlinearity and elastoplasticity. Firstly, a semi-analytical adjoint method for geometric nonlinear problems is explored. To eliminate the numerical errors introduced by element rotation in semi-analytical approximation, a correction term that can be analytically constructed is proposed. With this correction, the sensitivities become more accurate. More importantly, the stability of sensitivities is improved, thereby expanding the range of proper perturbation sizes in the semi-analytical approximation.

Secondly, an adjoint sensitivity analysis approach is explored for simultaneous consideration of geometric nonlinearity and elastoplasticity. The sensitivity must be evaluated through a stepwise backward procedure due to the history-dependency of plasticity. Consequently, both storage and computational costs increase in proportion to the number of load steps. To address this issue, rules for load step reduction in the sensitivity analysis are investigated. The proposed strategies are mathematically proven based on two special properties of adjoint variables. The effectiveness of these techniques is demonstrated through various numerical examples, including a large-scale engineering example under complex load histories.

The proposed load step reduction is first discussed and demonstrated under small strain conditions and an isotropic hardening material model. It is then extended to kinematic hardening and general mixed hardening cases, where back stresses and hardening ratios are taken into consideration. Finally, the applicability of the techniques to finite strain elastoplasticity is investigated. Multiple examples show that the presented techniques are well-suited to evaluate the sensitivity of these types of problems both accurately and efficiently.

Zusammenfassung

Die gradientenbasierte Strukturoptimierung hat in einer Vielzahl von industriellen Anwendungen in Verbindung mit linearer Finite-Elemente-Analyse großen Erfolg erzielt. Dennoch bleiben weitere Anwendungen in groß angelegten industriellen Problemen mit nichtlinearem Verhalten, darunter geometrische, materielle und Randbedingungs-Nichtlinearitäten, eine anspruchsvolle Aufgabe und stehen vor zahlreichen Hindernissen. Eine der grundlegenden Schwierigkeiten besteht in der Sensitivitätsanalyse, das heißt in der Bewertung von Ableitungen der Systemantworten im Hinblick auf Designvariablen. Angesichts der Eigenschaften nichtlinearer Finite-Elemente-Systeme ist eine erheblich höhere Komplexität und größerer Rechenaufwand absehbar, insbesondere wenn knotenbasierte Designvariablen verwendet werden. Die genaue und effiziente Ermittlung von Sensitivitäten ist daher von erheblicher Bedeutung.

Diese Dissertation untersucht mehrere Probleme im Zusammenhang mit der effizienten und genauen Sensitivitätsanalyse für zwei Arten nichtlinearer Struktursysteme: geometrische Nichtlinearität und Elastoplastizität. Zunächst wird eine semi-analytische adjungierte Methode für geometrisch nichtlineare Probleme erforscht. Um die durch die semi-analytischen Näherung eingeführten numerischen Fehler aufgrund der Elementrotation zu eliminieren, wird ein Korrekturterm vorgeschlagen, der analytisch konstruiert werden kann. Durch diese Korrektur werden die Sensitivitäten präziser. Noch wichtiger ist, dass die Stabilität der Sensitivitäten verbessert wird, was den Bereich geeigneter Perturbationsgrößen in der semi-analytischen Näherung erweitert.

Zweitens wird ein Ansatz für die adjungierte Sensitivitätsanalyse erforscht, der die gleichzeitige Berücksichtigung von geometrischer Nichtlinearität und Elastoplastizität ermöglicht. Aufgrund der geschichtsabhängigen Plastizität muss die Sensitivität durch ein schrittweises, rückwärts gerichtetes Verfahren ermittelt werden. Infolgedessen steigen sowohl die Speicher- als auch die Rechenkosten proportional zur Anzahl der Lastschritte an. Um dieses Problem zu lösen, werden Regeln zur Reduzierung der Lastschritte in der Sensitivitätsanalyse untersucht. Die vorgeschlagenen Strategien werden mathematisch basierend auf zwei

speziellen Eigenschaften der adjungierten Variablen nachgewiesen. Die Wirksamkeit dieser Verfahren wird durch verschiedene Beispiele, einschließlich eines groß angelegten industriellen Beispiels unter komplexen Lastverläufen, demonstriert.

Die vorgeschlagene Reduzierung der Lastschritte wird zuerst unter Bedingungen geringer Dehnung und einem isotropen Verfestigungsmaterialmodell diskutiert und demonstriert. Anschließend erfolgt die Erweiterung auf kinematische Verfestigung und allgemeine Mischverfestigungsfälle, in denen Rückspannungen und Verfestigungsverhältnisse berücksichtigt werden. Schließlich wird die Anwendbarkeit der Techniken auf die Elastoplastizität mit großen Dehnungen untersucht. Mehrere Beispiele zeigen, dass die vorgestellten Techniken gut geeignet sind, die Sensitivität dieser Art von Problemen genau und effizient zu bewerten.

Acknowledgements

This dissertation was written while I was research associate at the Chair of Structural Analysis (Lehrstuhl für Statik), Technische Universität München, as part of the LaSciSO project. The project aimed at promoting knowledge transfer between research institutions and enterprises in Europe in the field of large-scale industrial structural optimization.

First and foremost, I would like to express my sincere gratitude to my supervisor, Univ.-Prof. Dr.-Ing. Kai-Uwe Bletzinger, who provided enlightening guidance and remarkable support throughout all stages of my PhD study. He initiated this fascinating project, which significantly broadened my horizons in the industry. His permanent willingness to spare precious time for me, even when a short question turned into hours of discussion right after his all-day lectures, is truly appreciated. I am also grateful from the bottom of my heart for his sincere solicitude and encouragement when I encountered setbacks in my life. His valuable contributions to this thesis are highly respected.

I sincerely thank Univ.-Prof. Dr.-Ing. Axel Schumacher for his interest in my work, and his time and effort in reviewing my dissertation. I am also grateful to Univ.-Prof. Dr.-Ing. habil. Fabian Duddeck for chairing the board of examiners.

Furthermore, I owe a special thanks to Mr. Peter Michael Clausen, my supervisor and collaborator on the LaSciSO project in the Research & Development Department of Simulia Dassault Systèmes. He consistently provided encouragement for further innovation and generously shared his industrial experience without reservation. I would also like to express my appreciation to Mr. Peter Allinger and all my colleagues at Dassault Systèmes who facilitated various conveniences during my secondment.

Additionally, I am grateful to our project partners: Professor Ole Sigmund from the Technical University of Denmark, Professor Georgi Todorov from the Technical University of Sofia, and their colleagues, for their valuable discussions and advice in every project meeting.

Beyond that, I extend my thanks to all my colleagues at the Chair of Structural Analysis. I have greatly benefited from the motivating work environment and collaborative spirit among all co-workers at the institute. Special gratitude goes to Aditya Ghantasala, Daniel Baumgärtner, and Reza Najian Asl, who shared the same office with me, for fostering a friendly atmosphere and engaging in fruitful discussions during our work together.

Finally, I want to express my deepest gratitude to my parents for their unconditional love and unwavering support during my study in Germany.

Contents

List of Figures

List of Tables

1. Introduction

1.1 Motivation

Structural optimization, categorized into size optimization, shape optimization, and topology optimization, plays a crucial role in the modern design of structures to enhance product performance. In the field of shape optimization, a traditional method for describing structural shapes is through parametric representation. However, these geometric parameters automatically introduce additional constraints on the various modes of structures to be optimized.

Non-parametric shape optimization, also known as node-based shape optimization, overcomes this disadvantage by utilizing the coordinates of surface nodes in the finite element model of a structure as design variables. This approach provides a much more detailed description of structural shapes, significantly expanding the design freedom of structures. Another advantage of non-parametric shape optimization is its natural suitability for local improvements, such as local stress relief features.

To solve non-parametric shape optimization, two types of algorithms are usually employed: gradient-based algorithms and derivative-free algorithms. Starting from an initial point, gradient-based algorithms iteratively search for an optimal solution based on sensitivity information, i.e., derivatives of responses with respect to design variables. To obtain sensitivities for non-parametric shape descriptions, adjoint variable methods are normally preferable to direct methods because the number of design variables is often much larger than the number of responses. Accurate and efficient adjoint sensitivity analyses for linear structural systems have been widely investigated and have achieved great success in a wide range of industrial applications.

Among the challenges of nonlinear sensitivity analyses, efficiency cannot be overemphasized. For nonlinear structural systems, the solution procedure is often more complicated than that for linear problems, leading to increased complexity in nonlinear sensitivity analysis and resulting in higher computational and storage costs compared to the linear case. On the other

hand, the number of iterations in nonlinear optimization is often much larger than that in linear optimization for the same problem size. Therefore, the required number of sensitivity analyses in nonlinear optimization is correspondingly much larger. The efficiency issue becomes even more significant when the number of design nodes is large.

In addition to efficiency, the accuracy of sensitivities is also important in nonlinear optimization. It not only influences the search direction to optima but also affects the convergence speed, i.e., the number of iterations, in the optimization procedure. Hence, a highly efficient and accurate sensitivity analysis procedure is essential for a successful gradient-based nonlinear shape optimization. This dissertation makes every effort to investigate techniques to eliminate numerical errors and employ appropriate methods to improve efficiency in sensitivity analyses.

1.2 Literature survey

In this section, state-of-the-art sensitivity analysis methods are summarized, along with their advantages and disadvantages. An overview of research on sensitivity analysis for geometrical and material nonlinear problems is presented.

1.2.1 Design sensitivity analysis methodologies

There are various methods for conducting design sensitivity analysis (DSA) in structural optimization, as depicted in Figure 1-1. These methods can typically be categorized into [HA89, CK05a, CK05b]: global finite difference (GFD) approach, continuum approach, discrete approach, and other computational approaches.

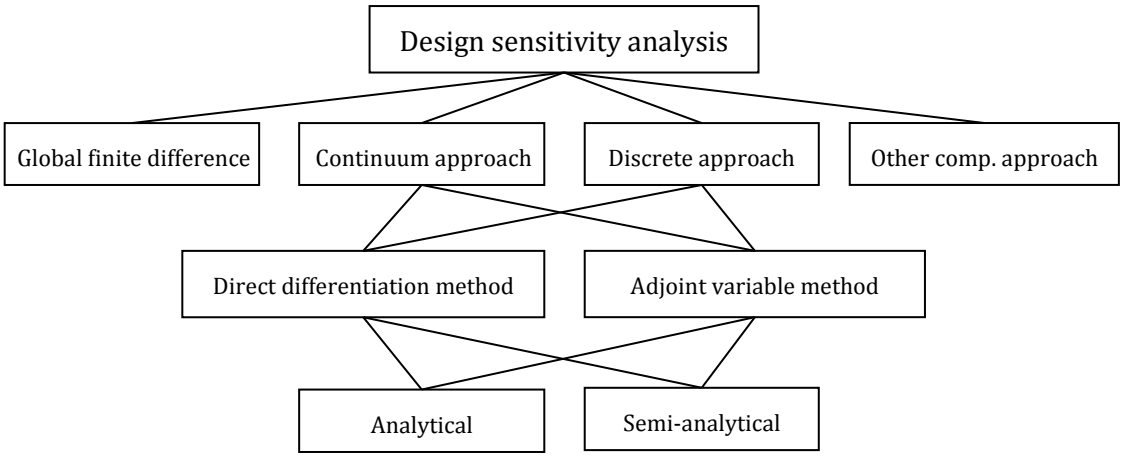

Figure 1-1. Hierarchy of design sensitivity analysis methods

The global finite difference method employs forward, backward, or central finite differencing schemes to calculate sensitivities. In the continuum method, derivatives are first taken on the variational equations of a structural system, and then the formulas are discretized. The discrete approach derives the sensitivity of structural systems based on discretized governing equations of finite element systems.

Other computational approaches employ specialized tools to compute or approximate sensitivities. Based on the chain rule, automatic differentiation methods compute sensitivities by differentiating elementary functions of structural systems [NQR98]. However, these methods have limitations for structural design sensitivity analysis due to their significant demand for computer memory. The complex variable method utilizes a complex finite element formulation and computes a system response by perturbing design parameters along the imaginary axis. It then takes the division of the imaginary function by the perturbation size as an estimation of the derivative of the response [MWB+13, HSM15]. The virtual distortion method evaluates sensitivities based on a so-called influence matrix, which describes the interaction between physical quantities related to design variables and the entire structure [KH98, KWH07]. Response surface methods first establish response functions between design variables and structural responses and then compute sensitivities analytically on the response surface [SC02, Kam11].

The global finite difference method is a computationally expensive method to calculate sensitivities and thus is not applicable to large-scale problems.

However, as the most straightforward way to evaluate derivatives, global finite difference results are good benchmarks for investigations of more sophisticated sensitivity analysis techniques. The continuum approach and the discrete approach are two general solutions for finite element based sensitivity analyses. The discrete methods are more commonly implemented in commercial finite element codes [KHK05].

Both the continuum approach and the discrete approach can be further classified into the direct differentiation method (DDM) and the adjoint variable method (AVM). The direct approach computes sensitivities based on the direct differentiation of state variables. In the adjoint variable method, direct differentiations are eliminated by introducing adjoint variables and governing equations. The adjoint sensitivity analysis method is more efficient when the number of design variables exceeds the number of response functions, which is usually the case in non-parametric shape optimization.

No matter whether a direct or adjoint approach is employed, derivatives of physical quantities such as the stiffness matrix or pseudo-load vectors are often required after discretization. The analytical derivatives of these quantities are difficult to obtain. Therefore, the semi-analytical technique, where analytical derivatives are approximated by finite differencing, is widely employed.

1.2.2 Sensitivity analysis with geometric and material nonlinearity

The design sensitivity analysis of a nonlinear system is often more complex than that of a linear system, with an exception being the elastic nonlinear problem. Geometrical nonlinearity and hyperelasticity are two typical issues that fall into this category. In this type of problem, sensitivity is determined solely by the final load step due to the path-independency [CD00, CK05b]. Linear sensitivity analysis approaches can be straightforwardly extended and applied to it. Additionally, based on the co-rotational formulation of geometric nonlinearity, element-independent analytical sensitivity expressions are presented [PM06]. The co-rotational framework utilizes only the linear finite element library and does not require kinematic nonlinear element formulations.

Sensitivity analysis for general nonlinear materials, which exhibit plasticity or viscosity, is essentially different from linear cases due to path-dependency. The responses and state variables of a load step are characterized not only by current loading conditions but also by previous loading histories. Therefore, sensitivity computations are often performed following each load step or time step in an incremental procedure [WA87, PC99b, SMR01, CK05b].

The direct differentiation method has been successfully applied to various material nonlinear sensitivity analyses in an incremental procedure. Sensitivity computations are presented for cases such as Norton-Soderberg power-law creep materials [VLH91], spread plasticity with geometric nonlinearity under seismic loading [HM10], in-plane stress elasto-viscoplasticity [KK96], anisotropic elastoplastic shells [Ho05], J2 plasticity with multi-yield-surface and nonlinear hardening [WKT03, GCE09], Prandtl-Reuss elastoplasticity with geometric nonlinearity [SR01, Sch01], beam elements with plastic hinges [Pe03], laminate composites with bilinear elastoplastic materials [CG95], nonlinear elasticity with frictionless contact [ST94], and elastoplasticity with frictional contact [KCC00, SKD02]. A non-differentiable problem that may occur at transition points, such as at points where material behavior turns from elastic to plastic or vice versa, has been discussed [OA94]. Taking the derivatives of adjacent points above or below the discontinuity will well solve the problem without leading to substantial errors. It is not necessary to compute the sensitivities at the initial yielding point in order to obtain sensitivities at the subsequent steps [SR01].

Unlike the direct differentiation approach, the applicability of adjoint variable methods for path-dependent problems was once an issue [RHW+85, KAH+97]. Since each adjoint variable corresponds to a response function at only one single step rather than the entire loading history, the sensitivities of state variables at all previous steps are still required [TA90, VH93, SR01]. These sensitivities at previous steps must be treated as additional response functions, which would significantly increase the total number of responses and jeopardize the advantage of the adjoint variable method [KK99, Hi95].

The key to solving the challenge is to avoid implicit derivatives of state variables in previous steps by introducing additional adjoint variables. Following this idea, adjoint sensitivities for transient non-linear coupled systems are achieved by introducing adequate adjoint variables for the

independent and dependent residuals [MTV94]. Adjoint sensitivity analysis with elastoplasticity is obtained as a direct extension of this method. By employing adjoint variables corresponding to nodal balance equations and the boundary conditions of material flow velocity, adjoint sensitivity analysis for non-steady forming could be implemented [CFC+03]. By introducing adjoint variables corresponding to boundary conditions on average residence time fields, sensitivity analysis and optimization of polymer sheet extrusion and molding processes are presented [Sm03]. Based on equilibrium governing equations, as well as a computational fluid grid induced by elastic deformations, adjoint sensitivity information for fluid-structure interaction problems is obtained [MNF03].

For path-dependent problems, it is shown that both direct and adjoint methods maintain their relative advantages as in linear or path-independent problems [Car05]. It has also been pointed out that sensitivity analysis for a path-dependent problem must be based on the consistent tangent operator, which specifies the variation of stress with respect to strain in the underlying finite element analysis [VLH91, VH93].

Both the computational cost and memory cost of path-dependent nonlinear sensitivity analysis increase significantly compared to single-step analysis. In the direct differentiation method, derivatives of state variables at each load step must be computed. In the adjoint variable method, additional adjoint variables at each load step must be solved. Some empirical experiences may be utilized to reduce the number of load steps or simplify the load history. Through numerical investigation involving a single tetrahedral element and a two-bar truss structure with bilinear elastoplastic material, it has been demonstrated that sensitivities only need to be calculated at the last step in a monotonic loading process [Köb15]. For a cyclical load history, design sensitivities must be computed at both the unloading starting point and the actual load point [Car05]. However, a theoretical justification for proper load step reduction is still lacking. The systematic investigation into load step reduction is particularly crucial for the application to large-scale problems.

1.2.3 Accuracy problem of semi-analytical approximation

In sensitivity analysis, derivatives of intermediate quantities, including the stiffness matrix and pseudo-load vectors, are often required. A widely

employed approach is to evaluate these derivatives using finite difference approximation, also known as semi-analytical approximation. The biggest advantage of this approach is that it leads to straightforward implementation, and there is no need to access specific finite element formulations.

However, the semi-analytical approach causes accuracy problems, even in linear sensitivity analysis [BCH88, PCR89, Mle92, CO93]. Rigid body rotation of finite elements is recognized as the source of the error, and various techniques have been presented to eliminate its influence on sensitivities. It has been shown that the first-order finite difference results, when multiplied by appropriate correction factors which can be easily pre-computed, are equal to the analytical derivatives of the stiffness matrix, mass matrix, and initial stress stiffness matrix for the isoparametric Mindlin plate element [PC99].

For general types of elements, "exact" semi-analytical sensitivity [ORL93, BFD08, Fi10] and refined semi-analytical analysis [BK97, KB98] are two effective methods in linear cases, although neither of them leads to the exact analytical derivatives. The "exact" semi-analytical approach corrects the finite difference approximation of the tangent stiffness matrix by adding an additional term, called the correction term, so that a set of rigid-body conditions is satisfied. The correction term is expressed as a member in the product space of a set of zero eigenvectors. The refined semi-analytical technique focuses on correcting the approximation error of the derivatives of internal force vectors, and the correction term is a linear combination of zero eigenvectors. The refined semi-analytical approach has also been extended to the geometric nonlinear case [BK00].

1.2.4 Implementation of sensitivity analysis in commercial finite element codes

Commercial finite element analysis software is favored for large-scale structural analysis in the industry due to its efficiency, robustness, and recognition. Therefore, optimization and sensitivity analysis techniques are often integrated with commercial finite element analysis codes to expand their fields of applications. However, commercial software always functions as a black box, where intermediate quantities needed in sensitivity analysis may not be available or accessible.

With limited information, linear sensitivity analysis with Kirchhoff flat shell elements is implemented in Abaqus based on the discrete direct differentiation method [ZD99]. Direct semi-analytical sensitivity analysis with refined correction is realized in ANSYS for linear problems with solid and shell elements [LYL04]. Sensitivities with linear elastic solid elements in a contact problem are attempted in MARC using the direct method [PRA93]. The complex variable finite element method and sensitivity analysis are implemented in Abaqus for pure elastoplastic problems with 16-node axisymmetric quadrilateral user elements [MWB+13, MFG+15]. There is still not much reported regarding the integration of geometric nonlinear sensitivity analysis into commercial codes, not to mention geometric nonlinear problems with material nonlinearities.

1.3 Scope and outline of thesis

This dissertation is based on the research in Work Package 2, Nonlinear Sensitivity-Based Shape Optimization of the LaSciSo project (Large Scale Industrial Structural Optimization for Advanced Applications). The focus of the work package is on high-quality sensitivity analysis for nonlinear, non-parametric shape optimization. The objective of this dissertation is to investigate methods to improve the accuracy and efficiency of adjoint sensitivity analysis in nonlinear, non-parametric shape optimization. Specifically, two types of nonlinearities are within the scope of this research: geometric nonlinearity and elastoplasticity.

The major contributions of this thesis to the research field are:

- Extension of the correction term in exact semi-analytical sensitivity analysis to the case of geometric nonlinearity.
- Analytical formulation of zero-eigenvectors, which are used in constructing the correction term efficiently.
- Proposal and theoretical proof of two numerical properties of adjoint variables for adjoint sensitivity analysis, considering simultaneous elastoplasticity and geometric nonlinearity.
- Proposal and theoretical proof of two load step reduction rules in the adjoint sensitivity analysis procedure to improve efficiency.

- Extension of proposed load step reduction techniques to elastoplasticity with a mixed-hardening material model.

- Extension of proposed load step reduction techniques to the case of finite strain elastoplasticity, along with a discussion on the applicability.

The dissertation is organized as follows.

In Chapter 2, an in-house finite element solver used in the study is presented. The solver can deal with simultaneous geometric nonlinearity and elastoplasticity. Although the ultimate and ideal industrial goal is to develop and implement the sensitivity analysis procedure in commercial finite element codes, an accurate in-house nonlinear finite element solver is highly demanded due to two reasons. Firstly, commercial finite element codes may not provide all necessary outputs to calculate sensitivities. Secondly, the intermediate quantities provided by commercial finite element codes may introduce numerical errors, which may lead to unreasonable sensitivity results and even fallacious conclusions.

Based on the solver, the semi-analytical adjoint sensitivity formulation for geometric nonlinear problems under both external force and prescribed displacement is derived in Chapter 3. The accuracy problem of the semi-analytical approach for geometric nonlinear sensitivity analysis is investigated. The "exact" semi-analytical correction is extended to this problem, and a correction term is constructed analytically to eliminate the errors. The sensitivity analysis procedure is integrated into the TOSCA optimization platform, and several non-parametric shape optimization examples are presented for demonstration.

In Chapter 4, the adjoint sensitivity approach for simultaneous geometric nonlinearity and small strain elastoplasticity with the isotropic hardening model is formulated and implemented. Techniques to reduce the number of load steps in the sensitivity analysis are proposed, theoretically proved, and demonstrated with multiple examples from small-scale bar truss examples to large-scale solid structures in Chapter 5. In Chapter 6, the presented techniques are extended to kinematic hardening and combined hardening material models with proof and demonstrations. In chapter 7, the applicability of the adjoint sensitivity analysis and load step reduction rules is investigated for a more general case, i.e. large strain elastoplasticity, where the logarithmic

strain measure and multiplicative decomposition of the deformation gradient are adopted.

The thesis is finally summarized in Chapter 8 with an outlook on further research work.

2. Introduction to nonlinear finite element analysis

In this chapter, the theory of nonlinear finite element analysis for geometric nonlinearity and elastoplasticity is briefly introduced. This serves as the basis for deducing the adjoint sensitivity formulation of structural responses. The mechanical quantities obtained from the finite element analysis form the foundation of sensitivity analysis. To overcome potential limitations of outputs from commercial finite element codes, an in-house nonlinear finite element solver is developed based on the theory and is employed in the research.

2.1 Geometric nonlinear analysis with secant stiffness matrix

2.1.1 The Newton-Raphson method

Geometric nonlinearity describes the nonlinear relationship between load and displacement when large structural deformation occurs. The Newton-Raphson method is commonly used at each load step of the finite element analysis to obtain the displacement of equilibrium iteratively. The flowchart of this method from load step *t* to the next load step *t+1* is depicted in Figure 2-1.

In the flowchart, ${}^{t}\boldsymbol{U}$ is the nodal displacement vector, ${}^{t}\boldsymbol{F}$ is the nodal external force. Throughout the paper, the upper left superscript denotes the load step. $\boldsymbol{R}$ is the residual force, $\boldsymbol{K}_{\mathrm{T}}$ denotes the tangent stiffness matrix, $\boldsymbol{F}^{\mathrm{int}}$ is the internal force vector corresponding to the displacement. In each iteration, an incremental displacement is obtained by solving a system of linear equations, with the residual force on the right-hand side. Then the displacement is updated by the increment, and the residual force is recomputed. The iterative procedure terminates if the residual force is sufficiently small.

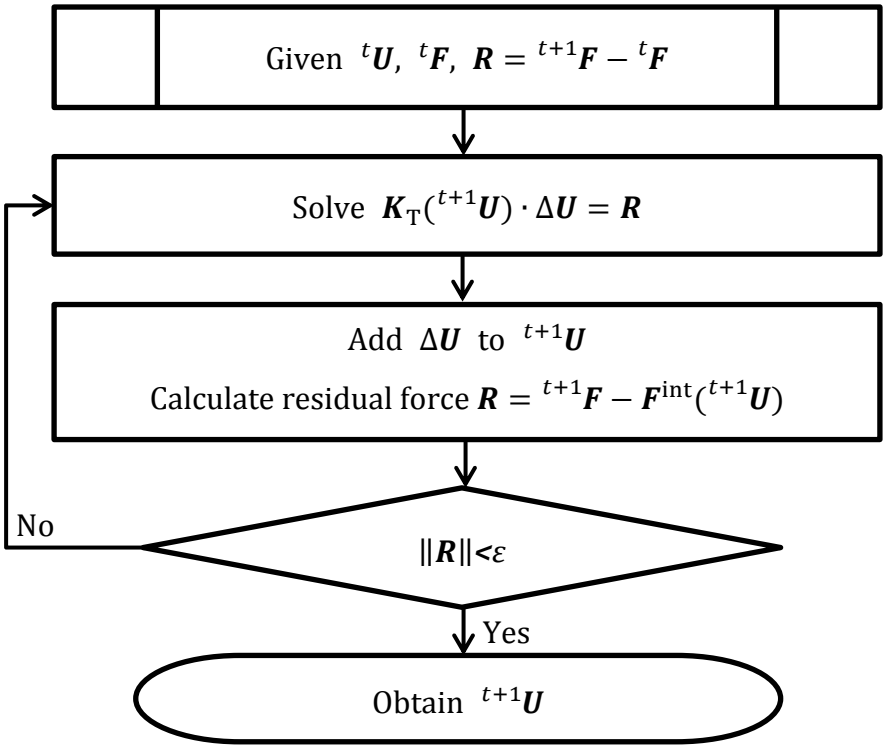

Figure 2-1. Newton-Raphson iterative solution procedure for geometric nonlinearity

On the element level, the internal force is obtained through stress integration:

$$\boldsymbol{F}^{\mathrm{int}} = \int_{V} \boldsymbol{B}\boldsymbol{\sigma} dv \tag{2.1}$$

where $\boldsymbol{B}$ is the deformation matrix, $\boldsymbol{\sigma}$ is the elemental stress and V stands for the volume of an element.

Instead of stress integration, when Green-Lagrangian strain is employed, the internal force vector can also be straightforwardly evaluated by multiplying a secant stiffness matrix $\boldsymbol{K}_{\mathrm{S}}$ by the displacement vector, as shown in the following equation [OOM+86, Pe05]:

$$\boldsymbol{F}^{\mathrm{int}} = \boldsymbol{K}_{\mathrm{S}}(\boldsymbol{U}) \cdot \boldsymbol{U} \tag{2.2}$$

This approach via secant stiffness matrix is introduced in the next section.

2.1.2 Introduction to the secant stiffness matrix

The secant stiffness matrix possesses a straightforward physical meaning that connects total displacement and internal force. The formulation and

application of the secant stiffness matrix in geometrically nonlinear finite element analyses have been investigated [OOM+86, Oñ91, MOM98]. Additionally, the secant stiffness matrix has been employed in the analysis of the stability of frame structures [CG96] and the estimation of buckling load factors [Oñ95].

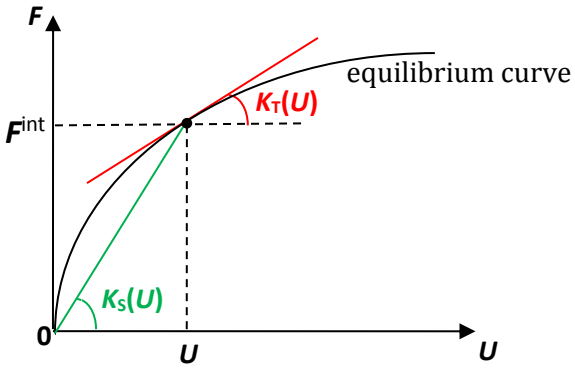

Figure 2-2. Tangent and secant stiffness matrices at an equilibrium point

Figure 2-2 depicts the force-displacement equilibrium curve of a general nonlinear problem. The secant stiffness matrix is the slope of the secant line connecting the initial point and the equilibrium point. While the tangent stiffness matrix reflects the relationship between incremental displacement and incremental force, the secant stiffness matrix describes the relationship between total displacement and total force.

There are three kinematic descriptions that are usually used in geometrically nonlinear finite element analysis: total Lagrangian formulation, updated Lagrangian formulation, and co-rotational formulation [No12, Cr00]. In the total Lagrangian formulation, strains and stresses are measured with reference to the initial undeformed configuration. The updated Lagrangian formulation uses the deformed configuration from the previous step as the reference state, and the reference configuration is updated as the solution procedure proceeds. In the co-rotational formulation, a local reference frame is attached to each element, and it translates and rotates with the corresponding element as a rigid body. In the context of the secant stiffness matrix approach, where the stiffness matrix is dependent on the total displacement, the total Lagrangian formulation could be naturally employed.

In the following, the formulations of the secant stiffness matrix for general finite elements under geometric nonlinearity is introduced. These

formulations have been derived by Pederson [Pe05, Pe06, Pe08], where Green–Lagrange strain and its conjugate second Piola-Kirchhoff stress are adopted.

The components of the nonlinear Green–Lagrange strain ε_{ij} in Cartesian coordinates are defined as

$$\varepsilon_{ij} = \frac{1}{2}\left(u_{i,j} + u_{j,i}\right) + \frac{1}{2}\left(u_{k,i} \cdot u_{k,j}\right) \tag{2.3}$$

where variable u is the displacement field and indices i, j, k represent the three directions in three-dimensional space. The Einstein summation convention applies to the index k. After discretization, the formulas can be expressed in matrix form using the Voigt notation for strain:

$$\boldsymbol{\varepsilon} = \boldsymbol{B}^{\mathrm{L}}\boldsymbol{U} + \frac{1}{2}\boldsymbol{U}^{\mathrm{T}}\boldsymbol{B}^{\mathrm{N}}\boldsymbol{U} \tag{2.4}$$

where $\boldsymbol{B}^{\mathrm{L}}$ is the linear strain–displacement matrix, $\boldsymbol{B}^{\mathrm{N}}$ is a symmetric matrix describes the nonlinear relation between displacement and strain, and the upper right superscript T represents the transpose operator. The variation of strain follows

$$\delta\boldsymbol{\varepsilon} = (\boldsymbol{B}^{\mathrm{L}} + \boldsymbol{U}^{\mathrm{T}}\boldsymbol{B}^{\mathrm{N}})\delta\boldsymbol{U} \tag{2.5}$$

The general equilibrium equation, according to the principle of virtual work over an element volume, is

$$\int_V \delta\boldsymbol{\varepsilon}^{\mathrm{T}}\boldsymbol{\sigma}\mathrm{d}v = \delta\boldsymbol{U} \cdot \boldsymbol{F} \tag{2.6}$$

By substituting Eq.(2.5) into Eq.(2.6), the equilibrium equation is derived:

$$\int_V (\boldsymbol{B}^{\mathrm{L}} + \boldsymbol{U}^{\mathrm{T}}\boldsymbol{B}^{\mathrm{N}})^{\mathrm{T}}\boldsymbol{\sigma}\mathrm{d}v = \boldsymbol{F} \tag{2.7}$$

Comparing Eq.(2.7) and Eq.(2.1), it follows that

$$\boldsymbol{B} = \boldsymbol{B}^{\mathrm{L}} + \boldsymbol{U}^{\mathrm{T}}\boldsymbol{B}^{\mathrm{N}} \tag{2.8}$$

The constitutive relationship between the second Piola-Kirchhoff stress and the Green–Lagrange strain is

$$\boldsymbol{\sigma} = \boldsymbol{D}\boldsymbol{\varepsilon} = \boldsymbol{D} \cdot \left(\boldsymbol{B}^{\mathrm{L}} + \frac{1}{2}\boldsymbol{U}^{\mathrm{T}}\boldsymbol{B}^{\mathrm{N}} \right) \cdot \boldsymbol{U} \tag{2.9}$$

where $\boldsymbol{D}$ represents the elastic constitutive relation between strain and stress.

For simplicity, denotes

$$\bar{\boldsymbol{B}} = \boldsymbol{B}^{\mathrm{L}} + \frac{1}{2}\boldsymbol{U}^{\mathrm{T}}\boldsymbol{B}^{\mathrm{N}} \tag{2.10}$$

The equilibrium equation is derived by substituting Eqs.(2.8) to (2.10) into Eq.(2.7),

$$\int_V \boldsymbol{B}^{\mathrm{T}}\boldsymbol{D}\bar{\boldsymbol{B}}\mathrm{d}v \cdot \boldsymbol{U} = \boldsymbol{F} \tag{2.11}$$

Thus, the general formulation of the secant stiffness matrix is obtained:

$$\boldsymbol{K}_{\mathrm{S}}(\boldsymbol{U}) = \int_V \boldsymbol{B}^{\mathrm{T}}\boldsymbol{D}\bar{\boldsymbol{B}}\mathrm{d}v \tag{2.12}$$

In addition, the tangent stiffness matrix can be derived from Eq.(2.12):

$$\begin{aligned} \boldsymbol{K}_{\mathrm{T}}(\boldsymbol{U}) = \nabla_{\boldsymbol{U}}(\boldsymbol{K}_{\mathrm{S}}(\boldsymbol{U}) \cdot \boldsymbol{U}) = \nabla_{\boldsymbol{U}} \int_V (\boldsymbol{B}^{\mathrm{L}} + \boldsymbol{U}^{\mathrm{T}}\boldsymbol{B}^{\mathrm{N}})^{\mathrm{T}}\boldsymbol{D}\left(\boldsymbol{B}^{\mathrm{L}}\boldsymbol{U} + \frac{1}{2}\boldsymbol{U}^{\mathrm{T}}\boldsymbol{B}^{\mathrm{N}}\boldsymbol{U} \right) dv \\ = \int_V \boldsymbol{B}^{\mathrm{T}}\boldsymbol{D}\boldsymbol{B}dv + \int_V \boldsymbol{\nabla}_{\boldsymbol{U}}\boldsymbol{B}^{\mathrm{T}}\boldsymbol{\sigma}dv \end{aligned} \tag{2.13}$$

The first term reflects the elastic stiffness matrix and displacement stiffness matrix, while the second term represents the stress stiffness matrix. It can be seen that, unlike the tangent stiffness matrix, the secant stiffness matrix in Eq. (2.12) is asymmetric.

Furthermore, both tangent and secant stiffness matrices for several element types can be analytically formulated using nodal coordinates and nodal displacements. An example is provided in Appendix A for the 3D 4-node tetrahedral element, as presented by Pederson [Pe06]. The analytical expressions of stiffness matrices offer a solid foundation for studies on

sensitivity analysis. In particular, they are helpful for tracing the source of errors.

2.2 Simultaneous geometric nonlinear and elastoplastic nonlinear analysis

In this section, nonlinear analysis is extended to simultaneous geometric nonlinearity and small strain elastoplasticity.

2.2.1 Elastoplastic material model

Plasticity describes a material undergoing irreversible deformation in response to an applied load. The elastoplastic material model depicts a material that possesses both elasticity and plasticity. Most ductile metals, widely used in mechanical engineering, fall into this category.

Figure 2-3 presents a 1D rheological model of elastoplasticity. It is composed of two springs with stiffness E (Young's modulus), E^{P} (Plastic modulus), respectively, and a frictional element with maximum friction force σ_{Y} (yield strength).

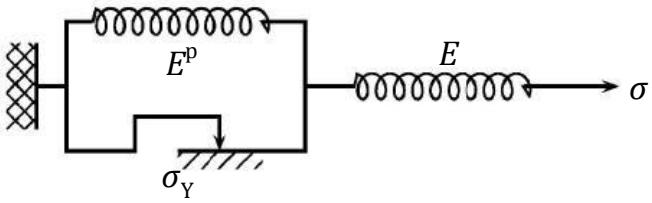

Figure 2-3. 1D rheological model of elastoplasticity

The elastoplastic material behavior in a loading-unloading procedure is illustrated in Figure 2-4. The material behaves elastically initially. Once the stress exceeds the initial yield strength σ_0, the plastic strain $\boldsymbol{\varepsilon}^{\mathrm{p}}$ gradually accumulates, which is the irreversible part after unloading.

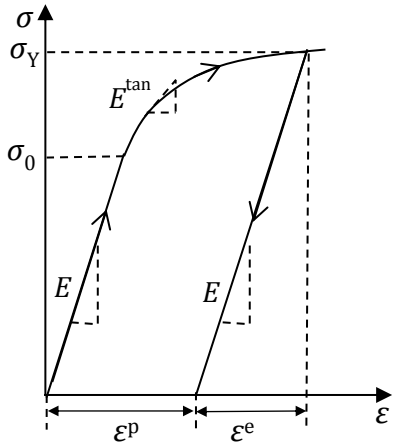

Figure 2-4. Elastoplastic material behavior in a loading-unloading procedure

In the small strain case, the total strain $\boldsymbol{\varepsilon}$ is additively decomposed into elastic strain part $\boldsymbol{\varepsilon}^{\mathrm{e}}$ and plastic strain part $\boldsymbol{\varepsilon}^{\mathrm{p}}$

$$\boldsymbol{\varepsilon} = \boldsymbol{\varepsilon}^{\mathrm{e}} + \boldsymbol{\varepsilon}^{\mathrm{p}} \tag{2.14}$$

The relationship between total stress and total strain is

$$\boldsymbol{\sigma} = \boldsymbol{D}^{\mathrm{e}}\boldsymbol{\varepsilon}^{\mathrm{e}} = \boldsymbol{D}^{\mathrm{e}}(\boldsymbol{\varepsilon} - \boldsymbol{\varepsilon}^{\mathrm{p}}) \tag{2.15}$$

where $\boldsymbol{D}^{\mathrm{e}}$ is the elastic constitutive relation matrix. In a 1D case, $\boldsymbol{D}^{\mathrm{e}}$ represents the elastic modulus E. In Figure 2-4, $E^{\tan}$ denotes the tangent modulus, which reflects the relationship between incremental stress and incremental strain

$$d\boldsymbol{\sigma} = E^{\tan} \cdot d\boldsymbol{\varepsilon} \tag{2.16}$$

The plastic modulus E^{p} denotes the relationship between incremental stress and incremental plastic strain

$$d\boldsymbol{\sigma} = E^{\mathrm{p}} \cdot d\boldsymbol{\varepsilon}^{\mathrm{p}} \tag{2.17}$$

Therefore, $E^{\tan}$ has the following relation to Young's modulus and the plastic modulus

$$E^{\tan} = \frac{EE^{\mathrm{p}}}{E + E^{\mathrm{p}}} \tag{2.18}$$

The total plastic strain results from the accumulation of incremental plastic strains from individual load step

$$\boldsymbol{\varepsilon}^{\mathrm{p}} = \sum_{t} {}^{t}\Delta\boldsymbol{\varepsilon}^{\mathrm{p}} \tag{2.19}$$

where the incremental plastic strain is the product of the incremental equivalent plastic strain and a vector $\mathbf{a}$ which is called the flow vector

$$\Delta\boldsymbol{\varepsilon}^{\mathrm{p}} = \Delta\varepsilon^{\mathrm{p}}_{\mathrm{eqv}} \cdot \mathbf{a} \tag{2.20}$$

The flow vector describes the direction of incremental plastic strain. In metal plasticity, it is typically assumed that flow vector is in the same direction as the normal to the yield surface. This is referred to as the associated-flow rule:

$$\mathbf{a} = \frac{df(\boldsymbol{\sigma})}{d\boldsymbol{\sigma}} = \frac{d|\boldsymbol{\sigma}|_{\mathrm{eqv}}}{d\boldsymbol{\sigma}} \tag{2.21}$$

Otherwise, it is referred to as a non-associated flow rule.

In Eq.(2.21), $f(\boldsymbol{\sigma})$ is a function of stress that defines the yield surface

$$f(\boldsymbol{\sigma}) = |\boldsymbol{\sigma}|_{\mathrm{eqv}} - \sigma_{\mathrm{Y}}(\varepsilon^{\mathrm{p}}_{\mathrm{eqv}}) = 0 \tag{2.22}$$

where $|\cdot|_{\mathrm{eqv}}$ is an equivalent stress measure, σ_{Y} is the yield strength, which is dependent on the material properties and equivalent plastic strain $\varepsilon^{\mathrm{p}}_{\mathrm{eqv}}$.

The equivalent stress measure is determined by the employed yield criterion. One widely used criterion for metal plasticity is the von Mises yield criterion. The von Mises equivalent stress is then determined by this criterion

$$\begin{aligned} &|\boldsymbol{\sigma}|_{\text{von Mises}} \\ &= \sqrt{\frac{(\sigma_{11}-\sigma_{22})^2 + (\sigma_{22}-\sigma_{33})^2 + (\sigma_{11}-\sigma_{33})^2 + 6({\sigma_{12}}^2 + {\sigma_{23}}^2 + {\sigma_{13}}^2)}{2}} \\ &= \sqrt{\frac{(\sigma_1-\sigma_2)^2 + (\sigma_2-\sigma_3)^2 + (\sigma_1-\sigma_3)^2}{2}} = \sqrt{\frac{3}{2}\sum_i \sum_j s_{ij}^2} \end{aligned} \tag{2.23}$$

where σ_1 to σ_3 represent the three principal stress components, and s_{ij} denotes the deviatoric stress components defined by

$$s_{ij} = \sigma_{ij} - \frac{1}{3}\sigma_{kk} \tag{2.24}$$

According to the development of yield strength, plasticity is categorized into three types: hardening, softening, and perfect plasticity. Hardening plasticity depicts an increase in yield strength as plastic strain accumulates, while softening plasticity depicts just the opposite, i.e. a decrease in yield strength. Perfect plasticity is an ideal model where the yield strength remains unchanged. These three types of plasticity are defined by the sign of the tangent modulus

$$E^{\tan} \text{ and } E^{\mathrm{p}} \begin{cases} > 0 & \text{hardening} \\ = 0 & \text{perfect plasticity} \\ < 0 & \text{softening} \end{cases} \tag{2.25}$$

For the hardening plasticity, three typical hardening rules describe the development of the yield surface: isotropic hardening, kinematic hardening, and mixed hardening, also known as combined hardening. The development of the yield surface under the isotropic hardening rule is depicted in Figure 2-5. It assumes that the yield surface expands uniformly in all directions as plastic strain increases.

The cases of kinematic hardening and mixed hardening will be discussed in Chapter 6.

2.2.2 Newton-Raphson iteration for elastoplasticity

The Newton-Raphson method is also employed to solve elastoplastic nonlinear problems. The flowchart for this method at a new load step *t+1* from the previous step *t* is depicted in Figure 2-6. In each iteration, an incremental displacement is obtained by solving a system of linear equations, similar to the process in geometric nonlinearity. Two major differences exist: the inclusion of the tangent stiffness in the linear equation system and the utilization of a return mapping algorithm.

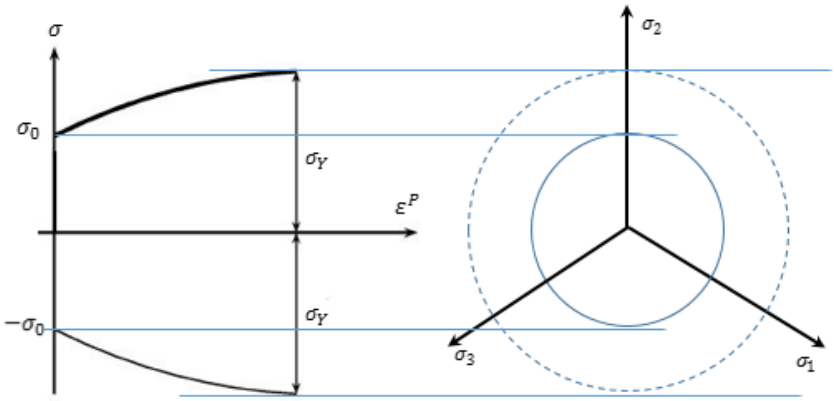

(a) 1D development of yield strength (b) 3D development of yield surface in the space of principal stress components, taking von Mises yield criterion as an example

Figure 2-5. Increase of yield strength and expansion of yield surface under isotropic hardening rule

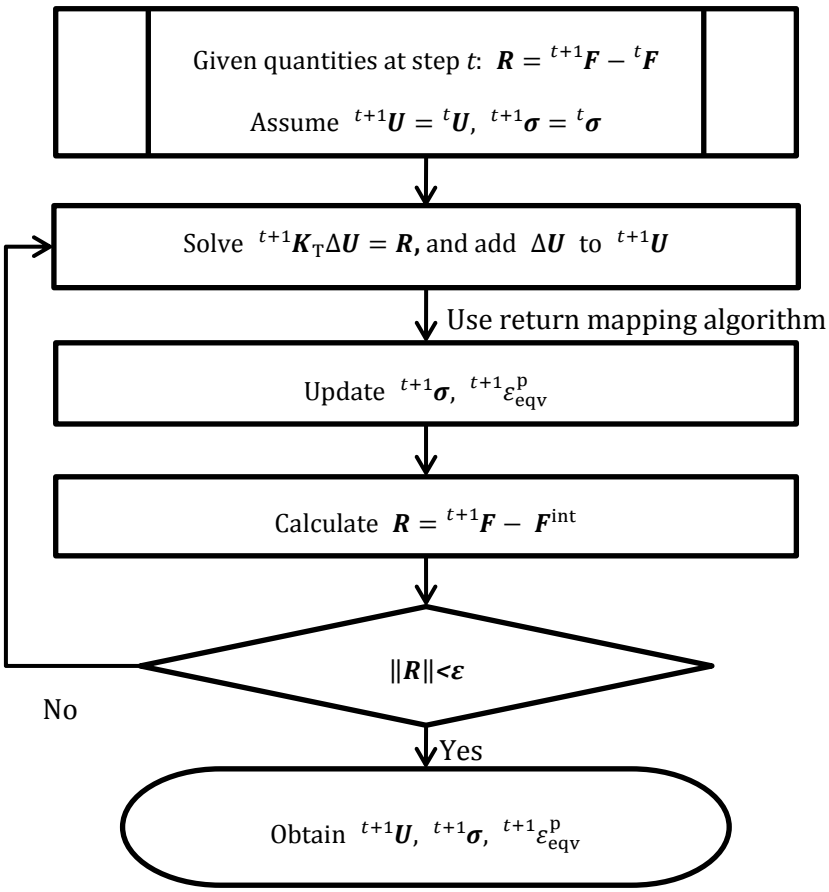

Figure 2-6. Newton-Raphson iteration for elastoplasticity

The tangent stiffness matrix follows the expression in Eq.(2.13), with the elastic constitutive matrix being replaced by $\boldsymbol{D}^{\mathrm{ep}}$. $\boldsymbol{D}^{\mathrm{ep}}$ describes the relationship between incremental stress and incremental strain in elastoplastic analysis

$$\Delta\boldsymbol{\sigma} = \boldsymbol{D}^{\mathrm{ep}} \cdot \Delta\boldsymbol{\varepsilon} \tag{2.26}$$

In an elastic step, it equals the elastic constitutive matrix $\boldsymbol{D}^{\mathrm{e}}$. During a plastic step, $\boldsymbol{D}^{\mathrm{ep}}$ is expressed as follows [Cr00]:

$$\boldsymbol{D}^{\mathrm{ep}} = \boldsymbol{Q}^{-1} \cdot \boldsymbol{D}^{\mathrm{e}} - \frac{\boldsymbol{d}}{\mathbf{a} \cdot \boldsymbol{r} + E^{\mathrm{p}}} \tag{2.27}$$

where

$$\boldsymbol{Q} = \boldsymbol{I} + \boldsymbol{D}^{\mathrm{e}} \cdot \frac{d\mathbf{a}}{d\boldsymbol{\sigma}} \cdot \Delta\varepsilon^{\mathrm{p}}_{\mathrm{eqv}}$$

$$\frac{d\mathbf{a}}{d\boldsymbol{\sigma}} = \frac{\mathbf{1}}{|\boldsymbol{\sigma}|_{\mathrm{eqv}}} \left(\begin{bmatrix} 1 & -0.5 & -0.5 & & & \\ -0.5 & 1 & -0.5 & & & \\ -0.5 & -0.5 & 1 & & & \\ & & & 3 & & \\ & & & & 3 & \\ & & & & & 3 \end{bmatrix} - \mathbf{a}^{\mathrm{T}} \cdot \mathbf{a} \right) \tag{2.28}$$

$$\boldsymbol{r} = \boldsymbol{Q}^{-1} \cdot \boldsymbol{D}^{\mathrm{e}} \cdot \mathbf{a}^{\mathrm{T}}$$

$$\boldsymbol{d} = \boldsymbol{r} \cdot \boldsymbol{r}^{\mathrm{T}}$$

After updating the nodal displacement, the stress and equivalent plastic strain will be updated to calculate the internal force and stiffness matrix in the next iteration. These quantities cannot be determined explicitly from nodal displacement when plasticity occurs. A return mapping algorithm is typically employed to perform this task implicitly. The algorithm is introduced in the next section.

2.2.3 Return mapping algorithm

The return mapping algorithm [Cr00] is usually used to determine the stress and equivalent plastic strain with a given incremental strain. The algorithm is described below, taking the von-Mises yield criterion as an example.

Given stress ${}^{t}\boldsymbol{\sigma}$ and equivalent plastic strain ${}^{t}\varepsilon_{\mathrm{eqv}}^{\mathrm{p}}$, firstly, calculate the incremental strain $\Delta\boldsymbol{\varepsilon}$ through the incremental displacement $\Delta\boldsymbol{U}$. Then, assume it is an elastic increment, i.e. $\Delta\varepsilon_{\mathrm{eqv}}^{\mathrm{p}} = 0$, and update the trial stress with

$$\begin{aligned} \Delta\boldsymbol{\sigma}_{\mathrm{try}} &= \boldsymbol{D}^{\mathrm{e}} \cdot \Delta\boldsymbol{\varepsilon} \\ \boldsymbol{\sigma}_{\mathrm{try}} &= {}^{t}\boldsymbol{\sigma} + \Delta\boldsymbol{\sigma}_{\mathrm{try}} \end{aligned} \tag{2.29}$$

Calculate the von Mises equivalent stress using $\boldsymbol{\sigma}_{\mathrm{try}}$ and check whether it is not larger than the yield strength at step *t*.

If it is true, then the element is indeed in an elastic state, and the assumption $\Delta\varepsilon_{\mathrm{eqv}}^{\mathrm{p}} = 0$ holds. Therefore, it follows ${}^{t+1}\boldsymbol{\sigma} = \boldsymbol{\sigma}_{\mathrm{try}}$, ${}^{t+1}\varepsilon_{\mathrm{eqv}}^{\mathrm{p}} = {}^{t}\varepsilon_{\mathrm{eqv}}^{\mathrm{p}}$, and $\boldsymbol{D}^{\mathrm{ep}} = \boldsymbol{D}^{\mathrm{e}}$. Otherwise, initiate the return mapping algorithm:

a) Calculate trial associated flow vector $\mathbf{a}$:

$$\mathbf{a} = \frac{d\left|\boldsymbol{\sigma}_{\mathrm{try}}\right|_{\mathrm{Mises}}}{d\boldsymbol{\sigma}} = \frac{3}{2\left|\boldsymbol{\sigma}_{\mathrm{try}}\right|_{\mathrm{Mises}}}[s_{11}, s_{22}, s_{33}, 2s_{12}, 2s_{13}, 2s_{23}] \tag{2.30}$$

b) Update the incremental plastic strain

$$\begin{aligned} \Delta\varepsilon_{\mathrm{eqv}}^{\mathrm{p}} &= \Delta\varepsilon_{\mathrm{eqv}}^{\mathrm{p}} + \frac{\left|\boldsymbol{\sigma}_{\mathrm{try}}\right|_{\mathrm{Mises}} - {}^{t}\sigma_{\mathrm{Y}} - E^{\mathrm{p}} \cdot \Delta\varepsilon_{\mathrm{eqv}}^{\mathrm{p}}}{\mathbf{a} \cdot \boldsymbol{D}^{\mathrm{e}} \cdot \mathbf{a}^{\mathrm{T}} + E^{\mathrm{p}}} \\ \Delta\boldsymbol{\varepsilon}^{\mathrm{p}} &= \Delta\varepsilon_{\mathrm{eqv}}^{\mathrm{p}} \cdot \mathbf{a} \end{aligned} \tag{2.31}$$

c) Update trial stress

$$\boldsymbol{\sigma}_{\mathrm{try}} = {}^{t}\boldsymbol{\sigma} + \boldsymbol{D}^{\mathrm{e}} \cdot \Delta\boldsymbol{\varepsilon} - \boldsymbol{D}^{\mathrm{e}} \cdot \Delta\boldsymbol{\varepsilon}^{\mathrm{p}} \tag{2.32}$$

d) Check if $\left|\boldsymbol{\sigma}_{\mathrm{try}}\right|_{\mathrm{Mises}} - {}^{t}\sigma_{\mathrm{Y}} - E^{\mathrm{p}} \cdot \Delta\varepsilon_{\mathrm{eqv}}^{\mathrm{p}} = 0$. If it is not satisfied, go back to step a). Otherwise, the algorithm stops and provides the result

$$\begin{aligned} {}^{t+1}\boldsymbol{\sigma} &= \boldsymbol{\sigma}_{\mathrm{try}} \\ {}^{t+1}\varepsilon_{\mathrm{eqv}}^{\mathrm{p}} &= {}^{t}\varepsilon_{\mathrm{eqv}}^{\mathrm{p}} + \Delta\varepsilon_{\mathrm{eqv}}^{\mathrm{p}} \end{aligned} \tag{2.33}$$

After updating the stress and equivalent plastic strain, the internal force could be calculated following Eq.(2.1).

3. Adjoint sensitivity analysis with geometric nonlinearity

In this chapter, the adjoint sensitivity formulation for geometric nonlinear problems is derived using the secant stiffness matrix. An analytical correction term is proposed to eliminate the rotation error in the semi-analytical approximation. Several optimization examples with the TOSCA shape optimization solver are presented.

3.1 Adjoint sensitivity analysis formulation under prescribed displacement and external force

Under both prescribed displacement and external force, the system response f of a geometric nonlinear system can be expressed as a function of unknown displacement, unknown reaction force, and design variables. The displacement and reaction force are also dependent on design variables. Therefore, the sensitivity of the system response with respect to a design variable s follows

$$\frac{df(\boldsymbol{U}(s),\boldsymbol{F}(s),s)}{ds}=\frac{\partial f}{\partial s}+\frac{\partial f}{\partial \boldsymbol{U}}^{\mathrm{T}}\cdot\frac{d\boldsymbol{U}}{ds}+\frac{\partial f}{\partial \boldsymbol{F}}^{\mathrm{T}}\cdot\frac{d\boldsymbol{F}}{ds} \tag{3.1}$$

where derivative of displacements and reaction forces need to be evaluated. The idea of the adjoint variable method is to avoid the calculation of these derivatives by cancelling them out with additional terms. These additional terms are products of adjoint variables with derivatives of governing equations, which are identical to zero and contain $d\boldsymbol{U}/ds$ and $d\boldsymbol{F}/ds$. Here, the equilibrium equation of the finite element system is utilized

$$\boldsymbol{R}(\boldsymbol{U}(s),\boldsymbol{F}(s),s)=\boldsymbol{K}_{\mathrm{S}}(\boldsymbol{U}(s),s)\cdot\boldsymbol{U}(s)-\boldsymbol{F}(s)\equiv\boldsymbol{0} \tag{3.2}$$

The total derivative of the residual force vector, which is identical to zero, is calculated as

$$\boldsymbol{0}=\frac{d\boldsymbol{R}}{ds}=\frac{\partial \boldsymbol{R}}{\partial s}+\frac{\partial \boldsymbol{R}}{\partial \boldsymbol{U}}^{\mathrm{T}}\cdot\frac{d\boldsymbol{U}}{ds}+\frac{\partial \boldsymbol{R}}{\partial \boldsymbol{F}}^{\mathrm{T}}\cdot\frac{d\boldsymbol{F}}{ds}=\frac{\partial \boldsymbol{K}_{\mathrm{S}}}{\partial s}\cdot\boldsymbol{U}+\boldsymbol{K}_{\mathrm{T}}\cdot\frac{d\boldsymbol{U}}{ds}-\frac{d\boldsymbol{F}}{ds} \tag{3.3}$$

Define the adjoint variable $\boldsymbol{\lambda}$ as a column vector given by $\boldsymbol{\lambda} = [\boldsymbol{\lambda}^{\mathrm{f}} \quad \boldsymbol{\lambda}^{\mathrm{d}}]^{\mathrm{T}}$, where $\boldsymbol{\lambda}^{\mathrm{f}}$ corresponds to degrees of freedom with external force, and $\boldsymbol{\lambda}^{\mathrm{d}}$ corresponds to degrees of freedom with prescribed displacement. Pre-multiply the transpose of the adjoint variable to Eq. (3.3) and then subtract it from Eq. (3.1), this yields

$$\frac{df}{ds} = \frac{\partial f}{\partial s} + \frac{\partial f}{\partial \boldsymbol{U}}^{\mathrm{T}} \cdot \frac{d\boldsymbol{U}}{ds} + \frac{\partial f}{\partial \boldsymbol{F}}^{\mathrm{T}} \cdot \frac{d\boldsymbol{F}}{ds} - \boldsymbol{\lambda}^{\mathrm{T}} \cdot \left(\frac{\partial \boldsymbol{K}_{\mathrm{S}}}{\partial s} \cdot \boldsymbol{U} + \boldsymbol{K}_{\mathrm{T}} \cdot \frac{d\boldsymbol{U}}{ds} - \frac{d\boldsymbol{F}}{ds} \right) \tag{3.4}$$

After merging similar terms, the sensitivity has been reformulated as

$$\frac{df}{ds} = \frac{\partial f}{\partial s} - \boldsymbol{\lambda}^{\mathrm{T}} \cdot \frac{\partial \boldsymbol{K}_{\mathrm{S}}}{\partial s} \cdot \boldsymbol{U} - \left(\boldsymbol{K}_{\mathrm{T}} \cdot \boldsymbol{\lambda} - \frac{\partial f}{\partial \boldsymbol{U}} \right)^{\mathrm{T}} \cdot \frac{d\boldsymbol{U}}{ds} + \left(\frac{\partial f}{\partial \boldsymbol{F}} + \boldsymbol{\lambda} \right)^{\mathrm{T}} \cdot \frac{d\boldsymbol{F}}{ds} \tag{3.5}$$

The external forces and prescribed displacements on a structure are given quantities, independent of design variables. Consequently, the components of the derivative of the displacement vector, which correspond to the degrees of freedom with prescribed displacement, are zero. Similarly, the components of the derivative of the reaction force vector, which correspond to the degrees of freedom with external force, are also zero. They are expressed as follows:

$$\begin{aligned} \frac{d\boldsymbol{U}}{ds} &= \begin{bmatrix} d\boldsymbol{U}^{\mathrm{f}}/ds \\ \mathbf{0} \end{bmatrix} \\ \frac{d\boldsymbol{F}}{ds} &= \begin{bmatrix} \mathbf{0} \\ d\boldsymbol{F}^{d}/ds \end{bmatrix} \end{aligned} \tag{3.6}$$

With Eq.(3.6), the fourth term in Eq. (3.5) is

$$\left(\frac{\partial f}{\partial \boldsymbol{F}} + \boldsymbol{\lambda} \right)^{\mathrm{T}} \cdot \frac{d\boldsymbol{F}}{ds} = \left(\nabla_{\boldsymbol{F}^{d}} f + \boldsymbol{\lambda}^{\mathrm{d}} \right)^{\mathrm{T}} \cdot \frac{d\boldsymbol{F}^{d}}{ds} \tag{3.7}$$

Enforcing Eq. (3.7) to be zero leads to

$$\boldsymbol{\lambda}^{d} = -\nabla_{\boldsymbol{F}^{d}} f \tag{3.8}$$

With Eq.(3.6) and Eq.(3.8), the third term in Eq. (3.5) is

$$\left(\boldsymbol{K}_{\mathrm{T}} \cdot \boldsymbol{\lambda} - \frac{\partial f}{\partial \boldsymbol{U}}\right)^{\mathrm{T}} \cdot \frac{d\boldsymbol{U}}{ds} = \left(\boldsymbol{K}_{\mathrm{T}} \cdot \begin{bmatrix} \boldsymbol{\lambda}^{f} \\ -\nabla_{\boldsymbol{F}^{d}} f \end{bmatrix} - \frac{\partial f}{\partial \boldsymbol{U}}\right)^{\mathrm{T}} \cdot \begin{bmatrix} d\boldsymbol{U}^{f}/ds \\ \mathbf{0} \end{bmatrix} \tag{3.9}$$

Enforcing Eq. (3.9) to be zero yields that $\boldsymbol{\lambda}^{\mathrm{f}}$ satisfies the system of linear equations

$$\boldsymbol{K}_{\mathrm{T}} \cdot \begin{bmatrix} \boldsymbol{\lambda}^{f} \\ -\nabla_{\boldsymbol{F}^{d}} f \end{bmatrix} = \begin{bmatrix} \nabla_{\boldsymbol{U}^{f}} f \\ \boldsymbol{X} \end{bmatrix} \tag{3.10}$$

$\boldsymbol{\lambda}^{\mathrm{f}}$ and $\boldsymbol{X}$ are unknown variables to be solved. Finally, the sensitivity of response f equals

$$\frac{df}{ds} = \frac{\partial f}{\partial s} - \begin{bmatrix} \boldsymbol{\lambda}^{f} \\ -\nabla_{\boldsymbol{F}^{d}} f \end{bmatrix}^{\mathrm{T}} \cdot \frac{\partial \boldsymbol{K}_{\mathrm{S}}}{\partial s} \cdot \boldsymbol{U} \tag{3.11}$$

According to Eq. (3.11), the adjoint sensitivity analysis could be obtained by following the flowchart in Figure 3-1.

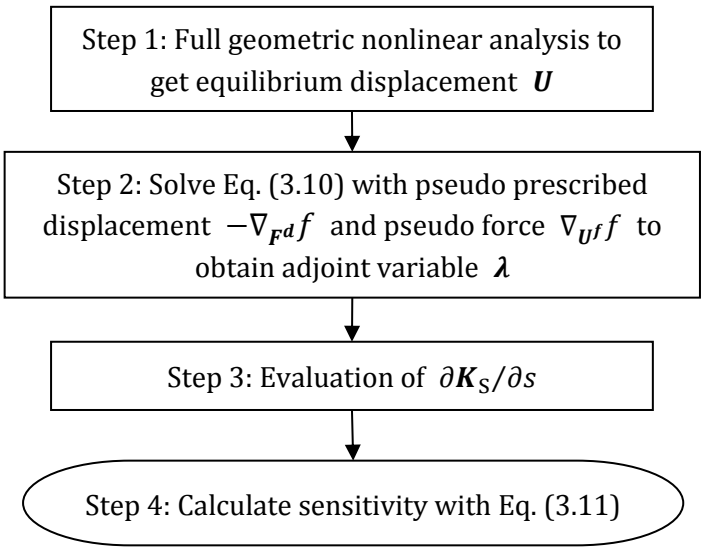

Figure 3-1. Flowchart of adjoint variable method for geometric nonlinear sensitivity analysis

In the flowchart, the linear perturbation analysis in step 2 involves solving a system of linear equations using the tangent stiffness matrix at the equilibrium point. The pseudo displacements and forces are determined through the appropriate partial derivatives of the response function.

In the third step, the partial derivative of the secant stiffness matrix with respect to design variables needs to be evaluated. This derivative can be approximated using a forward scheme semi-analytical approach

$$\frac{\partial \boldsymbol{K}_{\mathrm{S}}(\boldsymbol{U},s)}{\partial s} \approx \frac{\Delta \boldsymbol{K}_{\mathrm{S}}(\boldsymbol{U},\mathrm{s})}{\Delta s} = \frac{\boldsymbol{K}_{\mathrm{S}}(\boldsymbol{U},s+\Delta s) - \boldsymbol{K}_{\mathrm{S}}(\boldsymbol{U},s)}{\Delta s} \tag{3.12}$$

This semi-analytical approximation can be implemented with little effort for general types of elements. The disadvantage of this apporach is the well-known accuracy problem, which will be discussed later in Section 3.2 and 3.3.

It should be noted that, the design variables in non-parametric shape optimization are the nodal coordinates. Therefore, the finite difference of Eq.(3.12) is carried out at the element level, considering only those elements with design nodes as their vertices. This ensures the efficiency of the semi-analytical implementation.

3.2 Validation of adjoint sensitivity analysis

In this section, the semi-analytical sensitivity analysis procedure presented in the previous section is numerically validated.

A cantilever beam structure, depicted in Figure 3-2(a), is employed, and 3D 4-node tetrahedral elements are used to mesh the structure. The design variables consist of the vertical coordinates of nodes on the centerline of the bottom surface, as illustrated in red in Figure 3-2(b).

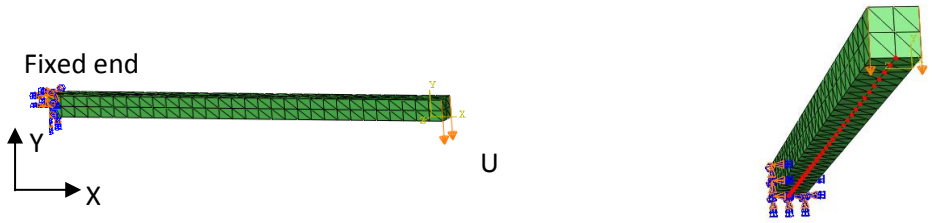

(a) Model description (b) Design nodes (red points) along the beam

Figure 3-2. Cantilever beam model (Length = 300 mm, width = 15 mm, height = 15 mm, Young's modulus = 209 GPa, Poisson's ratio = 0.3)

The structure is fixed at one end, and a prescribed displacement of 100mm in the vertically downward direction is applied at the other side. The total

vertical reaction force at the support is defined as one response function. In Figure 3-3, the sensitivities of this response obtained by the semi-analytical adjoint variable method are compared with the global finite difference results. The horizontal axis represents the x-coordinate of the design nodes. The perturbation size in the semi-analytical approximation is 10^{-5}mm, while the perturbation size in the global finite difference approach is 10^{-6}mm. It can be observed that the adjoint sensitivity results match quite well with the finite difference results from a real value perspective.

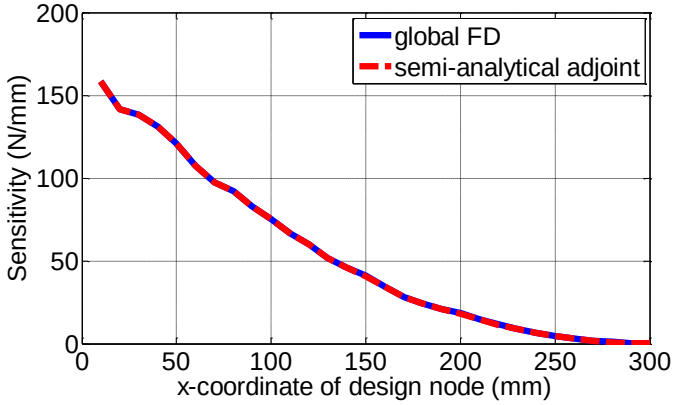

Figure 3-3. Sensitivity of reaction force obtained by semi-analytical adjoint variable method and global finite difference method

However, concerning the perspective of relative error, the accuracy issue mostly discussed in linear systems arises. Figure 3-4 illustrate the scaled sensitivity, defined as the ratio of semi-analytical adjoin sensitivities to global finite difference results:

$$\text{scaled sensitivity} = \frac{\text{Sensitivity of semi analytical adjoint method}}{\text{Sensitivity of global FD}} \qquad (3.13)$$

The scaled sensitivity measures the relative error between the two results. It indicates that, near the free end, the scaled sensitivity deviates significantly from 1, signifying a notable increase in relative error.

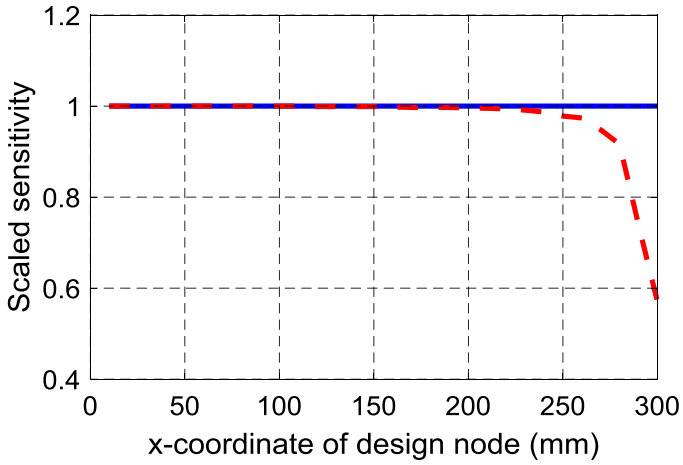

Figure 3-4. Scaled sensitivity of reaction force response

The perturbation size employed in the semi-analytical approximation influences the correctness of the sensitivity result. Figure 3-5 presents the semi-analytical sensitivity results using different perturbation sizes, ranging from 10^{-3} to 10^{-8} mm. It shows that if the perturbation size is too small or too large, incorrect sensitivity results could be obtained.

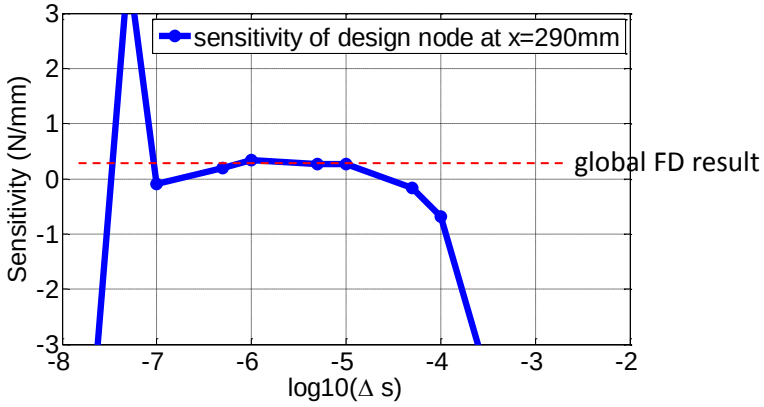

Figure 3-5. Sensitivity of reaction force response with different perturbation sizes. The design variable is the vertical coordinate of a design node near the loaded end

The maximum stress is usually another typical response in structural optimization. Since the location of the maximum stress point may change between iterations, stresses of a number of elements should be defined as responses to capture the maximum stress. To reduce the number of system responses, some aggregation functions are proposed to approximate the maximum stress with a single system response [QL10]. One of the typically used function is the P-norm of a set of interested elements:

$$\sigma_{max} \approx \left(\frac{1}{m} \sum_{e=1}^{m} {\sigma_e}^p \right)^{1/p} \tag{3.14}$$

where m is the number of selected elements, and p is the aggregation parameter, which is an integer.

The adjoint sensitivity analysis approach is validated with the P-norm of von-Mises equivalent stress as a response. The von Mises stress of 28 elements around the fixed end is included into the function evaluation. The parameter p is set to be 20. The sensitivities of the P-norm response obtained by semi-analytical adjoint variable method and global finite difference method are presented in Figure 3-6. The scaled sensitivity result is presented Figure 3-7.

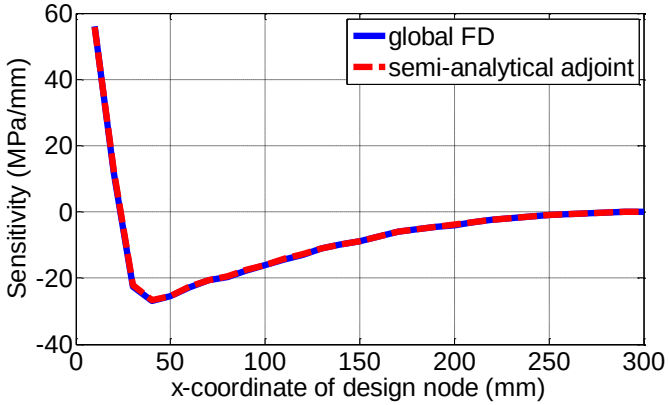

Figure 3-6. Sensitivity of P-norm stress obtained by semi-analytical adjoint variable method and global finite difference method

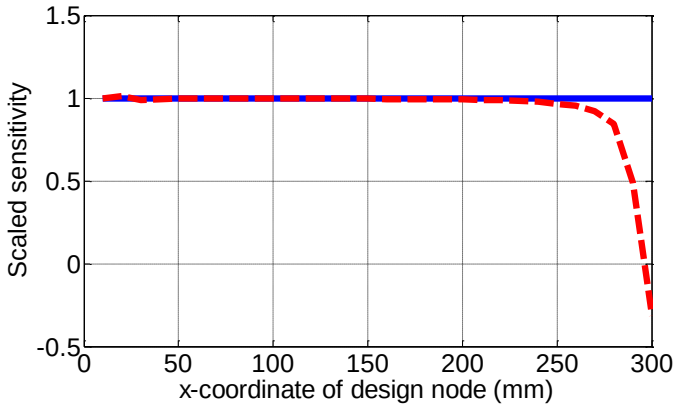

Figure 3-7. Scaled sensitivity of P-norm stress response

As it appears, the sensitivity results of both approaches match well with each other. However, the accuracy issue resurfaces at the free end.

3.3 Rotation error of semi-analytical approximation

As presented in Section 3.2, the semi-analytical approximation leads to an accuracy problem in the sensitivity analysis. The following example clearly illustrates that this error is caused by the rigid body rotation of elements.

In this example, the same cantilever beam model as in Section 3.2 is employed. As depicted in Figure 3-8, instead of applying a vertical prescribed displacement, a displacement of 30mm is applied in the axial direction at the free end.

Figure 3-8. Cantilever beam model under prescribed displacements in axial direction

This prescribed displacement leads to a pure extension of the beam. The total axial reaction force is defined as the response, utilizing the same design variables as presented in Section 3.2. The sensitivity and scaled sensitivities of semi-analytical adjoint approach and global finite difference approach are illustrated in Figure 3-9 and Figure 3-10, respectively.

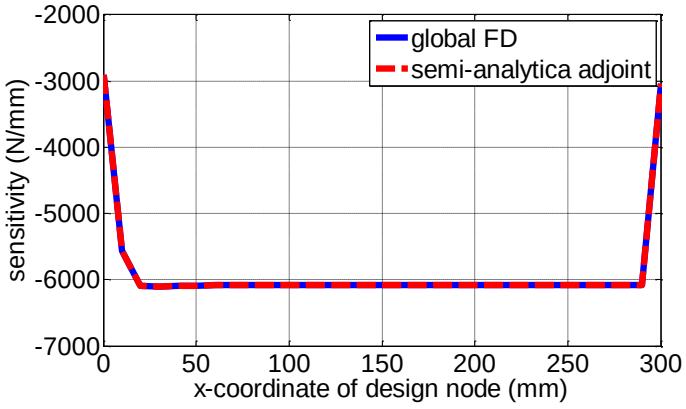

Figure 3-9. Sensitivity of reaction force under axial prescribed displacement

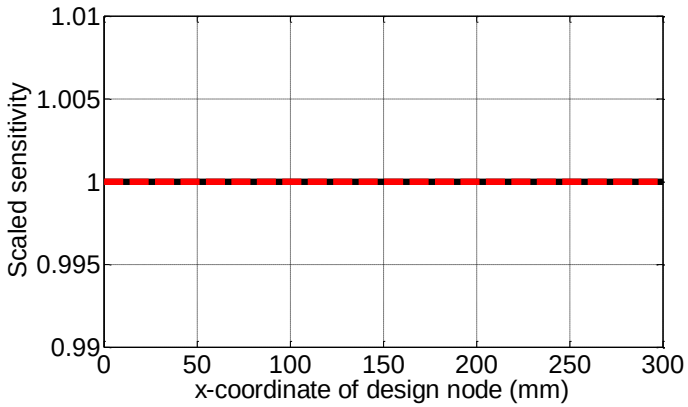

Figure 3-10. Scaled sensitivity of reaction force under axial prescribed displacement

The results show that, under pure extension, the semi-analytical sensitivity perfectly align with the benchmark without any accuracy issues. This numerical demonstration highlights that the accuracy problem only arise when there is elemental rotation in the underlying finite element system.

3.4 Correction term for semi-analytical approximation in adjoint sensitivity analysis

In the linear case, the rotation error has been successfully eliminated by both the "exact" semi-analytical approach and the refined semi-analytical approach. The idea behind both methods is to add a correction term to the finite difference of either the stiffness matrix or the internal force vector. This term is introduced to ensure that the semi-analytical approximation satisfies the so-called rigid body conditions or zero-eigenvector conditions. The correction term is constructed from the rigid body movement vectors of individual elements.

In this section, this idea is extended to the geometric nonlinear case. The construction of the correction term is based on the secant stiffness matrix outlined in Eq. (2.12).

Firstly, the zero-eigenvector conditions are deduced. Similar to every stiffness matrix, the secant stiffness matrix of a 3D element has a degree of rank

deficiency of 6. This means there are in total six zero eigenvectors $\{\boldsymbol{\varphi}_\mathrm{i}\}_{\mathrm{i}=1,\dots,6}$ that satisfy the condition

$$\boldsymbol{K}_\mathrm{S} \cdot \boldsymbol{\varphi}_\mathrm{i} = \mathbf{0} \tag{3.15}$$

Since the matrix transpose operator does not change the rank of a matrix, the rank deficiency of $\boldsymbol{K}_\mathrm{S}{}^\mathrm{T}$ is also 6. As a result, there must be six zero eigenvectors $\{\boldsymbol{\omega}_\mathrm{i}\}_{\mathrm{i}=1,\dots,6}$ such that

$$\boldsymbol{K}_\mathrm{S}{}^\mathrm{T} \cdot \boldsymbol{\omega}_\mathrm{i} = \mathbf{0} \tag{3.16}$$

When the secant stiffness matrix is asymmetrical, the sets $\{\boldsymbol{\varphi}_\mathrm{i}\}$ and $\{\boldsymbol{\omega}_\mathrm{i}\}$ are not identical. They are referred to as right and left eigenvectors, respectively. Both sets of eigenvectors can be orthogonalized using the Gram-Schmidt process, as presented in the following. The orthogonalized vectors are denoted by $\{\boldsymbol{\varphi}_\mathrm{i}^\mathrm{o}\}$ and $\{\boldsymbol{\omega}_\mathrm{i}^\mathrm{o}\}$.

$$\boldsymbol{\varphi}_1^\mathrm{o} = \boldsymbol{\varphi}_1$$

$$\boldsymbol{\varphi}_\mathrm{i}^\mathrm{o} = \boldsymbol{\varphi}_\mathrm{i} - \sum_{\mathrm{j}<i} \frac{\langle \boldsymbol{\varphi}_\mathrm{i}\,,\ \boldsymbol{\varphi}_\mathrm{j}^\mathrm{o} \rangle}{\langle \boldsymbol{\varphi}_\mathrm{j}^\mathrm{o}\,,\ \boldsymbol{\varphi}_\mathrm{j}^\mathrm{o} \rangle} \boldsymbol{\varphi}_\mathrm{j}^\mathrm{o} \quad (\text{for i} = 2, \dots, 6) \tag{3.17}$$

$$\boldsymbol{\omega}_1^\mathrm{o} = \boldsymbol{\omega}_1$$

$$\boldsymbol{\omega}_\mathrm{i}^\mathrm{o} = \boldsymbol{\omega}_i - \sum_{\mathrm{j}<i} \frac{\langle \boldsymbol{\omega}_\mathrm{i}\,,\ \boldsymbol{\omega}_\mathrm{j}^\mathrm{o} \rangle}{\langle \boldsymbol{\omega}_\mathrm{j}^\mathrm{o}\,,\ \boldsymbol{\omega}_\mathrm{j}^\mathrm{o} \rangle} \boldsymbol{\omega}_\mathrm{j}^\mathrm{o} \quad (\text{for i} = 2, \dots, 6) \tag{3.18}$$

The operator $\langle \cdot\,,\, \cdot \rangle$ represents the inner product of two vectors. The orthogonalized vectors $\{\boldsymbol{\varphi}_\mathrm{i}^\mathrm{o}\}$ and $\{\boldsymbol{\omega}_\mathrm{i}^\mathrm{o}\}$ are still eigenvectors of $\boldsymbol{K}_\mathrm{S}$ and $\boldsymbol{K}_\mathrm{S}{}^\mathrm{T}$, respectively.

Further, by replacing $\boldsymbol{\varphi}_\mathrm{i}$ with $\boldsymbol{\varphi}_\mathrm{i}^\mathrm{o}$ in Eq. (3.15) and taking partial derivative with respect to the design variable, pre-multiplying $\boldsymbol{\omega}_\mathrm{j}^{\mathrm{o}\,\mathrm{T}}$ on the left yields

$$\boldsymbol{\omega}_\mathrm{j}^{\mathrm{o}\,\mathrm{T}} \cdot \frac{\partial \boldsymbol{K}_\mathrm{S}}{\partial s} \cdot \boldsymbol{\varphi}_\mathrm{i}^\mathrm{o} + \boldsymbol{\omega}_\mathrm{j}^{\mathrm{o}\,\mathrm{T}} \cdot \boldsymbol{K}_\mathrm{S} \cdot \frac{\partial \boldsymbol{\varphi}_\mathrm{i}^\mathrm{o}}{\partial s} = \mathbf{0} \tag{3.19}$$

Using

$$\boldsymbol{\omega}_{\mathrm{j}}^{\mathrm{o}\mathrm{T}} \cdot \boldsymbol{K}_{\mathrm{S}} = \left(\boldsymbol{K}_{\mathrm{S}}{}^{\mathrm{T}} \cdot \boldsymbol{\omega}_{\mathrm{j}}^{\mathrm{o}}\right)^{\mathrm{T}} = \mathbf{0} \tag{3.20}$$

The second term in Eq. (3.19) vanishes, and the following 36 zero-eigenvector conditions are obtained

$$\boldsymbol{\omega}_{\mathrm{j}}^{\mathrm{o}\mathrm{T}} \cdot \frac{\partial \boldsymbol{K}_{\mathrm{S}}}{\partial s} \cdot \boldsymbol{\varphi}_{\mathrm{i}}^{\mathrm{o}} = 0 \quad (\text{for i, j} = 1, \dots, 6) \tag{3.21}$$

If a semi-analytical approximation of $\partial \boldsymbol{K}_{\mathrm{S}}/\partial s$ is accurate, it should satisfy all of these conditions. Unfortunately, this is usually not the case. Therefore, a correction term $\boldsymbol{T}$ must be added to the semi-analytical approximation result

$$\frac{\partial \boldsymbol{K}_{\mathrm{S}}}{\partial s} \approx \frac{\Delta \boldsymbol{K}_{\mathrm{S}}}{\Delta s} + \boldsymbol{T} \tag{3.22}$$

Substituting Eq. (3.22) into Eq. (3.21) results in

$$0 = \boldsymbol{\omega}_{\mathrm{j}}^{\mathrm{o}\mathrm{T}} \cdot \frac{\Delta \boldsymbol{K}_{\mathrm{S}}}{\Delta s} \cdot \boldsymbol{\varphi}_{\mathrm{i}}^{\mathrm{o}} + \boldsymbol{\omega}_{\mathrm{j}}^{\mathrm{o}\mathrm{T}} \cdot \boldsymbol{T} \cdot \boldsymbol{\varphi}_{\mathrm{i}}^{\mathrm{o}} \quad (\text{for i, j} = 1, \dots, 6) \tag{3.23}$$

Therefore, the correction term must satisfy

$$\boldsymbol{\omega}_{\mathrm{j}}^{\mathrm{o}\mathrm{T}} \cdot \boldsymbol{T} \cdot \boldsymbol{\varphi}_{\mathrm{i}}^{\mathrm{o}} = -\boldsymbol{\omega}_{\mathrm{j}}^{\mathrm{o}\mathrm{T}} \cdot \frac{\Delta \boldsymbol{K}_{\mathrm{S}}}{\Delta s} \cdot \boldsymbol{\varphi}_{\mathrm{i}}^{\mathrm{o}} \quad (\text{for i, j} = 1, \dots, 6) \tag{3.24}$$

Constructing the correction term in the production space of $\{\boldsymbol{\varphi}_{\mathrm{i}}^{\mathrm{o}}\}$ and $\{\boldsymbol{\omega}_{\mathrm{i}}^{\mathrm{o}}\}$

$$\boldsymbol{T} = \sum_{\mathrm{i}=1}^{6} \sum_{\mathrm{j}=1}^{6} \alpha_{\mathrm{ij}}\, \boldsymbol{\omega}_{\mathrm{j}}^{\mathrm{o}} \boldsymbol{\varphi}_{\mathrm{i}}^{\mathrm{o}\mathrm{T}} \tag{3.25}$$

By substituting Eq. (3.25) into Eq. (3.24), the coefficients $\{\alpha_{\mathrm{ij}}\}$ are obtained using the orthogonality of $\{\boldsymbol{\varphi}_{\mathrm{i}}^{\mathrm{o}}\}$ and $\{\boldsymbol{\omega}_{\mathrm{i}}^{\mathrm{o}}\}$

$$\alpha_{\mathrm{ij}} = \frac{-\boldsymbol{\omega}_{\mathrm{j}}^{\mathrm{o}\mathrm{T}} \cdot \frac{\Delta \boldsymbol{K}_{\mathrm{S}}}{\Delta s} \cdot \boldsymbol{\varphi}_{\mathrm{i}}^{\mathrm{o}}}{\langle \boldsymbol{\omega}_{\mathrm{j}}^{\mathrm{o}}, \boldsymbol{\omega}_{\mathrm{j}}^{\mathrm{o}} \rangle \langle \boldsymbol{\varphi}_{\mathrm{i}}^{\mathrm{o}}, \boldsymbol{\varphi}_{\mathrm{i}}^{\mathrm{o}} \rangle} \tag{3.26}$$

Usually, the sets of zero eigenvectors $\{\boldsymbol{\varphi}_{\mathrm{i}}\}$ and $\{\boldsymbol{\omega}_{\mathrm{i}}\}$ are obtained by solving the eigenvalue problems of Eqs. (3.15) and (3.16). The numerical solution may introduce extra numerical errors, and the errors will be further transmitted

to the sensitivity analysis. Therefore, efficient and accurate way to obtain these two sets of eigenvectors is valuable. The following analytical expressions of these eigenvectors are proposed in [WCB15], which avoid additional numerical calculations.

The set of $\{\boldsymbol{\omega}_i\}$ can be obtained from a mechanical point of view by pre-multiplying the displacement vector at the equilibrium point with Eq. (3.16)

$$\boldsymbol{U}^T \cdot \boldsymbol{K}_S{}^T \cdot \boldsymbol{\omega}_i = \boldsymbol{F}^T \cdot \boldsymbol{\omega}_i = 0 \tag{3.27}$$

It means that the work done by an external force $\boldsymbol{F}$ on $\{\boldsymbol{\omega}_i\}$ is zero. Therefore, $\{\boldsymbol{\omega}_i\}$ should be the rigid body movement under the deformed configuration. Taking the 3D 4-node tetrahedral element shown in Figure 3-11 as an example, where the four nodes are numbered from 0 to 3. Nodal coordinates in the undeformed configuration are denoted by $\{c_{i\alpha}\}$, nodal displacements by $\{u_{i\alpha}\}$, and the nodal coordinates of the deformed configuration by $\{d_{i\alpha}\}$, where i = 0, 1, 2, 3, and α = x, y, z. The following relations hold

$$d_{i\alpha} = c_{i\alpha} + u_{i\alpha} \tag{3.28}$$

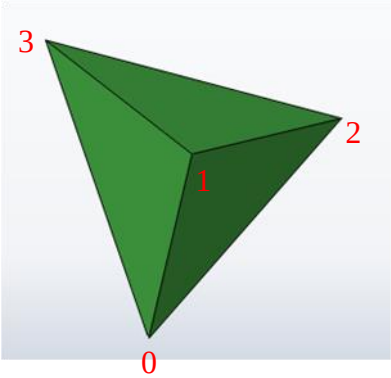

Figure 3-11. 3D 4-node linear tetrahedral element

Then, the three zero eigenvectors representing the rigid translation of the deformed element along x-, y-, and z- axes are

$$\begin{aligned} \boldsymbol{\omega}_1 &= [1 \quad 0 \quad 0 \quad 1 \quad 0 \quad 0 \quad 1 \quad 0 \quad 0 \quad 1 \quad 0 \quad 0]^T \\ \boldsymbol{\omega}_2 &= [0 \quad 1 \quad 0 \quad 0 \quad 1 \quad 0 \quad 0 \quad 1 \quad 0 \quad 0 \quad 1 \quad 0]^T \end{aligned} \tag{3.29}$$

$$\boldsymbol{\omega}_3 = [0 \quad 0 \quad 1 \quad 0 \quad 0 \quad 1 \quad 0 \quad 0 \quad 1 \quad 0 \quad 0 \quad 1]^{\mathrm{T}}$$

and the three zero eigenvectors representing rigid rotation of the deformed configuration around x-, y-, and z- axes are

$$\begin{aligned}
\boldsymbol{\omega}_4 &= [0 \quad -d_{0z} \quad d_{0y} \quad 0 \quad -d_{1z} \quad d_{1y} \quad 0 \quad -d_{2z} \quad d_{2y} \quad 0 \quad -d_{3z} \quad d_{3y}]^{\mathrm{T}} \\
\boldsymbol{\omega}_5 &= [d_{0z} \quad 0 \quad -d_{0x} \quad d_{1z} \quad 0 \quad -d_{1x} \quad d_{2z} \quad 0 \quad -d_{2x} \quad d_{3z} \quad 0 \quad -d_{3x}]^{\mathrm{T}} \\
\boldsymbol{\omega}_6 &= [-d_{0y} \quad d_{0x} \quad 0 \quad -d_{1y} \quad d_{1x} \quad 0 \quad -d_{2y} \quad d_{2x} \quad 0 \quad -d_{3y} \quad d_{3x} \quad 0]^{\mathrm{T}}
\end{aligned} \tag{3.30}$$

Eqs. (3.29) and (3.30) are the analytical expression for $\{\boldsymbol{\omega}_{\mathrm{i}}\}$.

The zero eigenvectors $\{\boldsymbol{\varphi}_{\mathrm{i}}\}$ can be assumed to have the same form as $\{\boldsymbol{\omega}_{\mathrm{i}}\}$, i.e. the position of zero entries in $\{\boldsymbol{\varphi}_{\mathrm{i}}\}$ are the same as those in $\{\boldsymbol{\omega}_{\mathrm{i}}\}$. With this restriction, a set of empirical formulas for $\{\boldsymbol{\varphi}_{\mathrm{i}}\}$ is found through numerical observation. Analytically, $\{\boldsymbol{\varphi}_{\mathrm{i}}\}$ contain three rigid body translation vectors that are identical to $\boldsymbol{\omega}_1$ to $\boldsymbol{\omega}_3$

$$\begin{aligned}
\boldsymbol{\varphi}_1 &= \boldsymbol{\omega}_1 \\
\boldsymbol{\varphi}_2 &= \boldsymbol{\omega}_2 \\
\boldsymbol{\varphi}_3 &= \boldsymbol{\omega}_3
\end{aligned} \tag{3.31}$$

and three rotational vectors as follows

$$\begin{aligned}
\boldsymbol{\varphi}_4 &= [0 \quad -(d_{0z}+c_{0z}) \quad d_{0y}+c_{0y} \quad 0 \quad -(d_{1z}+c_{1z}) \quad d_{1y}+c_{1y} \quad 0 \quad -(d_{2z}+c_{2z}) \quad d_{2y}+c_{2y} \quad 0 \quad -(d_{3z}+c_{3z}) \quad d_{3y}+c_{3y}]^{\mathrm{T}} \\
\boldsymbol{\varphi}_5 &= [d_{0z}+c_{0z} \quad 0 \quad -(d_{0x}+c_{0x}) \quad d_{1z}+c_{1z} \quad 0 \quad -(d_{1x}+c_{1x}) \quad d_{2z}+c_{2z} \quad 0 \quad -(d_{2x}+c_{2x}) \quad d_{3z}+c_{3z} \quad 0 \quad -(d_{3x}+c_{3x})]^{\mathrm{T}} \\
\boldsymbol{\varphi}_6 &= [-(d_{0y}+c_{0y}) \quad d_{0x}+c_{0x} \quad 0 \quad -(d_{1y}+c_{1y}) \quad d_{1x}+c_{1x} \quad 0 \quad -(d_{2y}+c_{2y}) \quad d_{2x}+c_{2x} \quad 0 \quad -(d_{3y}+c_{3y}) \quad d_{3x}+c_{3x} \quad 0]^{\mathrm{T}}
\end{aligned} \tag{3.32}$$

where $\boldsymbol{\varphi}_4$ to $\boldsymbol{\varphi}_6$ differ from $\boldsymbol{\omega}_4$ to $\boldsymbol{\omega}_6$ by replacing the terms $d_{\mathrm{i}\alpha}$ with $d_{\mathrm{i}\alpha} + c_{\mathrm{i}\alpha}$.

With analytical expressions of both $\{\boldsymbol{\varphi}_{\mathrm{i}}\}$ and $\{\boldsymbol{\omega}_{\mathrm{i}}\}$, there is no need to solve the eigenvalue problems, thereby improving both the efficiency and accuracy in constructing the correction term.

It should be noted that, the above formulas are obtained and verified based on the asymmetric secant stiffness matrix of the 3D 4-node tetrahedral element. Although it has not been verified in this dissertation, there is no foreseeable

reason that these formulas are not applicable to other types of 3D finite elements.

3.5 Numerical examples

In this section, the effectiveness of the correction term is demonstrated numerically with the same cantilever beam example presented in Section 3.2. The two responses, namely the reaction force and P-norm stress, are also the same.

Figure 3-12 presents the scaled sensitivity of the reaction force response with and without the correction term. These values are calculated by dividing the semi-analytical adjoint sensitivity by the global finite difference sensitivity. The figure clearly shows that the large relative error near the free end is significantly eliminated after incorporating the correction term into the semi-analytical approximation. Although not presented here, a similar phenomenon is also observed with the P-norm stress response.

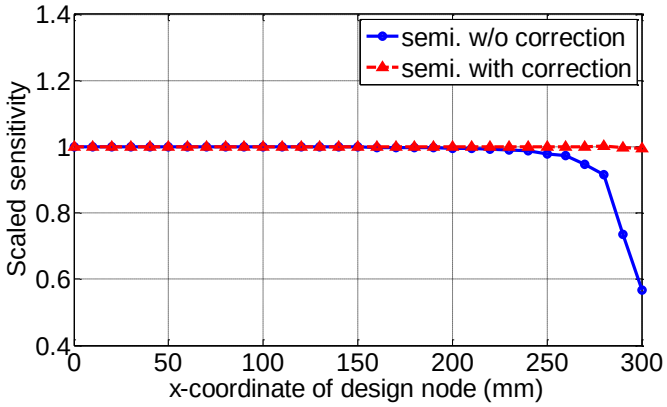

Figure 3-12. Scaled sensitivity of semi-analytical adjoint method with and without correction term

Sensitivity results for the two responses with different perturbation sizes are presented in Table 3-1 and Table 3-2, respectively. The design node is located near the free end, where the largest relative error occurs. It shows that, for all perturbation sizes, the accuracy of sensitivity is significantly improved by adding the correction term.

Table 3-1. Sensitivities of reaction force response at a design node near the free end (ref. result = 0.0500 N/mm)

Perturbation size (mm)	Semi w/o correction		Semi. with correction	
	Sensitivity(N/mm)	Error(%)	Sensitivity(N/mm)	Error(%)
10^{-3}	–3.02	–6131%	0.0582	16.2%
10^{-4}	–0.256	–612%	0.0509	1.62%
10^{-5}	0.029	–43%	0.0501	0.16%
10^{-6}	–0.001	–102%	0.0501	0.02%
10^{-7}	0.284	467%	0.0501	0.02%
10^{-8}	–2.76	–5612%	0.0503	0.51%
10^{-9}	6.22	12326%	0.0508	1.50%

Table 3-2. Sensitivities of the P-norm stress response at a design node near the free end (ref. result =–0.0072 MPa/mm)

Perturbation size (mm)	Semi w/o correction		Semi. with correction	
	Sensitivity (MPa/mm)	Error(%)	Sensitivity (MPa/mm)	Error(%)
10^{-3}	0.1833	–2637%	–0.0086	19.4%
10^{-4}	0.0118	–263.9%	–0.0074	1.82%
10^{-5}	–0.0054	–25.79%	–0.0072	0.06%
10^{-6}	–0.0073	1.53%	–0.0072	–0.12%
10^{-7}	–0.0095	31.8%	–0.0072	–0.14%
10^{-8}	–0.0469	550%	–0.0072	0.08%
10^{-9}	–0.2820	3804%	–0.0071	–1.77%

What's more, the results also demonstrate that sensitivity outcomes are significantly less reliant on the choice of perturbation size when the correction term is applied. In industrial applications, structures are often meshed with varying element sizes in different areas, and the element size may change when the structure is updated during optimization. Therefore, special attention must be given to the selection of the perturbation size for nodal coordinates. By incorporating the correction term, the stability of sensitivity results increases, facilitating the selection of perturbation size.

It is also interesting to investigate the relation between the accuracy of sensitivity and the degree of nonlinearity. The degree of nonlinearity could be measured by the magnitude of loading. In this cantilever beam example, it is the magnitude of the prescribed displacement. If the prescribed displacement

is sufficiently small, the problem is close to a linear one. A larger prescribed displacement leads to a higher degree of geometric nonlinearity.

Three different levels of prescribed displacement, i.e. 1 mm, 10 mm, and 100 mm, are applied to the free end of the beam. Sensitivity results with correction term for the reaction force response are listed in Table 3-3.

Table 3-3. Sensitivities of the reaction force response at a design node near the free end under different prescribed displacement

Perturbation size (mm)	u = 1 mm Ref. Sens.= 0.00035 N/mm		u = 10 mm Ref. Sens.= 0.0035 N/mm		u = 100 mm Ref. Sens.= 0.05N/mm	
	Sensitivity (N/mm)	Error(%)	Sensitivity (N/mm)	Error(%)	Sensitivity (N/mm)	Error(%)
10^{-3}	0.000397	13.5%	0.00399	14.1%	0.0582	16.2%
10^{-4}	0.000355	1.35%	0.00355	1.41%	0.0509	1.62%
10^{-5}	0.000350	0.13%	0.00350	0.14%	0.0501	0.16%
10^{-6}	0.000350	0.01%	0.00350	0.01%	0.0501	0.02%
10^{-7}	0.000350	0.00%	0.00350	0.02%	0.0501	0.02%
10^{-8}	0.000350	0.03%	0.00351	0.29%	0.0503	0.51%
10^{-9}	0.000354	1.06%	0.00353	0.88%	0.0508	1.50%

For the convenience of observation, the relative errors against the perturbation size under different prescribed displacements are depicted in Figure 3-13.

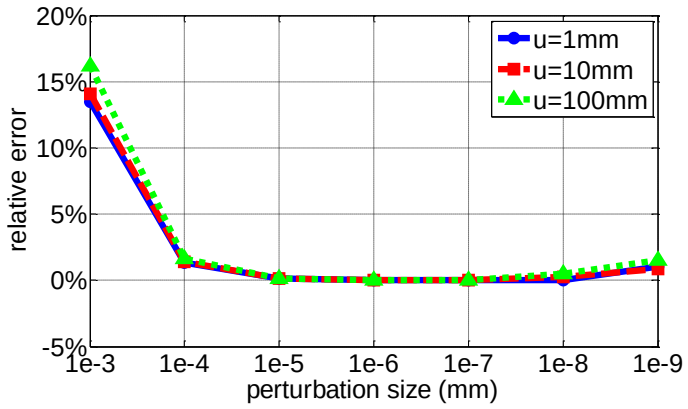

Figure 3-13. Sensitivity errors versus perturbation size under different levels of prescribed displacement

It shows that the relative error of the semi-analytical approach with the correction term are nearly independent of the level of nonlinearity. This

property is also important in practical applications when the load factor itself is a system response or when the linear behavior of a structural system changes to nonlinear due to change in the structure's shape.

3.6 Optimization examples with TOSCA Structure

In this chapter, the semi-analytical adjoint sensitivity method with a correction term is integrated into the TOSCA structure shape optimization environment. Several optimization examples are presented to demonstrate the applicability of the sensitivity analysis procedure in solving geometric nonlinear optimization problems.

3.6.1 Introduction to TOSCA Structure

TOSCA Structure is a software package that aims to enhance product development through topology and shape optimization. As depicted in Figure 3-14, TOSCA Structure can generate an optimized CAD model from a conceptual design space by combining topology optimization and shape optimization techniques.

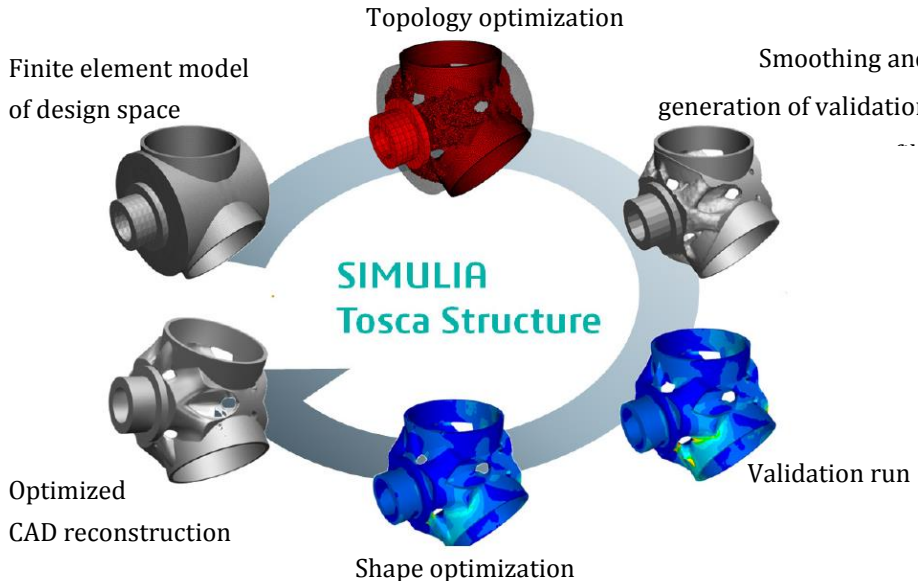

Figure 3-14. Production development circle of TOSCA Structure (Source: https://www.3ds.com/products-services/simulia/products/tosca/)

Both a derivative-free controller method, and a gradient-based algorithm (Method of Moving Asymptotes) are employed in the TOSCA optimization module. The controller method possesses the advantages of fast convergence and easy integration into general finite element solvers. It has already been extended to tackle both linear and nonlinear structural optimization problems demonstrating successful applications in lightweight optimization and stress concentration reduction problems [MSS05]. However, the limitation of the controller method is that it is difficult to handle constraints in optimization. To overcome this restriction, a sensitivity-based algorithm is employed. It is capable of handling multiple objectives and large number of constraints. The flowchart in Figure 3-15 depicts the sensitivity-based structural optimization procedure of TOSCA.

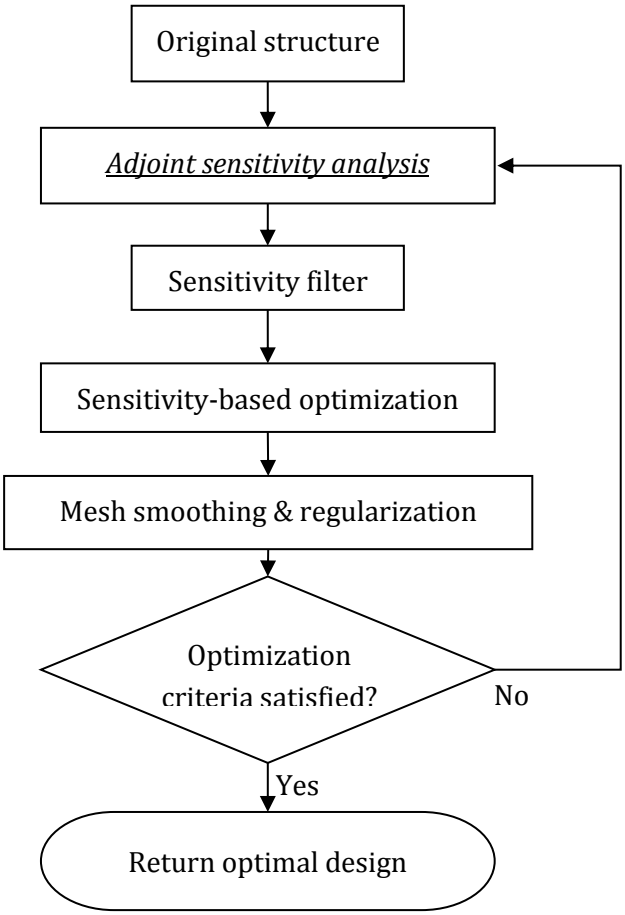

Figure 3-15. Flowchart of sensitivity-based shape optimization in TOSCA

The presented adjoint sensitivity analysis procedure is integrated into the TOSCA environment. After each sensitivity evaluation, a sensitivity filter is applied to eliminate oscillations in the sensitivities. Subsequently, mesh

smoothing and regularization tools are employed to ensure the smoothness of the optimized surface and maintain a high-quality mesh for the updated structure. The iteration continues until the optimization criteria are satisfied.

3.6.2 Optimization example of a cantilever beam under large prescribed displacement

In this example, an optimization example of a cantilever beam subjected to a large prescribed displacement is presented.

The original structure is the same as in Figure 3-2 (a), including the material properties. The prescribed vertical displacement is −94.7mm which leads to a total reaction force of 20000N in vertical direction. The vertical coordinate of all nodes at the bottom surface are the design variables, depicted by the red dots in Figure 3-16. The objective is to maximize the vertical reaction force at the fixed end. One constraint is that the total weight, measured by the volume of the structure, should not increase.

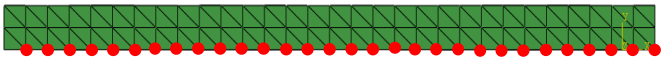

Figure 3-16. Design nodes at the bottom surface of the structure

With the presented semi-analytical adjoint sensitivity analysis procedure, sensitivity-based optimization is carried out in TOSCA Structure. The result after 30 iterations is depicted in Figure 3-17. The total reaction force increases from 20000N to 32336N, representing a 61.7% improvement. The total volume of the optimized structure is 67520mm^3 which remains almost the same as the original.

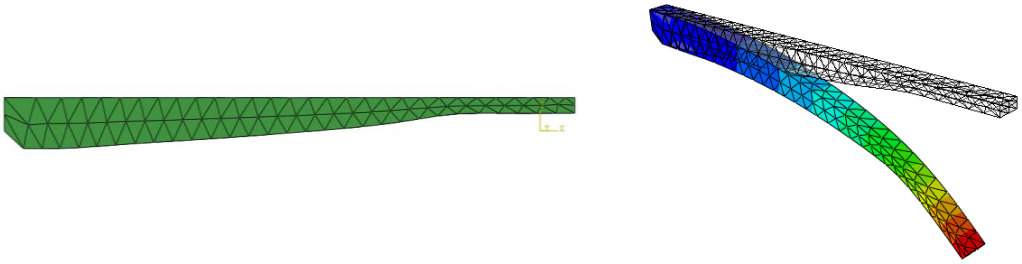

(a) Side-view of the optimized structure

(b) Deformation of the optimized beam under prescribed displacement

Figure 3-17. Optimization results of the cantilever beam after 30 iterations

3.6.3 Optimization example of a V-shaped beam with snap-through

In this section, a V-shaped beam optimization problem is presented. The structure is depicted in Figure 3-18, which is plane symmetric and fixed on both ends. The vertical coordinates of all nodes at the top and bottom surfaces are chosen as design variables. A prescribed displacement is applied at the center, and the total vertical reaction force is measured. The force-displacement curve at the loading point is depicted in Figure 3-19, showing a snap-through behavior of the structure.

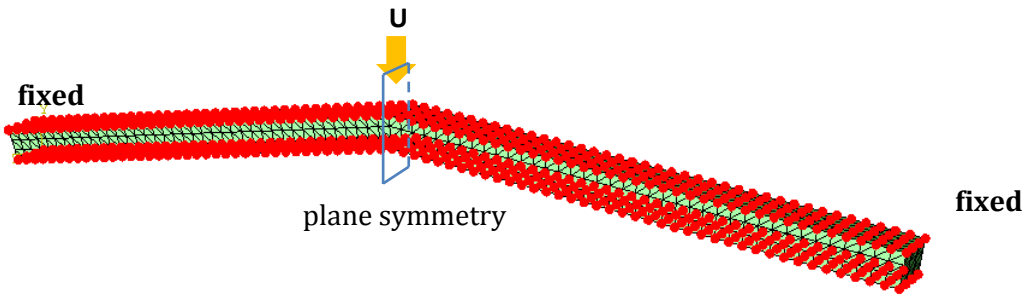

Figure 3-18. V-shaped beam structure (red dots depict design nodes at the top and bottom surfaces)

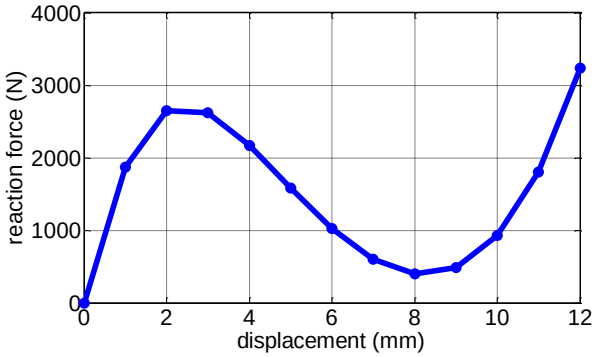

Figure 3-19. Reaction force-displacement curve of the original structure

The objective of the optimization is to maximize the reaction force when the prescribed displacement is 12mm. One constraint is that the total volume of the structure should not increase. The optimization converges after 50 iterations. The undeformed, optimized structure and its deformation under the prescribed displacement at the final load step are depicted in Figure 3-20.

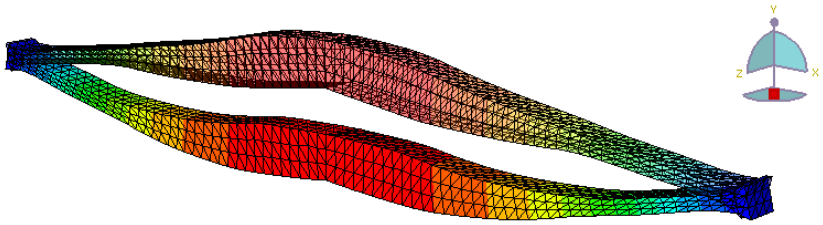

Figure 3-20. Optimized structure (top) with its deformation (bottom) under the prescribed load

The force-displacement curve of the original structure and the optimized structure is compared in Figure 3-21. It shows that the reaction force increases significantly after optimization, rising from 3383N to 14869N.

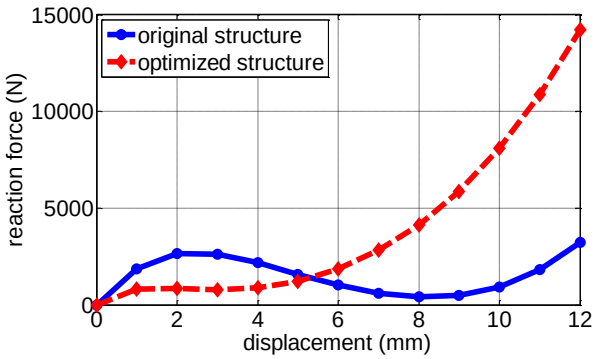

Figure 3-21. Reaction force-displacement curve of original and optimized structure

Another optimization is performed with the same original structure. The optimization aims to maximize the reaction force under a prescribed displacement of 1mm, i.e. to achieve the highest possible initial stiffness of the structure. The volume constraint still applies. Additionally, a lower bound of 300N is set for reaction force throughout the entire loading procedure, i.e. with prescribed displacement ranging from 1mm to 12mm.

The optimization procedure convergences after 74 iterations, and the optimized structure, along with its deformation at the final load step (u=12mm), is illustrated in Figure 3-22.

The force-displacement curves of the original structure and the optimized structure are depicted in Figure 3-23.

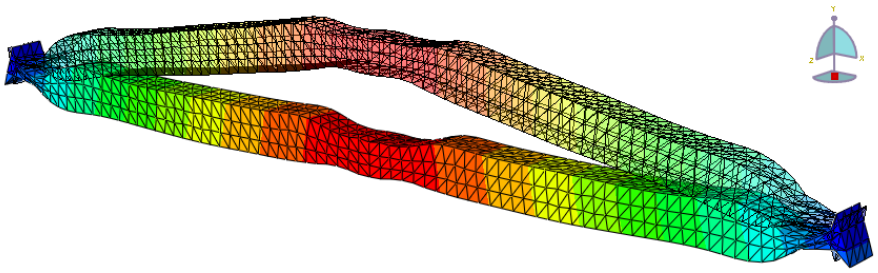

Figure 3-22. Optimized structure (transparent) with its deformation under the prescribed displacement

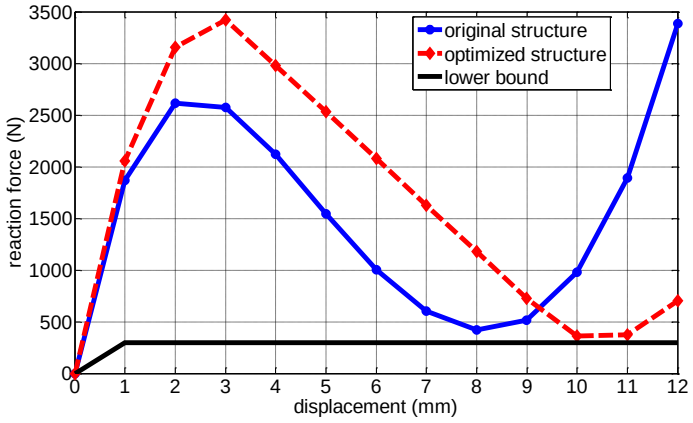

Figure 3-23. Reaction force-displacement equilibrium curve of original and optimized structure

The results show that the minimum reaction force of the optimized structure is 363N, which satisfies the constraint. The reaction force at the first step increases from 1865N to 2056N, representing a 10.2% increase.

4. Adjoint sensitivity analysis with isotropic hardening elastoplasticity and geometric nonlinearity

In this chapter, the adjoint sensitivity formulation for simultaneous isotropic hardening elastoplasticity and geometric nonlinearity is presented. The deduction follows the procedure outlined by [MTV94]. The formulation is confined to small strain elastoplasticity with large deformation. The derived approach is demonstrated through numerical examples. Extensions to more general hardening models and finite strain elastoplasticity will be discussed in later chapters.

4.1 Adjoint sensitivity formulation

4.1.1 Definition of state variables

For elastoplasticity analysis, the physical quantities at an equilibrium point are not determined solely by the current displacement due to path-dependency. Through the solution procedure presented in Section 2.2, sets of displacement vectors $\{{}^t\boldsymbol{U}\}_{t=1}^{\mathrm{N}}$, stress $\{{}^t\boldsymbol{\sigma}\}_{t=1}^{\mathrm{N}}$, equivalent plastic strains $\{{}^t\varepsilon_{\mathrm{eqv}}^{\mathrm{p}}\}_{t=1}^{\mathrm{N}}$ are obtained. These quantities serve as the basis for deriving all other physical quantities and mechanical responses. Here, N is the total number of load steps.

By introducing a state variable ${}^t\boldsymbol{V}$, which is composed of stress and equivalent plastic strain

$$ {}^t\boldsymbol{V} = \begin{pmatrix} {}^t\boldsymbol{\sigma} \\ {}^t\varepsilon_{\mathrm{eqv}}^{\mathrm{p}} \end{pmatrix} \tag{4.1} $$

For any system response f, it can be expressed either explicitly or implicitly as a function of $\{{}^t\boldsymbol{U}\}_{t=1}^{\mathrm{N}}$, $\{{}^t\boldsymbol{V}\}_{t=1}^{\mathrm{N}}$, and the design variables in optimization, i.e.

$$ f = f({}^1\boldsymbol{U}(s), {}^2\boldsymbol{U}(s), \dots, {}^{\mathrm{N}}\boldsymbol{U}(s), {}^1\boldsymbol{V}(s), {}^2\boldsymbol{V}(s), \dots, {}^{\mathrm{N}}\boldsymbol{V}(s), s) \tag{4.2} $$

4.1.2 Deduction of adjoint sensitivity formulation

According to Eq. (4.2), the sensitivity of a response function f with respect to a design variable is determined by

$$\frac{df}{ds} = \frac{\partial f}{\partial s} + \sum_{t=1}^{\mathrm{N}} \frac{\partial f}{\partial {}^t\boldsymbol{U}}^{\mathrm{T}} \frac{d\,{}^t\boldsymbol{U}}{ds} + \sum_{t=1}^{\mathrm{N}} \frac{\partial f}{\partial {}^t\boldsymbol{V}}^{\mathrm{T}} \frac{d\,{}^t\boldsymbol{V}}{ds} \tag{4.3}$$

Following the concept of adjoint sensitivity analysis, the computing of derivatives of displacements and state variables can be circumvented by cancelling them out with additional terms associated with adjoint variables. For this purpose, several governing equations are employed. Firstly, in accordance with the equilibrium condition, the residual forces must be equal to zero at all load steps

$$\mathbf{0} \equiv {}^t\boldsymbol{R}({}^t\boldsymbol{U}, {}^t\boldsymbol{V}, s) = \boldsymbol{F}^{\mathrm{ext}} - \boldsymbol{F}^{\mathrm{int}} = \boldsymbol{F}^{\mathrm{ext}} - \int_V {}^t\boldsymbol{B}^{\mathrm{T}}\,{}^t\boldsymbol{\sigma}\, dv \;\; (\mathrm{t} = 1,2,\dots,\mathrm{N}) \tag{4.4}$$

The total derivative of the residual force with respect to a design variable is

$$\frac{d\,{}^t\boldsymbol{R}}{ds} = \frac{\partial\,{}^t\boldsymbol{R}}{\partial s} + \frac{\partial\,{}^t\boldsymbol{R}}{\partial\,{}^t\boldsymbol{U}} \cdot \frac{d\,{}^t\boldsymbol{U}}{ds} + \frac{\partial\,{}^t\boldsymbol{R}}{\partial\,{}^t\boldsymbol{V}} \cdot \frac{d\,{}^t\boldsymbol{V}}{ds} \equiv \mathbf{0} \tag{4.5}$$

According to Eq. (2.15), the stress and plastic strain follow the incremental relation

$${}^t\boldsymbol{\sigma} = {}^{t-1}\boldsymbol{\sigma} + \boldsymbol{D}^{\mathrm{e}}[({}^t\boldsymbol{\varepsilon} - {}^{t-1}\boldsymbol{\varepsilon}) - {}^t\Delta\boldsymbol{\varepsilon}^{\mathrm{p}}] \tag{4.6}$$

where the increment of plastic strain, as per Eq. (2.20), is

$${}^t\Delta\boldsymbol{\varepsilon}^{\mathrm{p}} = {}^t\boldsymbol{\varepsilon}^{\mathrm{p}} - {}^{t-1}\boldsymbol{\varepsilon}^{\mathrm{p}} = \left({}^t\varepsilon^{\mathrm{p}}_{\mathrm{eqv}} - {}^{t-1}\varepsilon^{\mathrm{p}}_{\mathrm{eqv}}\right) \cdot {}^t\mathbf{a} \tag{4.7}$$

and according to the yield and consistency condition, it has

$$\left({}^t\varepsilon^{\mathrm{p}}_{\mathrm{eqv}} - {}^{t-1}\varepsilon^{\mathrm{p}}_{\mathrm{eqv}}\right) \cdot \left[|{}^t\boldsymbol{\sigma}|_{\mathrm{eqv}} - \sigma_{\mathrm{Y}}\left({}^t\varepsilon^{\mathrm{p}}_{\mathrm{eqv}}\right)\right] = 0 \tag{4.8}$$

Writing Eqs. (4.6) and (4.8) as a vector function ${}^{t}\boldsymbol{H}$:

$$ {}^{t}\boldsymbol{H}({}^{t}\boldsymbol{U}, {}^{t-1}\boldsymbol{U}, {}^{t}\boldsymbol{V}, {}^{t-1}\boldsymbol{V}, s) = \begin{pmatrix} {}^{t-1}\boldsymbol{\sigma} + \boldsymbol{D}^{\mathrm{e}}\left[\left({}^{t}\boldsymbol{\varepsilon} - {}^{t-1}\boldsymbol{\varepsilon}\right) - \left({}^{t}\varepsilon^{\mathrm{p}}_{\mathrm{eqv}} - {}^{t-1}\varepsilon^{\mathrm{p}}_{\mathrm{eqv}}\right) \cdot {}^{t}\mathbf{a}\right] - {}^{t}\boldsymbol{\sigma} \\ \left({}^{t}\varepsilon^{\mathrm{p}}_{\mathrm{eqv}} - {}^{t-1}\varepsilon^{\mathrm{p}}_{\mathrm{eqv}}\right) \cdot \left[\left|{}^{t}\boldsymbol{\sigma}\right|_{\mathrm{eqv}} - \sigma_{\mathrm{Y}}\left({}^{t}\varepsilon^{\mathrm{p}}_{\mathrm{eqv}}\right)\right] \end{pmatrix} \tag{4.9} $$

${}^{t}\boldsymbol{H}$ is referred to as dependent residual in literature [MTV94] and is identical to zero at each load step.

The dependent residual is a function of variables at both the current and the previous load step. The total derivative of the dependent residual with respect to a design variable is

$$ \frac{d^{t}\boldsymbol{H}}{ds} = \frac{\partial^{t}\boldsymbol{H}}{\partial s} + \frac{\partial^{t}\boldsymbol{H}}{\partial^{t}\boldsymbol{U}}\frac{d^{t}\boldsymbol{U}}{ds} + \frac{\partial^{t}\boldsymbol{H}}{\partial^{t-1}\boldsymbol{U}}\frac{d^{t-1}\boldsymbol{U}}{ds} + \frac{\partial^{t}\boldsymbol{H}}{\partial^{t}\boldsymbol{V}}\frac{d^{t}\boldsymbol{V}}{ds} + \frac{\partial^{t}\boldsymbol{H}}{\partial^{t-1}\boldsymbol{V}}\frac{d^{t-1}\boldsymbol{V}}{ds} \equiv \mathbf{0} \tag{4.10} $$

As the residual force and the dependent residual are both zero at each load step, pre-multiplying adjoint variable vectors ${}^{t}\boldsymbol{\lambda}$ to ${}^{t}\boldsymbol{R}$ and adjoint variable vectors ${}^{t}\boldsymbol{\gamma}$ to ${}^{t}\boldsymbol{H}$, and then subtracting them from the response function, will not alter the response value, i.e.

$$ f = f - \sum_{t=1}^{\mathrm{N}} {}^{t}\boldsymbol{\lambda}^{\mathrm{T}}\, {}^{t}\boldsymbol{R} - \sum_{t=1}^{\mathrm{N}} {}^{t}\boldsymbol{\gamma}^{\mathrm{T}}\, {}^{t}\boldsymbol{H} \tag{4.11} $$

Utilizing Eqs. (4.3), (4.5), (4.10) and Eq. (4.11), it follows

$$ \begin{aligned} \frac{df}{ds} = {} & \frac{\partial f}{\partial s} + \sum_{t=1}^{\mathrm{N}} \frac{\partial f}{\partial^{t}\boldsymbol{U}}^{\mathrm{T}} \frac{d^{t}\boldsymbol{U}}{ds} + \sum_{t=1}^{\mathrm{N}} \frac{\partial f}{\partial^{t}\boldsymbol{V}}^{\mathrm{T}} \frac{d^{t}\boldsymbol{V}}{ds} - \sum_{t=1}^{\mathrm{N}} {}^{t}\boldsymbol{\lambda}^{\mathrm{T}} \left(\frac{\partial^{t}\boldsymbol{R}}{\partial s} + \frac{\partial^{t}\boldsymbol{R}}{\partial^{t}\boldsymbol{U}} \cdot \frac{d^{t}\boldsymbol{U}}{ds} + \frac{\partial^{t}\boldsymbol{R}}{\partial^{t}\boldsymbol{V}} \cdot \frac{d^{t}\boldsymbol{V}}{ds} \right) \\ & - \sum_{t=1}^{\mathrm{N}} {}^{t}\boldsymbol{\gamma}^{\mathrm{T}} \left(\frac{\partial^{t}\boldsymbol{H}}{\partial s} + \frac{\partial^{t}\boldsymbol{H}}{\partial^{t}\boldsymbol{U}}\frac{d^{t}\boldsymbol{U}}{ds} + \frac{\partial^{t}\boldsymbol{H}}{\partial^{t-1}\boldsymbol{U}}\frac{d^{t-1}\boldsymbol{U}}{ds} + \frac{\partial^{t}\boldsymbol{H}}{\partial^{t}\boldsymbol{V}}\frac{d^{t}\boldsymbol{V}}{ds} + \frac{\partial^{t}\boldsymbol{H}}{\partial^{t-1}\boldsymbol{V}}\frac{d^{t-1}\boldsymbol{V}}{ds} \right) \end{aligned} \tag{4.12} $$

By merging similar terms and enforcing the coefficients of $d^{t}\boldsymbol{U}/ds$ and $d^{t}\boldsymbol{V}/ds$ to be zero, it yields

$$
\begin{aligned}
\frac{df}{ds} = \frac{\partial f}{\partial s} - \sum_{t=1}^{\mathrm{N}} {}^{t}\boldsymbol{\lambda}^{\mathrm{T}} \frac{\partial \boldsymbol{R}^{\mathrm{t}}}{\partial \mathrm{s}} - \sum_{t=1}^{\mathrm{N}} {}^{t}\boldsymbol{\gamma}^{\mathrm{T}} \frac{\partial^{t}\boldsymbol{H}}{\partial s} \\
+ \left(\underbrace{\frac{\partial f}{\partial^{\mathrm{N}}\boldsymbol{U}}^{\mathrm{T}} - {}^{\mathrm{N}}\boldsymbol{\lambda}^{\mathrm{T}} \frac{\partial^{\mathrm{N}}\boldsymbol{R}}{\partial^{\mathrm{N}}\boldsymbol{U}} - {}^{\mathrm{N}}\boldsymbol{\gamma}^{\mathrm{T}} \frac{\partial^{\mathrm{N}}\boldsymbol{H}}{\partial^{\mathrm{N}}\boldsymbol{U}}}_{=0} \right) \frac{d^{\mathrm{N}}\boldsymbol{U}}{ds} \\
+ \left(\underbrace{\frac{\partial f}{\partial^{\mathrm{N}}\boldsymbol{V}}^{\mathrm{T}} - {}^{\mathrm{N}}\boldsymbol{\lambda}^{\mathrm{T}} \frac{\partial^{\mathrm{N}}\boldsymbol{R}}{\partial^{\mathrm{N}}\boldsymbol{V}} - {}^{\mathrm{N}}\boldsymbol{\gamma}^{\mathrm{T}} \frac{\partial^{\mathrm{N}}\boldsymbol{H}}{\partial^{\mathrm{N}}\boldsymbol{V}}}_{=0} \right) \frac{d^{\mathrm{N}}\boldsymbol{V}}{ds} \\
- \sum_{t=1}^{\mathrm{N}-1} \left(\underbrace{{}^{t}\boldsymbol{\lambda}^{\mathrm{T}} \frac{\partial^{t}\boldsymbol{R}}{\partial^{t}\boldsymbol{U}} + {}^{t}\boldsymbol{\gamma}^{\mathrm{T}} \frac{\partial^{t}\boldsymbol{H}}{\partial^{t}\boldsymbol{U}} + {}^{t+1}\boldsymbol{\gamma}^{\mathrm{T}} \frac{\partial^{t+1}\boldsymbol{H}}{\partial^{t}\boldsymbol{U}} - \frac{\partial f}{\partial^{t}\boldsymbol{U}}^{\mathrm{T}}}_{=0} \right) \frac{d^{t}\boldsymbol{U}}{ds} \\
- \sum_{t=1}^{\mathrm{N}-1} \left(\underbrace{{}^{t}\boldsymbol{\lambda}^{\mathrm{T}} \frac{\partial^{t}\boldsymbol{R}}{\partial^{t}\boldsymbol{V}} + {}^{t}\boldsymbol{\gamma}^{\mathrm{T}} \frac{\partial^{t}\boldsymbol{H}}{\partial^{t}\boldsymbol{V}} + {}^{t+1}\boldsymbol{\gamma}^{\mathrm{T}} \frac{\partial^{t+1}\boldsymbol{H}}{\partial^{t}\boldsymbol{V}} - \frac{\partial f}{\partial^{t}\boldsymbol{V}}^{\mathrm{T}}}_{=0} \right) \frac{d^{t}\boldsymbol{V}}{ds} \\
- {}^{1}\boldsymbol{\gamma}^{\mathrm{T}} \left(\underbrace{\frac{\partial^{1}\boldsymbol{H}}{\partial^{0}\boldsymbol{U}} \frac{d^{0}\boldsymbol{U}}{ds} + \frac{\partial^{1}\boldsymbol{H}}{\partial^{0}\boldsymbol{V}} \frac{d^{0}\boldsymbol{V}}{ds}}_{\equiv 0} \right)
\end{aligned}
\tag{4.13}
$$

A series of systems of linear equations related to the adjoint variables is obtained

$$
\begin{pmatrix} \frac{\partial^{\mathrm{N}}\boldsymbol{R}}{\partial^{\mathrm{N}}\boldsymbol{U}}^{\mathrm{T}} & \frac{\partial^{\mathrm{N}}\boldsymbol{H}}{\partial^{\mathrm{N}}\boldsymbol{U}}^{\mathrm{T}} \\ \frac{\partial^{\mathrm{N}}\boldsymbol{R}}{\partial^{\mathrm{N}}\boldsymbol{V}}^{\mathrm{T}} & \frac{\partial^{\mathrm{N}}\boldsymbol{H}}{\partial^{\mathrm{N}}\boldsymbol{V}}^{\mathrm{T}} \end{pmatrix} \begin{pmatrix} {}^{\mathrm{N}}\boldsymbol{\lambda} \\ {}^{\mathrm{N}}\boldsymbol{\gamma} \end{pmatrix} = \begin{pmatrix} \frac{\partial f}{\partial^{\mathrm{N}}\boldsymbol{U}} \\ \frac{\partial f}{\partial^{\mathrm{N}}\boldsymbol{V}} \end{pmatrix} \tag{4.14}
$$

$$
\begin{pmatrix} \frac{\partial^{t}\boldsymbol{R}}{\partial^{t}\boldsymbol{U}}^{\mathrm{T}} & \frac{\partial^{t}\boldsymbol{H}}{\partial^{t}\boldsymbol{U}}^{\mathrm{T}} \\ \frac{\partial^{t}\boldsymbol{R}}{\partial^{t}\boldsymbol{V}}^{\mathrm{T}} & \frac{\partial^{t}\boldsymbol{H}}{\partial^{t}\boldsymbol{V}}^{\mathrm{T}} \end{pmatrix} \begin{pmatrix} {}^{t}\boldsymbol{\lambda} \\ {}^{t}\boldsymbol{\gamma} \end{pmatrix} = - \begin{pmatrix} \frac{\partial^{t+1}\boldsymbol{H}}{\partial^{t}\boldsymbol{U}} \\ \frac{\partial^{t+1}\boldsymbol{H}}{\partial^{t}\boldsymbol{V}} \end{pmatrix}^{\mathrm{T}} {}^{t+1}\boldsymbol{\gamma} + \begin{pmatrix} \frac{\partial f}{\partial^{t}\boldsymbol{U}} \\ \frac{\partial f}{\partial^{t}\boldsymbol{V}} \end{pmatrix} \quad (t = \mathrm{N}-1, \dots, 1) \tag{4.15}
$$

Then the sensitivity of the response is

$$\frac{df}{ds}=\frac{\partial f}{\partial s}-\sum_{t=1}^{\mathrm{N}}{}^{t}\boldsymbol{\lambda}^{\mathrm{T}}\frac{\partial^{t}\boldsymbol{R}}{\partial \mathrm{s}}-\sum_{t=1}^{\mathrm{N}}{}^{t}\boldsymbol{\gamma}^{\mathrm{T}}\frac{\partial^{t}\boldsymbol{H}}{\partial s} \tag{4.16}$$

Instead of computing derivatives of displacements and state variables, the partial derivatives of the residual force and dependent residuals are required to solve the adjoint variables and calculate sensitivity. For the convenience of further discussion, these partial derivatives are derived and presented in the following.

According to Eq. (2.1), it follows

$$\frac{\partial^{t}\boldsymbol{R}}{\partial^{t}\boldsymbol{U}}=-\frac{\partial\int_{V}{}^{t}\boldsymbol{B}^{\mathrm{T}\,t}\boldsymbol{\sigma}dv}{\partial\boldsymbol{U}^{\mathrm{t}}}=-\int_{V}\nabla_{\boldsymbol{U}}{}^{t}\boldsymbol{B}^{\mathrm{T}\,t}\boldsymbol{\sigma}dv \tag{4.17}$$

$$\frac{\partial^{t}\boldsymbol{R}}{\partial^{t}\boldsymbol{V}}=-\left(\frac{\partial}{\partial^{t}\boldsymbol{\sigma}}\quad\frac{\partial}{\partial^{t}\varepsilon_{\mathrm{eqv}}^{\mathrm{p}}}\right)\int_{V}{}^{t}\boldsymbol{B}^{\mathrm{T}\,t}\boldsymbol{\sigma}dv=-\left(\int_{V}{}^{t}\boldsymbol{B}^{\mathrm{T}}dv\quad 0\right) \tag{4.18}$$

If load step t is an elastic step, then the dependent residual is

$${}^{t}\boldsymbol{H}=\begin{pmatrix}{}^{t-1}\boldsymbol{\sigma}+\boldsymbol{D}^{\mathrm{e}}({}^{t}\boldsymbol{\varepsilon}-{}^{t-1}\boldsymbol{\varepsilon})-{}^{t}\boldsymbol{\sigma}\\ {}^{t}\varepsilon_{\mathrm{eqv}}^{\mathrm{p}}-{}^{t-1}\varepsilon_{\mathrm{eqv}}^{\mathrm{p}}\end{pmatrix}=0 \tag{4.19}$$

According to the expression of ${}^{t}\boldsymbol{\varepsilon}$ in Eq. (2.4), it yields

$$\frac{\partial^{t}\boldsymbol{H}}{\partial^{t}\boldsymbol{U}}=\begin{pmatrix}\boldsymbol{D}^{\mathrm{e}}\dfrac{\partial^{t}\boldsymbol{\varepsilon}}{\partial^{t}\boldsymbol{U}}\\ 0\end{pmatrix}=\begin{pmatrix}\boldsymbol{D}^{\mathrm{e}\,t}\boldsymbol{B}\\ 0\end{pmatrix} \tag{4.20}$$

$$\frac{\partial^{t}\boldsymbol{H}}{\partial^{t-1}\boldsymbol{U}}=\begin{pmatrix}-\boldsymbol{D}^{\mathrm{e}}\dfrac{\partial^{t-1}\boldsymbol{\varepsilon}}{\partial^{t-1}\boldsymbol{U}}\\ 0\end{pmatrix}=-\frac{\partial^{t-1}\boldsymbol{H}}{\partial^{t-1}\boldsymbol{U}} \tag{4.21}$$

$$\frac{\partial^{t}\boldsymbol{H}}{\partial s}=\begin{pmatrix}\boldsymbol{D}^{\mathrm{e}}\dfrac{\partial({}^{t}\boldsymbol{\varepsilon}-{}^{t-1}\boldsymbol{\varepsilon})}{\partial s}\\ 0\end{pmatrix}=\begin{pmatrix}\boldsymbol{D}^{\mathrm{e}}\dfrac{\partial^{t}\boldsymbol{\varepsilon}}{\partial s}\\ 0\end{pmatrix}-\begin{pmatrix}\boldsymbol{D}^{\mathrm{e}}\dfrac{\partial^{t-1}\boldsymbol{\varepsilon}}{\partial s}\\ 0\end{pmatrix} \tag{4.22}$$

$$\frac{\partial^{t}\boldsymbol{H}}{\partial^{t}\boldsymbol{V}}=\left(\frac{\partial}{\partial^{t}\boldsymbol{\sigma}}\quad\frac{\partial}{\partial^{t}\varepsilon_{\mathrm{eqv}}^{\mathrm{p}}}\right){}^{t}\boldsymbol{H}=\begin{pmatrix}-\boldsymbol{I} & -\boldsymbol{D}^{\mathrm{e}\,t}\mathbf{a}\\ 0 & 1\end{pmatrix}=\left(\frac{\partial^{t}\boldsymbol{H}}{\partial^{t}\boldsymbol{V}}\right)^{-1} \tag{4.23}$$

$$\frac{\partial^t \boldsymbol{H}}{\partial^{t-1}\boldsymbol{V}} = \begin{pmatrix} \frac{\partial}{\partial^{t-1}\boldsymbol{\sigma}} & \frac{\partial}{\partial^{t-1}\varepsilon^{\mathrm{p}}_{\mathrm{eqv}}} \end{pmatrix} {}^t\boldsymbol{H} = \begin{pmatrix} \boldsymbol{I} & \boldsymbol{D}^{\mathrm{e}}{}^t\mathbf{a} \\ 0 & -1 \end{pmatrix} = -\frac{\partial^t \boldsymbol{H}}{\partial^t \boldsymbol{V}} \tag{4.24}$$

If load step t is a plastic step, then the dependent residual is

$${}^t\boldsymbol{H} = \begin{pmatrix} {}^{t-1}\boldsymbol{\sigma} + \boldsymbol{D}^{\mathrm{e}}\left[\left({}^t\boldsymbol{\varepsilon} - {}^{t-1}\boldsymbol{\varepsilon}\right) - \left({}^t\varepsilon^{\mathrm{p}}_{\mathrm{eqv}} - {}^{t-1}\varepsilon^{\mathrm{p}}_{\mathrm{eqv}}\right) \cdot {}^t\mathbf{a}\right] - {}^t\boldsymbol{\sigma} \\ \left|{}^t\boldsymbol{\sigma}\right|_{\mathrm{eqv}} - \sigma_{\mathrm{Y}}\left({}^t\varepsilon^{\mathrm{p}}_{\mathrm{eqv}}\right) \end{pmatrix} = \mathbf{0} \tag{4.25}$$

where the yield strength for isotropic hardening follows

$$\sigma_{\mathrm{Y}}\left({}^t\varepsilon^{\mathrm{p}}_{\mathrm{eqv}}\right) = \sigma_0 + \int_0^{{}^t\varepsilon^{\mathrm{p}}_{\mathrm{eqv}}} E^{\mathrm{p}} d\varepsilon^{\mathrm{p}}_{\mathrm{eqv}} \tag{4.26}$$

The expression $\partial^t \boldsymbol{H}/\partial^t \boldsymbol{U}$, $\partial^t \boldsymbol{H}/\partial^{t-1}\boldsymbol{U}$, and $\partial^t \boldsymbol{H}/\partial s$ still follow Eqs. (4.20) and (4.22). Other partial derivatives of ${}^t\boldsymbol{H}$ are obtained as:

$$\frac{\partial^t \boldsymbol{H}}{\partial^t \boldsymbol{V}} = \begin{pmatrix} \frac{\partial}{\partial^t \boldsymbol{\sigma}} & \frac{\partial}{\partial^t \varepsilon^{\mathrm{p}}_{\mathrm{eqv}}} \end{pmatrix} {}^t\boldsymbol{H} = \begin{pmatrix} -\boldsymbol{I} - \boldsymbol{D}^{\mathrm{e}} \frac{d^t \mathbf{a}}{d^t \boldsymbol{\sigma}} \Delta\varepsilon^{\mathrm{p}}_{\mathrm{eqv}} & -\boldsymbol{D}^{\mathrm{e}}{}^t\mathbf{a} \\ {}^t\mathbf{a}^T & -E^{\mathrm{p}} \end{pmatrix} \tag{4.27}$$

$$\frac{\partial^t \boldsymbol{H}}{\partial^{t-1}\boldsymbol{V}} = \begin{pmatrix} \frac{\partial}{\partial^{t-1}\boldsymbol{\sigma}} & \frac{\partial}{\partial^{t-1}\varepsilon^{\mathrm{p}}_{\mathrm{eqv}}} \end{pmatrix} {}^t\boldsymbol{H} = \begin{pmatrix} \boldsymbol{I} & \boldsymbol{D}^{\mathrm{e}}{}^t\mathbf{a} \\ 0 & 0 \end{pmatrix} \tag{4.28}$$

4.1.3 Solution of adjoint variables

The adjoint variables are obtained by solving the linear systems in Eqs. (4.14) and (4.15). It should be noted that these equations must be solved backward, from the last step N to the first step 1. At step N, Eq. (4.14) yields

$$\left(\frac{\partial^{\mathrm{N}}\boldsymbol{R}}{\partial^{\mathrm{N}}\boldsymbol{U}} - \frac{\partial^{\mathrm{N}}\boldsymbol{R}}{\partial^{\mathrm{N}}\boldsymbol{V}} \frac{\partial^{\mathrm{N}}\boldsymbol{H}}{\partial^{\mathrm{N}}\boldsymbol{V}}^{-1} \frac{\partial^{\mathrm{N}}\boldsymbol{H}}{\partial^{\mathrm{N}}\boldsymbol{U}}\right)^{\mathrm{T}} {}^{\mathrm{N}}\boldsymbol{\lambda} = \frac{\partial f}{\partial^{\mathrm{N}}\boldsymbol{U}} - \frac{\partial^{\mathrm{N}}\boldsymbol{H}}{\partial^{\mathrm{N}}\boldsymbol{U}}^{\mathrm{T}} \frac{\partial^{\mathrm{N}}\boldsymbol{H}}{\partial^{\mathrm{N}}\boldsymbol{V}}^{-\mathrm{T}} \frac{\partial f}{\partial^{\mathrm{N}}\boldsymbol{V}} \tag{4.29}$$

The following will show that the matrix on the left-hand side conforms Eq.(4.30) for all load steps

$$\frac{\partial^t \boldsymbol{R}}{\partial^t \boldsymbol{U}} - \frac{\partial^t \boldsymbol{R}}{\partial^t \boldsymbol{V}} \frac{\partial^t \boldsymbol{H}}{\partial^t \boldsymbol{V}}^{-1} \frac{\partial^t \boldsymbol{H}}{\partial^t \boldsymbol{U}} = -{}^t\boldsymbol{K}_{\mathrm{T}} \tag{4.30}$$

Eq. (4.30) is proven separately for an elastic step and a plastic step. Firstly, if load step t is an elastic step, utilizing Eqs. (4.17), (4.18), (4.20), (4.23) and (2.13), it follows

$$\begin{aligned} &\frac{\partial^t \boldsymbol{R}}{\partial^t \boldsymbol{U}} - \frac{\partial^t \boldsymbol{R}}{\partial^t \boldsymbol{V}} \frac{\partial^t \boldsymbol{H}}{\partial^t \boldsymbol{V}}^{-1} \frac{\partial^t \boldsymbol{H}}{\partial^t \boldsymbol{U}} \\ &\qquad = -\int_V \nabla_{\boldsymbol{U}}{}^t\boldsymbol{B}^{\mathrm{T}}{}^t\boldsymbol{\sigma} dv + \left(\int_V {}^t\boldsymbol{B}^{\mathrm{T}} dv \quad 0\right) \begin{pmatrix} -\boldsymbol{I} & -\boldsymbol{D}^{\mathrm{e}\,t}\mathbf{a} \\ 0 & 1 \end{pmatrix} \begin{pmatrix} \boldsymbol{D}^{\mathrm{e}\,t}\boldsymbol{B} \\ 0 \end{pmatrix} \\ &\qquad = -\int_V {}^t\boldsymbol{B}^{\mathrm{T}} \boldsymbol{D}^{\mathrm{e}\,t}\boldsymbol{B} dv - \int_V \nabla_{\boldsymbol{U}}{}^t\boldsymbol{B}^{\mathrm{T}}{}^t\boldsymbol{\sigma} dv = -{}^t\boldsymbol{K}_{\mathrm{T}} \end{aligned} \tag{4.31}$$

Secondly, for a plastic load step t, denote

$$\frac{\partial^t \boldsymbol{H}}{\partial^t \boldsymbol{V}}^{-1} = \begin{pmatrix} \boldsymbol{W}_1 & \boldsymbol{W}_2 \\ \boldsymbol{W}_3 & \boldsymbol{W}_4 \end{pmatrix} \tag{4.32}$$

By referencing Eq. (4.27), it can be verified that

$$\boldsymbol{W}_1 = \boldsymbol{Q}^{-1} - \frac{\boldsymbol{d} \cdot \boldsymbol{D}^{\mathrm{e}-1}}{\mathbf{a} \cdot \boldsymbol{r} + E^{\mathrm{p}}} \tag{4.33}$$

where $\boldsymbol{Q}$, $\boldsymbol{r}$ and $\boldsymbol{d}$ follow Eq. (2.28).

Combing Eqs. (4.17), (4.18), (4.20), (4.32) and (2.13), it follows

$$\begin{aligned} &\frac{\partial^t \boldsymbol{R}}{\partial^t \boldsymbol{U}} - \frac{\partial^t \boldsymbol{R}}{\partial^t \boldsymbol{V}} \frac{\partial^t \boldsymbol{H}}{\partial^t \boldsymbol{V}}^{-1} \frac{\partial^t \boldsymbol{H}}{\partial^t \boldsymbol{U}} \\ &\qquad = -\int_V \nabla_{\boldsymbol{U}}{}^t\boldsymbol{B}^{\mathrm{T}}{}^t\boldsymbol{\sigma} dv \\ &\qquad + \left(\int_V \nabla_{\boldsymbol{U}}{}^t\boldsymbol{B}^{\mathrm{T}}{}^t\boldsymbol{\sigma} dv \quad 0\right) \begin{pmatrix} \boldsymbol{Q}^{-1} - \dfrac{\boldsymbol{d} \cdot \boldsymbol{D}^{\mathrm{e}-1}}{\mathbf{a} \cdot \boldsymbol{r} + E^{\mathrm{p}}} & \boldsymbol{W}_2 \\ \boldsymbol{W}_3 & \boldsymbol{W}_4 \end{pmatrix} \begin{pmatrix} \boldsymbol{D}^{\mathrm{e}\,t}\boldsymbol{B} \\ 0 \end{pmatrix} \\ &\qquad = -\int_V {}^t\boldsymbol{B}^{\mathrm{T}} \left(\boldsymbol{Q}^{-1}\boldsymbol{D}^{\mathrm{e}} - \frac{\boldsymbol{d}}{\mathbf{a} \cdot \boldsymbol{r} + E^{\mathrm{p}}}\right) {}^t\boldsymbol{B} dv - \int_V \nabla_{\boldsymbol{U}}{}^t\boldsymbol{B}^{\mathrm{T}}{}^t\boldsymbol{\sigma} dv \\ &\qquad = -\int_V {}^t\boldsymbol{B}^{\mathrm{T}} \boldsymbol{D}^{\mathrm{ep}\,t}\boldsymbol{B} dv - \int_V \nabla_{\boldsymbol{U}}{}^t\boldsymbol{B}^{\mathrm{T}}{}^t\boldsymbol{\sigma} dv = -{}^t\boldsymbol{K}_{\mathrm{T}} \end{aligned} \tag{4.34}$$

Therefore, Eq. (4.30) holds for both elastic and plastic steps. By substituting Eq. (4.30) into Eq.(4.29), the adjoint variable vectors ${}^{\mathrm{N}}\boldsymbol{\lambda}$ and ${}^{\mathrm{N}}\boldsymbol{\gamma}$ can be obtained:

$$
\begin{aligned}
{}^{\mathrm{N}}\boldsymbol{K}_{\mathrm{T}}{}^{\mathrm{N}}\boldsymbol{\lambda} &= \frac{\partial f}{\partial {}^{\mathrm{N}}\boldsymbol{U}} - \frac{\partial {}^{\mathrm{N}}\boldsymbol{H}^{\mathrm{T}}}{\partial {}^{\mathrm{N}}\boldsymbol{U}} \frac{\partial {}^{\mathrm{N}}\boldsymbol{H}^{-\mathrm{T}}}{\partial {}^{\mathrm{N}}\boldsymbol{V}} \frac{\partial f}{\partial {}^{\mathrm{N}}\boldsymbol{V}} \\
{}^{\mathrm{N}}\boldsymbol{\gamma} &= \frac{\partial {}^{\mathrm{N}}\boldsymbol{H}^{-\mathrm{T}}}{\partial {}^{\mathrm{N}}\boldsymbol{V}} \left(\frac{\partial f}{\partial {}^{\mathrm{N}}\boldsymbol{V}} - \frac{\partial {}^{\mathrm{N}}\boldsymbol{R}^{\mathrm{T}}}{\partial {}^{\mathrm{N}}\boldsymbol{V}} {}^{\mathrm{N}}\boldsymbol{\lambda} \right)
\end{aligned}
\tag{4.35}
$$

Adjoint variable vectors ${}^{t}\boldsymbol{\lambda}$ and ${}^{t}\boldsymbol{\gamma}$ are obtained backwardly by solving Eq.(4.15) from load step N-1 to load step 1, which yields

$$
\begin{aligned}
{}^{t}\boldsymbol{K}_{\mathrm{T}}{}^{t}\boldsymbol{\lambda} &= \left(\frac{\partial {}^{t}\boldsymbol{H}^{\mathrm{T}}}{\partial {}^{t}\boldsymbol{U}} \frac{\partial {}^{t}\boldsymbol{H}^{-\mathrm{T}}}{\partial {}^{t}\boldsymbol{V}} \frac{\partial {}^{t+1}\boldsymbol{H}^{\mathrm{T}}}{\partial {}^{t}\boldsymbol{V}} - \frac{\partial {}^{t+1}\boldsymbol{H}^{\mathrm{T}}}{\partial {}^{t}\boldsymbol{U}} \right) {}^{t+1}\boldsymbol{\gamma} + \frac{\partial f}{\partial {}^{t}\boldsymbol{U}} - \frac{\partial {}^{t}\boldsymbol{H}^{\mathrm{T}}}{\partial {}^{t}\boldsymbol{U}} \frac{\partial {}^{t}\boldsymbol{H}^{-\mathrm{T}}}{\partial {}^{t}\boldsymbol{V}} \frac{\partial f}{\partial {}^{t}\boldsymbol{V}} \\
{}^{t}\boldsymbol{\gamma} &= \frac{\partial {}^{t}\boldsymbol{H}^{-\mathrm{T}}}{\partial {}^{t}\boldsymbol{V}} \left(\frac{\partial f}{\partial {}^{t}\boldsymbol{V}} - \frac{\partial {}^{t+1}\boldsymbol{H}^{\mathrm{T}}}{\partial {}^{t}\boldsymbol{V}} {}^{t+1}\boldsymbol{\gamma} - \frac{\partial {}^{t}\boldsymbol{R}^{\mathrm{T}}}{\partial {}^{t}\boldsymbol{V}} {}^{t}\boldsymbol{\lambda} \right)
\end{aligned}
\tag{4.36}
$$

4.2 Numerical examples

In this section, two numerical examples are presented to demonstrate adjoint sensitivity analysis in Section 4.1. The first example involves a truss structure with bar elements, while the second example features a cantilever beam structure meshed with tetrahedral elements.

4.2.1 100-bar truss structure

In this example, a 100-bar truss, as depicted in Figure 4-1, is employed. Nodes on the left end of the structure are fixed, and an external force is applied to the right end. The material is assumed to be incompressible with a Young's modulus of 210GPa, an initial yield stress of 235MPa and a plastic modulus of 100GPa. A bilinear elastoplastic and isotropic hardening material model is assumed.

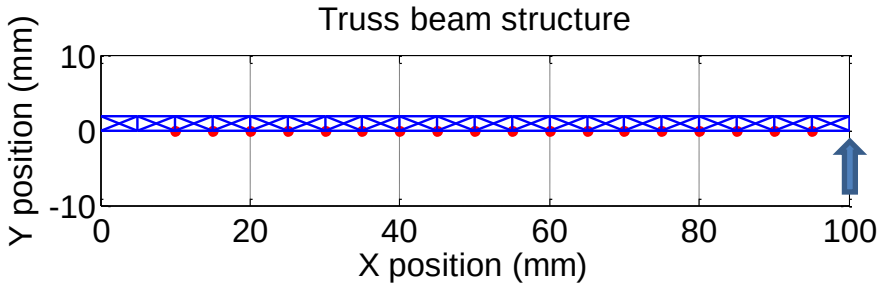

Figure 4-1. 100-bar truss structure (design nodes are highlighted by red dots)

The load history is presented in Figure 4-2 (a), consisting of a loading and a fully unloading stage. The force-displacement curve of the loaded end is shown in Figure 4-2 (b). The plastic strain history of a bar element at the fixed end is depicted in Figure 4-2 (c). The deformation of the structure at fully loading and fully unloading steps are illustrated in Figure 4-3.

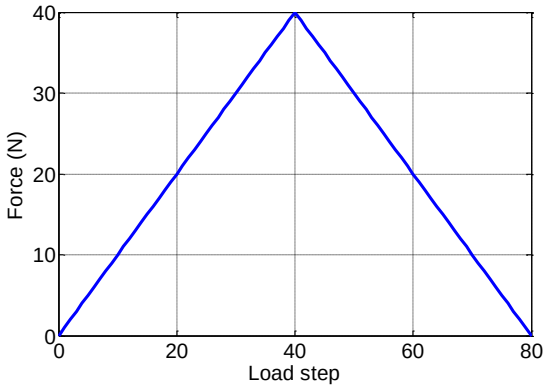

(a) Load history on the structure

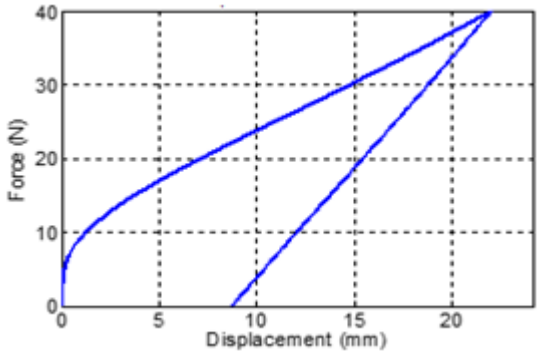

(b) Force-vertical displacement curve at the loaded end

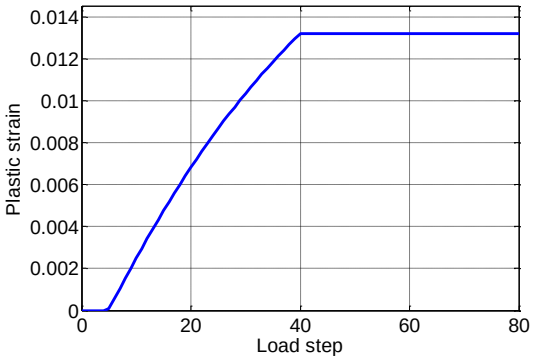

(c) Plastic strain history at the fixed end

Figure 4-2. Load history and finite element analysis results of the truss beam structure

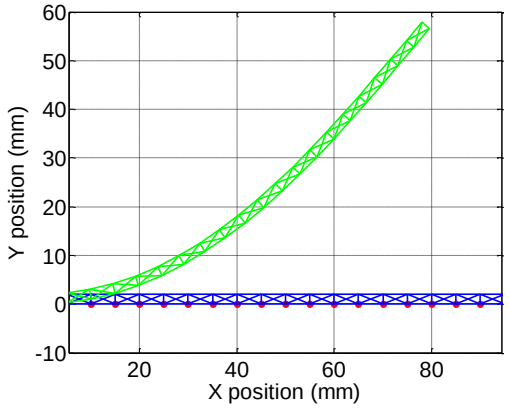

(a) Undeformed and deformed structure at fully loaded step (Load step 40)

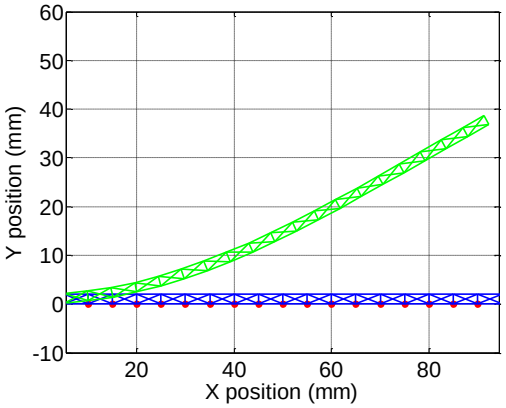

(b) Undeformed and deformed structure at fully unloaded step (Load step 80)

Figure 4-3. Deformed configuration of the 100-bar truss structure

In the sensitivity analysis, the remaining vertical displacement of the free end after fully unloading is defined as the system response. Design nodes, located at the bottom of the structure, are highlighted by red dots in Figure 4-1. The vertical coordinates of these nodes serve as the design variables. The sensitivities obtained using the adjoint variable method are compared with global finite difference results in Figure 4-4, where the horizontal axis represents the x-coordinate of the design nodes. The figure shows a perfect match between the two results.

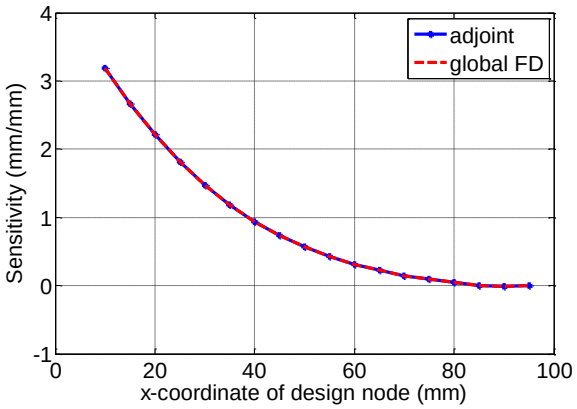

Figure 4-4. Adjoint sensitivity results and global FD results

4.2.2 Cantilever beam structure with tetrahedral elements

In this example, the adjoint sensitivity analysis approach is validated using an example of 3D solid elements. The cantilever beam structure, previously introduced in Section 3.2, is employed here for demonstration. The material

properties remain consistent with the bar truss example, with a Poisson's ratio of 0.3. The vertical coordinates of the design nodes, highlighted by red dots in Figure 4-5, serve as the designated design variables. Two different load histories are applied to the free end of the structure.

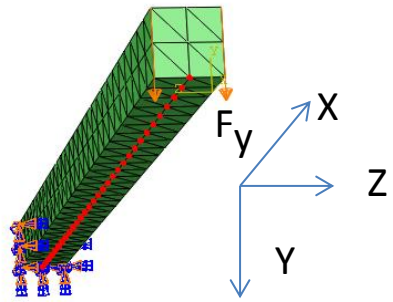

Figure 4-5. Illustration of the cantilever beam example

In the first load case, a procedure involves loading, partially unloading, and reloading is applied to the free end of the beam. The load history is depicted in Figure 4-6 (a). The contour of equivalent plastic strain at the final step is presented in both the original and deformed configuration in Figure 4-6 (b).

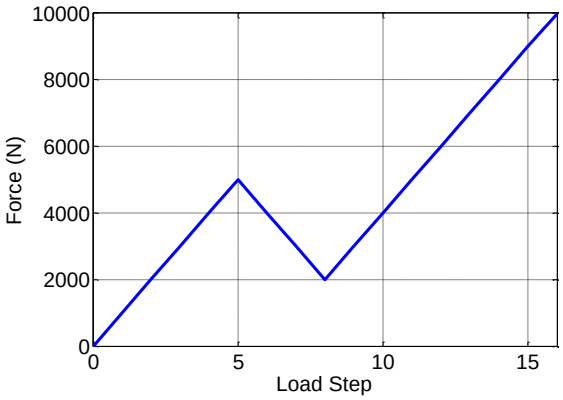

(a) Load history

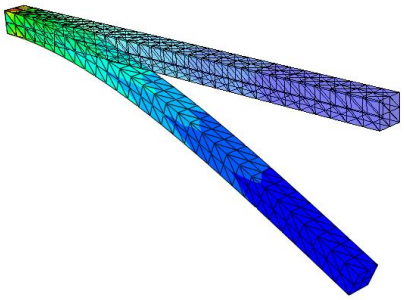

(b) Contour of equivalent plastic strains on the original and deformed structure

Figure 4-6. Load case one: load history and contour plot of equivalent plastic strain

The sensitivities of two system responses are evaluated: one pertains to the vertical displacement at the free end, while the other concerns the equivalent plastic strain of one element at the fixed end. The partial derivatives of the

second response with respect to displacement and state variables are as follows:

$$\frac{\partial f}{\partial {}^{t}\boldsymbol{U}} = 0 \ \ (t = 1,2,\dots,\mathrm{N})$$

$$\frac{\partial f}{\partial {}^{t}\boldsymbol{V}} = 0 \ \ (t = 1,2,\dots,\mathrm{N}-1)$$

$$\frac{\partial f}{\partial {}^{\mathrm{N}}\boldsymbol{V}} = \begin{bmatrix} 0 \\ \vdots \\ 0 \\ 1 \\ 0 \\ \vdots \\ 0 \end{bmatrix} \tag{4.37}$$

The non-zero entry is at the position that corresponds to the equivalent plastic strain of the element in the state variable vector.

The adjoint sensitivity results of the two responses are compared with global finite difference results in Figure 4-7. The horizontal axis represents the x-coordinate of the design nodes. The comparison reveals that the adjoint sensitivities closely align with the finite difference results for both responses.

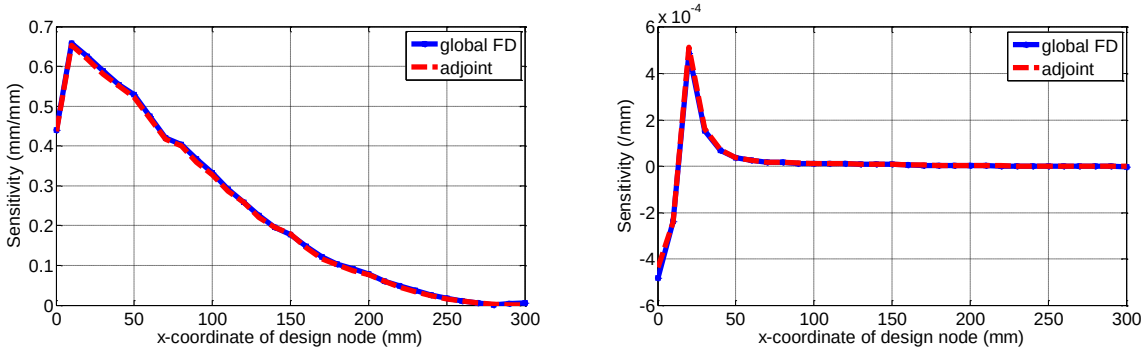

(a) Sensitivities of vertical displacement response

(b) Sensitivities of equivalent plastic strain response

Figure 4-7. Sensitivity results comparison for the first load case of cantilever beam example

In the second load case, two single forces are simultaneously applied in the vertical and horizontal directions to the free end. The vertical force follows a loading-partially unloading-holding constant procedure, while the horizontal force undergoes a monotonically loading procedure, starting from the load step when the vertical force begins to hold constant. The load histories in both

directions are depicted in Figure 4-8 (a). The contour of the equivalent plastic strain at the last load step is presented in Figure 4-8 (b).

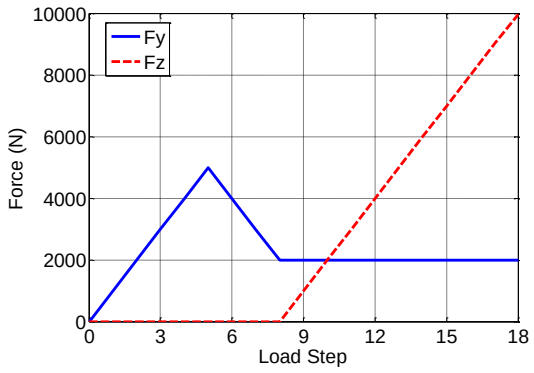

(a) Load history

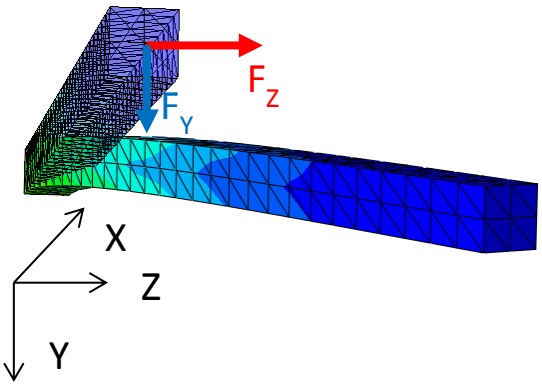

(b) Contour of equivalent plastic strain on both original and deformed configuration

Figure 4-8. Load case two: load history and contour plot of equivalent plastic strain on the original and deformed structure

Two responses are defined as system responses. One is the equivalent plastic strain, which remains the same as in the first load case. The other is the displacement in the horizontal z-direction at the free end. Sensitivities using the adjoint variable method and the global finite difference method are presented in Figure 4-9, showing good agreement between the results.

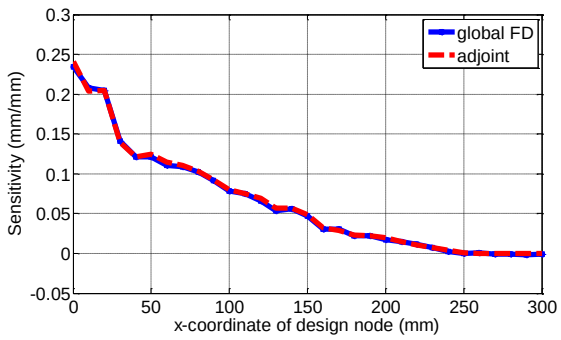

(a) Sensitivities of horizontal displacement response

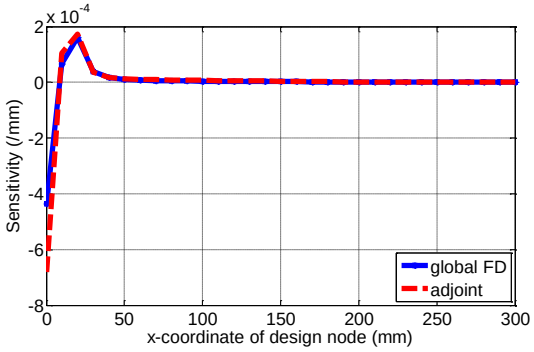

(b) Sensitivities of equivalent plastic strain response

Figure 4-9. Sensitivity results comparison for the second load case of cantilever beam example

The above examples demonstrate the adjoint variable sensitivity analysis approach for addressing simultaneous elastoplasticity and geometric nonlinearity problems.

5. Load step reduction in the adjoint sensitivity analysis

In this chapter, the computational cost and memory cost of the adjoint variable method presented in Chapter 4 are analyzed. Techniques to reduce both costs through load step reduction are discussed, and the efficiency and accuracy of the proposed methods are demonstrated through multiple examples.

5.1 Computational and memory cost of adjoint sensitivity analysis

Section 4.1.2 and Section 4.1.3 show that the primary computational cost of adjoint sensitivity analysis lies in solving adjoint variables.

The solution of $\{{}^t\boldsymbol{\lambda}\}_{t=1}^{\mathrm{N}}$ requires solving linear systems N times, where N is the total number of load steps. Each linear system is of the size of total number of degrees of freedom of the underlying finite element system. The solution of adjoint variables $\{{}^t\boldsymbol{\gamma}\}_{t=1}^{\mathrm{N}}$ could be carried out element by element. Therefore, the computational cost for ${}^t\boldsymbol{\gamma}$ is negligible. In sum, the total computational cost to obtain adjoint variables lies in the solution of $\{{}^t\boldsymbol{\lambda}\}_{t=1}^{\mathrm{N}}$, which is proportional to the total number of load steps.

The memory cost is measured by the number of non-zero values that must be stored simultaneously in a computer system. According to Eqs.(4.35) and (4.36), tangent stiffness matrices at the equilibrium point, partial derivatives of the residual force, and partial derivatives of the dependent residual are required in the solutions of adjoint variables. These quantities are gradually collected during nonlinear analysis at each step. Due to the backward solution procedure of adjoint variables, these quantities at all load steps must be kept in memory until the last step of finite element analysis is finished.

The direct storage of all these variables is not the most efficient way from the memory point of view. To minimize memory cost, it is suggested to store only displacement and state variables at all load steps. During sensitivity analysis, intermediate quantities are retrieved from them. Recomputation happens only at the element level. Therefore, the computational effort could be

neglected. However, the required storage space is still proportional to the number of load steps in sensitivity analysis.

Based on the discussion, the key to saving computational and memory costs in adjoint sensitivity analysis is the reduction of the total number of load steps. In the following sections, how to decrease the number of load steps without sacrificing accuracy is investigated. In Section 5.2, two properties regarding adjoint variables are claimed and theoretically proven. With these properties, Section 5.3 further proves that many load steps can be skipped in the sensitivity analysis. Adjoint variables needs to be solved only at much fewer load steps.

5.2 Two properties of adjoint variables

Before entering the discussion, it is important to clarify one assumption regarding system responses and establish a clear definition of load steps.

Firstly, given a sequence of load steps L= {1, 2, …, t-2, t-1, t, …, N}, a system response *f* investigated in this section is assumed to be dependent only on the displacement and state variables at the last step. This assumption is mathematically formulated as follows:

$$\begin{aligned} \frac{\partial f}{\partial {}^{t}\boldsymbol{U}} &= 0 \qquad \text{for } t < \mathrm{N} \\ \frac{\partial f}{\partial {}^{t}\boldsymbol{V}} &= 0 \qquad \text{for } t < \mathrm{N} \end{aligned} \tag{5.1}$$

Many practical mechanical responses fall into this category, including final displacement, maximum equivalent plastic strain and maximum equivalent stress. In addition, many responses can be expressed as a composition of functions of this type, i.e.

$$g({}^{1}\boldsymbol{U}, {}^{2}\boldsymbol{U}, \dots, {}^{\mathrm{N}}\boldsymbol{U}, {}^{1}\boldsymbol{V}, {}^{2}\boldsymbol{V}, \dots, {}^{\mathrm{N}}\boldsymbol{V}) = h^{\circ}(f_1({}^{1}\boldsymbol{U}, {}^{1}\boldsymbol{V}), f_2({}^{2}\boldsymbol{U}, {}^{2}\boldsymbol{V}), \dots, f_N({}^{\mathrm{N}}\boldsymbol{U}, {}^{\mathrm{N}}\boldsymbol{V})) \tag{5.2}$$

where function $f_k({}^{k}\boldsymbol{U}, {}^{k}\boldsymbol{V})$ is dependent only on the quantities at step k. The sensitivity of g is obtained using the chain rule with sensitivities of f_k. To calculate the sensitivity of f_k, just take step k as the last load step. Thus, f_k is a function satisfies the assumption in Eq. (5.1).

Secondly, in future discussions, an elastic load step is defined as a load step in which all finite elements behave elastically. Otherwise, the load step is called a plastic load step.

In the following, two properties regarding adjoint variables are claimed and proved.

Property 1. If a load step t is an intermediate (i.e. t<N) elastic load step, then ${}^{t}\boldsymbol{\lambda} = 0$.

Proof:

According to Eqs. (4.24) and (4.28)

$$\frac{\partial {}^{t+1}\boldsymbol{H}}{\partial {}^{t}\boldsymbol{V}} = \begin{pmatrix} \boldsymbol{I} & \boldsymbol{D}^{\mathrm{e}}\,{}^{t+1}\mathbf{a} \\ \mathbf{0} & c \end{pmatrix}$$
$$c = \begin{cases} -1 & if\ step\ t+1\ is\ elastic \\ 0 & if\ step\ t+1\ is\ plastic \end{cases} \tag{5.3}$$

By combining Eqs.(4.20), (4.21), (4.23) and (5.3), it yields

$$\begin{aligned} \frac{\partial {}^{t}\boldsymbol{H}^{\mathrm{T}}}{\partial {}^{t}\boldsymbol{U}} \frac{\partial {}^{t}\boldsymbol{H}^{-\mathrm{T}}}{\partial {}^{t}\boldsymbol{V}} \frac{\partial {}^{t+1}\boldsymbol{H}^{\mathrm{T}}}{\partial {}^{t}\boldsymbol{V}} - \frac{\partial {}^{t+1}\boldsymbol{H}^{\mathrm{T}}}{\partial {}^{t}\boldsymbol{U}} &= ({}^{t}\boldsymbol{B}^{\mathrm{T}}\boldsymbol{D}^{\mathrm{e}} \quad 0)\left(\begin{pmatrix} -\boldsymbol{I} & \mathbf{0} \\ -{}^{t}\mathbf{a}^{\mathrm{T}}\boldsymbol{D}^{\mathrm{e}} & 1 \end{pmatrix}\begin{pmatrix} \boldsymbol{I} & \mathbf{0} \\ {}^{t+1}\mathbf{a}^{\mathrm{T}}\boldsymbol{D}^{\mathrm{e}} & c \end{pmatrix} + \boldsymbol{I}\right) \\ &= ({}^{t}\boldsymbol{B}^{\mathrm{T}}\boldsymbol{D}^{\mathrm{e}} \quad 0)\begin{pmatrix} \mathbf{0} & \mathbf{0} \\ \left({}^{t+1}\mathbf{a}^{\mathrm{T}} - {}^{t}\mathbf{a}^{\mathrm{T}}\right)\boldsymbol{D}^{\mathrm{e}} & c+1 \end{pmatrix} = \mathbf{0} \end{aligned} \tag{5.4}$$

By substituting Eq.(5.1) and Eq.(5.4) into Eq.(4.36), it follows

$${}^{t}\boldsymbol{K}_{\mathrm{T}}\,{}^{t}\boldsymbol{\lambda} = \left(\frac{\partial {}^{t}\boldsymbol{H}^{\mathrm{T}}}{\partial {}^{t}\boldsymbol{U}} \frac{\partial {}^{t}\boldsymbol{H}^{-\mathrm{T}}}{\partial {}^{t}\boldsymbol{V}} \frac{\partial {}^{t+1}\boldsymbol{H}^{\mathrm{T}}}{\partial {}^{t}\boldsymbol{V}} - \frac{\partial {}^{t+1}\boldsymbol{H}^{\mathrm{T}}}{\partial {}^{t}\boldsymbol{U}}\right)^{t+1}\boldsymbol{\gamma} + \frac{\partial f}{\partial {}^{t}\boldsymbol{U}} - \frac{\partial {}^{t}\boldsymbol{H}^{\mathrm{T}}}{\partial {}^{t}\boldsymbol{U}} \frac{\partial {}^{t}\boldsymbol{H}^{-\mathrm{T}}}{\partial {}^{t}\boldsymbol{V}} \frac{\partial f}{\partial {}^{t}\boldsymbol{V}} = \mathbf{0} \tag{5.5}$$

which leads to

$${}^{t}\boldsymbol{\lambda} = \mathbf{0} \tag{5.6}$$

□

Property 2. If both load step t and $t+1$ are plastic, and the flow vectors satisfy ${}^{t}\mathbf{a} = {}^{t+1}\mathbf{a}$, $\frac{\mathrm{d}\,{}^{t}\mathbf{a}}{\mathrm{d}\,{}^{t}\boldsymbol{\sigma}} = 0$, then ${}^{t}\boldsymbol{\lambda} = 0$ and ${}^{t}\boldsymbol{\gamma} := \begin{pmatrix} {}^{t}\boldsymbol{\gamma}_{\boldsymbol{\sigma}} \\ {}^{t}\boldsymbol{\gamma}_{\varepsilon^{\mathrm{p}}_{\mathrm{eqv}}} \end{pmatrix} = \begin{pmatrix} {}^{t+1}\boldsymbol{\gamma}_{\boldsymbol{\sigma}} \\ 0 \end{pmatrix}$.

Proof:

Using the assumption of $d^t\mathbf{a}/d^t\boldsymbol{\sigma} = 0$, Eq.(4.27) is simplified to

$$\frac{\partial^t \boldsymbol{H}^{\mathrm{T}}}{\partial^t \boldsymbol{V}} = \begin{pmatrix} -\boldsymbol{I} & {}^t\mathbf{a} \\ -{}^t\mathbf{a}^{\mathrm{T}}\boldsymbol{D}^{\mathrm{e}} & -E^{\mathrm{P}} \end{pmatrix} \tag{5.7}$$

Using the assumption ${}^t\mathbf{a} = {}^{t+1}\mathbf{a}$ and Eq.(4.28), it follows

$$\frac{\partial^{t+1} \boldsymbol{H}^{\mathrm{T}}}{\partial^t \boldsymbol{V}} = \begin{pmatrix} \boldsymbol{I} & \mathbf{0} \\ {}^t\mathbf{a}^{\mathrm{T}}\boldsymbol{D}^{\mathrm{e}} & 0 \end{pmatrix} \tag{5.8}$$

The first column of Eq.(5.7) differs from that of Eq.(5.8) only by a negative sign. Therefore

$$\frac{\partial^t \boldsymbol{H}}{\partial^t \boldsymbol{V}}^{-\mathrm{T}} \frac{\partial^{t+1} \boldsymbol{H}^{\mathrm{T}}}{\partial^t \boldsymbol{V}} = \left(\frac{\partial^t \boldsymbol{H}^{\mathrm{T}}}{\partial^t \boldsymbol{V}}\right)^{-1} \begin{pmatrix} \boldsymbol{I} & \mathbf{0} \\ {}^t\mathbf{a}^{\mathrm{T}}\boldsymbol{D}^{\mathrm{e}} & 0 \end{pmatrix} = \begin{pmatrix} -\boldsymbol{I} & \mathbf{0} \\ \mathbf{0} & 0 \end{pmatrix} \tag{5.9}$$

By combining Eqs (4.20), (4.21) and (5.9), it follows

$$\frac{\partial^t \boldsymbol{H}^{\mathrm{T}}}{\partial^t \boldsymbol{U}} \frac{\partial^t \boldsymbol{H}}{\partial^t \boldsymbol{V}}^{-\mathrm{T}} \frac{\partial^{t+1} \boldsymbol{H}^{\mathrm{T}}}{\partial^t \boldsymbol{V}} - \frac{\partial^{t+1} \boldsymbol{H}^{\mathrm{T}}}{\partial^t \boldsymbol{U}} = ({}^t\boldsymbol{B}^{\mathrm{T}}\boldsymbol{D}^{\mathrm{e}} \quad 0) \begin{pmatrix} \mathbf{0} & \mathbf{0} \\ \mathbf{0} & 1 \end{pmatrix} = \mathbf{0} \tag{5.10}$$

Substituting Eq. (5.1) and Eq. (5.10) into Eq. (4.36), it follows

$${}^t\boldsymbol{K}_{\mathrm{T}}{}^t\boldsymbol{\lambda} = \left(\frac{\partial^t \boldsymbol{H}^{\mathrm{T}}}{\partial^t \boldsymbol{U}} \frac{\partial^t \boldsymbol{H}}{\partial^t \boldsymbol{V}}^{-\mathrm{T}} \frac{\partial^{t+1} \boldsymbol{H}^{\mathrm{T}}}{\partial^t \boldsymbol{V}} - \frac{\partial^{t+1} \boldsymbol{H}^{\mathrm{T}}}{\partial^t \boldsymbol{U}}\right) {}^{t+1}\boldsymbol{\gamma} + \frac{\partial f}{\partial^t \boldsymbol{U}} - \frac{\partial^t \boldsymbol{H}}{\partial^t \boldsymbol{U}}^{\mathrm{T}} \frac{\partial^t \boldsymbol{H}}{\partial^t \boldsymbol{V}}^{-\mathrm{T}} \frac{\partial f}{\partial^t \boldsymbol{V}} = \mathbf{0} \tag{5.11}$$

which leads to

$${}^t\boldsymbol{\lambda} = 0 \tag{5.12}$$

Furthermore, substitute Eqs.(5.1), (5.9) and ${}^t\boldsymbol{\lambda} = 0$ into Eq. (4.36). It has

$${}^t\boldsymbol{\gamma} = \frac{\partial^t \boldsymbol{H}}{\partial^t \boldsymbol{V}}^{-\mathrm{T}} \left(\frac{\partial f}{\partial^t \boldsymbol{V}} - \frac{\partial^{t+1} \boldsymbol{H}^{\mathrm{T}}}{\partial^t \boldsymbol{V}} {}^{t+1}\boldsymbol{\gamma} - \frac{\partial^t \boldsymbol{R}}{\partial^t \boldsymbol{V}}^{\mathrm{T}} {}^t\boldsymbol{\lambda}\right) = \begin{pmatrix} \boldsymbol{I} & \mathbf{0} \\ \mathbf{0} & 0 \end{pmatrix} {}^{t+1}\boldsymbol{\gamma} = \begin{pmatrix} {}^{t+1}\boldsymbol{\gamma}_{\boldsymbol{\sigma}} \\ 0 \end{pmatrix} \tag{5.13}$$

□

5.3 Load step reduction in the adjoint sensitivity analysis

Based on the properties of adjoint variables, this section proposes and proves load step reduction rules in adjoint sensitivity analysis. These rules demonstrate that certain load steps can be skipped in sensitivity analysis without altering the results.

Elastic load step reduction rule: Given a sequence of load steps L = {1, 2, ..., t-1, t, t+1, …, N}, if step *t* is an intermediate elastic load step, then skip step *t* as the load steps contain only S = {1, 2, ..., t-1, t+1, …, N} will not change the sensitivity results.

Before delving into the proof, it is important to clarify several points. Firstly, the load step reduction occurs only during the sensitivity analysis phase, with no impact on the nonlinear finite element analysis.

Secondly, when the load step *t* is skipped in the sensitivity analysis, step *t-1* becomes adjacent to step *t+1* in the backward calculation of adjoint variables.

Thirdly, it is obvious that by skipping step *t*, the adjoint variables obtained from step N to step *t+1* remain unchanged, as no step has been skipped in the backward procedure yet, i.e.,

$$\begin{aligned} {}^{n}_{\mathrm{S}}\boldsymbol{\gamma} &= {}^{n}_{\mathrm{L}}\boldsymbol{\gamma} \ \ (\text{for } n > t) \\ {}^{n}_{\mathrm{S}}\boldsymbol{\lambda} &= {}^{n}_{\mathrm{L}}\boldsymbol{\lambda} \ \ (\text{for } n > t) \end{aligned} \tag{5.14}$$

where the left subscript S and L denote quantities obtained with load steps sequence S and L, respectively.

Lastly, since the finite element analysis is independent of the sensitivity analysis, the quantities and partial derivatives in load step sequences S and L are the same if they are not related to step *t*. Mathematically, it follows

$$\begin{aligned} \frac{\partial {}^{n}_{\mathrm{S}}\boldsymbol{R}}{\partial s} &= \frac{\partial {}^{n}_{\mathrm{L}}\boldsymbol{R}}{\partial s} \ \ (\text{for } n \neq t) \\ \frac{\partial {}^{n}_{\mathrm{S}}\boldsymbol{H}}{\partial s} &= \frac{\partial {}^{n}_{\mathrm{L}}\boldsymbol{H}}{\partial s} \ \ (\text{for } n \neq t \text{ and } n \neq t+1) \end{aligned} \tag{5.15}$$

and

$$\begin{aligned}
\frac{\partial_{\mathrm{S}}^{n}\boldsymbol{H}}{\partial^{n}\boldsymbol{U}} &= \frac{\partial_{\mathrm{L}}^{n}\boldsymbol{H}}{\partial^{n}\boldsymbol{U}} \quad (\text{for } n < t) \\
\frac{\partial_{\mathrm{S}}^{n}\boldsymbol{H}}{\partial^{n}\boldsymbol{V}} &= \frac{\partial_{\mathrm{L}}^{n}\boldsymbol{H}}{\partial^{n}\boldsymbol{V}} \quad (\text{for } n < t) \\
\frac{\partial_{\mathrm{S}}^{n}\boldsymbol{H}}{\partial^{n-1}\boldsymbol{V}} &= \frac{\partial_{\mathrm{L}}^{n}\boldsymbol{H}}{\partial^{n-1}\boldsymbol{V}} \quad (\text{for } n < t) \\
\frac{\partial_{\mathrm{S}}^{n}\boldsymbol{H}}{\partial^{n-1}\boldsymbol{U}} &= \frac{\partial_{\mathrm{L}}^{n}\boldsymbol{H}}{\partial^{n-1}\boldsymbol{U}} \quad (\text{for } n < t) \\
{}_{\mathrm{S}}^{n}\boldsymbol{K}_{\mathrm{T}} &= {}_{\mathrm{L}}^{n}\boldsymbol{K}_{\mathrm{T}} \quad (\text{for } n < t)
\end{aligned} \tag{5.16}$$

Now, the proof of the first load step reduction rule is presented.

Proof:

Mathematically, it needs to show:

$$\frac{d_{\mathrm{L}}f}{ds} = \frac{d_{\mathrm{S}}f}{ds} \tag{5.17}$$

According to Eq.(4.16), the left-hand side and the right-hand side are

$$\begin{aligned}
\frac{d_{\mathrm{L}}f}{ds} &= \frac{\partial f}{\partial s} - {}_{\mathrm{L}}\Lambda - {}_{\mathrm{L}}\Gamma \\
\frac{d_{\mathrm{S}}f}{ds} &= \frac{\partial f}{\partial s} - {}_{\mathrm{S}}\Lambda - {}_{\mathrm{S}}\Gamma
\end{aligned} \tag{5.18}$$

where

$$\begin{aligned}
{}_{\mathrm{L}}\Lambda &= \sum_{n=1}^{t-1} {}_{\mathrm{L}}^{n}\boldsymbol{\lambda}^{\mathrm{T}} \frac{\partial_{\mathrm{L}}^{n}\boldsymbol{R}}{\partial s} + {}_{\mathrm{L}}^{t}\boldsymbol{\lambda}^{\mathrm{T}} \frac{\partial_{\mathrm{L}}^{t}\boldsymbol{R}^{\mathrm{T}}}{\partial s} + \sum_{n=t+1}^{\mathrm{N}} {}_{\mathrm{L}}^{n}\boldsymbol{\lambda}^{\mathrm{T}} \frac{\partial_{\mathrm{L}}^{n}\boldsymbol{R}}{\partial s} \\
{}_{\mathrm{S}}\Lambda &= \sum_{n=1}^{t-1} {}_{\mathrm{S}}^{n}\boldsymbol{\lambda}^{\mathrm{T}} \frac{\partial_{\mathrm{S}}^{n}\boldsymbol{R}}{\partial s} + \sum_{n=t+1}^{\mathrm{N}} {}_{\mathrm{S}}^{n}\boldsymbol{\lambda}^{\mathrm{T}} \frac{\partial_{\mathrm{S}}^{n}\boldsymbol{R}}{\partial s}
\end{aligned} \tag{5.19}$$

and

$$
\begin{aligned}
{}_{\mathrm{L}}\Gamma &= \sum_{n=1}^{t-1} {}_{\mathrm{L}}^{n}\boldsymbol{\gamma}^{\mathrm{T}} \frac{\partial {}_{\mathrm{L}}^{n}\boldsymbol{H}}{\partial s} + {}_{\mathrm{L}}^{t}\boldsymbol{\gamma}^{\mathrm{T}} \frac{\partial {}_{\mathrm{L}}^{t}\boldsymbol{H}}{\partial s} + {}_{\mathrm{L}}^{t+1}\boldsymbol{\gamma}^{\mathrm{T}} \frac{\partial {}_{\mathrm{L}}^{t+1}\boldsymbol{H}}{\partial s} + \sum_{n=t+2}^{\mathrm{N}} {}_{\mathrm{L}}^{n}\boldsymbol{\gamma}^{\mathrm{T}} \frac{\partial {}_{\mathrm{L}}^{n}\boldsymbol{H}}{\partial s} \\
{}_{\mathrm{S}}\Gamma &= \sum_{n=1}^{t-1} {}_{\mathrm{S}}^{n}\boldsymbol{\gamma}^{\mathrm{T}} \frac{\partial {}_{\mathrm{S}}^{n}\boldsymbol{H}}{\partial s} + {}_{\mathrm{S}}^{t+1}\boldsymbol{\gamma}^{\mathrm{T}} \frac{\partial {}_{\mathrm{S}}^{t+1}\boldsymbol{H}}{\partial s} + \sum_{n=t+2}^{\mathrm{N}} {}_{\mathrm{S}}^{n}\boldsymbol{\gamma}^{\mathrm{T}} \frac{\partial {}_{\mathrm{S}}^{n}\boldsymbol{H}}{\partial s}
\end{aligned}
\tag{5.20}
$$

Comparing both formulas in Eqs.(5.19) and (5.20) and taking Eqs.(5.14) to (5.16) into account, Eq.(5.17) holds if the following three items are all proven:

1. ${}_{\mathrm{L}}^{t}\boldsymbol{\lambda} = 0$
2. ${}_{\mathrm{S}}^{n}\boldsymbol{\lambda} = {}_{\mathrm{L}}^{n}\boldsymbol{\lambda}$ and ${}_{\mathrm{S}}^{n}\boldsymbol{\gamma} = {}_{\mathrm{L}}^{n}\boldsymbol{\gamma}$ for $n \leq t-1$
3. ${}_{\mathrm{L}}^{t}\boldsymbol{\gamma}^{\mathrm{T}} \frac{\partial {}_{\mathrm{L}}^{t}\boldsymbol{H}}{\partial s} + {}_{\mathrm{L}}^{t+1}\boldsymbol{\gamma}^{\mathrm{T}} \frac{\partial {}_{\mathrm{L}}^{t+1}\boldsymbol{H}}{\partial s} = {}_{\mathrm{S}}^{t+1}\boldsymbol{\gamma}^{\mathrm{T}} \frac{\partial {}_{\mathrm{S}}^{t+1}\boldsymbol{H}}{\partial s}$

Since step t is elastic, the first item is directly obtained from Property 1. in Section 5.2.

For the second item, firstly, show that it holds for $n = t-1$. Using the assumption in Eq.(5.1), it follows from Eq.(4.36) that

$$
{}_{\mathrm{L}}^{t-1}\boldsymbol{\lambda} = {}_{\mathrm{L}}^{t-1}\boldsymbol{K}_{\mathrm{T}}{}^{-1} \cdot \left(\frac{\partial {}_{\mathrm{L}}^{t-1}\boldsymbol{H}}{\partial \boldsymbol{U}}^{\mathrm{T}} \frac{\partial {}_{\mathrm{L}}^{t-1}\boldsymbol{H}}{\partial \boldsymbol{V}}^{-\mathrm{T}} \frac{\partial {}_{\mathrm{L}}^{t}\boldsymbol{H}}{\partial \boldsymbol{V}}^{\mathrm{T}} {}_{\mathrm{L}}^{t}\boldsymbol{\gamma} - \frac{\partial {}_{\mathrm{L}}^{t}\boldsymbol{H}}{\partial \boldsymbol{U}}^{\mathrm{T}} {}_{\mathrm{L}}^{t}\boldsymbol{\gamma} \right) \tag{5.21}
$$

By utilizing Eq.(5.16) and substituting the terms on the right-hand side with quantities from the load sequence S, it obtains

$$
{}_{\mathrm{L}}^{t-1}\boldsymbol{\lambda} = {}_{\mathrm{S}}^{t-1}\boldsymbol{K}_{\mathrm{T}}{}^{-1} \cdot \left(\frac{\partial {}_{\mathrm{S}}^{t-1}\boldsymbol{H}}{\partial \boldsymbol{U}}^{\mathrm{T}} \frac{\partial {}_{\mathrm{S}}^{t-1}\boldsymbol{H}}{\partial \boldsymbol{V}}^{-\mathrm{T}} \frac{\partial {}_{\mathrm{L}}^{t}\boldsymbol{H}}{\partial \boldsymbol{V}}^{\mathrm{T}} {}_{\mathrm{L}}^{t}\boldsymbol{\gamma} - \frac{\partial {}_{\mathrm{L}}^{t}\boldsymbol{H}}{\partial \boldsymbol{U}}^{\mathrm{T}} {}_{\mathrm{L}}^{t}\boldsymbol{\gamma} \right) \tag{5.22}
$$

Due to the assumption in Eq.(5.1) and ${}_{\mathrm{L}}^{t}\boldsymbol{\lambda} = 0$, it gets from Eq. (4.36) that

$$
{}_{\mathrm{L}}^{t}\boldsymbol{\gamma} = -\frac{\partial {}_{\mathrm{L}}^{t}\boldsymbol{H}}{\partial^{t}\boldsymbol{V}}^{-\mathrm{T}} \frac{\partial {}_{\mathrm{L}}^{t+1}\boldsymbol{H}}{\partial^{t}\boldsymbol{V}}^{\mathrm{T}} {}_{\mathrm{L}}^{t+1}\boldsymbol{\gamma} \tag{5.23}
$$

By substituting Eqs.(4.23), (4.24), (4.28) into Eq.(5.23) and using Eq.(5.14), it has

$$ {}^{t}_{\mathrm{L}}\boldsymbol{\gamma} = \begin{pmatrix} \boldsymbol{I} & 0 \\ {}^{t}\mathbf{a}^{\mathrm{T}}\boldsymbol{D}^{\mathrm{e}} & -1 \end{pmatrix} \begin{pmatrix} \boldsymbol{I} & 0 \\ {}^{t+1}\mathbf{a}^{\mathrm{T}}\boldsymbol{D}^{\mathrm{e}} & c \end{pmatrix} {}^{t+1}_{\mathrm{S}}\boldsymbol{\gamma} = \begin{pmatrix} \boldsymbol{I} & 0 \\ ({}^{t}\mathbf{a}^{\mathrm{T}} - {}^{t+1}\mathbf{a}^{\mathrm{T}})\boldsymbol{D}^{\mathrm{e}} & -c \end{pmatrix} {}^{t+1}_{\mathrm{S}}\boldsymbol{\gamma} \tag{5.24} $$

where c equals -1 if step *t+1* is elastic and c equals 0 if step *t+1* is plastic.

When step t is skipped, step *t-1* and step *t+1* become adjacent. Therefore, according to Eqs.(4.24) and (5.24), it follows

$$ \frac{\partial {}^{t}_{\mathrm{L}}\boldsymbol{H}}{\partial {}^{t-1}\boldsymbol{V}}^{\mathrm{T}} {}^{t}_{\mathrm{L}}\boldsymbol{\gamma} = \begin{pmatrix} \boldsymbol{I} & 0 \\ {}^{t}\mathbf{a}^{\mathrm{T}}\boldsymbol{D}^{\mathrm{e}} & -1 \end{pmatrix} \begin{pmatrix} \boldsymbol{I} & 0 \\ ({}^{t}\mathbf{a}^{\mathrm{T}} - {}^{t+1}\mathbf{a}^{\mathrm{T}})\boldsymbol{D}^{\mathrm{e}} & -c \end{pmatrix} {}^{t+1}_{\mathrm{S}}\boldsymbol{\gamma} = \begin{pmatrix} \boldsymbol{I} & 0 \\ {}^{t+1}\mathbf{a}^{\mathrm{T}}\boldsymbol{D}^{\mathrm{e}} & c \end{pmatrix} {}^{t+1}_{\mathrm{S}}\boldsymbol{\gamma} = \frac{\partial {}^{t+1}_{\mathrm{S}}\boldsymbol{H}}{\partial {}^{t-1}\boldsymbol{V}}^{\mathrm{T}} {}^{t+1}_{\mathrm{S}}\boldsymbol{\gamma} \tag{5.25} $$

According to Eqs. (4.21) and (5.24), it follows that

$$ \begin{aligned} \frac{\partial {}^{t}_{\mathrm{L}}\boldsymbol{H}}{\partial {}^{t-1}\boldsymbol{U}}^{\mathrm{T}} {}^{t}_{\mathrm{L}}\boldsymbol{\gamma} &= -({}^{t-1}\boldsymbol{B}^{\mathrm{T}}\boldsymbol{D}^{\mathrm{e}} \quad 0) \begin{pmatrix} \boldsymbol{I} & 0 \\ ({}^{t}\mathbf{a}^{\mathrm{T}} - {}^{t+1}\mathbf{a}^{\mathrm{T}})\boldsymbol{D}^{\mathrm{e}} & -c \end{pmatrix} {}^{t+1}_{\mathrm{S}}\boldsymbol{\gamma} \\ &= -({}^{t-1}\boldsymbol{B}^{\mathrm{T}}\boldsymbol{D}^{\mathrm{e}} \quad 0) {}^{t+1}_{\mathrm{S}}\boldsymbol{\gamma} = \frac{\partial {}^{t+1}_{\mathrm{S}}\boldsymbol{H}}{\partial {}^{t-1}\boldsymbol{U}}^{\mathrm{T}} {}^{t+1}_{\mathrm{S}}\boldsymbol{\gamma} \end{aligned} \tag{5.26} $$

By substituting Eqs.(5.25) and (5.26) into Eq.(5.22), and using Eq.(4.36), it obtains

$$ {}^{t-1}_{\mathrm{L}}\boldsymbol{\lambda} = {}^{t-1}_{\mathrm{S}}\boldsymbol{K}_{\mathrm{T}}^{-1} \cdot \left(\frac{\partial {}^{t-1}_{\mathrm{S}}\boldsymbol{H}}{\partial {}^{t-1}\boldsymbol{U}}^{\mathrm{T}} \frac{\partial {}^{t-1}_{\mathrm{S}}\boldsymbol{H}}{\partial {}^{t-1}\boldsymbol{V}}^{-\mathrm{T}} \frac{\partial {}^{t+1}_{\mathrm{S}}\boldsymbol{H}}{\partial {}^{t-1}\boldsymbol{V}}^{\mathrm{T}} - \frac{\partial {}^{t+1}_{\mathrm{S}}\boldsymbol{H}}{\partial {}^{t-1}\boldsymbol{U}}^{\mathrm{T}} \right) {}^{t+1}_{\mathrm{S}}\boldsymbol{\gamma} = {}^{t-1}_{\mathrm{S}}\boldsymbol{\lambda} \tag{5.27} $$

Using the assumption in Eq. (5.1), it follows from Eq. (4.36) that

$$ {}^{t-1}_{\mathrm{L}}\boldsymbol{\gamma} = -\frac{\partial {}^{t-1}_{\mathrm{L}}\boldsymbol{H}}{\partial {}^{t-1}\boldsymbol{V}}^{-\mathrm{T}} \cdot \left(\frac{\partial {}^{t}_{\mathrm{L}}\boldsymbol{H}}{\partial {}^{t-1}\boldsymbol{V}}^{\mathrm{T}} {}^{t}_{\mathrm{L}}\boldsymbol{\gamma} + \frac{\partial {}^{t-1}_{\mathrm{L}}\boldsymbol{R}}{\partial {}^{t-1}\boldsymbol{V}}^{\mathrm{T}} {}^{t-1}_{\mathrm{L}}\boldsymbol{\lambda} \right) \tag{5.28} $$

Finally, using Eqs.(5.16), (5.25), (5.27) and replacing terms on the right-hand side by quantities in the load sequence S, it gets

$$ {}^{t-1}_{\mathrm{L}}\boldsymbol{\gamma} = -\frac{\partial {}^{t-1}_{\mathrm{S}}\boldsymbol{H}}{\partial {}^{t-1}\boldsymbol{V}}^{-\mathrm{T}} \cdot \left(\frac{\partial {}^{t+1}_{\mathrm{S}}\boldsymbol{H}}{\partial {}^{t-1}\boldsymbol{V}}^{\mathrm{T}} {}^{t+1}_{\mathrm{S}}\boldsymbol{\gamma} + \frac{\partial {}^{t-1}_{\mathrm{S}}\boldsymbol{R}}{\partial {}^{t-1}\boldsymbol{V}}^{\mathrm{T}} {}^{t-1}_{\mathrm{S}}\boldsymbol{\lambda} \right) = {}^{t-1}_{\mathrm{S}}\boldsymbol{\gamma} \tag{5.29} $$

From Eqs.(5.27) and (5.29) at step *t-1*, it easily gets

$$ {}^{n}_{\mathrm{S}}\boldsymbol{\lambda} = {}^{n}_{\mathrm{L}}\boldsymbol{\lambda} \ \text{ and } \ {}^{n}_{\mathrm{S}}\boldsymbol{\gamma} = {}^{n}_{\mathrm{L}}\boldsymbol{\gamma} \ \ (for\ n \le t-2) \tag{5.30} $$

Thirdly, from Eqs.(4.22), (5.14) and (5.24), it gets

$$ \begin{aligned} &{}^{t}_{\mathrm{L}}\boldsymbol{\gamma}^{\mathrm{T}} \frac{\partial {}^{t}_{\mathrm{L}}\boldsymbol{H}}{\partial s} + {}^{t+1}_{\mathrm{L}}\boldsymbol{\gamma}^{\mathrm{T}} \frac{\partial {}^{t+1}_{L}\boldsymbol{H}}{\partial s} \\ &\quad = {}^{t+1}_{\mathrm{S}}\boldsymbol{\gamma}^{\mathrm{T}} \begin{pmatrix} \boldsymbol{I} & \boldsymbol{D}^{\mathrm{e}}({}^{t}\mathbf{a} - {}^{t+1}\mathbf{a}) \\ \mathbf{0} & -c \end{pmatrix} \begin{pmatrix} \boldsymbol{D}^{\mathrm{e}}\left(\frac{\partial {}^{t}\boldsymbol{\varepsilon}}{\partial s} - \frac{\partial {}^{t-1}\boldsymbol{\varepsilon}}{\partial s}\right) \\ 0 \end{pmatrix} + {}^{t+1}_{\mathrm{S}}\boldsymbol{\gamma}^{\mathrm{T}} \begin{pmatrix} \boldsymbol{D}^{\mathrm{e}}\left(\frac{\partial {}^{t+1}\boldsymbol{\varepsilon}}{\partial s} - \frac{\partial {}^{t}\boldsymbol{\varepsilon}}{\partial s}\right) \\ 0 \end{pmatrix} \\ &\quad = {}^{t+1}_{\mathrm{S}}\boldsymbol{\gamma}^{\mathrm{T}} \begin{pmatrix} \boldsymbol{D}^{\mathrm{e}}\left(\frac{\partial {}^{t+1}\boldsymbol{\varepsilon}}{\partial s} - \frac{\partial {}^{t-1}\boldsymbol{\varepsilon}}{\partial s}\right) \\ 0 \end{pmatrix} = {}^{t+1}_{\mathrm{S}}\boldsymbol{\gamma}^{\mathrm{T}} \frac{\partial {}^{t}_{\mathrm{S}}\boldsymbol{H}}{\partial s} \end{aligned} \tag{5.31} $$

The proof of the three items is concluded here.

□

To reduce a plastic load step *t*, the following rule is proposed and proven.

Plastic load step reduction rule: Given a sequence of load steps L = {1, 2, ..., t-1, t, t+1, ..., N}, if step *t* and step *t+1* are both plastic load steps, ${}^{t}\mathbf{a} = {}^{t+1}\mathbf{a}$ and $\frac{\mathrm{d}\,{}^{t}\mathbf{a}}{\mathrm{d}\,{}^{t}\boldsymbol{\sigma}} = 0$, then skip step *t* as the load steps contains only S = {1, 2, ..., t-1, t+1, ..., N} will not change the sensitivity results.

Proof:

The same as the previous proof, it is suffice to show

1. ${}^{t}_{\mathrm{L}}\boldsymbol{\lambda} = 0$
2. ${}^{n}_{\mathrm{S}}\boldsymbol{\lambda} = {}^{n}_{\mathrm{L}}\boldsymbol{\lambda}$ and ${}^{n}_{\mathrm{S}}\boldsymbol{\gamma} = {}^{n}_{\mathrm{L}}\boldsymbol{\gamma}$ for $n \le t-1$
3. ${}^{t}_{\mathrm{L}}\boldsymbol{\gamma}^{\mathrm{T}} \frac{\partial {}^{t}_{\mathrm{L}}\boldsymbol{H}}{\partial s} + {}^{t+1}_{\mathrm{L}}\boldsymbol{\gamma}^{\mathrm{T}} \frac{\partial {}^{t+1}_{\mathrm{L}}\boldsymbol{H}}{\partial s} = {}^{t+1}_{\mathrm{S}}\boldsymbol{\gamma}^{\mathrm{T}} \frac{\partial {}^{t+1}_{\mathrm{S}}\boldsymbol{H}}{\partial s}$

The first item is directly obtained from the Property 2 in Section 5.2.

For the second item, firstly show that it holds for *n=t-1*. Obviously, Eq.(5.22) still holds here

$$ {}^{t-1}_{\mathrm{L}}\boldsymbol{\lambda} = {}^{t-1}_{\mathrm{S}}\boldsymbol{K}_{\mathrm{T}}{}^{-1} \cdot \left(\frac{\partial {}^{t-1}_{\mathrm{S}}\boldsymbol{H}}{\partial {}^{t-1}\boldsymbol{U}}^{\mathrm{T}} \frac{\partial {}^{t-1}_{\mathrm{S}}\boldsymbol{H}}{\partial {}^{t-1}\boldsymbol{V}}^{-\mathrm{T}} \frac{\partial {}^{t}_{\mathrm{L}}\boldsymbol{H}}{\partial {}^{t-1}\boldsymbol{V}}^{\mathrm{T}} {}^{t}_{\mathrm{L}}\boldsymbol{\gamma} - \frac{\partial {}^{t}_{\mathrm{L}}\boldsymbol{H}}{\partial {}^{t-1}\boldsymbol{U}}^{\mathrm{T}} {}^{t}_{\mathrm{L}}\boldsymbol{\gamma} \right) \tag{5.32} $$

Using Eq.(4.21) and Property 2 in Section 5.2, it follows

$$\frac{\partial {}^{t}_{\mathrm{L}}\boldsymbol{H}}{\partial {}^{t-1}\boldsymbol{U}}^{\mathrm{T}} {}^{t}_{\mathrm{L}}\boldsymbol{\gamma} = -\begin{pmatrix} {}^{t-1}\boldsymbol{B}^{\mathrm{T}}\boldsymbol{D}^{\mathrm{e}} & 0 \end{pmatrix}\begin{pmatrix} {}^{t+1}_{\mathrm{S}}\boldsymbol{\gamma}_{\boldsymbol{\sigma}} \\ 0 \end{pmatrix} = -\begin{pmatrix} {}^{t-1}\boldsymbol{B}^{\mathrm{T}}\boldsymbol{D}^{\mathrm{e}} & 0 \end{pmatrix}\begin{pmatrix} {}^{t+1}_{\mathrm{S}}\boldsymbol{\gamma}_{\boldsymbol{\sigma}} \\ {}^{t+1}_{\mathrm{S}}\boldsymbol{\gamma}_{\varepsilon^{\mathrm{p}}_{\mathrm{eqv}}} \end{pmatrix} = \frac{\partial {}^{t+1}_{\mathrm{S}}\boldsymbol{H}}{\partial {}^{t-1}\boldsymbol{U}}^{\mathrm{T}} {}^{t+1}_{\mathrm{S}}\boldsymbol{\gamma} \tag{5.33}$$

According to Eq.(4.28) and the assumption of ${}^{t}\mathbf{a} = {}^{t+1}\mathbf{a}$, it has

$$\frac{\partial {}^{t}_{\mathrm{L}}\boldsymbol{H}}{\partial {}^{t-1}\boldsymbol{V}}^{\mathrm{T}} = \begin{pmatrix} \boldsymbol{I} & 0 \\ {}^{t+1}\mathbf{a}^{\mathrm{T}}\boldsymbol{D}^{\mathrm{e}} & 0 \end{pmatrix} \tag{5.34}$$

Using Property 2 in Section 5.2, it follows

$$\frac{\partial {}^{t}_{\mathrm{L}}\boldsymbol{H}}{\partial {}^{t-1}\boldsymbol{V}}^{\mathrm{T}} {}^{t}_{\mathrm{L}}\boldsymbol{\gamma} = \begin{pmatrix} \boldsymbol{I} & 0 \\ {}^{t+1}\mathbf{a}^{\mathrm{T}}\boldsymbol{D}^{\mathrm{e}} & 0 \end{pmatrix}\begin{pmatrix} {}^{t+1}_{\mathrm{S}}\boldsymbol{\gamma}_{\boldsymbol{\sigma}} \\ 0 \end{pmatrix} = \begin{pmatrix} \boldsymbol{I} & 0 \\ {}^{t+1}\mathbf{a}^{\mathrm{T}}\boldsymbol{D}^{\mathrm{e}} & 0 \end{pmatrix}\begin{pmatrix} {}^{t+1}_{\mathrm{S}}\boldsymbol{\gamma}_{\boldsymbol{\sigma}} \\ {}^{t+1}_{\mathrm{S}}\boldsymbol{\gamma}_{\varepsilon^{\mathrm{p}}_{\mathrm{eqv}}} \end{pmatrix} = \frac{\partial {}^{t+1}_{\mathrm{S}}\boldsymbol{H}}{\partial {}^{t-1}\boldsymbol{V}}^{\mathrm{T}} {}^{t+1}_{\mathrm{S}}\boldsymbol{\gamma} \tag{5.35}$$

By substituting Eqs.(5.32) and (5.35) into Eq.(5.32) and using Eq.(4.36), it obtains

$${}^{t-1}_{\mathrm{L}}\boldsymbol{\lambda} = {}^{t-1}_{\mathrm{S}}\boldsymbol{K}_{\mathrm{T}}{}^{-1} \cdot \left(\frac{\partial {}^{t-1}_{\mathrm{S}}\boldsymbol{H}}{\partial {}^{t-1}\boldsymbol{U}}^{\mathrm{T}} \frac{\partial {}^{t-1}_{\mathrm{S}}\boldsymbol{H}}{\partial {}^{t-1}\boldsymbol{V}}^{-\mathrm{T}} \frac{\partial {}^{t+1}_{\mathrm{S}}\boldsymbol{H}}{\partial {}^{t-1}\boldsymbol{V}}^{\mathrm{T}} - \frac{\partial {}^{t+1}_{\mathrm{S}}\boldsymbol{H}}{\partial {}^{t-1}\boldsymbol{U}}^{\mathrm{T}} \right) {}^{t+1}_{\mathrm{S}}\boldsymbol{\gamma} = {}^{t-1}_{\mathrm{S}}\boldsymbol{\lambda} \tag{5.36}$$

Using the assumption in Eq.(5.1), it follows from Eq.(4.36) that

$${}^{t-1}_{\mathrm{L}}\boldsymbol{\gamma} = -\frac{\partial {}^{t-1}_{\mathrm{L}}\boldsymbol{H}}{\partial {}^{t-1}\boldsymbol{V}}^{-\mathrm{T}} \cdot \left(\frac{\partial {}^{t}_{\mathrm{L}}\boldsymbol{H}}{\partial {}^{t-1}\boldsymbol{V}}^{\mathrm{T}} {}^{t}_{\mathrm{L}}\boldsymbol{\gamma} + \frac{\partial {}^{t-1}_{\mathrm{L}}\boldsymbol{R}}{\partial {}^{t-1}\boldsymbol{V}}^{\mathrm{T}} {}^{t-1}_{\mathrm{L}}\boldsymbol{\lambda} \right) \tag{5.37}$$

Finally, using Eqs.(5.16), (5.35), (5.36) and replacing terms on the right-hand side by quantities in the load sequence S, it obtains

$${}^{t-1}_{\mathrm{L}}\boldsymbol{\gamma} = -\frac{\partial {}^{t-1}_{\mathrm{S}}\boldsymbol{H}}{\partial {}^{t-1}\boldsymbol{V}}^{-\mathrm{T}} \cdot \left(\frac{\partial {}^{t+1}_{\mathrm{S}}\boldsymbol{H}}{\partial {}^{t-1}\boldsymbol{V}}^{\mathrm{T}} {}^{t+1}_{\mathrm{S}}\boldsymbol{\gamma} + \frac{\partial {}^{t-1}_{\mathrm{S}}\boldsymbol{R}}{\partial {}^{t-1}\boldsymbol{V}}^{\mathrm{T}} {}^{t-1}_{\mathrm{S}}\boldsymbol{\lambda} \right) = {}^{t-1}_{\mathrm{S}}\boldsymbol{\gamma} \tag{5.38}$$

From Eqs.(5.36) and (5.38) at step *t-1*, it easily gets

$${}^{n}_{\mathrm{S}}\boldsymbol{\lambda} = {}^{n}_{\mathrm{L}}\boldsymbol{\lambda} \text{ and } {}^{n}_{\mathrm{S}}\boldsymbol{\gamma} = {}^{n}_{\mathrm{L}}\boldsymbol{\gamma} \ \ (for\ n \le t-2) \tag{5.39}$$

Lastly, according to the Property 2 in Section 5.2 and ${}^{t+1}_{\mathrm{L}}\boldsymbol{\gamma} = {}^{t+1}_{\mathrm{S}}\boldsymbol{\gamma}$, the third item is proven by

$$
\begin{aligned}
{}_{\mathrm{L}}^{t}\boldsymbol{\gamma}^{\mathrm{T}}\frac{\partial\,{}_{\mathrm{L}}^{t}\boldsymbol{H}}{\partial s}+{}_{\mathrm{L}}^{t+1}\boldsymbol{\gamma}^{\mathrm{T}}\frac{\partial\,{}_{\mathrm{L}}^{t+1}\boldsymbol{H}}{\partial s}&=\begin{pmatrix}{}_{\mathrm{S}}^{t+1}\boldsymbol{\gamma}_{\boldsymbol{\sigma}}\\0\end{pmatrix}^{\mathrm{T}}\begin{pmatrix}\boldsymbol{D}^{\mathrm{e}}\left(\frac{\partial^{t}\boldsymbol{\varepsilon}}{\partial s}-\frac{\partial^{t-1}\boldsymbol{\varepsilon}}{\partial s}\right)\\0\end{pmatrix}+\begin{pmatrix}{}_{\mathrm{S}}^{t+1}\boldsymbol{\gamma}_{\boldsymbol{\sigma}}\\{}_{\mathrm{S}}^{t+1}\boldsymbol{\gamma}_{\varepsilon_{\mathrm{eqv}}^{\mathrm{p}}}\end{pmatrix}^{\mathrm{T}}\begin{pmatrix}\boldsymbol{D}^{\mathrm{e}}\left(\frac{\partial^{t+1}\boldsymbol{\varepsilon}}{\partial s}-\frac{\partial^{t}\boldsymbol{\varepsilon}}{\partial s}\right)\\0\end{pmatrix}\\
&=\begin{pmatrix}{}_{\mathrm{S}}^{t+1}\boldsymbol{\gamma}_{\boldsymbol{\sigma}}\\{}_{\mathrm{S}}^{t+1}\boldsymbol{\gamma}_{\varepsilon_{\mathrm{eqv}}^{\mathrm{p}}}\end{pmatrix}^{\mathrm{T}}\begin{pmatrix}\boldsymbol{D}^{\mathrm{e}}\left(\frac{\partial^{t+1}\boldsymbol{\varepsilon}}{\partial s}-\frac{\partial^{t-1}\boldsymbol{\varepsilon}}{\partial s}\right)\\0\end{pmatrix}={}_{\mathrm{S}}^{t+1}\boldsymbol{\gamma}^{\mathrm{T}}\frac{\partial\,{}_{\mathrm{S}}^{t}\boldsymbol{H}}{\partial s}
\end{aligned}
\tag{5.40}
$$

□

The elastic load step reduction rule is applicable to all types of elements. It theoretically proves that, in the adjoint sensitivity analysis, all intermediate elastic load steps can be skipped without losing accuracy.

The plastic load step reduction rule states that, for two consecutive plastic steps, the former plastic step can be skipped without changing the sensitivity results if two conditions are satisfied. The prerequisites include ${}^{t}\mathbf{a}={}^{t+1}\mathbf{a}$ and $\frac{\mathrm{d}\,{}^{t}\mathbf{a}}{\mathrm{d}\,{}^{t}\boldsymbol{\sigma}}=0$.

For a bar element undergoing tension or compression, the flow vector equals

$$
\mathbf{a}=\begin{cases}1 & \text{in tension}\\-1 & \text{in compression}\end{cases}
\tag{5.41}
$$

Hence, its derivative is equal to 0, i.e.

$$
\frac{\mathrm{d}\mathbf{a}}{\mathrm{d}\boldsymbol{\sigma}}=\mathbf{0}
\tag{5.42}
$$

Therefore, the two prerequisites could be strictly satisfied by bar elements when two adjacent plastic steps are both in tension or in compression. In such cases, sensitivity analysis following plastic reduction rule will yield the same results as using all load steps.

However, for general 3D elements with the von Mises yield criterion, $d\mathbf{a}/d\boldsymbol{\sigma}$ follows Eq.(2.28) and it is always non-zero. Therefore, the second prerequisite in the plastic load step reduction rule can't be satisfied. The same holds true for general 2D elements. Thus, the plastic reduction rule cannot be used directly.

The prerequisites in plastic case require that the flow vectors in two consecutive plastic steps remain constant. It is expected that if the flow

vectors do not change too much, the sensitivity results could still be valid. Therefore, the following empirical rule is proposed to reduce the plastic load steps in the sensitivity analysis with 2D and 3D elements.

Empirical rule: Given a sequence of load steps L = {1, 2, ..., t-1, t, t+1, …, N}, if step *t* and step *t+1* are in a monotonic loading stage, then step *t* could be skipped in the sensitivity analysis.

Sensitivity analysis following the empirical rule will not yield exact results. The effectiveness and influence on result accuracy will be investigated through numerical examples in Section 5.5 and 5.6.

5.4 Demonstration with a 100-bar truss structure

In this section, the presented load step reduction techniques are verified using the same 100-bar truss structure presented in Figure 4-1. The material properties and design variables are also consistent with those in Section 4.2.1. Three load cases are applied to the structure to demonstrate the reduction in load steps under different situations.

In the first load case, the vertical force at the free end of the structure follows a total of 35 load steps, as depicted in Figure 5-1. The load history could be divided into three stages: an initial stage with the load monotonically increasing from step 1 to step 12, followed by a partial unloading stage from step 13 to step 22, and finally, a reloading stage from step 23 to step 35. The force at the final step is greater than that in the intermediate steps. The green dots in Figure 5-1 represent elastic load steps in the nonlinear finite element analysis, while the red diamond points illustrate plastic load steps.

According to the reduction rule for elastic load steps, all the elastic load steps can be skipped in this example. For the plastic steps, since the load monotonically increases during the initial loading and the reloading stage, all bars maintain their status either in tension or in compression between two consecutive steps. According to the plastic reduction rule, the former one in each pair of consecutive plastic steps can be skipped. This results in only two steps, step 12 and step 35, remaining in the sensitivity analysis. Now, step 12 and step 35 become two consecutive plastic steps. They have the same load

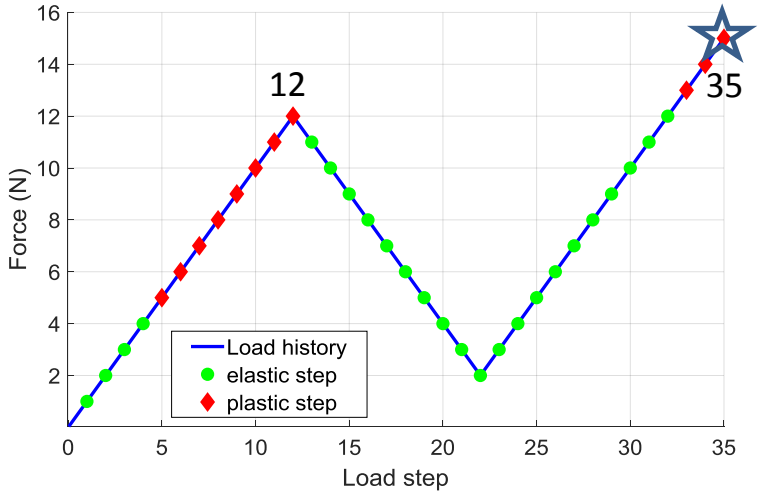

Figure 5-1. Load history of the first load case. The pentagram depicts the reduced load step in sensitivity analysis

direction, and hence there is no alternation of tension and compression for any bar element between these two steps. Therefore, step 12 can once again be skipped. Finally, only the last load step is needed in the sensitivity analysis, which is listed in Table 5-1 and highlighted by a pentagram in Figure 5-1.

Table 5-1. The reduced load step for load case 1 of the 100-bar truss example

Reduced load step	Corresponding FEA load step	Load (N)
1	35	15

The sensitivity result calculated with the reduced load step is compared with that employing all load steps in Figure 5-2. The two system responses considered are the vertical displacement at the free end and the maximum equivalent plastic strain at the fixed end.

To assess the accuracy of sensitivities, the relative value is defined as the ratio of sensitivity calculated using the reduced load steps to sensitivity calculated using all load steps:

$$\text{relative value} = \frac{\text{Sensitivity with reduced load steps}}{\text{Sensitivity with all load steps}} \tag{5.43}$$

The relative values are presented in the subfigures on the right. The results show that, for both responses, sensitivities with the reduced load step are the same as those obtained using all load steps.

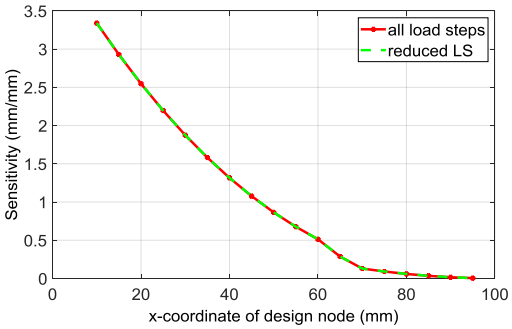

(a) Sensitivities of vertical displacement response in load case 1

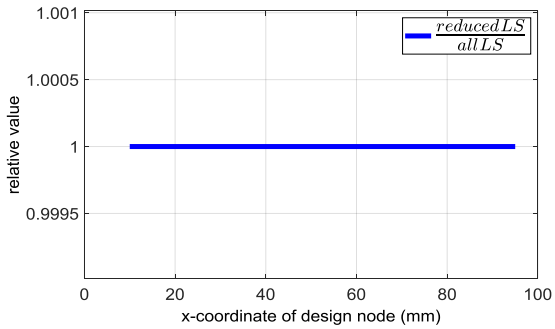

(b) Sensitivity relative value of vertical displacement response in load case 1

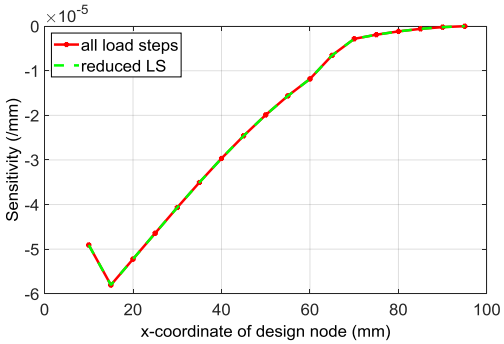

(c) Sensitivity of equivalent plastic strain response in load case 1

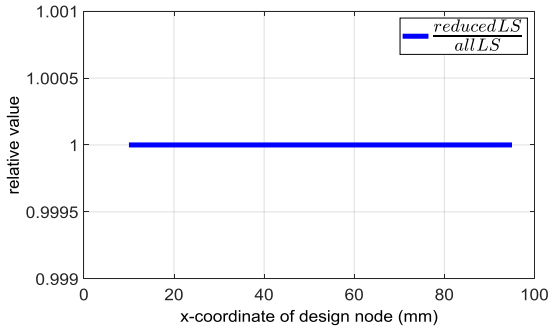

(d) Sensitivity relative value of equivalent plastic strain response in load case 1

Figure 5-2. Sensitivities comparison for load case 1 of the 100-bar truss example

In the second load case, the vertical force follows a total of 50 load steps, as depicted in Figure 5-3. The load history comprises four stages: initial loading from step 1 to step 10, complete unloading from step 11 to step 20, reverse loading in the opposite direction from step 21 to step 35, and finally, a fully unloading stage from step 36 to step 50. The maximum force of the load in the opposite direction is larger than that in the initial loading stage.

According to the load step reduction rules, all elastic steps, except the last one, can be skipped in the sensitivity analysis. Since the force monotonically increases during loading and reverse loading, the states of tension or compression remain unchanged for each bar in either stage. Hence, the former one in each pair of consecutive plastic steps can be skipped in the sensitivity analysis. Therefore, only plastic steps 10, 35, and elastic step 50 remain. Now, steps 10 and 35 are two consecutive plastic steps with opposite external force directions. Some bars change from tension to compression, and some change

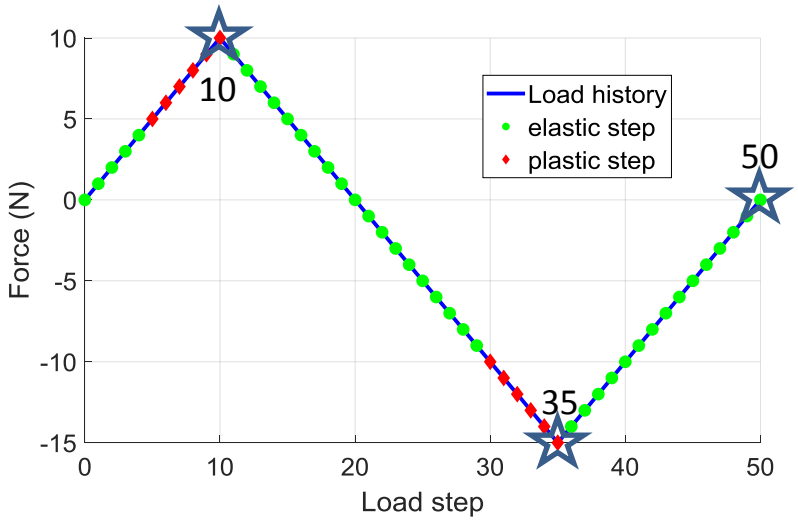

Figure 5-3. Load history of the second load case. Pentagrams depict the reduced load steps in sensitivity analysis

from compression to tension. Therefore, the former step 10 can't be skipped in this case. In summary, steps 10, 35, and 50 are needed in the sensitivity analysis. They are listed in Table 5-2 and highlighted in Figure 5-3 by pentagrams.

Table 5-2. Reduced load steps for load case 2 of the 100-bar truss example

Reduced load step	Corresponding FEA load step	Load (N)
1	10	10
2	35	-15
3	50	0

The sensitivity results are presented in Figure 5-4. The two system responses are the same as in load case 1. The results show that the sensitivities with reduced load steps match exactly with those obtained using all load steps.

In the third load case, a force with both horizontal and vertical components is applied at the free end. The load history is depicted in Figure 5-5. defining three stages: an initial loading stage from step 1 to step 5, horizontal unloading and vertical loading from step 6 to step 38, and finally, a vertically plastic loading stage from step 39 to step 50.

In the first stage, the stress state of bars is primarily influenced by the monotonically increasing extensional force in the horizontal direction. Consequently, there is no transition between tension and compression in bars.

Following the plastic load step reduction rule, the first four steps can be skipped. Applying the elastic load step reduction rule allows for the omission of all elastic steps in the sensitivity analysis.

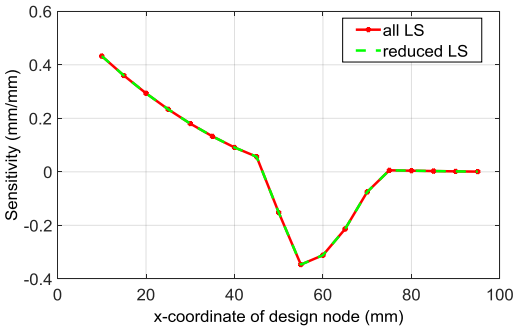

(a) Sensitivities of vertical displacement response in load case 2

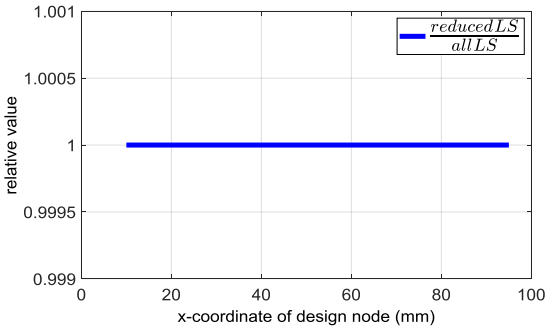

(b) Sensitivity relative value of vertical displacement response in load case 2

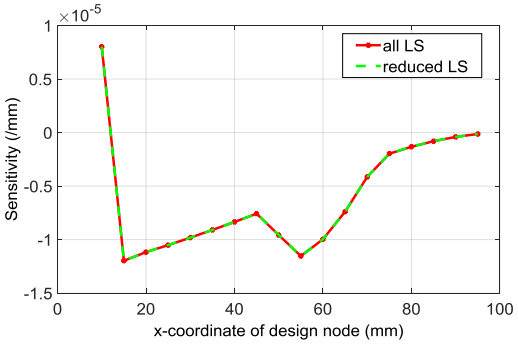

(d) Sensitivity of equivalent plastic strain response in load case 2

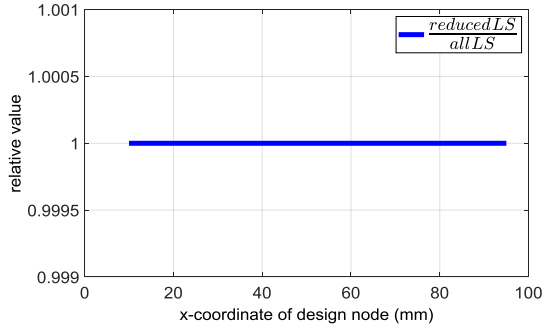

(e) Sensitivity relative value of equivalent plastic strain response in load case 2

Figure 5-4. Sensitivities comparison for load case 2 of the 100-bar truss example

In the last vertically plastic loading stage, tension or compression is determined by the bending moment caused by the vertical force. As the vertical force monotonically increases, all steps except the last one can be skipped in the sensitivity analysis. At this point, only steps 5 and 50 remain in the sensitivity analysis.

The horizontal force in step 5 induces tensional stress in all the bars. In step 50, the vertical force leads to bending deformation of the structure, resulting in some bars being in compression. Therefore, both steps 5 and 50 must be included in the sensitivity analysis.

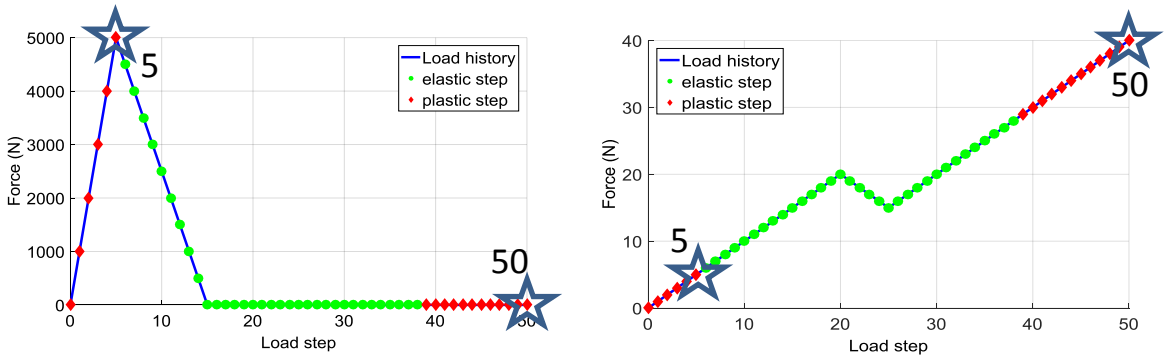

(a) Load history in horizontal x-direction (b) Load history in vertical y-direction

Figure 5-5. Load history of the third load case. Pentagrams depict the reduced load steps in sensitivity analysis

The reduced load steps are listed Table 5-3 and highlighted in Figure 5-5.

Table 5-3. Reduced load steps for load case 3 of the 100-bar truss example

Reduced load step	Corresponding FEA load step	Load (N)
1	5	Fx=5000, Fy=5
2	50	Fx=0, Fy=40

Sensitivities of the two system responses are evaluated, and the results are presented in Figure 5-6. It shows that the sensitivities with the reduced load steps match exactly with those obtained using all load steps.

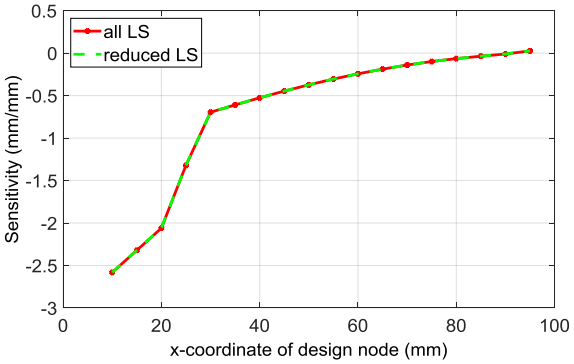

(a) Sensitivities of vertical displacement response in load case 3

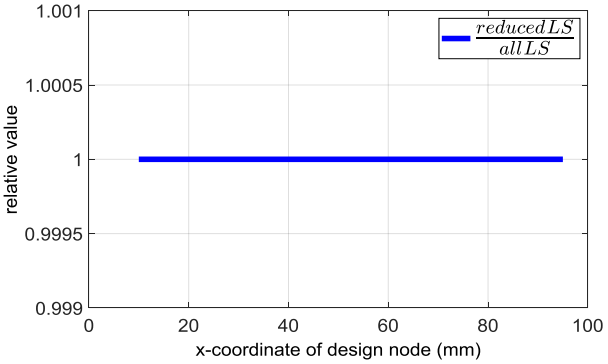

(b) Sensitivity relative value of vertical displacement response in load case 3

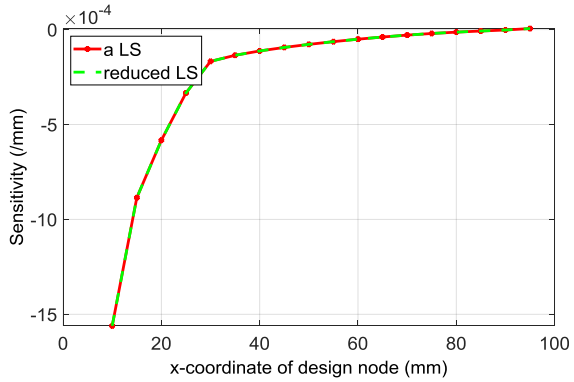

(c) Sensitivity of equivalent plastic strain response in load case 3

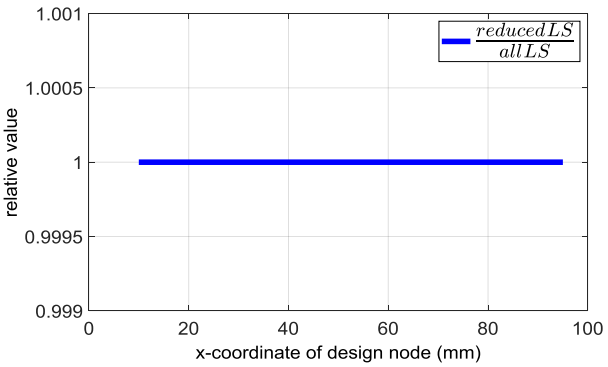

(d) Sensitivity relative value of equivalent plastic strain response in load case 3

Figure 5-6. Sensitivities comparison for load case 3 of the 100-bar truss example

5.5 Demonstration with a cantilever beam structure meshed with 3D solid elements

As discussed in Section 5.3, theoretically, plastic load steps of finite element systems with general 2D and 3D elements should not be skipped in the sensitivity analysis. However, the number of load steps can be significantly reduced by following the proposed empirical rule. Therefore, it is worth evaluating the inaccuracy that the empirical rule will introduce into the sensitivities. In this section, the load step reduction rules are demonstrated with a cantilever beam example meshed with 3D 4-node tetrahedral elements. The accuracy of sensitivities will be quantified.

The structure is the same as in Figure 4-5, including material properties and design variables. Three typical load cases are applied on the structure. Both geometric nonlinearity and small strain elastoplasticity are considered.

The first load case is depicted in Figure 5-7, where the load history is composed of three stages: the initial loading stage from step 1 to step 5, the unloading stage from step 6 to step 8, and the reloading stage from step 9 to step 16. In this example, the average vertical displacement at the free end and the maximum equivalent plastic strain at the fixed end are the two system responses.

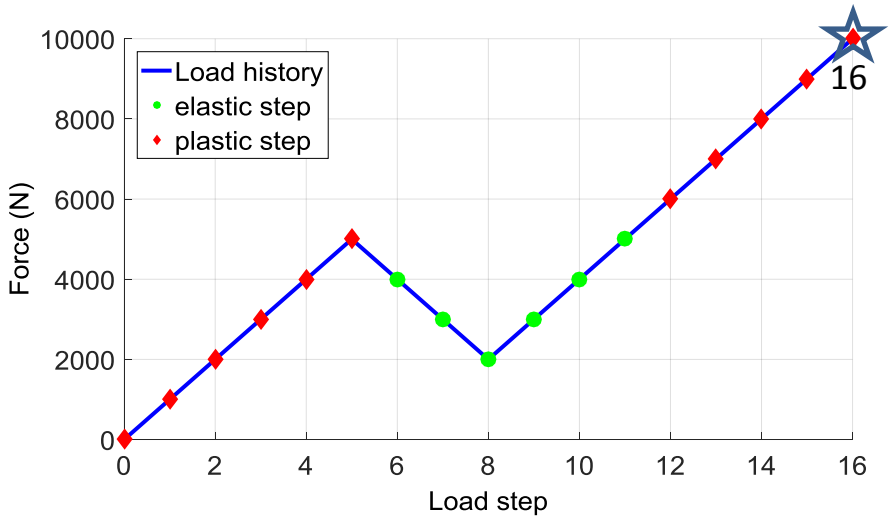

Figure 5-7. Load history of load case 1 for the cantilever beam example. The pentagram depicts the reduced load step

This load history is similar to the load case 1 in Section 5.4. Following the elastic load step reduction rule and the empirical rule for plastic steps, only the last load step is left in the sensitivity analysis. The reduced load step is listed in Table 5-4 and highlighted with a pentagram in Figure 5-7.

Table 5-4. Reduced load step for load case 1 of 3D cantilever beam example

Reduced load step	Corresponding FEA load step	Load (N)
1	16	10000

Sensitivities calculated with the reduced load step are compared in Figure 5-8, with those calculated using all load steps, from both real and relative value perspectives.

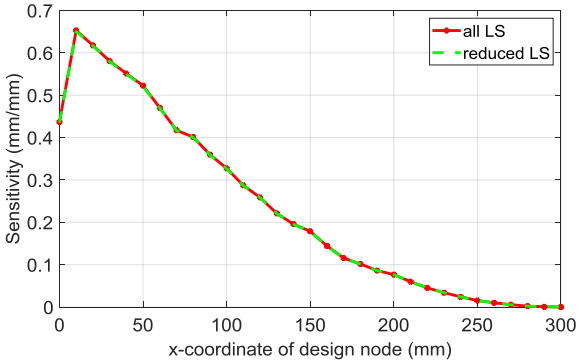

(a)Sensitivities of the vertical displacement response in load case 1

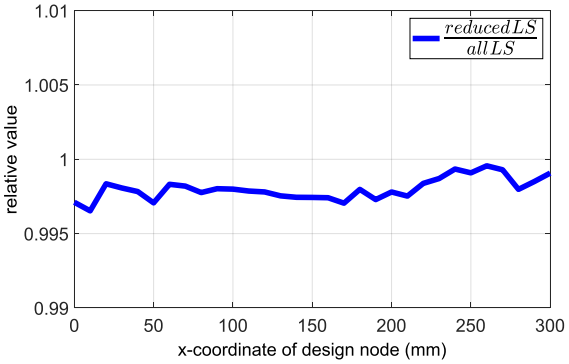

(b) Sensitivity relative value of vertical displacement response in load case 1

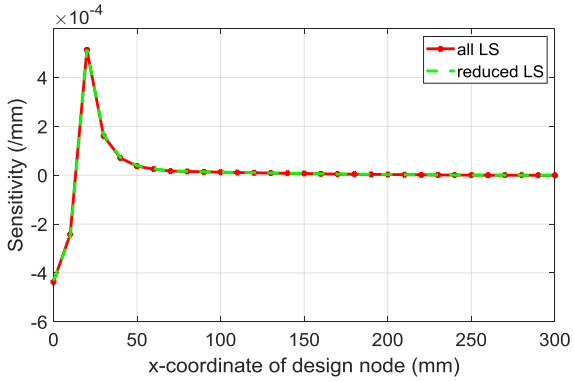

(c) Sensitivity of equivalent plastic strain response in load case 1

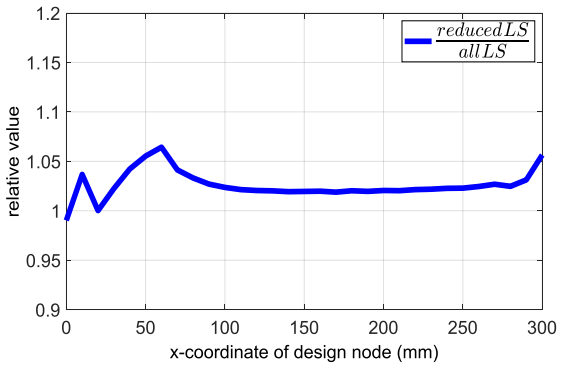

(d) Sensitivity relative value of equivalent plastic strain response in load case 1

Figure 5-8. Sensitivity comparison for load case 1 of 3D cantilever beam example

From a real value point of view, it shows that the sensitivities with the reduced load step match well with those using all load steps. From a relative value point of view, sensitivities with a reduced load step have errors of less than 0.5% for the displacement response. The error of sensitivities for the equivalent plastic strain response is 3% on average, with a maximum of 7%.

The second load case is illustrated in Figure 5-9, where the load history comprises loading, unloading, reverse loading, and unloading stages. By excluding monotonic plastic load steps and elastic steps, plastic step 4, plastic step 14, and elastic step 20 remain in the sensitivity analysis. It is important to note that, even though steps 4 and 14 are consecutive, they experience force in opposite directions. The load history progresses from 0N to 4000N (step 4) and then to -6000N (step 14), making it non-monotonic. Consequently, both

steps must be included in the sensitivity analysis. The three reduced load steps are listed in Table 5-5 and highlighted with pentagrams in Figure 5-9.

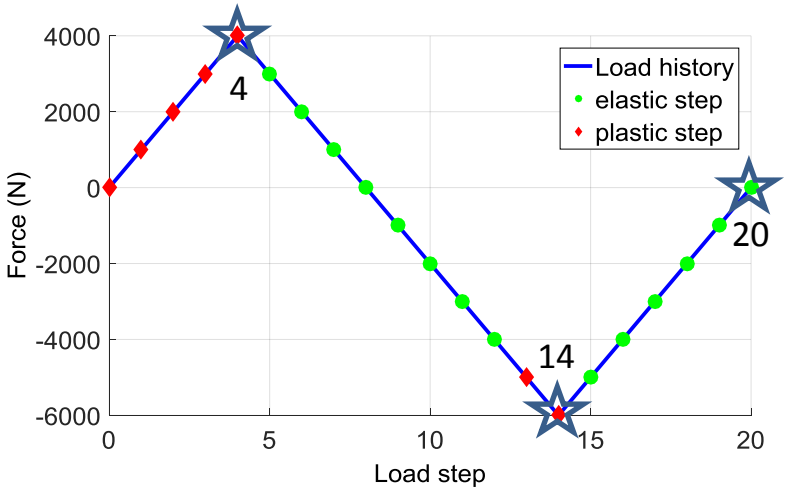

Figure 5-9. Load history of load case 2 for the cantilever beam example. Pentagrams depict the reduced load step

Table 5-5. Reduced load steps for load case 2 of 3D cantilever beam example

Reduced load step	Corresponding FEA load step	Load (N)
1	4	4000
2	14	-6000
3	20	0

The sensitivities results are compared with those using full load steps in Figure 5-10.

The results indicate a good match between sensitivities obtained with reduced load steps and those obtained with all load steps from a real-value perspective. Errors in sensitivities for the displacement response average 2%, while errors in sensitivities for equivalent plastic strain response average 3.5%. The change in force direction during loading and reverse loading stages results in a more significant alteration of flow vectors. This more pronounced change in flow vectors leads to an increase in errors following the empirical rule.

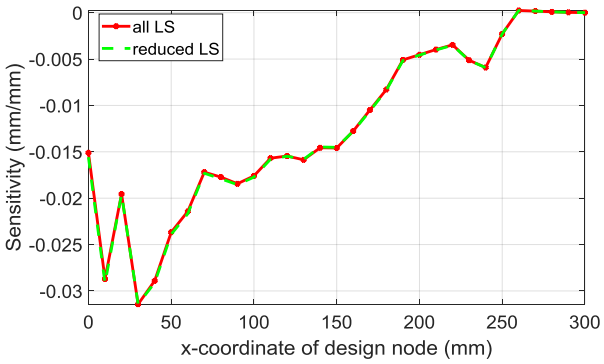

(a) Sensitivities of the vertical displacement response in load case 2

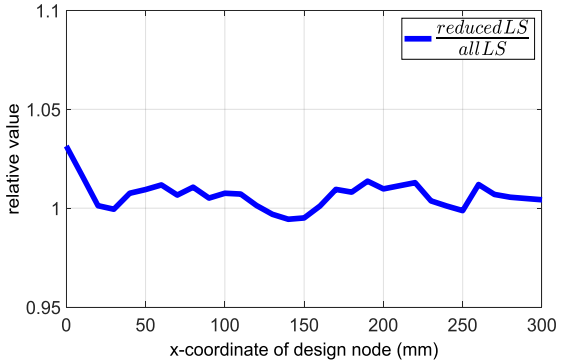

(b) Sensitivity relative value of vertical displacement response in load case 2

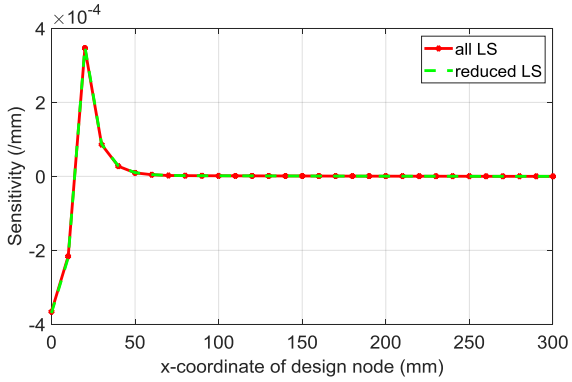

(c) Sensitivity of equivalent plastic strain response in load case 2

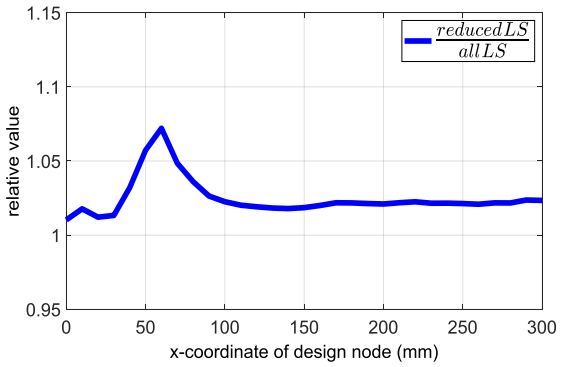

(d) Sensitivity relative value of equivalent plastic strain response in load case 2

Figure 5-10. Sensitivity comparison for load case 2 of 3D solid beam example

To demonstrate the necessity of load step 4 in sensitivity analysis, two situations are discussed. In one scenario, step 4 is skipped in the sensitivity analysis, meaning only steps 14 and 20 are considered, as shown in Figure 5-11(a). The resulting vertical displacement sensitivities are presented in Figure 5-11(b). Clearly, if step 4 is omitted, the sensitivity results are entirely incorrect.

In another scenario, step 3 is employed in the sensitivity analysis instead of step 4, as illustrated in Figure 5-12(a). The vertical displacement sensitivities obtained are presented in Figure 5-12(b). Clearly, the sensitivity results are also entirely incorrect.

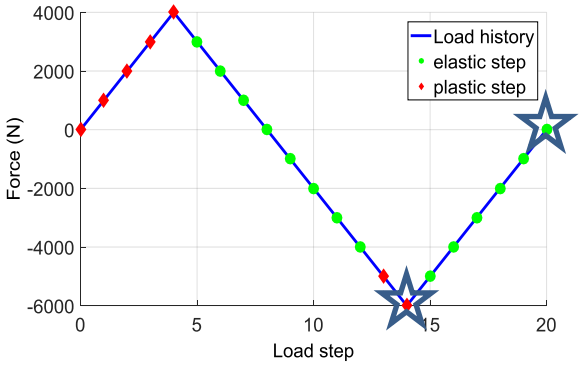

(a) Reduced load steps with step 4 being skipped

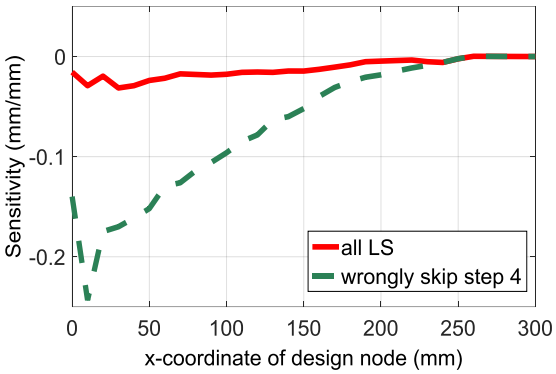

(b) Sensitivity of the vertical displacement response

Figure 5-11. Sensitivity results if load step 4 is wrongly skipped in load case 2

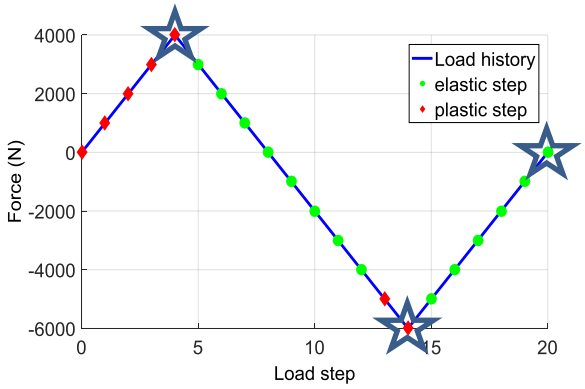

(a) Reduced load steps with step 3 instead of step 4

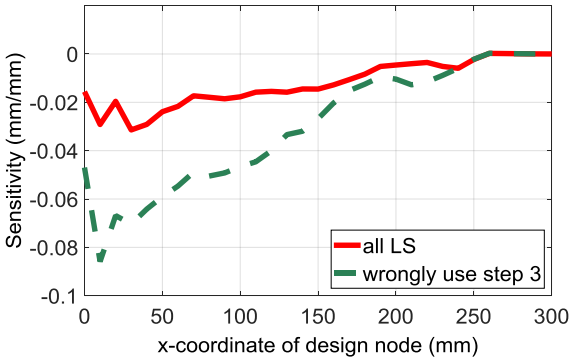

(b) Sensitivity of the vertical displacement response

Figure 5-12. Sensitivity results if step 3 is included instead of step 4

The two situations mentioned above demonstrate that the load step reduction rules proposed in Section 5.3 are not only sufficient for obtaining accurate sensitivity results but also necessary. Adhering to these rules is essential, as skipping load steps that violate these principles will result in inaccurate outcomes.

The third load case on the cantilever beam is depicted in Figure 5-13, where the load applies in the vertical y-direction and horizontal z-direction simultaneously. Together, they define three stages: a vertically plastic loading stage from step 1 to step 5, an elastic stage from step 6 to step 8, and a horizontally plastic loading stage from step 9 to step 18. The deformation and contour plot of the equivalent plastic strain at the last load step are depicted in Figure 5-14.

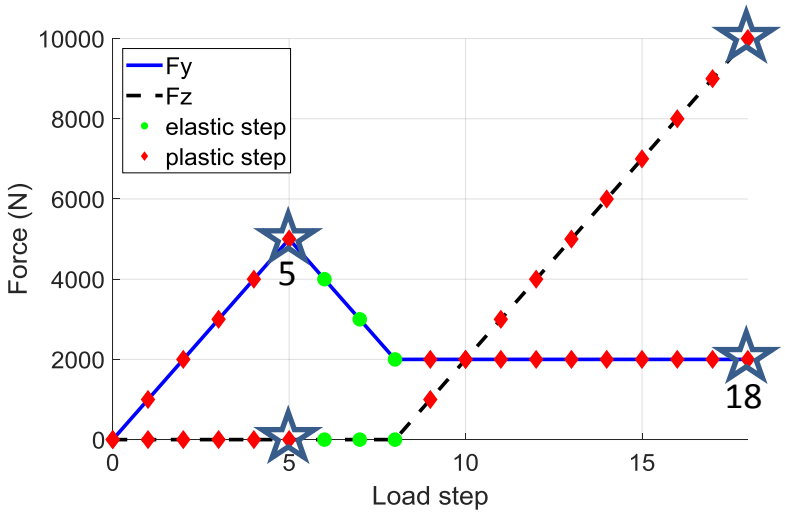

Figure 5-13. Load history of load case 3 for the cantilever beam example. Pentagrams depict the reduced load step

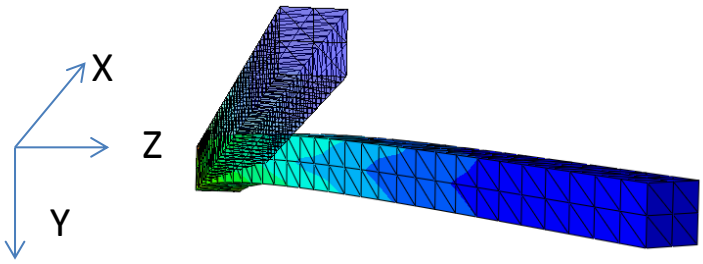

Figure 5-14. Contour plot of equivalent plastic strain at the last step on undeformed and deformed structure

In the sensitivity analysis, the first four plastic steps are skipped according to the empirical rule. The three intermediate elastic steps are also skipped due to the elastic load step reduction rule. In the horizontally plastic loading stage, the force in the y-direction holds constant, and the force in the z-direction monotonically increases. In this situation, the empirical rule still applies. Hence, steps 9 to 17 are skipped in the sensitivity analysis. In summary, only steps 5 and 18, as listed in Table 5-6 and highlighted in Figure 5-13, are employed in the sensitivity analysis.

Figure 5-15 compares the sensitivity results obtained using both reduced load steps and all load steps.

From the perspective of real values, sensitivities obtained with reduced load steps still match well with sensitivities obtained with all load steps. However,

Table 5-6. Reduced load steps for load case 3 of 3D cantilever beam example

Reduced load step	Corresponding FEA load step	Load (N)
1	5	Fy=5000, Fz=0
2	18	Fy=2000, Fz=10000

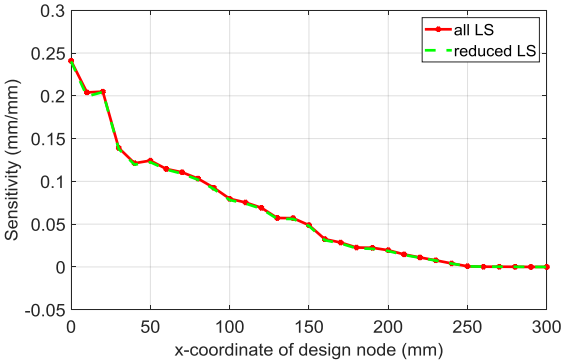

(a) Sensitivities of the vertical displacement response in load case 3

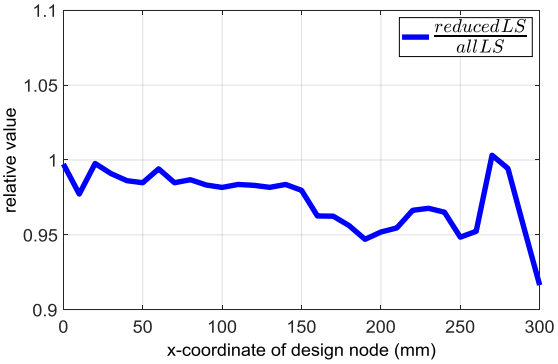

(b) Sensitivity relative value of vertical displacement response in load case 3

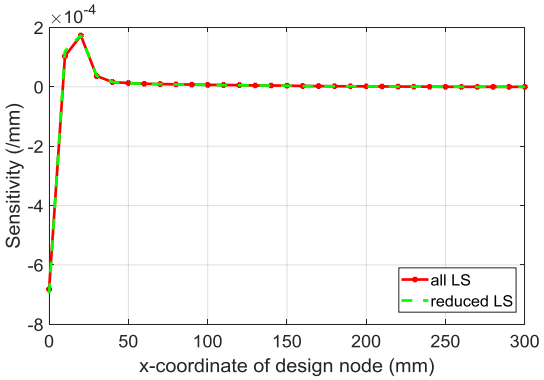

(c) Sensitivity of equivalent plastic strain response in load case 3

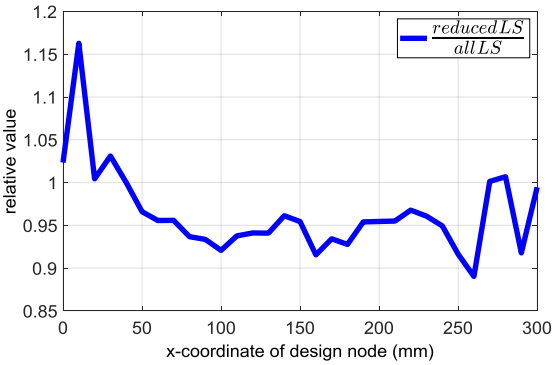

(d) Sensitivity relative value of equivalent plastic strain response in load case 3

Figure 5-15. Sensitivity comparison for load case 3 of 3D cantilever beam example

the relative error in this case is larger than in the previous two cases. The maximum error of the displacement response is 8%, with an average of 5%. The maximum error of the equivalent plastic strain response reaches 17%, with an average of 8%. This can be explained by the change in the direction of the resultant load force during the horizontally plastic loading stage. The resultant load force changes its direction in every load step. Correspondingly,

the flow vectors also change direction in every step. Therefore, a more severe change in the flow vectors could be imagined, leading to larger errors in sensitivities.

5.6 Demonstration with a connecting rod example

In this section, the rules for reducing load steps are demonstrated using a large-scale industrial example, specifically, a connecting rod structure in an internal combustion piston engine, also known as a conrod. Figure 5-16 shows the finite element model of a typical connecting rod structure, meshed with 6584 nodes and 27160 3D 4-node tetrahedral elements. The material properties are listed Table 5-7.

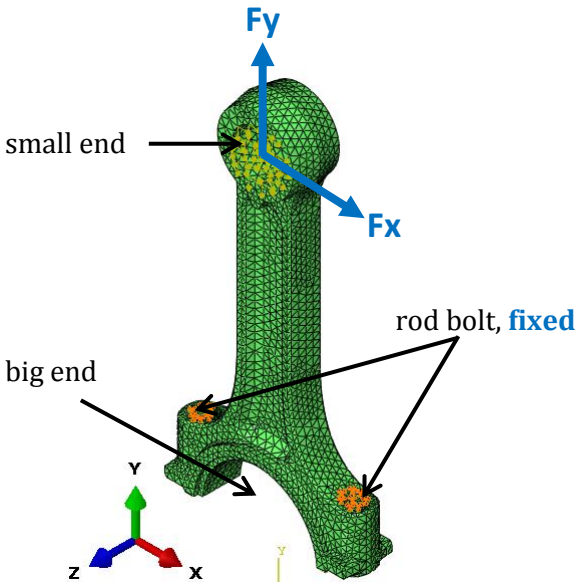

Figure 5-16. Finite element model of a connecting rod structure

Table 5-7. Material properties of the connecting rod example

E-modulus (GPa)	Plastic modulus (GPa)	Initial yield strength (MPa)	Poisson's ratio
210	100	450	0.3

The rod bolt is fixed, and a horizontal force in the x-direction and a vertical force in the y-direction are uniformly applied to the inner surface nodes of the small end. The load history contains 19 load steps, as depicted in Figure 5-17.

The structure is initially compressed in the y direction in step 1. From step 2 to step 7, the compressive load monotonically increases, and additionally, a horizontal force is gradually applied, leading to the bending of the rod. From step 8 to step 12, the horizontal force is fully unloaded, while the vertical force is partially released. The bending load increases in the negative x direction, accompanied by a slight increase in the compressive load from step 13 to step 16. Finally, from step 17 to step 19, the horizontal force is fully unloaded again, while the vertical force gradually increases to the same value as in step 1.

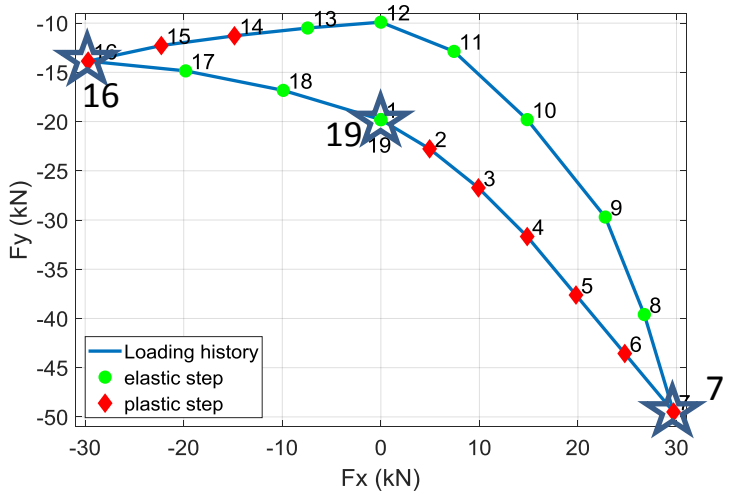

Figure 5-17. Load history on the small end of the connecting rod

Nonlinear finite element analysis shows that there are 10 elastic steps and 9 plastic steps, as illustrated in Figure 5-17. Under the given load history, the maximum horizontal displacement is 15.0 mm, occurring at step 7 at the top of the small end. The contour of displacement at step 7 is depicted in Figure 5-18, showing both the original and deformed structures. When compared to the dimensions of the model, the displacement is significant, making the problem geometrically nonlinear.

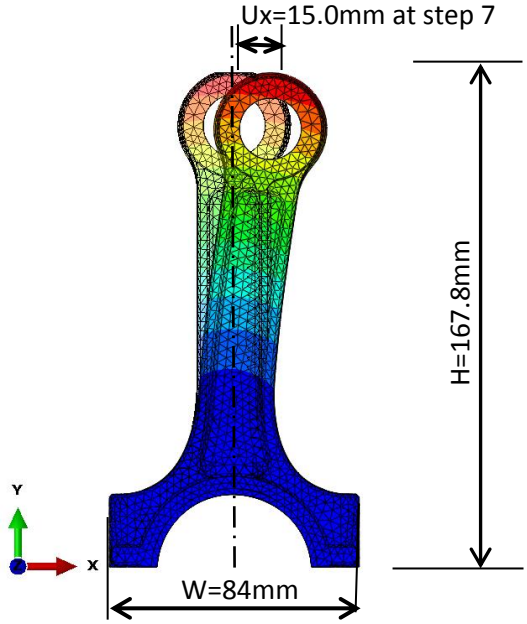

Figure 5-18. Contour plot of displacement on original and deformed structure at step 7

The contour plot of equivalent plastic strain at the last load step 19 is depicted in Figure 5-19 (a). The maximum equivalent plastic strain is 2.34%, located on the surface of the neck near the larger end. A total of 106 elements around this point are selected, as shown in Figure 5-19 (b), and the average equivalent plastic strain of these elements at the last step is defined as one system response.

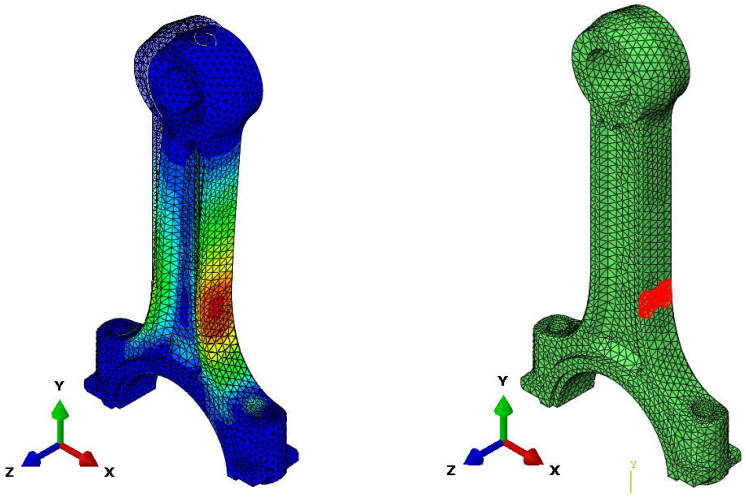

(a) Contour plot of equivalent plastic strain at load step 19, max=2.34%

(b) Selected elements around the maximum equivalent plastic strain point

Figure 5-19. Contour of equivalent plastic strain at the last load step

Figure 5-20 shows the deformation of the structure at the last load step. The average x-displacement and y-displacement at the small end are defined as the second and third system responses, respectively.

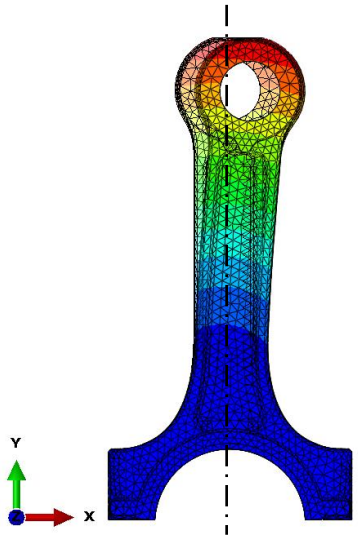

Figure 5-20. Contour plot of displacement on both original and deformed configuration at the last load step. Average displacement of small end nodes: Ux=6.48mm, Uy=-0.47mm

The design variables for the structure consist of the x-coordinates of 228 nodes highlighted in Figure 5-21. These nodes are situated on one side of the surface between the small end and the big end.

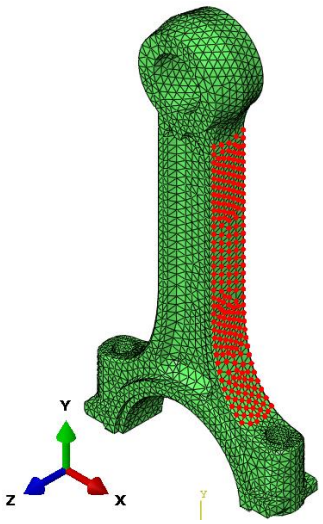

Figure 5-21. Design nodes of the structure

According to the rules for reducing elastic load steps, all elastic load steps are disregarded in the sensitivity analysis, except for the last step. Following the empirical rule, plastic steps 2 to 6, 14, and 15 are also omitted due to the monotonic load history. However, the remaining plastic steps, 7 and 16, are necessary since their loads are in opposite directions. The three reduced load steps in the sensitivity analysis are highlighted by pentagrams in Figure 5-17 and listed in Table 5-8.

Table 5-8. Reduced load steps in sensitivity analysis of the conrod example

Reduced load step	Corresponding FEA load step	Load (kN)
1	7	Fx= 29.7, Fy= -49.5
2	16	Fx= -29.7, Fy= -13.9
3	19	Fx= 0, Fy= -19.8

The contours of sensitivities for the three responses are depicted in Figure 5-22. As shown in Figure 5-22 (b), the sensitivities of the equivalent plastic strain response are close to zero for nodes far away from the maximum equivalent strain point. This is reasonable because the equivalent plastic strain is a local response influenced mainly by the local structure shape. The negative value means that if the node moves along the positive x-direction, which is the outer direction of the surface, the equivalent plastic strain will decrease.

In Figure 5-22 (c), sensitivity results show that if design nodes move along the outer surface direction, the final displacement in the horizontal direction will decrease. In Figure 5-22 (d), the sensitivity results reveal that if design nodes move along the outer surface direction, the final displacement in the vertical direction will increase. This is attributed to the decrease in plastic strains when the design nodes move outwardly. In the final step, the small end of the conrod returns closer to the centerline due to less plastic deformation. Consequently, this results in a decrease in horizontal displacement and an increase in vertical displacement.

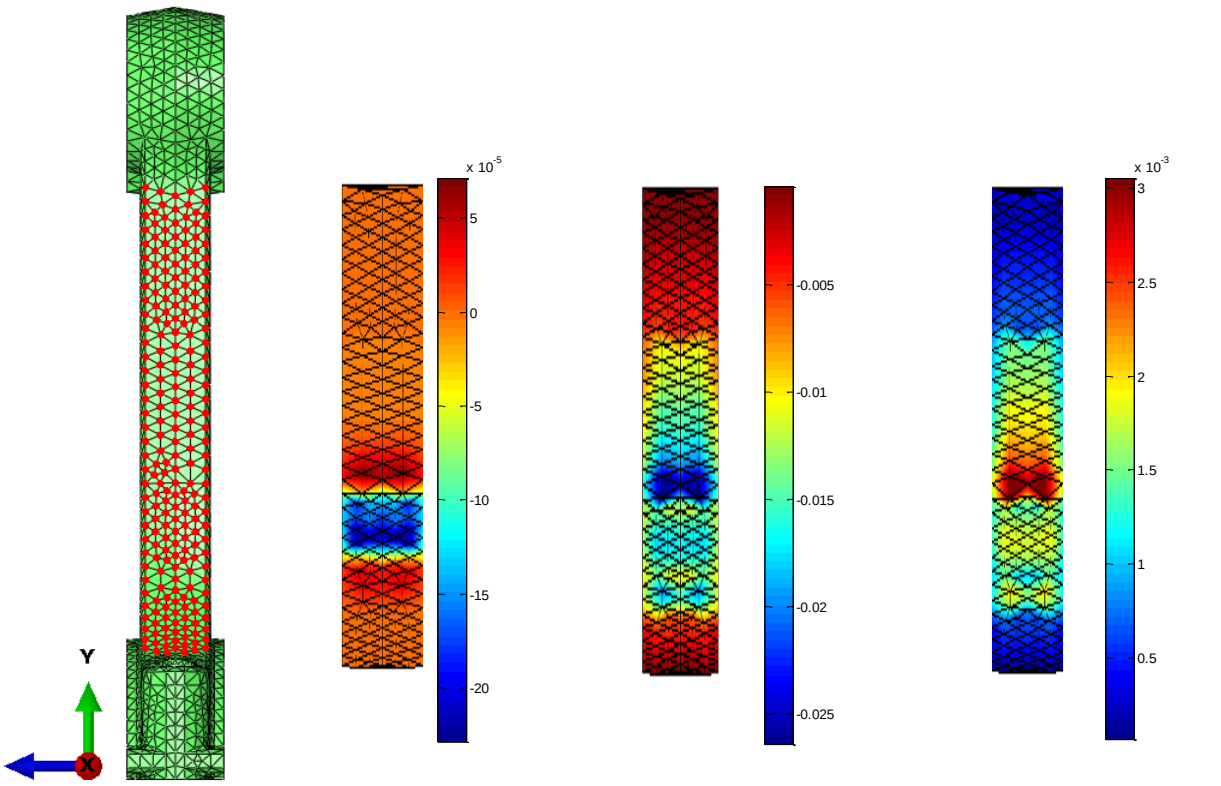

(a) Side view of design nodes

(b) Sensitivity of the equivalent plastic strain response (/mm)

(c) Sensitivity of x-displacement response (mm/mm)

(d) Sensitivity of y-displacement response (mm/mm)

Figure 5-22. Contour of sensitivities for the connecting rod example

To verify the accuracy of the results, the relative values of sensitivities are calculated and depicted in Figure 5-23. The figures show that the relative values are close to 1 for all three responses, demonstrating that the sensitivity results with the reduced load steps closely match the results obtained using all load steps.

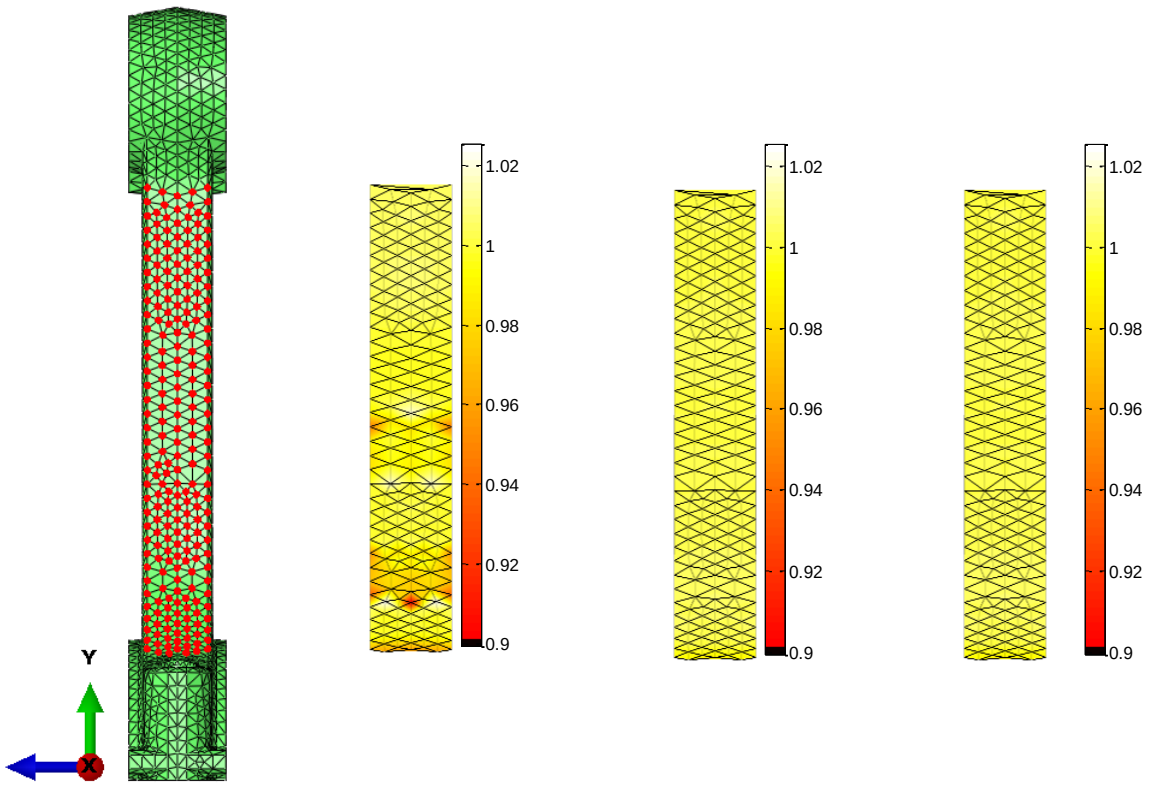

(a) Side view of design nodes

(b) Relative value of the equivalent plastic strain sensitivity

(c) Relative value of x-displacement sensitivity

(d) Relative value of y-displacement sensitivity

Figure 5-23. Relative values of sensitivities for the connecting rod example

The maximum and average relative errors of sensitivities are summarized in Table 5-9. They show that sensitivity errors with reduced load steps are small.

Table 5-9. Relative error of sensitivities for the connecting rod example

Response	Maximum error	Average error
equivalent plastic strain	10.0%	0.9%
x-displacement	1.2%	0.3%
y-displacement	1.3%	0.2%

6. Adjoint sensitivity analysis and load step reduction for mixed hardening elastoplasticity

In this chapter, the presented adjoint variable method for sensitivity analysis and load step reduction techniques is extended to a mixed hardening material model. Pure kinematic hardening is a special case of this discussion.

The major difference from isotropic hardening arises from an additional quantity, i.e., the back stress, in nonlinear finite element analysis. Its influence on the adjoint sensitivity analysis formulations is presented. The properties of adjoint variables and the load step reduction rules are verified. Finally, numerical examples are provided to demonstrate the applicability of load step reduction rules.

6.1 Nonlinear analysis procedure and consistent tangent stiffness matrix for mixed hardening elastoplasticity

The fundamental difference between mixed hardening elastoplasticity and the isotropic hardening case lies in the development of the yield surface. In the isotropic hardening model, the yield surface expands uniformly in all directions. Mixed hardening elastoplasticity assumes that not only does the size of the yield surface expand, but also the center of the yield surface shifts in the stress space. As depicted in Figure 6-1, the stress tensor $\boldsymbol{\alpha}$, referred to as back stress, measures the translation of yield surface's center.

The yield strength at a step t is equal to

$$ {}^{t}\sigma_{\mathrm{Y}} = \sigma_0 + \int_0^{{}^{t}\varepsilon^{\mathrm{p}}_{\mathrm{eqv}}} E^{\mathrm{p}} \beta d\varepsilon^{\mathrm{p}}_{\mathrm{eqv}} \tag{6.1} $$

where β is the hardening ratio, which lies between 0 and 1. If β equals 1, it describes pure isotropic hardening behavior. When β is equal to 0, the size of the yield surface remains constant, describing a pure kinematic hardening rule.

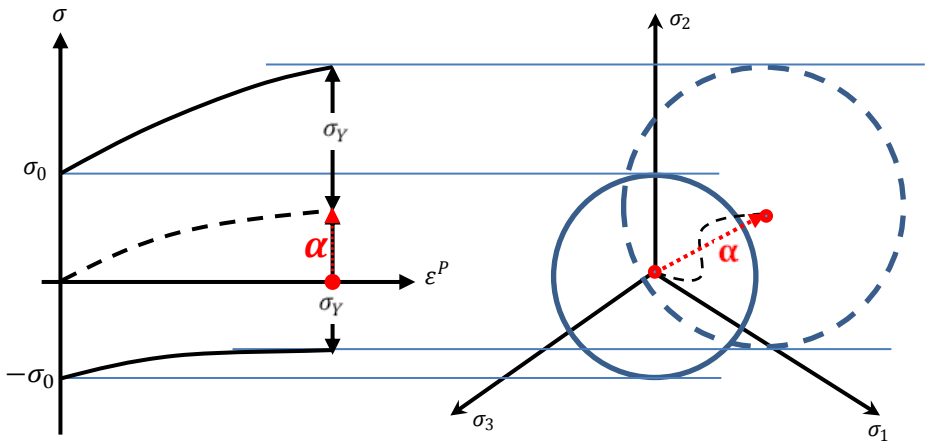

(a) 1D development of yield strength

(b) 3D development of yield surface in the space of principal stress components, taking von Mises yield criterion as an example

Figure 6-1. Development of yield strength and yield surface of mixed hardening elastoplasticity

The nonlinear Newton-Raphson iterative solution procedure in Section 2.2.2 still applies to the mixed hardening case, except that the back stress is an additional quantity to be determined through the return mapping algorithm.

Given stress ${}^{t}\boldsymbol{\sigma}$, back stress ${}^{t}\boldsymbol{\alpha}$, equivalent plastic strain ${}^{t}\varepsilon^{\mathrm{p}}_{\mathrm{eqv}}$ at step *t*, and an incremental strain $\Delta\boldsymbol{\varepsilon}$ determined by the incremental displacement, the trial stress is calculated as follows:

$$\begin{aligned} \Delta\boldsymbol{\sigma}_{\mathrm{try}} &= \boldsymbol{D}^{\mathrm{e}} \cdot \Delta\boldsymbol{\varepsilon} \\ \boldsymbol{\sigma}_{\mathrm{try}} &= {}^{t}\boldsymbol{\sigma} + \Delta\boldsymbol{\sigma}_{\mathrm{try}} \end{aligned} \tag{6.2}$$

where $\Delta\varepsilon^{\mathrm{p}}_{\mathrm{eqv}} = 0$, $\Delta\boldsymbol{\alpha} = 0$ are assumed. Then the equivalent stress is calculated with $\boldsymbol{\sigma}_{\mathrm{try}} - {}^{t}\boldsymbol{\alpha}$. If the equivalent stress is smaller or equal to the yield strength at step t, then the element behaves elastically and ${}^{t+1}\boldsymbol{\sigma} = \boldsymbol{\sigma}_{\mathrm{try}}$, ${}^{t+1}\boldsymbol{\alpha} = {}^{t}\boldsymbol{\alpha}$, ${}^{t+1}\varepsilon^{\mathrm{p}}_{\mathrm{eqv}} = {}^{t}\varepsilon^{\mathrm{p}}_{\mathrm{eqv}}$. Otherwise, the return mapping algorithm is employed to determine the increments [SH98]:

Set $\Delta\varepsilon^{\mathrm{p}}_{\mathrm{eqv}} = 0, \Delta\boldsymbol{\alpha} = 0,\ \Delta\boldsymbol{\sigma}_{\mathrm{try}} = \boldsymbol{D}^{\mathrm{e}} \cdot \Delta\boldsymbol{\varepsilon}, \boldsymbol{\sigma}_{\mathrm{try}} = {}^{t}\boldsymbol{\sigma} + \Delta\boldsymbol{\sigma}_{\mathrm{try}},\ \boldsymbol{\alpha}_{\mathrm{try}} = {}^{t}\boldsymbol{\alpha} + \Delta\boldsymbol{\alpha}$

a) Calculate trial associated flow vector $\mathbf{a}$ based on $\boldsymbol{\sigma}_{\text{try}}$ and $\boldsymbol{\alpha}_{\text{try}}$:

$$\mathbf{a} = \frac{d\left|\boldsymbol{\sigma}_{\text{try}} - \boldsymbol{\alpha}_{\text{try}}\right|_{\text{eqv}}}{d\boldsymbol{\sigma}} \tag{6.3}$$

b) Update the incremental plastic strain:

$$\Delta\varepsilon^{\text{p}}_{\text{eqv}} = \Delta\varepsilon^{\text{p}}_{\text{eqv}} + \frac{\left|\boldsymbol{\sigma}_{\text{try}} - \boldsymbol{\alpha}_{\text{try}}\right|_{\text{eqv}} - {}^{t}\sigma_{\text{Y}} - E^{\text{p}} \cdot \Delta\varepsilon^{\text{p}}_{\text{eqv}} \cdot \beta}{\mathbf{a} \cdot \boldsymbol{D}^{\text{e}} \cdot \mathbf{a}^{\text{T}} + E^{\text{p}}}$$
$$\Delta\boldsymbol{\varepsilon}^{\text{p}} = \Delta\varepsilon^{\text{p}}_{\text{eqv}} \cdot \mathbf{a} \tag{6.4}$$

c) Update trial stress:

$$\boldsymbol{\sigma}_{\text{try}} = {}^{t}\boldsymbol{\sigma} + \boldsymbol{D}^{\text{e}} \cdot \Delta\boldsymbol{\varepsilon} - \boldsymbol{D}^{\text{e}} \cdot \Delta\boldsymbol{\varepsilon}^{\text{p}} \tag{6.5}$$

d) Compute trial back stress:

$$\Delta\boldsymbol{\alpha} = (1-\beta) \cdot \boldsymbol{D}^{\alpha} \cdot \Delta\boldsymbol{\varepsilon}^{\text{p}}$$
$$\boldsymbol{\alpha}_{\text{try}} = {}^{t}\boldsymbol{\alpha} + \Delta\boldsymbol{\alpha} \tag{6.6}$$

where

$$\boldsymbol{D}^{\alpha} = \frac{E^{\text{p}}}{3}\begin{bmatrix} 2 & & & & & \\ & 2 & & & & \\ & & 2 & & & \\ & & & 1 & & \\ & & & & 1 & \\ & & & & & 1 \end{bmatrix} \tag{6.7}$$

Check if $\left|\boldsymbol{\sigma}_{\text{try}} - \boldsymbol{\alpha}_{\text{try}}\right|_{\text{eqv}} - {}^{t}\sigma_{\text{Y}} - E^{\text{p}} \cdot \Delta\varepsilon^{\text{p}}_{\text{eqv}} \cdot \beta = 0$. If it is not satisfied, then go back to step a. Otherwise the algorithm stops.

When the stopping condition of the algorithm is met, it provides:

$$^{t+1}\boldsymbol{\sigma} = \boldsymbol{\sigma}_{\text{try}}$$
$$^{t+1}\boldsymbol{\alpha} = \boldsymbol{\alpha}_{\text{try}} \tag{6.8}$$
$$^{t+1}\varepsilon^{\text{p}}_{\text{eqv}} = {}^{t}\varepsilon^{\text{p}}_{\text{eqv}} + \Delta\varepsilon^{\text{p}}_{\text{eqv}}$$

The consistent tangent stiffness matrix has the same expression as in Eq.(2.13). The constitutive matrix $\boldsymbol{D}^{\mathrm{ep}}$ at a plastic step is:

$$\boldsymbol{D}^{\mathrm{ep}} = \boldsymbol{Q}^{-1} \cdot \boldsymbol{D}^{\mathrm{e}} - \frac{\boldsymbol{d}}{\mathbf{a} \cdot \boldsymbol{r} + E^{\mathrm{p}} \cdot \beta + \mathbf{a} \cdot \boldsymbol{D}^{\alpha} \cdot \mathbf{a}^{\mathrm{T}} \cdot (1-\beta)} \tag{6.9}$$

where $\boldsymbol{Q}$, $\boldsymbol{r}$ and $\boldsymbol{d}$ follow in Eq.(2.28).

6.2 State variables and adjoint sensitivity analysis

In mixed hardening elastoplasticity, the back stress is also a state variable. Define the state vector as follows

$${}^{t}\boldsymbol{V} = \begin{pmatrix} {}^{t}\boldsymbol{\sigma} \\ {}^{t}\varepsilon_{\mathrm{eqv}}^{\mathrm{p}} \\ {}^{t}\boldsymbol{\alpha} \end{pmatrix} \tag{6.10}$$

For a system response f, it can be either explicitly or implicitly expressed as a function of $\{{}^{t}\boldsymbol{V}\}_{t=1}^{\mathrm{N}}$ and $\{{}^{t}\boldsymbol{U}\}_{t=1}^{\mathrm{N}}$:

$$f = f({}^{1}\boldsymbol{U}(s), {}^{2}\boldsymbol{U}(s), \dots, {}^{\mathrm{N}}\boldsymbol{U}(s), {}^{1}\boldsymbol{V}(s), {}^{2}\boldsymbol{V}(s), \dots, {}^{\mathrm{N}}\boldsymbol{V}(s), s) \tag{6.11}$$

To derive the adjoint sensitivity formulation, the dependent residual ${}^{t}\boldsymbol{H}$ should be defined. The two governing equations in Eqs. (4.6) and (4.8) still hold in mixed hardening case. Additionally, as described in the return mapping algorithm, the incremental back stress and incremental plastic strain have a relation

$${}^{t}\boldsymbol{\alpha} - {}^{t-1}\boldsymbol{\alpha} = (1-\beta) \cdot \boldsymbol{D}^{\alpha} \cdot {}^{t}\Delta\boldsymbol{\varepsilon}^{\mathrm{p}} \tag{6.12}$$

where the incremental plastic strain is:

$${}^{t}\Delta\boldsymbol{\varepsilon}^{\mathrm{p}} = {}^{t}\boldsymbol{\varepsilon}^{\mathrm{p}} - {}^{t-1}\boldsymbol{\varepsilon}^{\mathrm{p}} = \left({}^{t}\varepsilon_{\mathrm{eqv}}^{\mathrm{p}} - {}^{t-1}\varepsilon_{\mathrm{eqv}}^{\mathrm{p}}\right) \cdot {}^{t}\mathbf{a} \tag{6.13}$$

Therefore, the dependent residual ${}^{t}\boldsymbol{H}$ could be defined as

$$ {}^{t}\boldsymbol{H}({}^{t}\boldsymbol{U},{}^{t-1}\boldsymbol{U},{}^{t}\boldsymbol{V},{}^{t-1}\boldsymbol{V},s)=\begin{pmatrix} {}^{t-1}\boldsymbol{\sigma}+\boldsymbol{D}^{\mathrm{e}}\left[({}^{t}\boldsymbol{\varepsilon}-{}^{t-1}\boldsymbol{\varepsilon})-\left({}^{t}\varepsilon_{\mathrm{eqv}}^{\mathrm{p}}-{}^{t-1}\varepsilon_{\mathrm{eqv}}^{\mathrm{p}}\right)\cdot{}^{t}\mathbf{a}\right]-{}^{t}\boldsymbol{\sigma} \\ \left({}^{t}\varepsilon_{\mathrm{eqv}}^{\mathrm{p}}-{}^{t-1}\varepsilon_{\mathrm{eqv}}^{\mathrm{p}}\right)\cdot\left[|{}^{t}\boldsymbol{\sigma}-{}^{t}\boldsymbol{\alpha}|_{\mathrm{eqv}}-\sigma_{\mathrm{Y}}({}^{t}\varepsilon_{\mathrm{eqv}}^{\mathrm{p}})\right] \\ {}^{t-1}\boldsymbol{\alpha}+(1-\beta)\cdot\boldsymbol{D}^{\alpha}\cdot\left({}^{t}\varepsilon_{\mathrm{eqv}}^{\mathrm{p}}-{}^{t-1}\varepsilon_{\mathrm{eqv}}^{\mathrm{p}}\right)\cdot{}^{t}\mathbf{a}-{}^{t}\boldsymbol{\alpha} \end{pmatrix}\equiv\mathbf{0} \quad (6.14) $$

The adjoint sensitivity formulation is then derived in the same way as in Section 4.1.2, which leads to

$$ \frac{df}{ds}=\frac{\partial f}{\partial s}-\sum_{t=1}^{\mathrm{N}}{}^{t}\boldsymbol{\lambda}^{\mathrm{T}}\frac{\partial^{t}\boldsymbol{R}}{\partial s}-\sum_{t=1}^{\mathrm{N}}{}^{t}\boldsymbol{\gamma}^{\mathrm{T}}\frac{\partial^{t}\boldsymbol{H}}{\partial s} \quad (6.15) $$

The adjoint variables ${}^{t}\boldsymbol{\lambda}$ and ${}^{t}\boldsymbol{\gamma}$ are solved backwardly through

$$ \begin{aligned} {}^{t}\boldsymbol{K}_{\mathrm{T}}{}^{t}\boldsymbol{\lambda}&=\left(\frac{\partial^{t}\boldsymbol{H}^{\mathrm{T}}}{\partial^{t}\boldsymbol{U}}\frac{\partial^{t}\boldsymbol{H}}{\partial^{t}\boldsymbol{V}}^{-\mathrm{T}}\frac{\partial^{t+1}\boldsymbol{H}^{\mathrm{T}}}{\partial^{t}\boldsymbol{V}}-\frac{\partial^{t+1}\boldsymbol{H}^{\mathrm{T}}}{\partial^{t}\boldsymbol{U}}\right){}^{t+1}\boldsymbol{\gamma}+\frac{\partial f}{\partial^{t}\boldsymbol{U}}-\frac{\partial^{t}\boldsymbol{H}^{\mathrm{T}}}{\partial^{t}\boldsymbol{U}}\frac{\partial^{t}\boldsymbol{H}}{\partial^{t}\boldsymbol{V}}^{-\mathrm{T}}\frac{\partial f}{\partial^{t}\boldsymbol{V}} \\ {}^{t}\boldsymbol{\gamma}&=\frac{\partial^{t}\boldsymbol{H}}{\partial^{t}\boldsymbol{V}}^{-\mathrm{T}}\left(\frac{\partial f}{\partial^{t}\boldsymbol{V}}-\frac{\partial^{t+1}\boldsymbol{H}^{\mathrm{T}}}{\partial^{t}\boldsymbol{V}}\,{}^{t+1}\boldsymbol{\gamma}-\frac{\partial^{t}\boldsymbol{R}^{\mathrm{T}}}{\partial^{t}\boldsymbol{V}}\,{}^{t}\boldsymbol{\lambda}\right) \end{aligned} \quad (6.16) $$

The derivatives of the residual force vector and the dependent residual for mixed hardening elastoplasticity with an associated flow rule are presented below for the convenience of further discussion.

According to Eq.(2.1), it has

$$ \frac{\partial^{t}\boldsymbol{R}}{\partial^{t}\boldsymbol{U}}=-\frac{\partial\int_{V}{}^{t}\boldsymbol{B}^{\mathrm{T}}{}^{t}\boldsymbol{\sigma}dv}{\partial^{t}\boldsymbol{U}}=-\int_{V}\nabla_{\boldsymbol{U}}{}^{t}\boldsymbol{B}^{\mathrm{T}}{}^{t}\boldsymbol{\sigma}dv \quad (6.17) $$

$$ \frac{\partial^{t}\boldsymbol{R}}{\partial^{t}\boldsymbol{V}}=-\left(\frac{\partial}{\partial^{t}\boldsymbol{\sigma}}\quad\frac{\partial}{\partial^{t}\varepsilon_{\mathrm{eqv}}^{\mathrm{p}}}\quad\frac{\partial}{\partial^{t}\boldsymbol{\alpha}}\right)\int_{V}{}^{t}\boldsymbol{B}^{\mathrm{T}}{}^{t}\boldsymbol{\sigma}dv=-\left(\int_{V}{}^{t}\boldsymbol{B}^{\mathrm{T}}dv\quad 0\quad\mathbf{0}\right) \quad (6.18) $$

If a load step t is an elastic step, then the dependent residual is

$$ {}^{t}\boldsymbol{H}=\begin{pmatrix} {}^{t-1}\boldsymbol{\sigma}+\boldsymbol{D}^{\mathrm{e}}({}^{t}\boldsymbol{\varepsilon}-{}^{t-1}\boldsymbol{\varepsilon})-{}^{t}\boldsymbol{\sigma} \\ {}^{t}\varepsilon_{\mathrm{eqv}}^{\mathrm{p}}-{}^{t-1}\varepsilon_{\mathrm{eqv}}^{\mathrm{p}} \\ {}^{t-1}\boldsymbol{\alpha}-{}^{t}\boldsymbol{\alpha} \end{pmatrix}=\mathbf{0} \quad (6.19) $$

According to Eq.(2.4), the derivatives of ${}^{t}\boldsymbol{H}$ are

$$\frac{\partial^t \boldsymbol{H}}{\partial^t \boldsymbol{U}} = \begin{pmatrix} \boldsymbol{D}^{\mathrm{e}} \dfrac{\partial^t \boldsymbol{\varepsilon}}{\partial^t \boldsymbol{U}} \\ 0 \\ \mathbf{0} \end{pmatrix} = \begin{pmatrix} \boldsymbol{D}^{\mathrm{e}\,t}\boldsymbol{B} \\ 0 \\ \mathbf{0} \end{pmatrix} \tag{6.20}$$

$$\frac{\partial^t \boldsymbol{H}}{\partial^{t-1} \boldsymbol{U}} = \begin{pmatrix} -\boldsymbol{D}^{\mathrm{e}} \dfrac{\partial^{t-1} \boldsymbol{\varepsilon}}{\partial^{t-1} \boldsymbol{U}} \\ 0 \\ \mathbf{0} \end{pmatrix} = -\frac{\partial^{t-1} \boldsymbol{H}}{\partial^{t-1} \boldsymbol{U}} \tag{6.21}$$

$$\frac{\partial^t \boldsymbol{H}}{\partial s} = \begin{pmatrix} \boldsymbol{D}^{\mathrm{e}} \dfrac{\partial ({}^t\boldsymbol{\varepsilon} - {}^{t-1}\boldsymbol{\varepsilon})}{\partial s} \\ 0 \\ \mathbf{0} \end{pmatrix} = \begin{pmatrix} \boldsymbol{D}^{\mathrm{e}} \dfrac{\partial^t \boldsymbol{\varepsilon}}{\partial s} \\ 0 \\ \mathbf{0} \end{pmatrix} - \begin{pmatrix} \boldsymbol{D}^{\mathrm{e}} \dfrac{\partial^{t-1} \boldsymbol{\varepsilon}}{\partial s} \\ 0 \\ \mathbf{0} \end{pmatrix} \tag{6.22}$$

$$\frac{\partial^t \boldsymbol{H}}{\partial^t \boldsymbol{V}} = \begin{pmatrix} \dfrac{\partial}{\partial^t \boldsymbol{\sigma}} & \dfrac{\partial}{\partial^t \varepsilon^{\mathrm{p}}_{\mathrm{eqv}}} & \dfrac{\partial}{\partial^t \boldsymbol{\alpha}} \end{pmatrix} {}^t\boldsymbol{H} = \begin{pmatrix} -\boldsymbol{I} & -\boldsymbol{D}^{\mathrm{e}}\,{}^t\mathbf{a} & 0 \\ 0 & 1 & 0 \\ 0 & 0 & -\boldsymbol{I} \end{pmatrix} = \frac{\partial^t \boldsymbol{H}^{-1}}{\partial^t \boldsymbol{V}} \tag{6.23}$$

$$\frac{\partial^t \boldsymbol{H}}{\partial^{t-1} \boldsymbol{V}} = \begin{pmatrix} \dfrac{\partial}{\partial^{t-1} \boldsymbol{\sigma}} & \dfrac{\partial}{\partial^{t-1} \varepsilon^{\mathrm{p}}_{\mathrm{eqv}}} & \dfrac{\partial}{\partial^{t-1} \boldsymbol{\alpha}} \end{pmatrix} {}^t\boldsymbol{H} = \begin{pmatrix} \boldsymbol{I} & \boldsymbol{D}^{\mathrm{e}}\,{}^t\mathbf{a} & 0 \\ 0 & -1 & 0 \\ 0 & 0 & \boldsymbol{I} \end{pmatrix} = -\frac{\partial^t \boldsymbol{H}}{\partial^t \boldsymbol{V}} \tag{6.24}$$

If a load step t is a plastic step, then the dependent residual follows

$${}^t\boldsymbol{H} = \begin{pmatrix} {}^{t-1}\boldsymbol{\sigma} + \boldsymbol{D}^{\mathrm{e}}\left[({}^t\boldsymbol{\varepsilon} - {}^{t-1}\boldsymbol{\varepsilon}) - \left({}^t\varepsilon^{\mathrm{p}}_{\mathrm{eqv}} - {}^{t-1}\varepsilon^{\mathrm{p}}_{\mathrm{eqv}} \right) \cdot {}^t\mathbf{a} \right] - {}^t\boldsymbol{\sigma} \\ |{}^t\boldsymbol{\sigma} - {}^t\boldsymbol{\alpha}|_{\mathrm{eqv}} - \sigma_{\mathrm{Y}}\left({}^t\varepsilon^{\mathrm{p}}_{\mathrm{eqv}} \right) \\ {}^{t-1}\boldsymbol{\alpha} + (1-\beta) \cdot \boldsymbol{D}^{\alpha} \cdot \left({}^t\varepsilon^{\mathrm{p}}_{\mathrm{eqv}} - {}^{t-1}\varepsilon^{\mathrm{p}}_{\mathrm{eqv}} \right) \cdot {}^t\mathbf{a} - {}^t\boldsymbol{\alpha} \end{pmatrix} = \mathbf{0} \tag{6.25}$$

$\partial^t \boldsymbol{H}/\partial^t \boldsymbol{U}$, $\partial^t \boldsymbol{H}/\partial^{t-1} \boldsymbol{U}$ and $\partial^t \boldsymbol{H}/\partial s$ are the same as Eqs.(6.20) to (6.22). Other partial derivatives are

$$\frac{\partial^t \boldsymbol{H}}{\partial^t \boldsymbol{V}} = \begin{pmatrix} \dfrac{\partial}{\partial^t \boldsymbol{\sigma}} & \dfrac{\partial}{\partial^t \varepsilon^{\mathrm{p}}_{\mathrm{eqv}}} & \dfrac{\partial}{\partial^t \boldsymbol{\alpha}} \end{pmatrix} {}^t\boldsymbol{H} = \begin{pmatrix} -\boldsymbol{I} - \boldsymbol{D}^{\mathrm{e}} \dfrac{d^t \mathbf{a}}{d^t \boldsymbol{\sigma}} \Delta\varepsilon^{\mathrm{p}}_{\mathrm{eqv}} & -\boldsymbol{D}^{\mathrm{e}}\,{}^t\mathbf{a} & 0 \\ {}^t\mathbf{a}^{\mathrm{T}} & -E^{\mathrm{p}} \cdot \beta & -{}^t\mathbf{a}^{\mathrm{T}} \\ 0 & (1-\beta) \cdot \boldsymbol{D}^{\alpha} \cdot {}^t\mathbf{a} & -\boldsymbol{I} \end{pmatrix} \tag{6.26}$$

$$\frac{\partial^t \boldsymbol{H}}{\partial^{t-1} \boldsymbol{V}} = \begin{pmatrix} \dfrac{\partial}{\partial^{t-1} \boldsymbol{\sigma}} & \dfrac{\partial}{\partial^{t-1} \varepsilon^{\mathrm{p}}_{\mathrm{eqv}}} & \dfrac{\partial}{\partial^{t-1} \boldsymbol{\alpha}} \end{pmatrix} {}^t\boldsymbol{H} = \begin{pmatrix} \boldsymbol{I} & \boldsymbol{D}^{\mathrm{e}}\,{}^t\mathbf{a} & 0 \\ 0 & 0 & 0 \\ 0 & -(1-\beta) \cdot \boldsymbol{D}^{\alpha} \cdot {}^t\mathbf{a} & \boldsymbol{I} \end{pmatrix} \tag{6.27}$$

6.3 Load step reduction for mixed hardening elastoplasticity

In this section, the properties of adjoint variables in Section 5.2 and the load step reductions rules in Section 5.3 are extended to mixed hardening elastoplasticity. They are also theoretically proven. The system responses discussed here are assumed to still satisfy Eq.(5.1).

Property 1. If a load step t is an intermediate elastic load step, then ${}^t\boldsymbol{\lambda} = 0$.

Proof:

According to Eqs.(6.24) and (6.27)

$$\frac{\partial {}^{t+1}\boldsymbol{H}}{\partial {}^t\boldsymbol{V}} = \begin{pmatrix} \boldsymbol{I} & \boldsymbol{D}^{\mathrm{e}}\,{}^{t+1}\mathbf{a} & 0 \\ 0 & c & 0 \\ 0 & d & \boldsymbol{I} \end{pmatrix} \tag{6.28}$$

where

$$c = \begin{cases} -1 & \text{if step } t \text{ is elastic} \\ 0 & \text{if step } t \text{ is plastic} \end{cases}$$
$$\boldsymbol{d} = \begin{cases} 0 & \text{if step } t \text{ is elastic} \\ -(1-\beta)\cdot \boldsymbol{D}^{\alpha}\cdot {}^t\mathbf{a} & \text{if step } t \text{ is plastic} \end{cases} \tag{6.29}$$

Combining Eqs.(6.20), (6.21), (6.23) and (6.29) yields

$$\begin{aligned} &\frac{\partial {}^t\boldsymbol{H}^{\mathrm{T}}}{\partial {}^t\boldsymbol{U}} \frac{\partial {}^t\boldsymbol{H}^{-\mathrm{T}}}{\partial {}^t\boldsymbol{V}} \frac{\partial {}^{t+1}\boldsymbol{H}^{\mathrm{T}}}{\partial {}^t\boldsymbol{V}} - \frac{\partial {}^{t+1}\boldsymbol{H}^{\mathrm{T}}}{\partial {}^t\boldsymbol{U}} \\ &\quad = ({}^t\boldsymbol{B}^{\mathrm{T}}\boldsymbol{D}^{\mathrm{e}} \quad 0 \quad 0)\left(\begin{pmatrix} -\boldsymbol{I} & 0 & 0 \\ -{}^t\mathbf{a}^{\mathrm{T}}\boldsymbol{D}^{\mathrm{e}} & 1 & 0 \\ 0 & 0 & -\boldsymbol{I} \end{pmatrix} \begin{pmatrix} \boldsymbol{I} & 0 & 0 \\ {}^{t+1}\mathbf{a}^{\mathrm{T}}\boldsymbol{D}^{\mathrm{e}} & c & \boldsymbol{d}^{\mathrm{T}} \\ 0 & 0 & \boldsymbol{I} \end{pmatrix} + \boldsymbol{I} \right) \\ &\quad = ({}^t\boldsymbol{B}^{\mathrm{T}}\boldsymbol{D}^{\mathrm{e}} \quad 0 \quad 0)\begin{pmatrix} 0 & 0 & 0 \\ \left({}^{t+1}\mathbf{a}^{\mathrm{T}} - {}^t\mathbf{a}^{\mathrm{T}}\right)\boldsymbol{D}^{\mathrm{e}} & c+1 & \boldsymbol{d}^{T} \\ 0 & 0 & 0 \end{pmatrix} = \mathbf{0} \end{aligned} \tag{6.30}$$

By substituting Eq.(5.1) and Eq.(6.30) into Eq.(6.16), it follows

$${}^t\boldsymbol{K}_{\mathrm{T}}\,{}^t\boldsymbol{\lambda} = \left(\frac{\partial {}^t\boldsymbol{H}^{\mathrm{T}}}{\partial {}^t\boldsymbol{U}} \frac{\partial {}^t\boldsymbol{H}^{-\mathrm{T}}}{\partial {}^t\boldsymbol{V}} \frac{\partial {}^{t+1}\boldsymbol{H}^{\mathrm{T}}}{\partial {}^t\boldsymbol{V}} - \frac{\partial {}^{t+1}\boldsymbol{H}^{\mathrm{T}}}{\partial {}^t\boldsymbol{U}} \right) {}^{t+1}\boldsymbol{\gamma} + \frac{\partial f}{\partial {}^t\boldsymbol{U}} - \frac{\partial {}^t\boldsymbol{H}^{\mathrm{T}}}{\partial {}^t\boldsymbol{U}} \frac{\partial {}^t\boldsymbol{H}^{-\mathrm{T}}}{\partial {}^t\boldsymbol{V}} \frac{\partial f}{\partial {}^t\boldsymbol{V}} = \mathbf{0} \tag{6.31}$$

which leads to

$$ {}^{t}\boldsymbol{\lambda} = \mathbf{0} \tag{6.32} $$

□

Property 2. If load steps *t* and *t+1* are both plastic, and the flow vectors satisfy ${}^{t}\mathbf{a} = {}^{t+1}\mathbf{a}$, $\frac{\mathrm{d}^{t}\mathbf{a}}{\mathrm{d}^{t}\boldsymbol{\sigma}} = 0$, then ${}^{t}\boldsymbol{\lambda} = 0$ and ${}^{t}\boldsymbol{\gamma} = \begin{pmatrix} {}^{t+1}\boldsymbol{\gamma}_{\sigma} \\ 0 \\ {}^{t+1}\boldsymbol{\gamma}_{\alpha} \end{pmatrix}$.

Proof:

By employing the assumption that $d^{t}\mathbf{a}/d^{t}\boldsymbol{\sigma} = 0$, Eq.(6.26) is thereby simplified to

$$ \frac{\partial^{t}\boldsymbol{H}^{\mathrm{T}}}{\partial^{t}\boldsymbol{V}} = \begin{pmatrix} -\boldsymbol{I} & {}^{t}\mathbf{a} & \mathbf{0} \\ -{}^{t}\mathbf{a}^{\mathrm{T}}\boldsymbol{D}^{\mathrm{e}} & -E^{\mathrm{P}}\cdot\beta & (1-\beta){}^{t}\mathbf{a}^{\mathrm{T}}\boldsymbol{D}^{\alpha} \\ \mathbf{0} & -{}^{t}\mathbf{a} & -\boldsymbol{I} \end{pmatrix} \tag{6.33} $$

Using the assumption ${}^{t}\mathbf{a} = {}^{t+1}\mathbf{a}$, it follows from Eq.(6.27) that

$$ \frac{\partial^{t+1}\boldsymbol{H}^{\mathrm{T}}}{\partial^{t}\boldsymbol{V}} = \begin{pmatrix} \boldsymbol{I} & \mathbf{0} & \mathbf{0} \\ {}^{t}\mathbf{a}^{\mathrm{T}}\boldsymbol{D}^{\mathrm{e}} & 0 & -(1-\beta){}^{t}\mathbf{a}^{\mathrm{T}}\boldsymbol{D}^{\alpha} \\ \mathbf{0} & \mathbf{0} & \boldsymbol{I} \end{pmatrix} \tag{6.34} $$

It follows from Eqs.(6.33) and (6.34) that

$$ \frac{\partial^{t}\boldsymbol{H}^{-\mathrm{T}}}{\partial^{t}\boldsymbol{V}} \frac{\partial^{t+1}\boldsymbol{H}^{\mathrm{T}}}{\partial^{t}\boldsymbol{V}} = \begin{pmatrix} -\boldsymbol{I} & \mathbf{0} & \mathbf{0} \\ \mathbf{0} & 0 & \mathbf{0} \\ \mathbf{0} & \mathbf{0} & -\boldsymbol{I} \end{pmatrix} \tag{6.35} $$

By combining Eqs.(6.20), (6.21) and (6.35), it has

$$ \frac{\partial^{t}\boldsymbol{H}^{\mathrm{T}}}{\partial^{t}\boldsymbol{U}} \frac{\partial^{t}\boldsymbol{H}^{-\mathrm{T}}}{\partial^{t}\boldsymbol{V}} \frac{\partial^{t+1}\boldsymbol{H}^{\mathrm{T}}}{\partial^{t}\boldsymbol{V}} - \frac{\partial^{t+1}\boldsymbol{H}^{\mathrm{T}}}{\partial^{t}\boldsymbol{U}} = ({}^{t}\boldsymbol{B}^{\mathrm{T}}\boldsymbol{D}^{\mathrm{e}} \quad 0 \quad \mathbf{0}) \begin{pmatrix} \mathbf{0} & \mathbf{0} & \mathbf{0} \\ \mathbf{0} & 1 & \mathbf{0} \\ \mathbf{0} & \mathbf{0} & \mathbf{0} \end{pmatrix} = \mathbf{0} \tag{6.36} $$

Substituting Eq.(5.1) and Eq.(6.36) into Eq.(6.16) yields

$$ {}^{t}\boldsymbol{K}_{\mathrm{T}}{}^{t}\boldsymbol{\lambda}=\left(\frac{\partial^{t}\boldsymbol{H}^{\mathrm{T}}}{\partial^{t}\boldsymbol{U}}\frac{\partial^{t}\boldsymbol{H}^{-\mathrm{T}}}{\partial^{t}\boldsymbol{V}}\frac{\partial^{t+1}\boldsymbol{H}^{\mathrm{T}}}{\partial^{t}\boldsymbol{V}}-\frac{\partial^{t+1}\boldsymbol{H}^{\mathrm{T}}}{\partial^{t}\boldsymbol{U}}\right){}^{t+1}\boldsymbol{\gamma}+\frac{\partial f}{\partial^{t}\boldsymbol{U}}-\frac{\partial^{t}\boldsymbol{H}^{\mathrm{T}}}{\partial^{t}\boldsymbol{U}}\frac{\partial^{t}\boldsymbol{H}^{-\mathrm{T}}}{\partial^{t}\boldsymbol{V}}\frac{\partial f}{\partial^{t}\boldsymbol{V}}=\boldsymbol{0} \qquad (6.37) $$

which leads to

$$ {}^{t}\boldsymbol{\lambda}=\boldsymbol{0} \qquad (6.38) $$

Furthermore, by substituting Eqs.(6.35), (6.38) and Eq.(5.1) into Eq.(6.16), it yields

$$ {}^{t}\boldsymbol{\gamma}=\frac{\partial^{t}\boldsymbol{H}^{-\mathrm{T}}}{\partial^{t}\boldsymbol{V}}\left(\frac{\partial f}{\partial^{t}\boldsymbol{V}}-\frac{\partial^{t+1}\boldsymbol{H}^{\mathrm{T}}}{\partial^{t}\boldsymbol{V}}{}^{t+1}\boldsymbol{\gamma}-\frac{\partial^{t}\boldsymbol{R}^{\mathrm{T}}}{\partial^{t}\boldsymbol{V}}{}^{t}\boldsymbol{\lambda}\right)=\begin{pmatrix}\boldsymbol{I}&\boldsymbol{0}&\boldsymbol{0}\\\boldsymbol{0}&\boldsymbol{0}&\boldsymbol{0}\\\boldsymbol{0}&\boldsymbol{0}&\boldsymbol{I}\end{pmatrix}{}^{t+1}\boldsymbol{\gamma}=\begin{pmatrix}{}^{t+1}\boldsymbol{\gamma}_{\sigma}\\0\\{}^{t+1}\boldsymbol{\gamma}_{\alpha}\end{pmatrix} \qquad (6.39) $$

□

Building upon the two properties mentioned above, the load step reduction rules proposed in Section 5.3 can be extended to mixed hardening elastoplasticity as follows.

Elastic load step reduction rule: Given a sequence of load steps L = {1, 2, ..., t-1, t, t+1, …, N}, if step *t* is an intermediate elastic load step, then skip step *t* as the load steps contain only S = {1, 2, ..., t-1, t+1, …, N} will not change the sensitivity results.

Proof:

Following the same discussion as in Section 5.3, it is suffice to prove

1. ${}^{t}_{\mathrm{L}}\boldsymbol{\lambda}=0$
2. ${}^{n}_{\mathrm{S}}\boldsymbol{\lambda}={}^{n}_{\mathrm{L}}\boldsymbol{\lambda}$ and ${}^{n}_{\mathrm{S}}\boldsymbol{\gamma}={}^{n}_{\mathrm{L}}\boldsymbol{\gamma}$ for $n\leq t-1$
3. ${}^{t}_{\mathrm{L}}\boldsymbol{\gamma}^{\mathrm{T}}\frac{\partial{}^{t}_{\mathrm{L}}\boldsymbol{H}}{\partial s}+{}^{t+1}_{\mathrm{L}}\boldsymbol{\gamma}^{\mathrm{T}}\frac{\partial^{t+1}_{\mathrm{L}}\boldsymbol{H}}{\partial s}={}^{t+1}_{\mathrm{S}}\boldsymbol{\gamma}^{\mathrm{T}}\frac{\partial^{t+1}_{\mathrm{S}}\boldsymbol{H}}{\partial s}$

The first item is obtained directly from the first property of adjoint variables.

For the second item, firstly, prove that it holds at $n=t-1$. By substituting Eqs.(5.1) and (5.16) into Eq.(6.16), it has

$$ {}^{t-1}_{\mathrm{L}}\boldsymbol{\lambda} = {}^{t-1}_{\mathrm{S}}\boldsymbol{K}_{\mathrm{T}}{}^{-1} \cdot \left(\frac{\partial {}^{t-1}_{\mathrm{S}}\boldsymbol{H}}{\partial {}^{t-1}\boldsymbol{U}}^{\mathrm{T}} \frac{\partial {}^{t-1}_{\mathrm{S}}\boldsymbol{H}}{\partial {}^{t-1}\boldsymbol{V}}^{-\mathrm{T}} \frac{\partial {}^{t}_{\mathrm{L}}\boldsymbol{H}}{\partial {}^{t-1}\boldsymbol{V}}^{\mathrm{T}} {}^{t}_{\mathrm{L}}\boldsymbol{\gamma} - \frac{\partial {}^{t}_{\mathrm{L}}\boldsymbol{H}}{\partial {}^{t-1}\boldsymbol{U}}^{\mathrm{T}} {}^{t}_{\mathrm{L}}\boldsymbol{\gamma} \right) \tag{6.40} $$

Using Eq.(5.1) and ${}^{t}_{\mathrm{L}}\boldsymbol{\lambda} = 0$, it follows from Eq.(6.16) that

$$ {}^{t}_{\mathrm{L}}\boldsymbol{\gamma} = -\frac{\partial {}^{t}_{\mathrm{L}}\boldsymbol{H}}{\partial {}^{t}\boldsymbol{V}}^{-\mathrm{T}} \frac{\partial {}^{t+1}_{\mathrm{L}}\boldsymbol{H}}{\partial {}^{t}\boldsymbol{V}}^{\mathrm{T}} {}^{t+1}_{\mathrm{L}}\boldsymbol{\gamma} \tag{6.41} $$

By substituting Eqs.(6.23) and (6.28) into Eq.(6.41) and using Eq.(5.16), it has

$$ {}^{t}_{\mathrm{L}}\boldsymbol{\gamma} = \begin{pmatrix} \boldsymbol{I} & 0 & 0 \\ {}^{t}\mathbf{a}^{\mathrm{T}}\boldsymbol{D}^{\mathrm{e}} & -1 & 0 \\ 0 & 0 & \boldsymbol{I} \end{pmatrix} \begin{pmatrix} \boldsymbol{I} & 0 & 0 \\ {}^{t+1}\mathbf{a}^{\mathrm{T}}\boldsymbol{D}^{\mathrm{e}} & c & \boldsymbol{d}^{\mathrm{T}} \\ 0 & 0 & \boldsymbol{I} \end{pmatrix} {}^{t+1}_{\mathrm{L}}\boldsymbol{\gamma} = \begin{pmatrix} \boldsymbol{I} & 0 & 0 \\ ({}^{t+1}\mathbf{a}^{\mathrm{T}} - {}^{t}\mathbf{a}^{\mathrm{T}})\boldsymbol{D}^{\mathrm{e}} & -c & -\boldsymbol{d}^{\mathrm{T}} \\ 0 & 0 & \boldsymbol{I} \end{pmatrix} {}^{t+1}_{\mathrm{S}}\boldsymbol{\gamma} \tag{6.42} $$

Step *t-1* and step *t+1* are adjacent steps in load sequences S. Therefore, using Eqs.(6.24) and (6.42), it follows

$$ \begin{aligned} \frac{\partial {}^{t}_{\mathrm{L}}\boldsymbol{H}}{\partial {}^{t-1}\boldsymbol{V}}^{\mathrm{T}} {}^{t}_{\mathrm{L}}\boldsymbol{\gamma} &= \begin{pmatrix} \boldsymbol{I} & 0 & 0 \\ {}^{t}\mathbf{a}^{\mathrm{T}}\boldsymbol{D}^{\mathrm{e}} & -1 & 0 \\ 0 & 0 & \boldsymbol{I} \end{pmatrix} \begin{pmatrix} \boldsymbol{I} & 0 & 0 \\ ({}^{t}\mathbf{a}^{\mathrm{T}} - {}^{t+1}\mathbf{a}^{\mathrm{T}})\boldsymbol{D}^{\mathrm{e}} & -c & -\boldsymbol{d}^{\mathrm{T}} \\ 0 & 0 & \boldsymbol{I} \end{pmatrix} {}^{t+1}_{\mathrm{S}}\boldsymbol{\gamma} \\ &= \begin{pmatrix} \boldsymbol{I} & 0 & 0 \\ {}^{t+1}\mathbf{a}^{\mathrm{T}}\boldsymbol{D}^{\mathrm{e}} & c & \boldsymbol{d}^{\mathrm{T}} \\ 0 & 0 & \boldsymbol{I} \end{pmatrix} {}^{t+1}_{\mathrm{S}}\boldsymbol{\gamma} = \frac{\partial {}^{t+1}_{\mathrm{S}}\boldsymbol{H}}{\partial {}^{t-1}\boldsymbol{V}}^{\mathrm{T}} {}^{t+1}_{\mathrm{S}}\boldsymbol{\gamma} \end{aligned} \tag{6.43} $$

Additionally, using Eqs.(6.21) and (6.42), it has

$$ \begin{aligned} \frac{\partial {}^{t}_{\mathrm{L}}\boldsymbol{H}}{\partial {}^{t-1}\boldsymbol{U}}^{\mathrm{T}} {}^{t}_{\mathrm{L}}\boldsymbol{\gamma} &= -({}^{t-1}\boldsymbol{B}^{\mathrm{T}}\boldsymbol{D}^{\mathrm{e}} \quad 0 \quad \mathbf{0}) \begin{pmatrix} \boldsymbol{I} & \mathbf{0} & \mathbf{0} \\ ({}^{t}\mathbf{a}^{\mathrm{T}} - {}^{t+1}\mathbf{a}^{\mathrm{T}})\boldsymbol{D}^{\mathrm{e}} & -c & -\boldsymbol{d}^{\mathrm{T}} \\ \mathbf{0} & \mathbf{0} & \boldsymbol{I} \end{pmatrix} {}^{t+1}_{\mathrm{S}}\boldsymbol{\gamma} \\ &= -({}^{t-1}\boldsymbol{B}^{\mathrm{T}}\boldsymbol{D}^{\mathrm{e}} \quad 0 \quad \mathbf{0}) {}^{t}_{\mathrm{S}}\boldsymbol{\gamma} = \frac{\partial {}^{t+1}_{\mathrm{S}}\boldsymbol{H}}{\partial {}^{t-1}\boldsymbol{U}}^{\mathrm{T}} {}^{t+1}_{\mathrm{S}}\boldsymbol{\gamma} \end{aligned} \tag{6.44} $$

Finally, by substituting Eqs.(6.43) and (6.44) into Eq.(6.40), it yields

$$ {}^{t-1}_{\mathrm{L}}\boldsymbol{\lambda} = {}^{t-1}_{\mathrm{S}}\boldsymbol{K}_{\mathrm{T}}{}^{-1} \cdot \left(\frac{\partial {}^{t-1}_{\mathrm{S}}\boldsymbol{H}}{\partial {}^{t-1}\boldsymbol{U}}^{\mathrm{T}} \frac{\partial {}^{t-1}_{\mathrm{S}}\boldsymbol{H}}{\partial {}^{t-1}\boldsymbol{V}}^{-\mathrm{T}} \frac{\partial {}^{t+1}_{\mathrm{S}}\boldsymbol{H}}{\partial {}^{t-1}\boldsymbol{V}}^{\mathrm{T}} - \frac{\partial {}^{t+1}_{\mathrm{S}}\boldsymbol{H}}{\partial {}^{t-1}\boldsymbol{U}}^{\mathrm{T}} \right) {}^{t+1}_{\mathrm{S}}\boldsymbol{\gamma} = {}^{t-1}_{\mathrm{S}}\boldsymbol{\lambda} \tag{6.45} $$

Further, by combining Eqs.(6.16), (6.43), (6.45) and (5.16), it obtains

$$
\begin{aligned}
{}^{t-1}_{\mathrm{L}}\boldsymbol{\gamma} &= -\frac{\partial^{t-1}_{\mathrm{L}}\boldsymbol{H}}{\partial^{t-1}\boldsymbol{V}}^{-\mathrm{T}} \cdot \left(\frac{\partial^{t}_{\mathrm{L}}\boldsymbol{H}}{\partial^{t-1}\boldsymbol{V}}^{\mathrm{T}} {}^{t}_{\mathrm{L}}\boldsymbol{\gamma} + \frac{\partial^{t-1}_{\mathrm{L}}\boldsymbol{R}}{\partial^{t-1}\boldsymbol{V}}^{\mathrm{T}} {}^{t-1}_{\mathrm{L}}\boldsymbol{\lambda} \right) = \\
&= -\frac{\partial^{t-1}_{\mathrm{S}}\boldsymbol{H}}{\partial^{t-1}\boldsymbol{V}}^{-\mathrm{T}} \cdot \left(\frac{\partial^{t+1}_{\mathrm{S}}\boldsymbol{H}}{\partial^{t-1}\boldsymbol{V}}^{\mathrm{T}} {}^{t+1}_{\mathrm{S}}\boldsymbol{\gamma} + \frac{\partial^{t-1}_{\mathrm{S}}\boldsymbol{R}}{\partial^{t-1}\boldsymbol{V}}^{\mathrm{T}} {}^{t-1}_{\mathrm{S}}\boldsymbol{\lambda} \right) = {}^{t-1}_{\mathrm{S}}\boldsymbol{\gamma}
\end{aligned}
\tag{6.46}
$$

From the proof at $n = t-1$ and backward calculation with Eq.(6.16), it can be easily derived that

$$
{}^{n}_{\mathrm{S}}\boldsymbol{\lambda} = {}^{n}_{\mathrm{L}}\boldsymbol{\lambda} \text{ and } {}^{n}_{\mathrm{S}}\boldsymbol{\gamma} = {}^{n}_{\mathrm{L}}\boldsymbol{\gamma} \ \ (for\ n \le t-2) \tag{6.47}
$$

Thirdly, from Eqs.(5.14), (6.22) and (6.42), it has

$$
\begin{aligned}
{}^{t}_{\mathrm{L}}\boldsymbol{\gamma}^{\mathrm{T}} \frac{\partial^{t}_{\mathrm{L}}\boldsymbol{H}}{\partial s} + {}^{t+1}_{\mathrm{L}}\boldsymbol{\gamma}^{\mathrm{T}} \frac{\partial^{t+1}_{\mathrm{L}}\boldsymbol{H}}{\partial s} &= {}^{t+1}_{\mathrm{S}}\boldsymbol{\gamma}^{\mathrm{T}} \begin{pmatrix} \boldsymbol{I} & \boldsymbol{D}^{\mathrm{e}}({}^{t}\mathbf{a} - {}^{t+1}\mathbf{a}) & \mathbf{0} \\ \mathbf{0} & -c & \mathbf{0} \\ \mathbf{0} & \boldsymbol{d} & \boldsymbol{I} \end{pmatrix} \begin{pmatrix} \boldsymbol{D}^{\mathrm{e}}\left(\frac{\partial^{t}\boldsymbol{\varepsilon}}{\partial s} - \frac{\partial^{t-1}\boldsymbol{\varepsilon}}{\partial s} \right) \\ 0 \\ \mathbf{0} \end{pmatrix} + {}^{t+1}_{\mathrm{S}}\boldsymbol{\gamma}^{\mathrm{T}} \begin{pmatrix} \boldsymbol{D}^{\mathrm{e}}\left(\frac{\partial^{t+1}\boldsymbol{\varepsilon}}{\partial s} - \frac{\partial^{t}\boldsymbol{\varepsilon}}{\partial s} \right) \\ 0 \\ \mathbf{0} \end{pmatrix} \\
&= {}^{t+1}_{\mathrm{S}}\boldsymbol{\gamma}^{\mathrm{T}} \begin{pmatrix} \boldsymbol{D}^{\mathrm{e}}\left(\frac{\partial^{t+1}\boldsymbol{\varepsilon}}{\partial s} - \frac{\partial^{t-1}\boldsymbol{\varepsilon}}{\partial s} \right) \\ 0 \\ 0 \end{pmatrix} = {}^{t+1}_{\mathrm{S}}\boldsymbol{\gamma}^{\mathrm{T}} \frac{\partial^{t}_{\mathrm{S}}\boldsymbol{H}}{\partial s}
\end{aligned}
\tag{6.48}
$$

□

Plastic load step reduction rule: Given a sequence of load steps L = {1, 2, ..., t-1, t, t+1, …, N}, if step *t* and step *t+1* are both plastic load steps, ${}^{t}\mathbf{a} = {}^{t+1}\mathbf{a}$ and $\frac{\mathrm{d}^{t}\mathbf{a}}{\mathrm{d}^{t}\boldsymbol{\sigma}} = 0$, then skip step *t* as the load steps contains only S = {1, 2, ..., t-1, t+1, …, N} will not change the sensitivity results.

Proof:

The same as in the previous proof, it is suffice to show

1. ${}^{t}_{\mathrm{L}}\boldsymbol{\lambda} = 0$
2. ${}^{n}_{\mathrm{S}}\boldsymbol{\lambda} = {}^{n}_{\mathrm{L}}\boldsymbol{\lambda}$ and ${}^{n}_{\mathrm{S}}\boldsymbol{\gamma} = {}^{n}_{\mathrm{L}}\boldsymbol{\gamma}$ for $n \le t-1$
3. ${}^{t}_{\mathrm{L}}\boldsymbol{\gamma}^{\mathrm{T}} \frac{\partial^{t}_{\mathrm{L}}\boldsymbol{H}}{\partial s} + {}^{t+1}_{\mathrm{L}}\boldsymbol{\gamma}^{\mathrm{T}} \frac{\partial^{t+1}_{\mathrm{L}}\boldsymbol{H}}{\partial s} = {}^{t+1}_{\mathrm{S}}\boldsymbol{\gamma}^{\mathrm{T}} \frac{\partial^{t+1}_{\mathrm{S}}\boldsymbol{H}}{\partial s}$

The first item is directly obtained from the second property of adjoint variables.

The second item will be obtained if it holds at $n = t-1$. To prove that, Substituting Eqs.(5.1) and (5.16) into Eq.(6.16), it has

$$ {}^{\mathrm{t-1}}_{\mathrm{L}}\boldsymbol{\lambda} = {}^{\mathrm{t-1}}_{\mathrm{S}}\boldsymbol{K}_{\mathrm{T}}{}^{-1} \cdot \left(\frac{\partial {}^{\mathrm{t-1}}_{\mathrm{S}}\boldsymbol{H}}{\partial {}^{\mathrm{t-1}}\boldsymbol{U}}^{\mathrm{T}} \frac{\partial {}^{\mathrm{t-1}}_{\mathrm{S}}\boldsymbol{H}}{\partial {}^{\mathrm{t-1}}\boldsymbol{V}}^{-\mathrm{T}} \frac{\partial {}^{\mathrm{t}}_{\mathrm{L}}\boldsymbol{H}}{\partial {}^{\mathrm{t-1}}\boldsymbol{V}}^{\mathrm{T}} {}^{\mathrm{t}}_{\mathrm{L}}\boldsymbol{\gamma} - \frac{\partial {}^{\mathrm{t}}_{\mathrm{L}}\boldsymbol{H}}{\partial {}^{\mathrm{t-1}}\boldsymbol{U}}^{\mathrm{T}} {}^{\mathrm{t}}_{\mathrm{L}}\boldsymbol{\gamma} \right) \tag{6.49} $$

Since step *t-1* and step *t+1* are two consecutive steps in load sequences S, therefore, by combining Eqs.(6.20), (6.21) and the second property of adjoint variables, it yields

$$ \frac{\partial {}^{t}_{\mathrm{L}}\boldsymbol{H}}{\partial {}^{t-1}\boldsymbol{U}}^{\mathrm{T}} {}^{t}_{\mathrm{L}}\boldsymbol{\gamma} = -({}^{t-1}\boldsymbol{B}^{\mathrm{T}}\boldsymbol{D}^{\mathrm{e}} \quad 0 \quad \boldsymbol{0}) \begin{pmatrix} {}^{t+1}_{\mathrm{L}}\boldsymbol{\gamma}_{\boldsymbol{\sigma}} \\ 0 \\ {}^{t+1}_{\mathrm{L}}\boldsymbol{\gamma}_{\boldsymbol{\alpha}} \end{pmatrix} = -({}^{t-1}\boldsymbol{B}^{\mathrm{T}}\boldsymbol{D}^{\mathrm{e}} \quad 0 \quad \boldsymbol{0}) \begin{pmatrix} {}^{t+1}_{\mathrm{L}}\boldsymbol{\gamma}_{\boldsymbol{\sigma}} \\ {}^{t+1}_{\mathrm{L}}\boldsymbol{\gamma}_{\varepsilon^{\mathrm{p}}_{\mathrm{eqv}}} \\ {}^{t+1}_{\mathrm{L}}\boldsymbol{\gamma}_{\boldsymbol{\alpha}} \end{pmatrix} = \frac{\partial {}^{t+1}_{\mathrm{S}}\boldsymbol{H}}{\partial {}^{t-1}\boldsymbol{U}}^{\mathrm{T}} {}^{t+1}_{\mathrm{S}}\boldsymbol{\gamma} \tag{6.50} $$

Utilizing Eq.(6.27), it obtains

$$ \begin{aligned} \frac{\partial {}^{t}_{\mathrm{L}}\boldsymbol{H}}{\partial {}^{t-1}\boldsymbol{V}}^{\mathrm{T}} {}^{t}_{\mathrm{L}}\boldsymbol{\gamma} &= \begin{pmatrix} \boldsymbol{I} & 0 & 0 \\ {}^{t}\mathbf{a}^{\mathrm{T}}\boldsymbol{D}^{\mathrm{e}} & 0 & -(1-\beta){}^{t}\mathbf{a}^{\mathrm{T}}\boldsymbol{D}^{\boldsymbol{\alpha}} \\ 0 & 0 & \boldsymbol{I} \end{pmatrix} \begin{pmatrix} {}^{t+1}_{\mathrm{L}}\boldsymbol{\gamma}_{\boldsymbol{\sigma}} \\ 0 \\ {}^{t+1}_{\mathrm{L}}\boldsymbol{\gamma}_{\boldsymbol{\alpha}} \end{pmatrix} \\ &= \begin{pmatrix} \boldsymbol{I} & 0 & 0 \\ {}^{t}\mathbf{a}^{\mathrm{T}}\boldsymbol{D}^{\mathrm{e}} & 0 & -(1-\beta){}^{t}\mathbf{a}^{\mathrm{T}}\boldsymbol{D}^{\boldsymbol{\alpha}} \\ 0 & 0 & \boldsymbol{I} \end{pmatrix} \begin{pmatrix} {}^{t+1}_{\mathrm{L}}\boldsymbol{\gamma}_{\boldsymbol{\sigma}} \\ {}^{t+1}_{\mathrm{L}}\boldsymbol{\gamma}_{\varepsilon^{\mathrm{p}}_{\mathrm{eqv}}} \\ {}^{t+1}_{\mathrm{L}}\boldsymbol{\gamma}_{\boldsymbol{\alpha}} \end{pmatrix} = \frac{\partial {}^{t+1}_{\mathrm{S}}\boldsymbol{H}}{\partial {}^{t-1}\boldsymbol{V}}^{\mathrm{T}} {}^{t+1}_{\mathrm{S}}\boldsymbol{\gamma} \end{aligned} \tag{6.51} $$

Finally, substituting Eqs.(6.50) and (6.51) into Eq.(6.49) yields

$$ {}^{t-1}_{\mathrm{L}}\boldsymbol{\lambda} = {}^{t-1}_{\mathrm{S}}\boldsymbol{K}_{\mathrm{T}}{}^{-1} \cdot \left(\frac{\partial {}^{t-1}_{\mathrm{S}}\boldsymbol{H}}{\partial {}^{t-1}\boldsymbol{U}}^{\mathrm{T}} \frac{\partial {}^{t-1}_{\mathrm{S}}\boldsymbol{H}}{\partial {}^{t-1}\boldsymbol{V}}^{-\mathrm{T}} \frac{\partial {}^{t+1}_{\mathrm{S}}\boldsymbol{H}}{\partial {}^{t-1}\boldsymbol{V}}^{\mathrm{T}} - \frac{\partial {}^{t+1}_{\mathrm{S}}\boldsymbol{H}}{\partial {}^{t-1}\boldsymbol{U}}^{\mathrm{T}} \right) {}^{t+1}_{\mathrm{S}}\boldsymbol{\gamma} = {}^{t-1}_{\mathrm{S}}\boldsymbol{\lambda} \tag{6.52} $$

Further, substituting Eqs.(6.51), (6.52) and (5.16) into Eq.(6.16), it has

$$ \begin{aligned} {}^{t-1}_{\mathrm{L}}\boldsymbol{\gamma} &= -\frac{\partial {}^{t-1}_{\mathrm{L}}\boldsymbol{H}}{\partial {}^{t-1}\boldsymbol{V}}^{-\mathrm{T}} \left(\frac{\partial {}^{t}_{\mathrm{L}}\boldsymbol{H}}{\partial {}^{t-1}\boldsymbol{V}}^{\mathrm{T}} {}^{t}_{\mathrm{L}}\boldsymbol{\gamma} + \frac{\partial {}^{t-1}_{\mathrm{L}}\boldsymbol{R}}{\partial {}^{t-1}\boldsymbol{V}}^{\mathrm{T}} {}^{t-1}_{\mathrm{L}}\boldsymbol{\lambda} \right) = \\ &= -\frac{\partial {}^{t-1}_{\mathrm{S}}\boldsymbol{H}}{\partial {}^{t-1}\boldsymbol{V}}^{-\mathrm{T}} \left(\frac{\partial {}^{t+1}_{\mathrm{S}}\boldsymbol{H}}{\partial {}^{t-1}\boldsymbol{V}}^{\mathrm{T}} {}^{t+1}_{\mathrm{S}}\boldsymbol{\gamma} + \frac{\partial {}^{t-1}_{\mathrm{S}}\boldsymbol{R}}{\partial {}^{t-1}\boldsymbol{V}}^{\mathrm{T}} {}^{t-1}_{\mathrm{S}}\boldsymbol{\lambda} \right) = {}^{t-1}_{\mathrm{S}}\boldsymbol{\gamma} \end{aligned} \tag{6.53} $$

From Eqs.(6.22) and the second property of adjoint variables, the third item is obtained

$$
\begin{aligned}
&{}^{t}_{\mathrm{L}}\boldsymbol{\gamma}^{\mathrm{T}}\frac{\partial\,{}^{t}_{\mathrm{L}}\boldsymbol{H}}{\partial s}+{}^{t+1}_{\mathrm{L}}\boldsymbol{\gamma}^{\mathrm{T}}\frac{\partial\,{}^{t+1}_{\mathrm{L}}\boldsymbol{H}}{\partial s}\\
&\quad=\begin{pmatrix}{}^{t+1}_{\mathrm{L}}\boldsymbol{\gamma}_{\boldsymbol{\sigma}}\\ 0\\ {}^{t+1}_{\mathrm{L}}\boldsymbol{\gamma}_{\boldsymbol{\alpha}}\end{pmatrix}^{\mathrm{T}}\begin{pmatrix}\boldsymbol{D}^{\mathrm{e}}\left(\dfrac{\partial^{t}\boldsymbol{\varepsilon}}{\partial s}-\dfrac{\partial^{t-1}\boldsymbol{\varepsilon}}{\partial s}\right)\\ 0\\ 0\end{pmatrix}+\begin{pmatrix}{}^{t+1}_{\mathrm{L}}\boldsymbol{\gamma}_{\boldsymbol{\sigma}}\\ {}^{t+1}_{\mathrm{L}}\boldsymbol{\gamma}_{\varepsilon^{\mathrm{p}}_{\mathrm{eqv}}}\\ {}^{t+1}_{\mathrm{L}}\boldsymbol{\gamma}_{\boldsymbol{\alpha}}\end{pmatrix}^{\mathrm{T}}\begin{pmatrix}\boldsymbol{D}^{\mathrm{e}}\left(\dfrac{\partial^{t+1}\boldsymbol{\varepsilon}}{\partial s}-\dfrac{\partial^{t}\boldsymbol{\varepsilon}}{\partial s}\right)\\ 0\\ 0\end{pmatrix} \qquad (6.54)\\
&\quad=\begin{pmatrix}{}^{t+1}_{\mathrm{S}}\boldsymbol{\gamma}_{\boldsymbol{\sigma}}\\ {}^{t+1}_{\mathrm{S}}\boldsymbol{\gamma}_{\varepsilon^{\mathrm{p}}_{\mathrm{eqv}}}\\ {}^{t+1}_{\mathrm{S}}\boldsymbol{\gamma}_{\boldsymbol{\alpha}}\end{pmatrix}^{\mathrm{T}}\begin{pmatrix}\boldsymbol{D}^{\mathrm{e}}\left(\dfrac{\partial^{t+1}\boldsymbol{\varepsilon}}{\partial s}-\dfrac{\partial^{t-1}\boldsymbol{\varepsilon}}{\partial s}\right)\\ 0\\ 0\end{pmatrix}={}^{t+1}_{\mathrm{S}}\boldsymbol{\gamma}^{\mathrm{T}}\frac{\partial\,{}^{t+1}_{\mathrm{S}}\boldsymbol{H}}{\partial s}
\end{aligned}
$$

□

The elastic load step reduction rule, the same as in the case of isotropic hardening, applies to all types of elements. The plastic load step reduction rule strictly applies to 1D elements. For general 2D and 3D elements, the following empirical rule is proposed to reduce the plastic load steps.

Empirical rule: Given a sequence of load steps L = {1, 2, ..., t-1, t, t+1, …, N}, if step *t* and step *t+1* are in a monotonic loading stage, then step *t* could be skipped in the sensitivity analysis.

Sensitivity analysis following the empirical rule will sacrifice some accuracy in exchange for efficiency. Its effectiveness and influence on the accuracy of sensitivity are investigated through numerical examples in the following.

6.4 Demonstration with a 100-bar truss structure

In this section, the load step reduction rules for mixed hardening elastoplasticity are demonstrated through 100-bar truss examples presented in Section 5.4. The only difference is that the material is assumed to follow mixed hardening rule with a hardening ratio equal to 0.1.

The load history, comprising a total of 50 load steps, is illustrated in Figure 6-2. It is the same as the second load case in Section 5.4. This load history consists of four stages: the initial loading stage from step 1 to step 10, the fully unloading stage from step 11 to step 20, the reverse loading stage from step 21 to step 35, and finally, the fully unloading stage from step 36 to step 50. In comparison with Figure 5-3, where an isotropic hardening model is assumed, more steps exhibit plastic behavior here under the mixed hardening model.

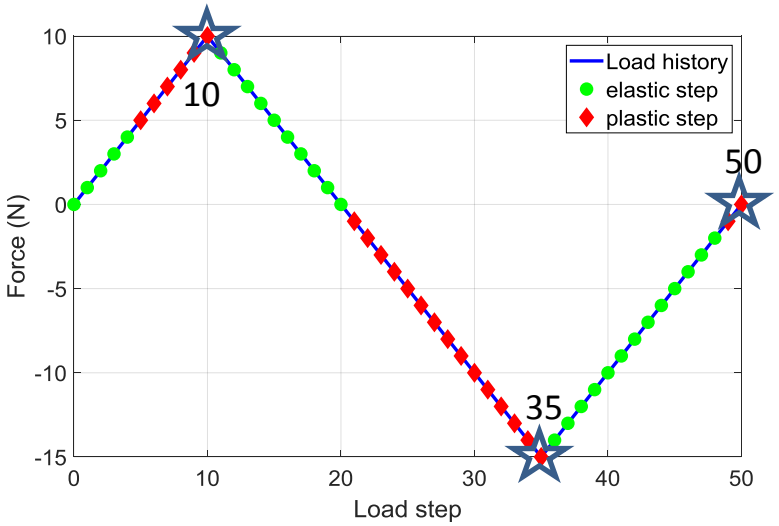

Figure 6-2. Load history of the 100-bar truss example under mixed hardening model. Pentagrams depict the reduced load steps in the sensitivity analysis

All elastic load steps could be skipped in the sensitivity analysis according to the elastic load step reduction rule. In the monotonic loading and reverse loading stages, flow vectors remain constant. The former in each pair of consecutive plastic steps can be skipped following the plastic load step reduction rule. Therefore, only plastic steps 10, 35, and 50 remain in the sensitivity analysis. The force directions in these three steps are opposite, causing the flow vector of some bars to change direction. Hence, the load steps can't be further reduced. In summary, steps 10, 35, and 50 are necessary in the sensitivity analysis. They are highlighted in Figure 6-2 by pentagrams and listed in Table 6-1.

Table 6-1. Reduced load step for the 100-bar truss example with mixed hardening elastoplasticity

Reduced load step	Corresponding FEA load step	Load (N)
1	10	10
2	35	-15
3	50	0

The system responses are the vertical displacement at the free end and the equivalent plastic strain of an element at the fixed end. The sensitivity results, calculated by reduced load steps, are compared with those using all load steps in Figure 6-3 (a) and (c). Their relative values are presented in Figure 6-3 (b) and (d). They show that the sensitivities with reduced load steps are perfectly accurate in this 1D element example.

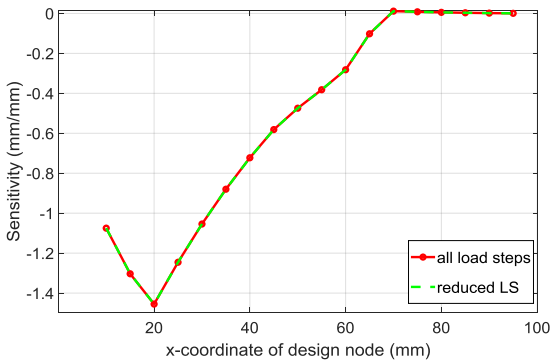

(a) Sensitivity of vertical displacement response

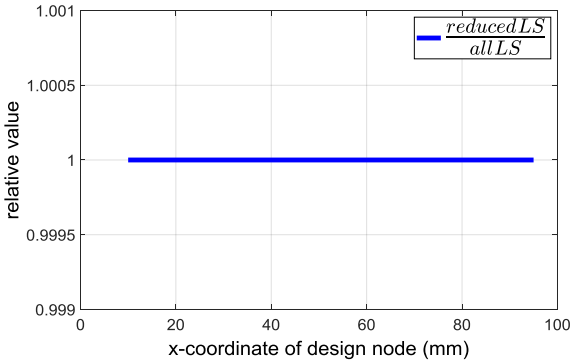

(b) Sensitivity relative value of vertical displacement response

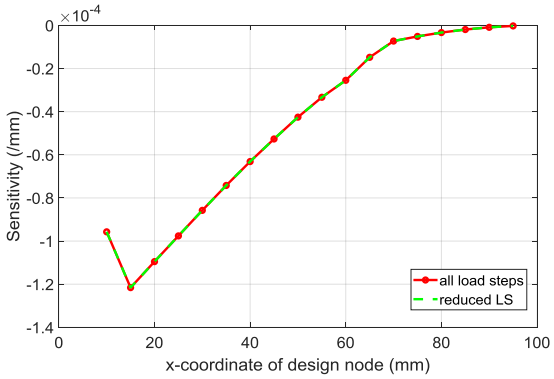

(c) Sensitivity of equivalent plastic strain response

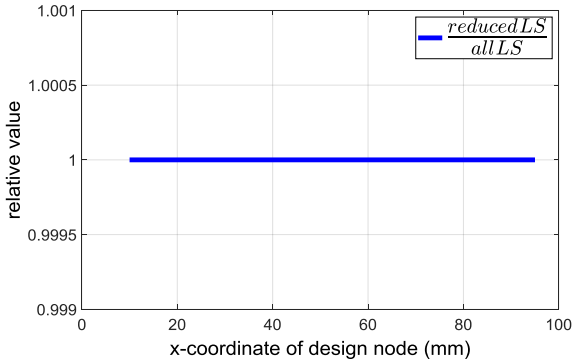

(d) Sensitivity relative value of equivalent plastic strain response

Figure 6-3. Sensitivity comparison for the 100-bar truss example with mixed hardening elastoplasticity

6.5 Demonstration with a connecting rod example

In this section, the applicability of load step reduction rules for mixed hardening model is demonstrated through the conrod example in Section 5.6. All the setups of the problem are the same except a hardening ratio 0.3 is assumed for the material. The load history, identical to that in Section 5.6, is depicted in Figure 6-4. It illustrates that, due to the change in the hardening model, the elastic and plastic steps in the nonlinear analysis differ.

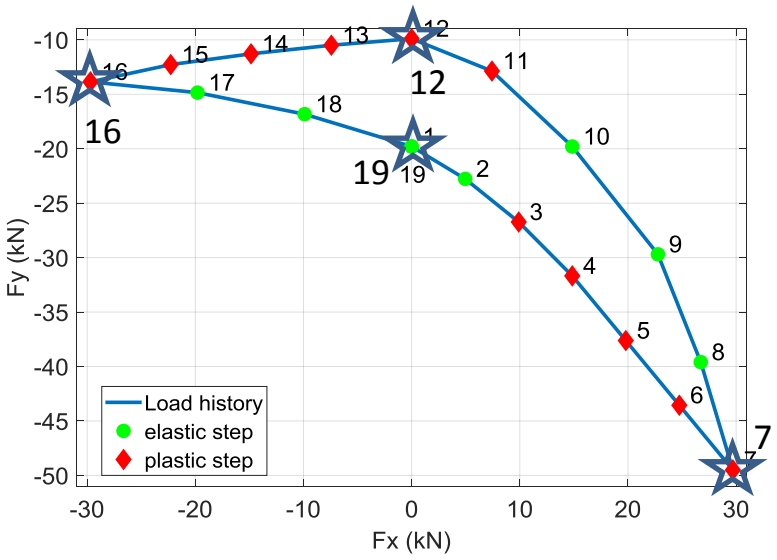

Figure 6-4. Load history on the small end of the conrod with hardening ratio of 0.3. Pentagrams depict the reduced load steps.

According to the elastic load step reduction rule, all intermediate elastic load steps are skipped in the sensitivity analysis. Based on the empirical rule, plastic steps 2 to step 6, step 11, step 13 to step 15 could be skipped because they lie in monotonically loading procedures. The four load steps needed in the sensitivity analysis are highlighted by pentagrams in Figure 6-4 and listed in Table 6-2. In contrast to the isotropic hardening case, the inclusion of plastic step 12 is necessary in this scenario.

Table 6-2. Reduced load steps in sensitivity analysis with hardening ratio 0.3

Reduced load step	Corresponding FEA load step	Load (kN)
1	7	Fx= 29.7, Fy= -49.5
2	12	Fx=0.0, Fy= -9.9
3	16	Fx= -29.7, Fy= -13.9
4	19	Fx= 0.0, Fy= -19.8

The three system responses are the same as in Section 5.6, i.e., average equivalent plastic strain around critical area, and average x and y displacements at the small end. The sensitivities obtained with reduced load steps are compared with those using all load steps in Figure 6-5. They show that the sensitivities match very well.

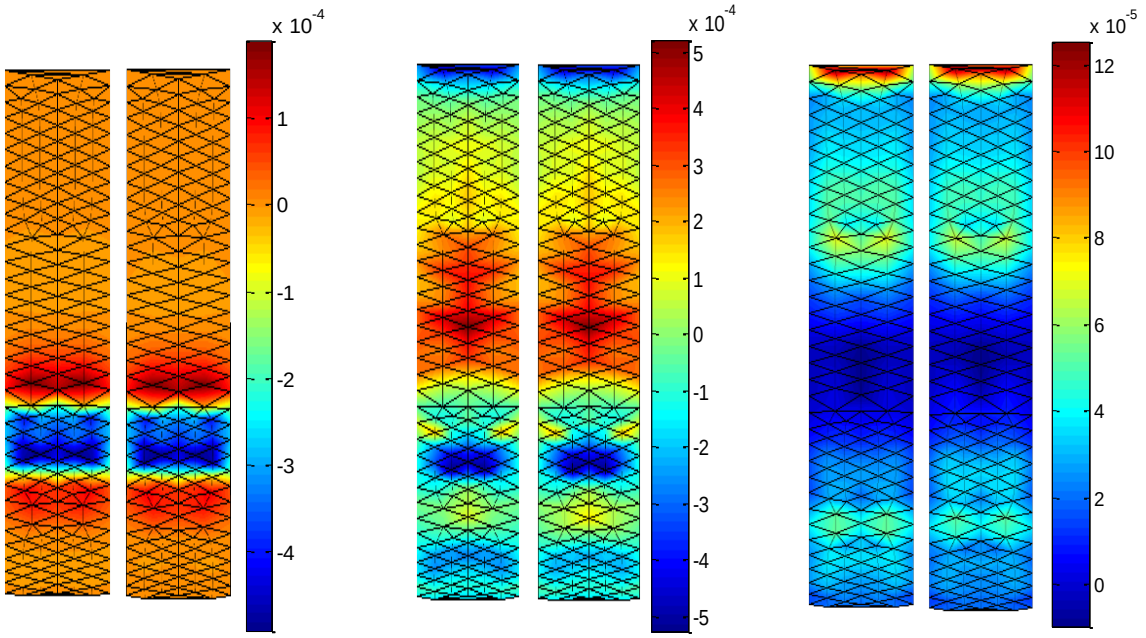

(a) Sensitivity of average equivalent plastic strain response

(b) Sensitivity of average x-displacement response

(c) Sensitivity of average y-displacement response

Figure 6-5. Comparison of sensitivity results. In each of these three figures, the result with reduced load steps is depicted on the left and result with all load steps is presented on the right

To investigate the influence of the hardening ratio on sensitivity accuracy, the percentage errors of sensitivities under isotropic hardening (β=1), kinematic hardening (β=0) and mixed hardening with β=0.3 are compared in Table 6-3. The errors are calculated by comparing sensitivities using reduced load steps to sensitivities obtained with all load steps.

Table 6-3. Relative error of sensitivities under different hardening ratio

Response	Isotropic hardening ($\beta = 1$)		Mixed hardening ($\beta = 0.3$)		Kinematic hardening ($\beta = 0$)	
	Maximum error	Average error	Maximum error	Average error	Maximum error	Average error
equiv. plastic strain	4.3%	0.3%	5.9%	2.3%	31.3%	6.2%
x-displacement	1.2%	0.3%	17%	6.5%	19.1%	4.5%
y-displacement	1.2%	0.2%	28%	10.0%	51.9%	10.3%

It should be noted that sensitivities are typically used to determine the direction in which to update the design variables in gradient-based optimization. The directional vector is primarily influenced by relatively large

values, while sensitivities with relatively small values are considered less important. However, the relative error at these small value points could be extremely large due to small denominators, introducing unnecessary noise in the assessment of sensitivity accuracy. For this reason, the average and maximum relative errors listed in Table 6-3 are evaluated only with sensitivities whose absolute values are not less than 1% of the maximum absolute value.

Table 6-3 shows that the levels of accuracy for the mixed hardening model and pure kinematic hardening model are similar. The errors under the pure isotropic hardening model are the least. The increase in errors in kinematic hardening and mixed hardening can be explained by the more severe violation of the constant flow vector condition in reducing plastic load steps. Under these two models, the flow vectors and their derivatives are not only dependent on the stress tensor but also on the back stress tensor. Therefore, even in a monotonic loading procedure, the flow vector may change its direction more significantly than in the pure isotropic hardening case.

7. Adjoint sensitivity analysis and load step reduction for finite strain elastoplasticity

In this chapter, load step reduction rules for finite strain elastoplasticity are investigated. The finite strain elastoplasticity analysis is briefly introduced, followed by the presentation of adjoint sensitivity formulations. The discussion on load step reduction is then extended to this type of problem. Applicability and limitations are demonstrated through several examples.

7.1 Finite strain elastoplasticity

The extension of the small strain plasticity to the finite strain plasticity is not straightforward. The fundamental difference lies in the strain measure and how the total deformation is decomposed into elastic and plastic parts.

In the small strain case, the Green-Lagrangian strain could be used, and the total strain is additively decomposed into an elastic and a plastic term. For finite strain nonlinearity, the logarithmic strain, or the so-called Hencky strain measure, is always employed as a proper measure. The elastic and plastic parts are obtained based on the multiplicative decomposition of the total deformation gradient.

Given the total deformation gradient ${}^{t}_{0}\boldsymbol{X}$, which is the derivative of deformed configuration at step t with respect to the original configuration at step 0, it can be decomposed into the multiplication of an elastic deformation gradient ${}^{t}\boldsymbol{X}^{\mathrm{e}}$ and a plastic deformation gradient ${}^{t}\boldsymbol{X}^{\mathrm{p}}$

$$ {}^{t}_{0}\boldsymbol{X} = {}^{t}\boldsymbol{X}^{\mathrm{e}} \cdot {}^{t}\boldsymbol{X}^{\mathrm{p}} \tag{7.1} $$

This multiplicative decomposition is proposed by Lee and Liu [LL67, Lee69], and widely accepted in the finite strain elastoplasticity analysis. The elastic deformation gradient can further be decomposed through right polar decomposition:

$$ {}^{t}\boldsymbol{X}^{\mathrm{e}} = {}^{t}\boldsymbol{R}^{\mathrm{e}} \cdot {}^{t}\boldsymbol{U}^{\mathrm{e}} \tag{7.2} $$

where ${}^t\boldsymbol{R}^{\mathrm{e}}$ is an orthonormal matrix, referred to as the elastic rotation tensor, and ${}^t\boldsymbol{U}^{\mathrm{e}}$ is a symmetric positive-definite matrix, called the elastic right stretch tensor. The elastic logarithmic strain is then defined by

$$ {}^t\boldsymbol{\varepsilon}^{\mathrm{e}} = \frac{1}{2} ln {}^t\boldsymbol{X}^{\mathrm{e}\mathrm{T}} {}^t\boldsymbol{X}^{\mathrm{e}} = ln {}^t\boldsymbol{U}^{\mathrm{e}} \tag{7.3} $$

The work-conjugate stress measure of this strain is the rotated Kirchhoff stress $\bar{\boldsymbol{\tau}}$ [GB95, CMB11, NEM16]. The constitutive relationship between them is

$$ {}^t\bar{\boldsymbol{\tau}} = \boldsymbol{D}^{\mathrm{e}} {}^t\boldsymbol{\varepsilon}^{\mathrm{e}} \tag{7.4} $$

The rotated Kirchhoff stress is the spatial Kirchhoff stress $\boldsymbol{\tau}$ rotated to the intermediate stress-free configuration by ${}^t\boldsymbol{R}^{\mathrm{e}}$. The spatial Kirchhoff stress is eventually obtained by back-rotating $\bar{\boldsymbol{\tau}}$ as

$$ {}^t\boldsymbol{\tau} = {}^t\boldsymbol{R}^{\mathrm{e}} {}^t\bar{\boldsymbol{\tau}} {}^t\boldsymbol{R}^{\mathrm{e}\mathrm{T}} \tag{7.5} $$

The Kirchhoff stress is related to the Cauchy stress $\boldsymbol{\sigma}$ through the Jacobian determinant of the deformation gradient by:

$$ {}^t\boldsymbol{\tau} = J {}^t\boldsymbol{\sigma} = \det|{}^t_0\boldsymbol{X}| \cdot {}^t\boldsymbol{\sigma} \tag{7.6} $$

The internal force can be obtained by integration either under the deformed volume or the initial volume:

$$ \boldsymbol{F}^{\mathrm{int}} = \int_V {}^t\boldsymbol{B} {}^t\boldsymbol{\sigma} dv = \int_{V^0} {}^t\boldsymbol{B} {}^t\boldsymbol{\tau} dv \tag{7.7} $$

The nonlinear Newton-Raphson solution procedure for finite strain finite element analysis is illustrated in Figure 7-1. In contrast to the small strain case, the plastic deformation gradient is an additional quantity to be solved at each step. To simplify the discussion, isotropic hardening plasticity is assumed initially. The extension to mixed-hardening and kinematic hardening cases will be presented in Section 7.5.

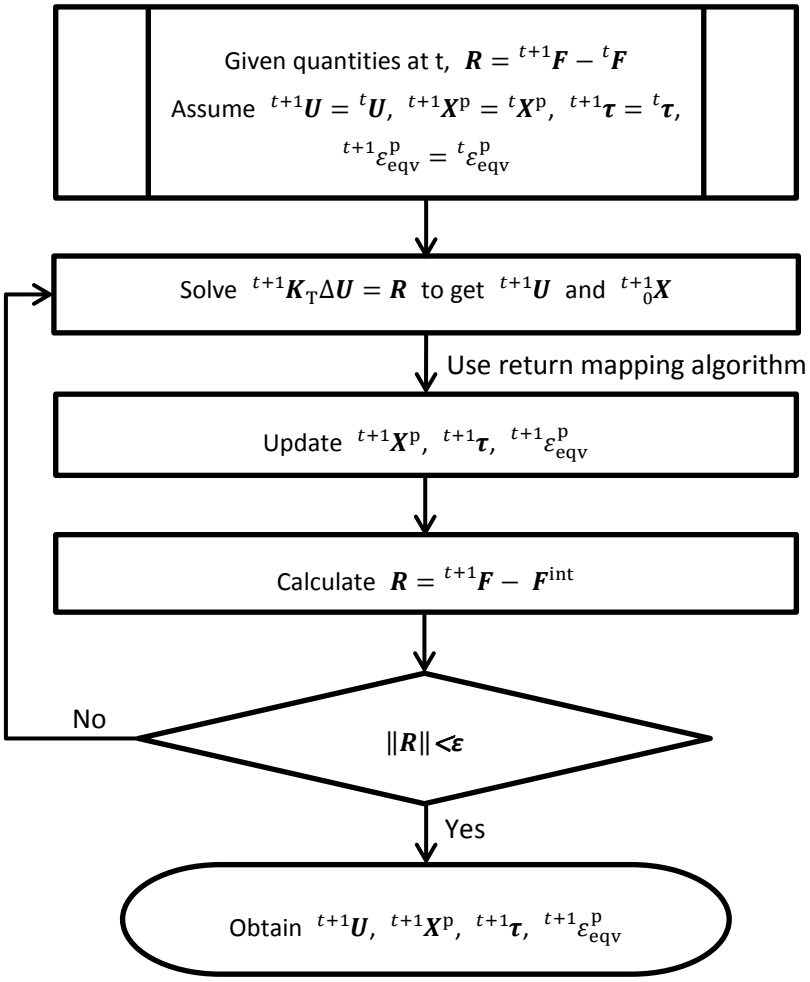

Figure 7-1. Newton-Raphson solution procedure for finite strain elastoplasticity

The return mapping algorithm is employed to determine stress, equivalent plastic strain, and plastic deformation gradient at step *t+1* based on the total deformation gradient at *t+1* and quantities from the preceding step at *t*. The algorithm's procedure is summarized as follows [EB90, DPR94]:

Given ${}^{t+1}_{0}\boldsymbol{X}$, and quantities of ${}^{t}\boldsymbol{X}^{\mathrm{p}}$, ${}^{t}\varepsilon_{\mathrm{eqv}}^{\mathrm{p}}$, ${}^{t}\boldsymbol{\tau}$ at previous step *t*,

(a) Assume a trial elastic state, i.e. $\Delta\varepsilon_{\mathrm{eqv}}^{\mathrm{p}} = 0$ and $\Delta\boldsymbol{\varepsilon}^{\mathrm{p}} = \boldsymbol{0}$. Obtain the trial elastic deformation gradient by

$$ {}^{t+1}\boldsymbol{X}_{*}^{\mathrm{e}} = {}^{t+1}_{0}\boldsymbol{X} \cdot {}^{t}\boldsymbol{X}^{\mathrm{p}-1} \tag{7.8} $$

(b) Perform the right polar decomposition

$$^{t+1}\boldsymbol{X}_*^{\mathrm{e}} = {}^{t+1}\boldsymbol{R}_*^{\mathrm{e}} \cdot {}^{t+1}\boldsymbol{U}_*^{\mathrm{e}} \tag{7.9}$$

(c) Calculate the trial elastic logarithmic strain and trial stress

$$^{t+1}\boldsymbol{\varepsilon}_*^{\mathrm{e}} = \frac{1}{2} ln^{t+1}\boldsymbol{X}_*^{\mathrm{e}\mathrm{T}}{}^{t+1}\boldsymbol{X}_*^{\mathrm{e}} = ln^{t+1}\boldsymbol{U}_*^{\mathrm{e}} \tag{7.10}$$

$$^{t+1}\bar{\boldsymbol{\tau}}_* = \boldsymbol{D}^{\mathrm{e}}{}^{t+1}\boldsymbol{\varepsilon}_*^{\mathrm{e}} \tag{7.11}$$

(d) Check for the yield condition. If $|^{t+1}\bar{\boldsymbol{\tau}}_*|_{\mathrm{eqv}} - {}^{t}\sigma_{\mathrm{Y}} - E^{\mathrm{p}} \cdot \Delta\varepsilon_{\mathrm{eqv}}^{\mathrm{p}} \leq 0$, then $^{t+1}\bar{\boldsymbol{\tau}} = {}^{t+1}\bar{\boldsymbol{\tau}}_*$, and the algorithm stops. If not, continues to step (e).

(e) Calculate the trial associated flow vector:

$$^{t+1}\mathbf{a} = \frac{d\left|^{t+1}\bar{\boldsymbol{\tau}}_*\right|_{\mathrm{eqv}}}{d^{t+1}\bar{\boldsymbol{\tau}}_*} \tag{7.12}$$

(f) Update the increment equivalent plastic strain and incremental plastic stretch

$$\Delta\varepsilon_{\mathrm{eqv}}^{\mathrm{p}} = \Delta\varepsilon_{\mathrm{eqv}}^{\mathrm{p}} + \frac{|^{t+1}\bar{\boldsymbol{\tau}}_*|_{\mathrm{eqv}} - {}^{t}\sigma_{\mathrm{Y}} - E^{\mathrm{p}} \cdot \Delta\varepsilon_{\mathrm{eqv}}^{\mathrm{p}}}{{}^{t+1}\mathbf{a} \cdot D^{\mathrm{e}} \cdot {}^{t+1}\mathbf{a}^{\mathrm{T}} + E^{\mathrm{p}}} \tag{7.13}$$

$$\Delta\boldsymbol{\varepsilon}^{\mathrm{p}} = \Delta\varepsilon_{\mathrm{eqv}}^{\mathrm{p}} \cdot {}^{t+1}\mathbf{a} \tag{7.14}$$

(g) Update trial elastic deformation gradient and trial elastic strain

$$^{t+1}\boldsymbol{X}^{\mathrm{e}} = {}^{t+1}\boldsymbol{X}_*^{\mathrm{e}} e^{-\Delta\boldsymbol{\varepsilon}^{\mathrm{p}}} \tag{7.15}$$

$$^{t+1}\boldsymbol{\varepsilon}^{\mathrm{e}} = \frac{1}{2} ln^{t+1}\boldsymbol{X}^{\mathrm{e}\mathrm{T}}{}^{t+1}\boldsymbol{X}^{\mathrm{e}} \tag{7.16}$$

(h) Update trial elastic stress and go back to step (d).

$$^{t+1}\bar{\boldsymbol{\tau}} = \boldsymbol{D}^{\mathrm{e}}{}^{t+1}\boldsymbol{\varepsilon}^{\mathrm{e}} \tag{7.17}$$

For moderately large elastic strain, such as those encountered in metal plasticity, it has been noted [MB05, CMB11] that Eqs.(7.15) and (7.16) could be approximated by

$$^{t+1}\boldsymbol{\varepsilon}^{\mathrm{e}} \approx {}^{t+1}\boldsymbol{\varepsilon}_{*}^{\mathrm{e}} - \Delta\boldsymbol{\varepsilon}^{\mathrm{p}} \tag{7.18}$$

This approximation is exact for isotropic hardening plasticity with associated flow rule or combined hardening and kinematic hardening cases where the stress and back stress tensors commute [EB90]. Substituting Eq.(7.18) into Eq.(7.4), it follows

$$^{t+1}\bar{\boldsymbol{\tau}} = \boldsymbol{D}^{\mathrm{e}}\boldsymbol{\varepsilon}_{*}^{\mathrm{e}} - \boldsymbol{D}^{\mathrm{e}}\Delta\boldsymbol{\varepsilon}^{\mathrm{p}} \tag{7.19}$$

When the return mapping algorithm stops, the following quantities are obtained

$$^{t+1}\boldsymbol{\tau} = {}^{t+1}\boldsymbol{R}_{*}^{\mathrm{e}} \cdot {}^{t+1}\bar{\boldsymbol{\tau}} \cdot {}^{t+1}\boldsymbol{R}_{*}^{\mathrm{e}^{\mathrm{T}}} \tag{7.20}$$

$$^{t+1}\varepsilon_{\mathrm{eqv}}^{\mathrm{p}} = {}^{t}\varepsilon_{\mathrm{eqv}}^{\mathrm{p}} + \Delta\varepsilon_{\mathrm{eqv}}^{\mathrm{p}} \tag{7.21}$$

$$^{t+1}\boldsymbol{X}^{\mathrm{p}} = e^{\Delta\boldsymbol{\varepsilon}^{\mathrm{p}}}\,{}^{t}\boldsymbol{X}^{\mathrm{p}} \tag{7.22}$$

In Eq.(7.20), the trial elastic rotation tensor is employed to back-rotate the stress tensor. Under the associated flow rule, the incremental plastic stretch $\Delta\boldsymbol{\varepsilon}^{\mathrm{p}}$ and the trial elastic stress tensor $^{\mathrm{t+1}}\boldsymbol{U}_{*}^{\mathrm{e}}$ have the same eigenvectors. Consequently, it can be verified that the trial elastic rotation tensor $^{t+1}\boldsymbol{R}_{*}^{\mathrm{e}}$ equals the real elastic rotation tensor $^{t+1}\boldsymbol{R}^{\mathrm{e}}$.

According to Eq.(7.7), the tangent stiffness matrix at step t is calculated by

$$\begin{aligned} {}^{t}\boldsymbol{K}_{\tan} = \frac{d\boldsymbol{F}^{\mathrm{int}}}{d^{t}\boldsymbol{U}} &= \int_{V^{0}} \frac{d^{t}\boldsymbol{B}}{d^{t}\boldsymbol{U}}\,{}^{t}\boldsymbol{\tau}\,dv + \int_{V^{0}} {}^{t}\boldsymbol{B}\,\frac{d^{t}\boldsymbol{R}^{\mathrm{e}}}{d^{t}\boldsymbol{U}}\,{}^{t}\bar{\boldsymbol{\tau}}\,{}^{t}\boldsymbol{R}^{\mathrm{e}^{\mathrm{T}}}dv \\ &+ \int_{V^{0}} {}^{t}\boldsymbol{B}\,{}^{t}\boldsymbol{R}^{\mathrm{e}}\boldsymbol{D}\,\frac{d^{t}\boldsymbol{\varepsilon}_{*}^{\mathrm{e}}}{d^{t}\boldsymbol{U}}\,{}^{t}\boldsymbol{R}^{\mathrm{e}^{\mathrm{T}}}dv + \int_{V^{0}} {}^{t}\boldsymbol{B}\,{}^{t}\boldsymbol{R}^{\mathrm{e}}\,{}^{t}\bar{\boldsymbol{\tau}}\,\frac{d^{t}\boldsymbol{R}^{\mathrm{e}^{\mathrm{T}}}}{d^{t}\boldsymbol{U}}dv \end{aligned} \tag{7.23}$$

where the constitutive relation matrix is

$$\boldsymbol{D} = \begin{cases} \boldsymbol{D}^{\mathrm{e}} & \text{(elastic state)} \\ \boldsymbol{D}^{\mathrm{ep}} \text{ in Eq. (2.27)} & \text{(plastic state)} \end{cases} \tag{7.24}$$

7.2 Adjoint sensitivity analysis with logarithmic strain elastoplasticity

The formulation of adjoint sensitivity with logarithmic strain elastoplasticity is derived in this section.

Firstly, a set of state variables sufficient for deriving other physical quantities at each time step should be selected. The selection of state variables is not unique. To achieve a less complicated expression in the sensitivity formulation, the following four quantities are chosen: displacement, rotated Kirchhoff stress, equivalent plastic strain, and the inverse of the plastic deformation gradient.

$$ {}^{t}\boldsymbol{U}, {}^{t}\boldsymbol{V} \stackrel{\text{def}}{=} \left\{ {}^{t}\bar{\boldsymbol{\tau}}, {}^{t}\varepsilon^{\mathrm{p}}_{\mathrm{eqv}}, {}^{t}\boldsymbol{X}^{\mathrm{p}^{-1}} \right\} \tag{7.25} $$

In comparison with the small strain case in Eq.(4.1), a variable describing plastic deformation is included due to the multiplicative decomposition of the deformation gradient.

The adjoint sensitivity formulation can be derived in a manner similar to that of the small strain case, employing several governing equations. The equilibrium condition serves as one of them:

$$ \mathbf{0} \equiv {}^{t}\boldsymbol{R}({}^{t}\boldsymbol{U}, {}^{t}\boldsymbol{V}, {}^{t-1}\boldsymbol{V}, s) = {}^{t}\boldsymbol{F} - \int_{V^0} {}^{t}\boldsymbol{B}\, {}^{t}\boldsymbol{R}^{e}\, {}^{t}\bar{\boldsymbol{\tau}}\, {}^{t}\boldsymbol{R}^{e\mathrm{T}} dv \quad (\mathrm{t} = 1,2,\ldots,\mathrm{N}) \tag{7.26} $$

As stated in Eq.(7.9), ${}^{t}\boldsymbol{R}^{\mathrm{e}}$ s a function of the total deformation gradient at step t and the inverse of the plastic deformation gradient at the previous step *t-1*. Therefore, the residual force is a function of the current displacement and state vectors at the current and previous steps. The total derivative of the residual force with respect to a design variable is

$$ \frac{d\,{}^{t}\boldsymbol{R}}{ds} = \frac{\partial\,{}^{t}\boldsymbol{R}}{\partial s} + \frac{\partial\,{}^{t}\boldsymbol{R}}{\partial\,{}^{t}\boldsymbol{U}} \cdot \frac{d\,{}^{t}\boldsymbol{U}}{ds} + \frac{\partial\,{}^{t}\boldsymbol{R}}{\partial\,{}^{t}\boldsymbol{V}} \cdot \frac{d\,{}^{t}\boldsymbol{V}}{ds} + \frac{\partial\,{}^{t}\boldsymbol{R}}{\partial\,{}^{t-1}\boldsymbol{V}} \cdot \frac{d\,{}^{t-1}\boldsymbol{V}}{ds} \tag{7.27} $$

Besides the equilibrium condition, according to Eq.(7.19), the stress and elastic right stretch tensor follow the relation

$$ {}^{t}\bar{\boldsymbol{\tau}} = \boldsymbol{D}^{\mathrm{e}} ln {}^{t}\boldsymbol{U}_{*}^{\mathrm{e}} - \boldsymbol{D}^{\mathrm{e}} \cdot {}^{t}\Delta\boldsymbol{\varepsilon}^{\mathrm{p}} \tag{7.28} $$

where the trial elastic stretch tensor is a function of the total deformation gradient at step *t* and inverse of plastic deformation gradient at previous step *t-1*.

The yield and consistency condition is

$$ \left({}^{t}\varepsilon_{\mathrm{eqv}}^{\mathrm{p}} - {}^{t-1}\varepsilon_{\mathrm{eqv}}^{\mathrm{p}}\right) \cdot \left[|{}^{t}\bar{\boldsymbol{\tau}}|_{\mathrm{eqv}} - \sigma_{\mathrm{Y}}\left({}^{t}\varepsilon_{\mathrm{eqv}}^{\mathrm{p}}\right)\right] = 0 \tag{7.29} $$

And the inverse plastic deformation gradient is updated by

$$ {}^{t}\boldsymbol{X}^{\mathrm{p}^{-1}} = {}^{t-1}\boldsymbol{X}^{\mathrm{p}^{-1}} \cdot e^{-{}^{t}\Delta\boldsymbol{\varepsilon}^{\mathrm{p}}} \tag{7.30} $$

Eqs.(7.28) to (7.30) form the dependent residual ${}^{\mathrm{t}}\boldsymbol{H}$, which is identical to zero at each load step

$$ {}^{t}\boldsymbol{H}({}^{t}\boldsymbol{U}, {}^{t}\boldsymbol{V}, {}^{t-1}\boldsymbol{V}, s) = \begin{pmatrix} {}^{t}\bar{\boldsymbol{\tau}} - \boldsymbol{D}^{\mathrm{e}} ln {}^{t}\boldsymbol{U}_{*}^{\mathrm{e}} + \boldsymbol{D}^{\mathrm{e}} \cdot {}^{t}\Delta\boldsymbol{\varepsilon}^{\mathrm{p}} \\ \left({}^{t}\varepsilon_{\mathrm{eqv}}^{\mathrm{p}} - {}^{t-1}\varepsilon_{\mathrm{eqv}}^{\mathrm{p}}\right) \cdot \left[|{}^{t}\bar{\boldsymbol{\tau}}|_{\mathrm{eqv}} - \sigma_{\mathrm{Y}}\left({}^{t}\varepsilon_{\mathrm{eqv}}^{\mathrm{p}}\right)\right] \\ {}^{t}\boldsymbol{X}^{\mathrm{p}^{-1}} - {}^{t-1}\boldsymbol{X}^{\mathrm{p}^{-1}} \cdot e^{-{}^{t}\Delta\boldsymbol{\varepsilon}^{\mathrm{p}}} \end{pmatrix} \equiv \boldsymbol{0} \tag{7.31} $$

The total derivative of the dependent residual with respect to a design variable is

$$ \frac{d\,{}^{t}\boldsymbol{H}}{ds} = \frac{\partial\,{}^{t}\boldsymbol{H}}{\partial s} + \frac{\partial\,{}^{t}\boldsymbol{H}}{\partial\,{}^{t}\boldsymbol{U}} \cdot \frac{d\,{}^{t}\boldsymbol{U}}{ds} + \frac{\partial\,{}^{t}\boldsymbol{H}}{\partial\,{}^{t}\boldsymbol{V}} \cdot \frac{d\,{}^{t}\boldsymbol{V}}{ds} + \frac{\partial\,{}^{t}\boldsymbol{H}}{\partial\,{}^{t-1}\boldsymbol{V}} \cdot \frac{d\,{}^{t-1}\boldsymbol{V}}{ds} \tag{7.32} $$

Then, following the same procedure as in small strain case, the adjoint sensitivity formulation of a response f is

$$ \frac{df}{ds} = \frac{\partial f}{\partial s} - \sum_{t=1}^{\mathrm{N}} {}^{t}\boldsymbol{\lambda}^{\mathrm{T}} \frac{\partial\,{}^{t}\boldsymbol{R}}{\partial s} - \sum_{\mathrm{t}=1}^{\mathrm{N}} {}^{t}\boldsymbol{\gamma}^{\mathrm{T}} \frac{\partial\,{}^{t}\boldsymbol{H}}{\partial s} \tag{7.33} $$

where the adjoint variables ${}^{t}\boldsymbol{\lambda}$ and ${}^{t}\boldsymbol{\gamma}$ are obtained by solving the following systems of linear equations in a backward manner:

$$\begin{pmatrix} \frac{\partial^{\mathrm{N}}\boldsymbol{R}}{\partial^{\mathrm{N}}\boldsymbol{U}} & \frac{\partial^{\mathrm{N}}\boldsymbol{H}}{\partial^{\mathrm{N}}\boldsymbol{U}} \\ \frac{\partial^{\mathrm{N}}\boldsymbol{R}}{\partial^{\mathrm{N}}\boldsymbol{V}} & \frac{\partial^{\mathrm{N}}\boldsymbol{H}}{\partial^{\mathrm{N}}\boldsymbol{V}} \end{pmatrix}^{\mathrm{T}} \begin{pmatrix} {}^{\mathrm{N}}\boldsymbol{\lambda} \\ {}^{\mathrm{N}}\boldsymbol{\gamma} \end{pmatrix} = \begin{pmatrix} \frac{\partial f}{\partial^{\mathrm{N}}\boldsymbol{U}} \\ \frac{\partial f}{\partial^{\mathrm{N}}\boldsymbol{V}} \end{pmatrix} \tag{7.34}$$

$$\begin{pmatrix} \frac{\partial^{t}\boldsymbol{R}}{\partial^{t}\boldsymbol{U}} & \frac{\partial^{t}\boldsymbol{H}}{\partial^{t}\boldsymbol{U}} \\ \frac{\partial^{t}\boldsymbol{R}}{\partial^{t}\boldsymbol{V}} & \frac{\partial^{t}\boldsymbol{H}}{\partial^{t}\boldsymbol{V}} \end{pmatrix}^{\mathrm{T}} \begin{pmatrix} {}^{t}\boldsymbol{\lambda} \\ {}^{t}\boldsymbol{\gamma} \end{pmatrix} = -\begin{pmatrix} 0 \\ \frac{\partial^{t+1}\boldsymbol{H}}{\partial^{t}\boldsymbol{V}} \end{pmatrix}^{\mathrm{T}} {}^{t+1}\boldsymbol{\gamma} - \begin{pmatrix} 0 \\ \frac{\partial^{t+1}\boldsymbol{R}}{\partial^{t}\boldsymbol{V}} \end{pmatrix}^{\mathrm{T}} {}^{t+1}\boldsymbol{\lambda} + \begin{pmatrix} \frac{\partial f}{\partial^{t}\boldsymbol{U}} \\ \frac{\partial f}{\partial^{t}\boldsymbol{V}} \end{pmatrix} (t = N-1, \dots, 1) \tag{7.35}$$

The formulation of partial derivatives for the residual force and the dependent residual is presented in Appendix B, from which it easily shows that by solving Eqs.(7.34) and (7.35), the adjoint variables are

$${}^{t}\boldsymbol{K}_{\mathrm{T}} \cdot {}^{t}\boldsymbol{\lambda} = \frac{\partial f}{\partial^{t}\boldsymbol{U}} - \frac{\partial^{t}\boldsymbol{H}}{\partial^{t}\boldsymbol{U}}^{\mathrm{T}} \frac{\partial^{t}\boldsymbol{H}}{\partial^{t}\boldsymbol{V}}^{-\mathrm{T}} \left(\frac{\partial f}{\partial^{t}\boldsymbol{V}} - \frac{\partial^{t+1}\boldsymbol{H}}{\partial^{t}\boldsymbol{V}}^{\mathrm{T}} {}^{t+1}\boldsymbol{\gamma} - \frac{\partial^{t+1}\boldsymbol{R}}{\partial^{t}\boldsymbol{V}}^{\mathrm{T}} {}^{t+1}\boldsymbol{\lambda} \right) \tag{7.36}$$

$${}^{t}\boldsymbol{\gamma} = \frac{\partial^{t}\boldsymbol{H}}{\partial^{t}\boldsymbol{V}}^{-\mathrm{T}} \left(\frac{\partial f}{\partial^{t}\boldsymbol{V}} - \frac{\partial^{t+1}\boldsymbol{H}}{\partial^{t}\boldsymbol{V}}^{\mathrm{T}} {}^{t+1}\boldsymbol{\gamma} - \frac{\partial^{t+1}\boldsymbol{R}}{\partial^{t}\boldsymbol{V}}^{\mathrm{T}} {}^{t+1}\boldsymbol{\lambda} - \frac{\partial^{t}\boldsymbol{R}}{\partial^{t}\boldsymbol{V}}^{\mathrm{T}} {}^{t}\boldsymbol{\lambda} \right) \tag{7.37}$$

7.3 Load step reduction in the adjoint sensitivity analysis

In this section, the properties of adjoint variables and load step reduction rules for finite strain elastoplasticity are discussed. The assumptions about the system response in Eq.(5.1) still apply.

Firstly, for an intermediate elastic load step, it is the same as in the small strain case.

Property 1. If a load step *t* is an intermediate elastic load step, then ${}^{t}\boldsymbol{\lambda} = \boldsymbol{0}$.

Elastic load step reduction rule: Given a sequence of load steps L = {1, 2, ..., *t-1*, *t*, *t+1*, …, N}, if step *t* is an intermediate elastic load step, then skip step *t* as the load steps contain only S = {1, 2, ..., *t-1*, *t+1*, …, N} will not change the sensitivity results.

The theoretical proofs of the property and load step reduction rule can be found in [WCB22]. They essentially follow the same idea as in the small strain

case, except that the expressions are more complicated due to the logarithmic strain measure and the multiplicative decomposition of the total deformation gradient.

At an intermediate plastic step, the adjoint variable $\boldsymbol{\lambda}$ could also be zero under four conditions. The following property is proved for such a plastic step.

Property2: If $\frac{\partial {}^{t}\mathbf{a}}{\partial {}^{t}\bar{\boldsymbol{\tau}}} = \mathbf{0}$, ${}^{t}\mathbf{a} = {}^{\mathrm{t+1}}\mathbf{a}$, $\frac{\partial {}^{t+1}\boldsymbol{R}^{\mathrm{e}}}{\partial {}^{t}\boldsymbol{X}^{\mathrm{p}-1}} = \mathbf{0}$, ${}^{t+1}\Delta\boldsymbol{\varepsilon}^{\mathrm{p}}$ and ${}^{t}\boldsymbol{X}^{\mathrm{p}}$ commute, then ${}^{t}\boldsymbol{\lambda} = \mathbf{0}$.

The first two conditions require that the flow vector be in the same direction at adjacent load steps, which is the same as in the small strain case. The other two conditions require that the elastic rotation tensor should be constant with respect to the plastic deformation gradient, and the incremental plastic strain should have the same principal directions as the accumulated plastic strain.

If all these conditions are met, and furthermore, the last two conditions are also satisfied in the previous step, then the following plastic load step reduction rule is proven in [WCB22].

Plastic load step reduction rule: Given a sequence of load steps L={1, 2,.., *t-1*, *t*, *t+1*,..., N}, if the prerequisites in Property 2 are fulfilled, additionally $\frac{\partial {}^{\mathrm{t}}\boldsymbol{R}^{\mathrm{e}}}{\partial {}^{\mathrm{t-1}}\boldsymbol{X}^{\mathrm{p}-1}} = \mathbf{0}$, ${}^{\mathrm{t}}\Delta\boldsymbol{\varepsilon}^{\mathrm{p}}$ and ${}^{\mathrm{t-1}}\boldsymbol{X}^{\mathrm{p}}$ also commute, then skip step *t* as the load steps contain only S = {1, 2, ..., *t-1*, *t+1*, ..., N} will not change the sensitivity results.

The plastic load step reduction applies strictly only to 1D element. For general types of elements, the following empirical rule is suggested in practice.

Empirical rule: Given a sequence of load steps L = {1, 2, ..., *t-1*, *t*, *t+1*, ..., N}, if step *t* and step *t+1* are in a monotonic loading procedure, and the incremental plastic flow is in close direction to the accumulated plastic flow, then step *t* can be skipped in the sensitivity analysis.

The application of the empirical rule in finite strain elastoplasticity is demonstrated through several examples in the next section. Additionally, one example is presented to show a situation where the load step could not be significantly reduced.

7.4 Numerical examples

7.4.1 Cantilever beam under severe bending

In this example, the 3D cantilever beam is employed once again. The structure is depicted in Figure 7-2. A bilinear isotropic hardening material is assumed, with a Young's modulus of 210 GPa, a plastic modulus of 50 GPa, an initial yield stress of 235 MPa, and a Poisson's ratio of 0.3.

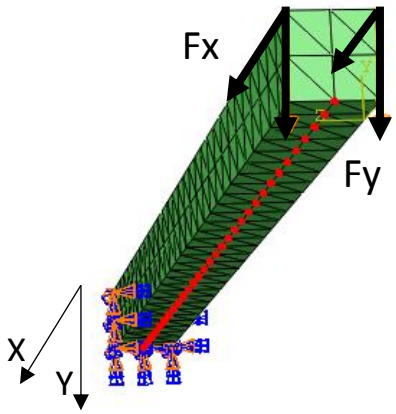

Figure 7-2. Cantilever beam structure in size 300mm×15mm×15mm. Red dots are design nodes

Two external forces in the horizontal x-direction and in the vertical y-direction are applied to the free end of the structure simultaneously. There are 11 load steps, as described in Figure 7-3. The downward vertical load increases in the first three steps and then decreases gradually. The horizontal load in the x-direction increases throughout the procedure.

Before proceeding to the sensitivity analysis, it is essential to verify the accuracy of the primal finite element analysis. Figure 7-4 presents the results of the finite element analysis with an in-house code, following the procedure outlined in Section 7.1. The x and y displacements at the free end are compared with those obtained from ABAQUS. The curves demonstrate that the displacements obtained by the in-house solver match perfectly with the benchmark results at all load steps.

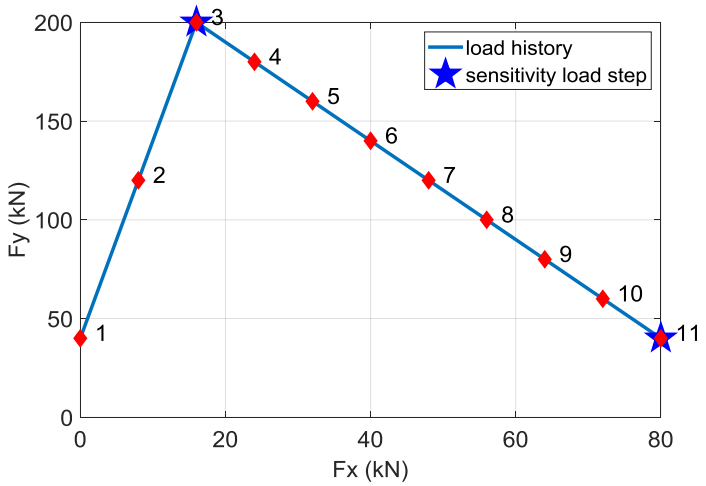

Figure 7-3. Load history in horizontal and vertical direction on the free end of the cantilever beam. Pentagrams depict the reduced load steps in the sensitivity analysis

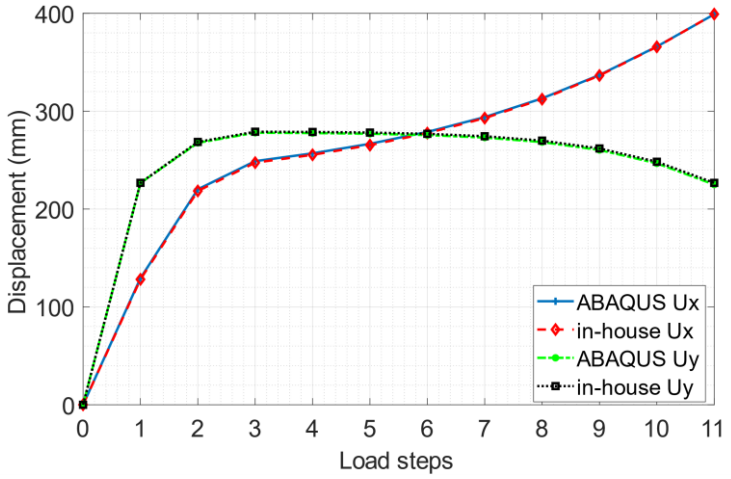

Figure 7-4. Comparison of nodal displacement of finite element analysis using in-house code and ABAQUS

The finite element analysis show that all the load steps are plastic. The maximum equivalent plastic strain at the last step is 25.2%. The contour of the equivalent plastic strain is presented in both initial and deformed configurations in Figure 7-5. Areas where the equivalent plastic strain is larger than 5% are depicted in red. The deformation shows that the beam structure is severely bent under the given loads.

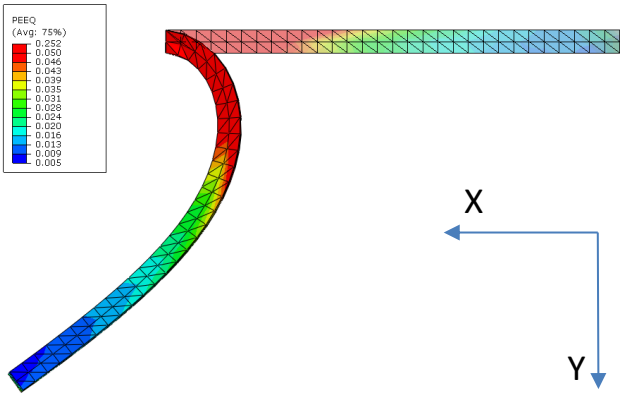

Figure 7-5. Contour of the equivalent plastic strain under original and deformed configurations

In the sensitivity analysis, the design variables are the vertical coordinates of center nodes on the bottom surface of the beam, as indicated by the red dots in Figure 7-2. The two system responses include the maximum equivalent plastic strain at the fixed end and the vertical displacement at the free end.

Under the given load, the structure is undergoing an increasingly bending procedure. The plastic flows are all in close directions. According to empirical rules, all intermediate load steps of a monotonic loading stage could be skipped. Therefore, only step 3, where the vertical load transitions from increasing to decreasing, and the last load step must be included in the sensitivity analysis. The sensitivity results with only these two steps and sensitivities with all load steps are compared in Figure 7-6. Additionally, in Figure 7-6, the central finite differencing sensitivities are also presented, where a perturbation size of 10^{-5} mm is adopted.

The results show that, the adjoint sensitivities match well with finite differencing results. Therefore, the adjoint sensitivity analysis procedure is demonstrated.

The results also show that, from a real value point of view, the sensitivities with reduced load steps match well with those using all load steps. Therefore, the empirical rule also applies to finite strain.

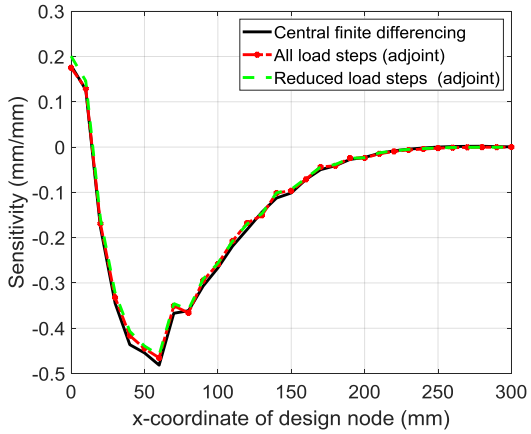

(a) Sensitivity of vertical displacement

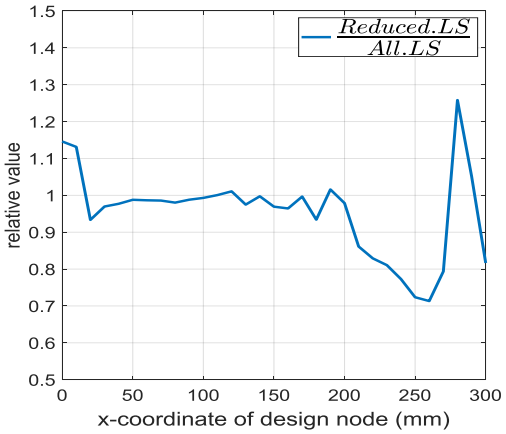

(b) Relative sensitivity of vertical displacement

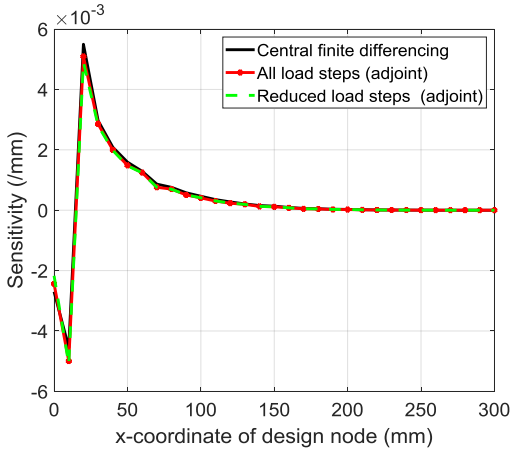

(c) Sensitivity of equivalent plastic strain

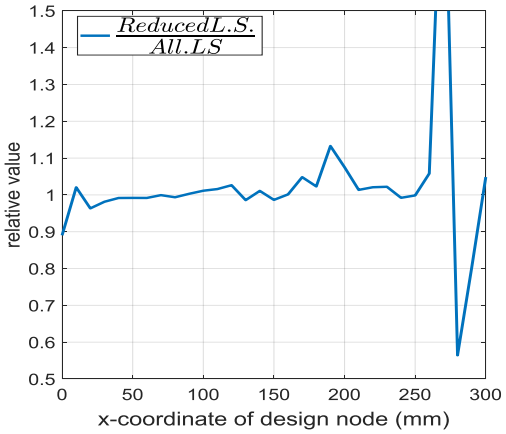

(d) Relative sensitivity of equivalent plastic strain

Figure 7-6. Comparison of sensitivity results using all load steps and using only the reduced load steps (step3+step11)

From a relative value perspective, it shows that the error increases significantly as we approach the free end of the beam. This increase in error is partially due to the sensitivities near the free end being close to zero. As a result, the relative error is calculated with a smaller denominator, leading to its amplification. After filtering out sensitivities whose absolute values are smaller than 1% of the maximum sensitivity, the sensitivity errors for both responses are summarized in Table 7-1. The average errors are smaller than 3%, demonstrating a good match of sensitivities when the load steps are reduced.

Table 7-1. Error of sensitivities of the cantilever beam example

Response	Maximum error	Average error
Vertical displacement	15%	2.3%
Eqv. plastic strain	11%	0.8%

7.4.2 Cantilever beam under severe bending and twisting

One of the requirement of the empirical rule is that the incremental plastic flow should be in close direction to the accumulated plastic flow. Due to the vagueness of this statement, it is worth presenting an example to illustrate a scenario where the load steps can't be reduced, even under a monotonic loading procedure.

In this example, the cantilever beam structure is still used. The horizontal and vertical load history are depicted in Figure 7-7. In addition to these two forces, a constant force of 2kN is applied at the free end in the horizontal z direction.

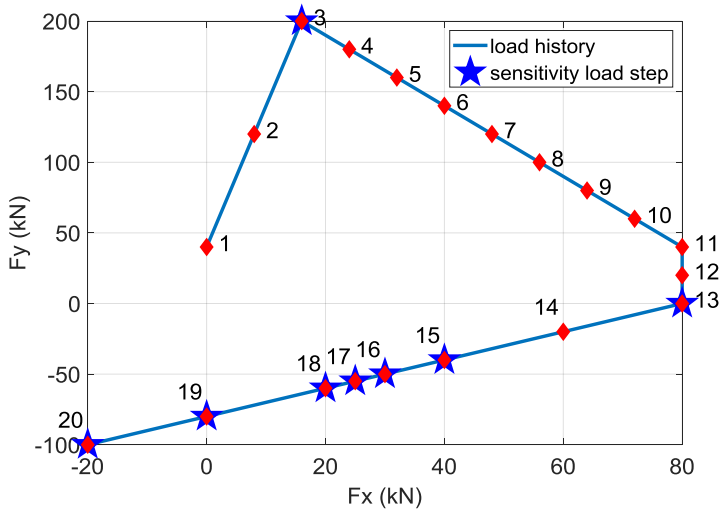

Figure 7-7. Load history for cantilever beam under bending and twisting. Pentagrams depict the reduced load steps in the sensitivity analysis

The deformation of the beam at representative load steps are depicted Figure 7-8 with contour of equivalent plastic strain. All twenty load steps are plastic steps. The maximum equivalent plastic strain at the final step is 36.3%. Areas with equivalent plastic strain larger than 5% are depicted in red. The deformations show that the beam slightly bends out of the x-y plane at the beginning under the force in the z direction. After a large enough plastic strain

is accumulated at the fixed end, the out-of-plane load causes the beam to twist severely.

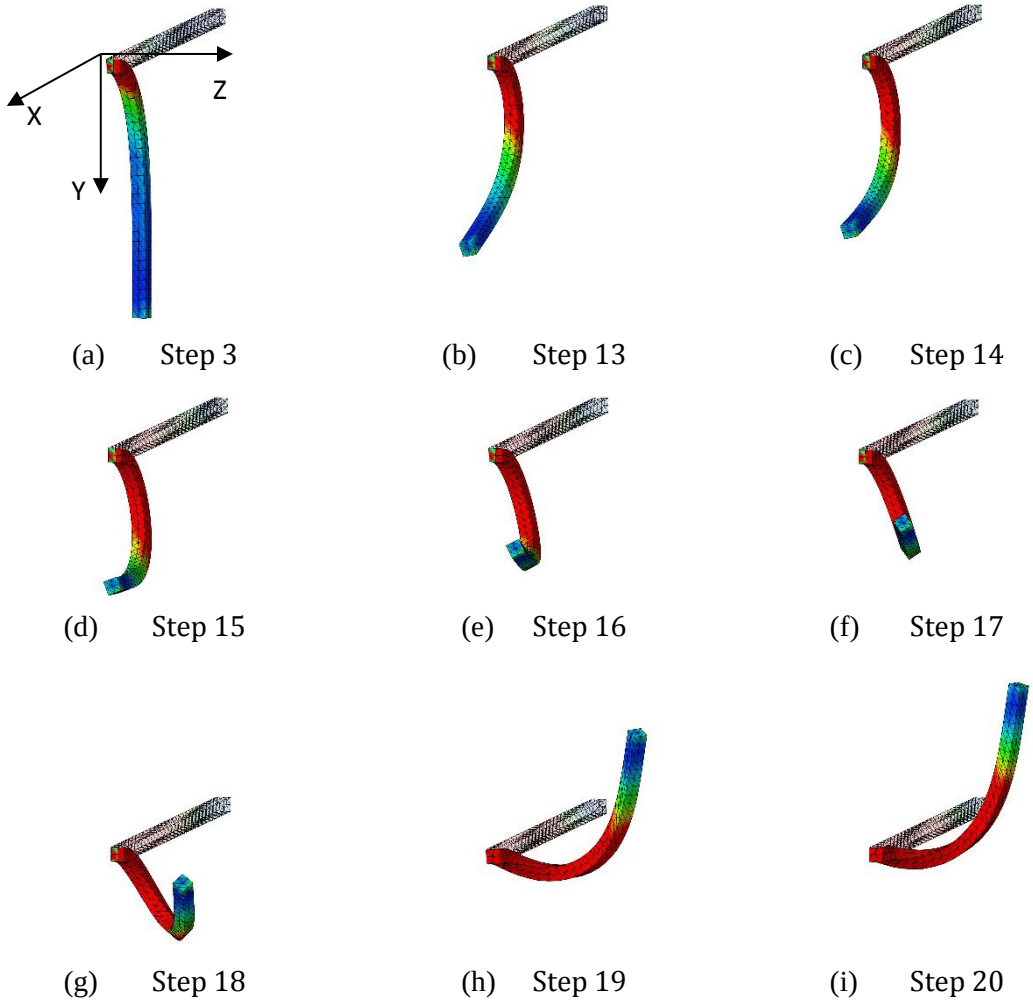

(a) Step 3 (b) Step 13 (c) Step 14

(d) Step 15 (e) Step 16 (f) Step 17

(g) Step 18 (h) Step 19 (i) Step 20

Figure 7-8. Deformation and contour of equivalent plastic strain at representative load steps of cantilever beam example under severe bending and twisting

According to the empirical rule, the turning points between monotonic loading procedures should be included in the sensitivity analysis. These points are at step 3, step 13, and step 20. During the twisting of the beam, the principal directions of stress change significantly. This leads to a change in the directions of the associated plastic flow. Therefore, the prerequisite of the empirical rule is violated. Consequently, from step 15 onward, all steps must be included in the sensitivity analysis, even if they are part of a monotonic loading procedure. The load steps in the sensitivity analysis must include step 3, step 13, and steps 15 to 20, as depicted by pentagrams in Figure 7-8. These reduced load steps are also listed in Table 7-2.

Table 7-2. Reduced load steps for cantilever beam under severe bending and twisting

Reduced load step	Corresponding FEA load step	Load (kN)
1	3	Fx=16, Fy=200, Fz=2
2	13	Fx=80, Fy=0, Fz=2
3	15	Fx=40, Fy=-40, Fz=2
4	16	Fx=30, Fy=-50, Fz=2
5	17	Fx=25, Fy=-55, Fz=2
6	18	Fx=20, Fy=-60, Fz=2
7	19	Fx=0, Fy=-80, Fz=2
8	20	Fx=-20, Fy=-100, Fz=2

The sensitivity of vertical displacement response is presented in Figure 7-9. The results obtained with reduced load steps (blue dashed line) perfectly match those obtained with all load steps (red straight line). The maximum percentage error is 2.0%, and the average error is 1.1%.

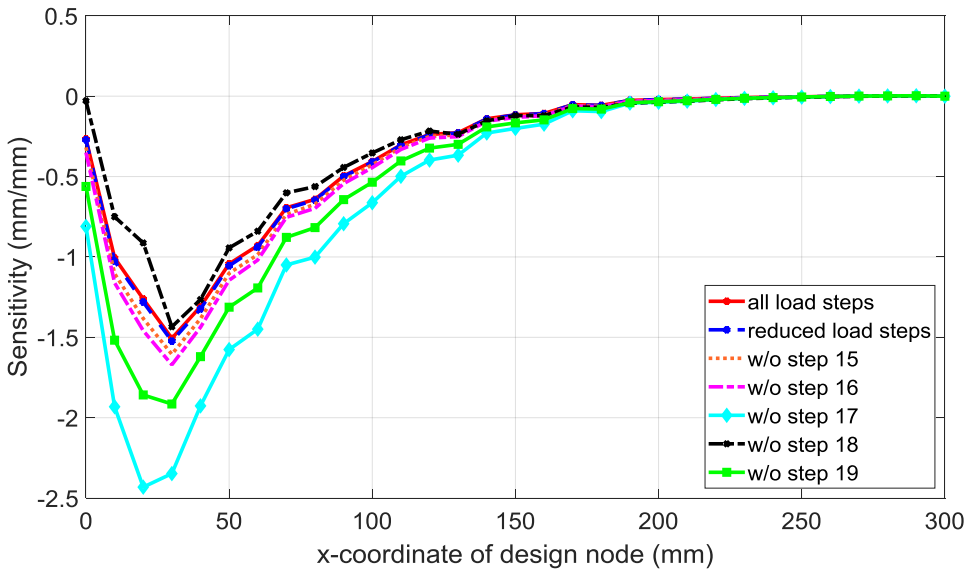

Figure 7-9. Sensitivity of vertical displacement response

To demonstrate the necessity of step 15 to step 19 in the sensitivity analysis, results of several trials are also presented in Figure 7-9. In each of these results, the reduced load steps in Table 7-2 are used except that one additional step between 15 and 19 is skipped. The results show that if any step between 15 and 19 is skipped in the sensitivity analysis, the sensitivity will be incorrect or have significant errors.

7.4.3 Demonstration with a connecting rod example

In this section, the load step reduction rules are demonstrated using the conrod example. The structure is identical to that shown in Figure 5-16. The load history on the small end of the conrod is depicted in Figure 7-10, with force magnitudes intentionally exaggerated to represent an extreme load case during engine failure.

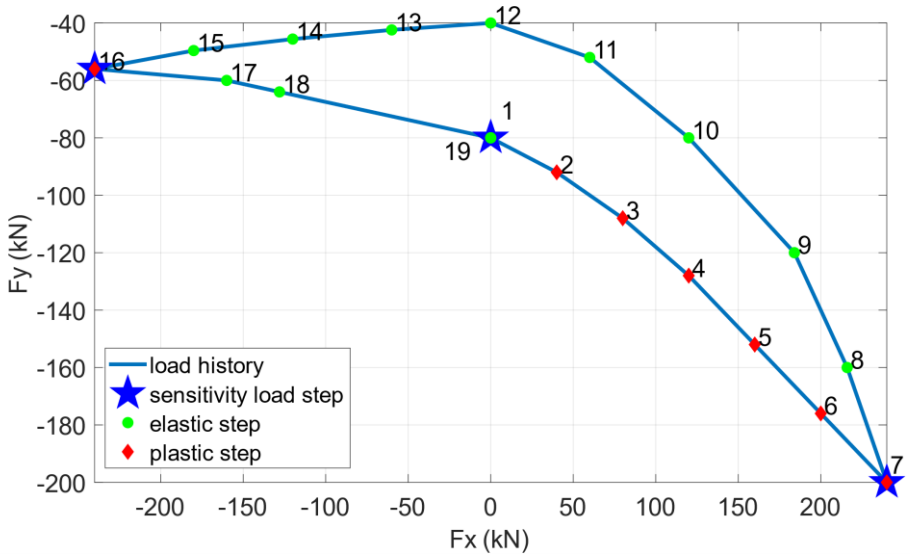

Figure 7-10. Load history on the small end of the conrod. Pentagrams depict the reduced load steps in the sensitivity analysis

The contour of the equivalent plastic strain at the final step is presented in both the initial and deformed configurations in Figure 7-11. The maximum equivalent plastic strain is 22.3%. Areas where the equivalent plastic strain is larger than 10% are depicted in red.

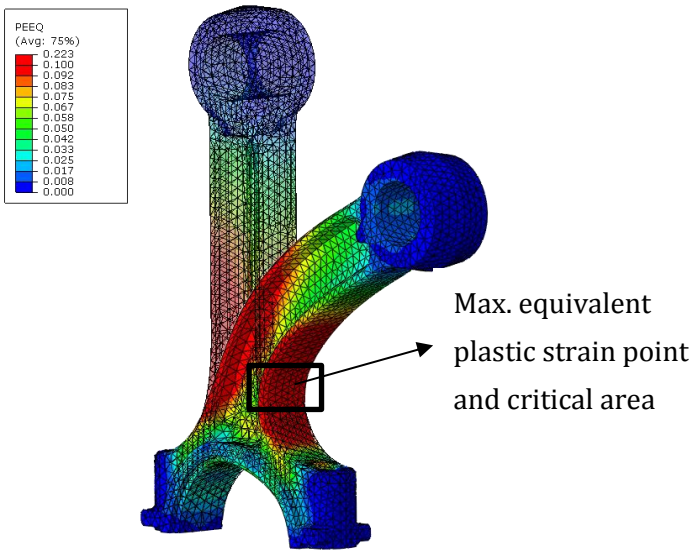

Figure 7-11. Equivalent plastic strain of the connecting rod at the last load step

According to nonlinear analysis, steps 2 to 7 and step 16 are considered plastic, while the remaining load steps are elastic. Following the rule for reducing elastic load steps, all elastic loads are skipped in the sensitivity analysis, except for step 19. According to the empirical rule, plastic steps 2 to 6 are also omitted since they follow a monotonic loading procedure. The three load steps that must be included in the sensitivity analysis are highlighted by pentagrams in Figure 7-10 and listed in Table 7-3.

Table 7-3. Reduced load steps for finite strain conrod example

Reduced load step	Corresponding FEA load step	Load (kN)
1	7	Fx= 240kN, Fy= -200kN
2	16	Fx= -240kN, Fy= -56kN
3	19	Fx= 0kN, Fy= -80kN

Three system responses are defined the same as in Section 5.6, i.e., average equivalent plastic strain around the critical area, and average x and y displacement of the small end. The sensitivities calculated with reduced load steps are compared with those using all load steps in Figure 7-12. All of them show that the results match very well.

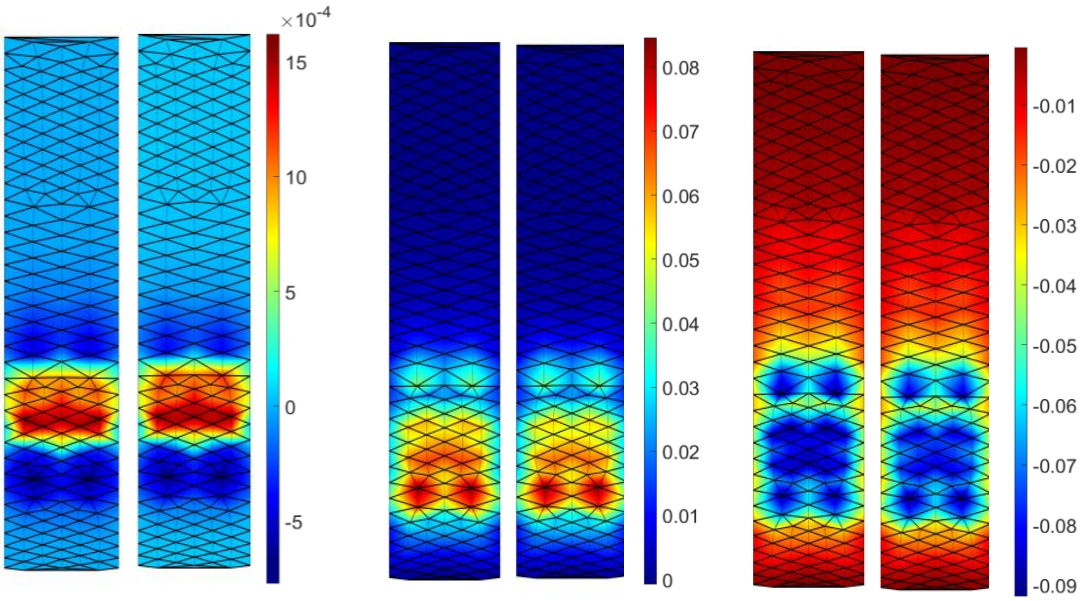

(a) Sensitivities of average equivalent plastic strain around critical point

(b) Sensitivities of average x-displacement response

(c) Sensitivities of average y-displacement response

Figure 7-12. Comparison of sensitivity results of three system responses. In each subfigure, the result with reduced load steps is depicted on the left and the result using all load steps is presented on the right

The relative error of sensitivities is calculated and summarized in Table 7-4. It should be mentioned that, in order to eliminate the effect of small denominators, sensitivities with an absolute value less than 1% of the maximum sensitivity are ignored.

Table 7-4. Relative errors of sensitivities for the finite strain conrod example

Response	Maximum error	Average error
Equivalent plastic strain	25%	8.5%
x-displacement	19%	6.6%
y-displacement	8.7%	4.6%

In comparison with the small strain case in Table 5-9, the relative errors are generally larger. However, the average relative errors of sensitivities for all three responses are still less than 10%. Therefore, the load step reduction rules still apply well for finite strain elastoplasticity.

7.5 Extension to finite strain elastoplasticity with mixed-hardening model

In this section, a brief discussion demonstrates that the reduction rules for finite strain elastoplasticity can be extended to the mixed-hardening model.

For the mixed hardening model, an additional state variable and governing equation should be introduced for the back stress. Denote the back stress under stress-free configuration by $\overline{\boldsymbol{\alpha}}$. The following five quantities are taken as state variables in this case: displacement, rotated Kirchhoff stress, equivalent plastic strain, inverse of plastic deformation gradient and the rotated back stress:

$$ {}^{t}\boldsymbol{U},\ {}^{t}\boldsymbol{V} = \left\{ {}^{t}\overline{\boldsymbol{\tau}},\ {}^{t}\varepsilon^{\mathrm{p}}_{\mathrm{eqv}},\ {}^{t}\boldsymbol{X}^{\mathrm{p}^{-1}},\ {}^{t}\overline{\boldsymbol{\alpha}} \right\} \tag{7.38} $$

For bilinear mixed hardening elastoplasticity, the yield surface is

$$ \left| {}^{t}\overline{\boldsymbol{\tau}} - {}^{t}\overline{\boldsymbol{\alpha}} \right|_{\mathrm{eqv}} = {}^{0}\sigma_{Y} + \beta \cdot E^{\mathrm{p}} \cdot {}^{t}\varepsilon^{\mathrm{p}}_{\mathrm{eqv}} \tag{7.39} $$

The rotated back stress of two consecutive steps follows

$$ {}^{t}\overline{\boldsymbol{\alpha}} = {}^{t-1}\overline{\boldsymbol{\alpha}} + (1-\beta) \cdot \boldsymbol{D}^{\alpha} \cdot \left({}^{t}\varepsilon^{\mathrm{p}}_{\mathrm{eqv}} - {}^{t-1}\varepsilon^{\mathrm{p}}_{\mathrm{eqv}} \right) {}^{t}\mathbf{a} \tag{7.40} $$

The dependent residual defined by governing equations are

$$ {}^{t}\boldsymbol{H}({}^{t}\boldsymbol{U}, {}^{t}\boldsymbol{V}, {}^{t-1}\boldsymbol{V}, s) = \begin{pmatrix} {}^{t}\overline{\boldsymbol{\tau}} - \boldsymbol{D}^{\mathrm{e}} ln \boldsymbol{U}^{\mathrm{e}}_{*} + \boldsymbol{D}^{\mathrm{e}} \left({}^{t}\varepsilon^{\mathrm{p}}_{\mathrm{eqv}} - {}^{t-1}\varepsilon^{\mathrm{p}}_{\mathrm{eqv}} \right) {}^{t}\mathbf{a} \\ \left({}^{t}\varepsilon^{\mathrm{p}}_{\mathrm{eqv}} - {}^{t-1}\varepsilon^{\mathrm{p}}_{\mathrm{eqv}} \right) \cdot \left[\left| {}^{t}\overline{\boldsymbol{\tau}} - {}^{t}\overline{\boldsymbol{\alpha}} \right|_{\mathrm{eqv}} - \sigma_{\mathrm{Y}} \left({}^{t}\varepsilon^{\mathrm{p}}_{\mathrm{eqv}} \right) \right] \\ {}^{t}\boldsymbol{X}^{\mathrm{p}^{-1}} - {}^{t-1}\boldsymbol{X}^{\mathrm{p}^{-1}} \cdot e^{-\left({}^{t}\varepsilon^{\mathrm{p}}_{\mathrm{eqv}} - {}^{t-1}\varepsilon^{\mathrm{p}}_{\mathrm{eqv}} \right) {}^{t}\mathbf{a}} \\ {}^{t}\overline{\boldsymbol{\alpha}} - {}^{t-1}\overline{\boldsymbol{\alpha}} - (1-\beta) \cdot \boldsymbol{D}^{\alpha} \cdot \left({}^{t}\varepsilon^{\mathrm{p}}_{\mathrm{eqv}} - {}^{t-1}\varepsilon^{\mathrm{p}}_{\mathrm{eqv}} \right) {}^{t}\mathbf{a} \end{pmatrix} \equiv \mathbf{0} \tag{7.41} $$

There are no changes in the adjoint sensitivity analysis, as in the isotropic hardening model. The two properties and two load steps reduction rules presented in Section 7.3 can be proven following the same procedures. Additionally, the same empirical rule is proposed to reduce plastic load steps in the sensitivity analysis.

The following example demonstrates the applicability of the empirical rule for the kinematic hardening case. In this example, the same conrod model as in Section 7.4.3 is employed and a hardening ratio $\beta = 0$ is assumed. The load history on the small end of the conrod is depicted in Figure 7-13, which is the same as the isotropic hardening case in Section 7.4.3. However, it shows that all the load steps behave plastically with the kinematic hardening material model.

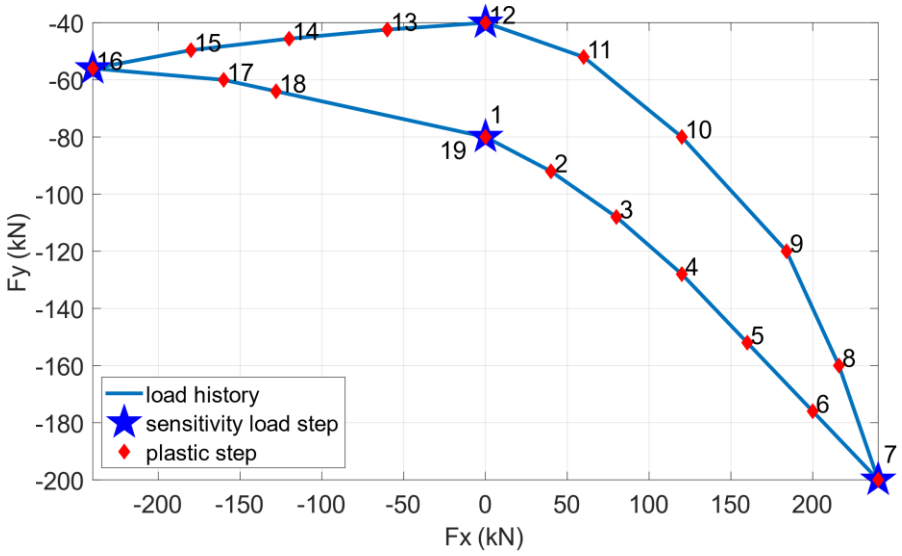

Figure 7-13. Load history on the small end of the conrod with kinematic hardening model. Pentagrams depict the reduced load steps in the sensitivity analysis.

Before entering the sensitivity analysis, the accuracy of the primal finite element analysis is validated. Figure 7-14 presents the results of the finite element analysis using in-house code. The x and y displacements at the small end are compared with those obtained from ABAQUS. The curves show that the displacements obtained by the in-house solver match perfectly with the ABAQUS results at all load steps.

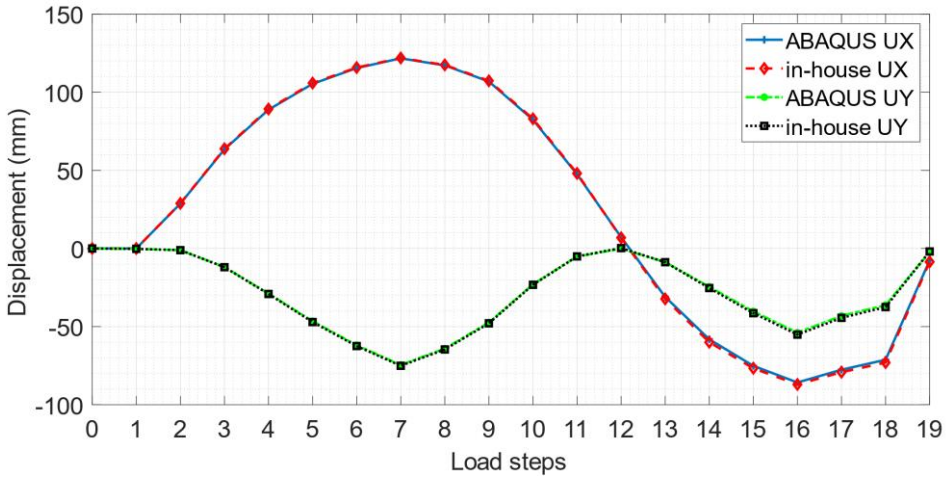

Figure 7-14. Comparison of nodal displacement of finite element analysis with in-house code and ABAQUS

The deformation and equivalent plastic strain at turning points of the load history are depicted in Figure 7-15. Areas where the equivalent plastic strain is larger than 20% are shown in red. The maximum equivalent plastic strain at the final step is 73%. This indicates that the structure undergoes severe back-and-forth bending under the given load history.

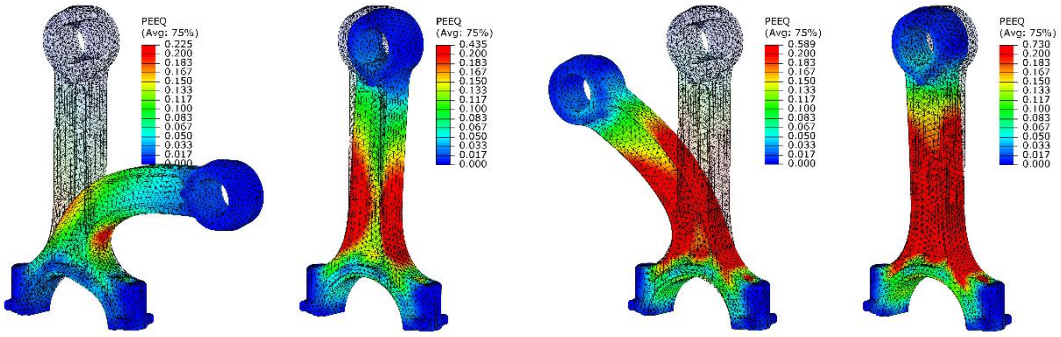

(a) Step 7 (b) Step 12 (c) Step 16 (d) Step 19

Figure 7-15. Deformation and contour of equivalent plastic strain at representative load steps of conrod example under kinematic hardening model

According to the empirical rule, sensitivity analysis should involve all turning steps: step 7, step 12, step 16, and step 19. In contrast to the isotropic hardening case, step 12 is an additional step. This is due to step 12 being a plastic step under the kinematic hardening model. The sensitivity results of equivalent plastic strain at the critical area are presented in Figure 7-16.

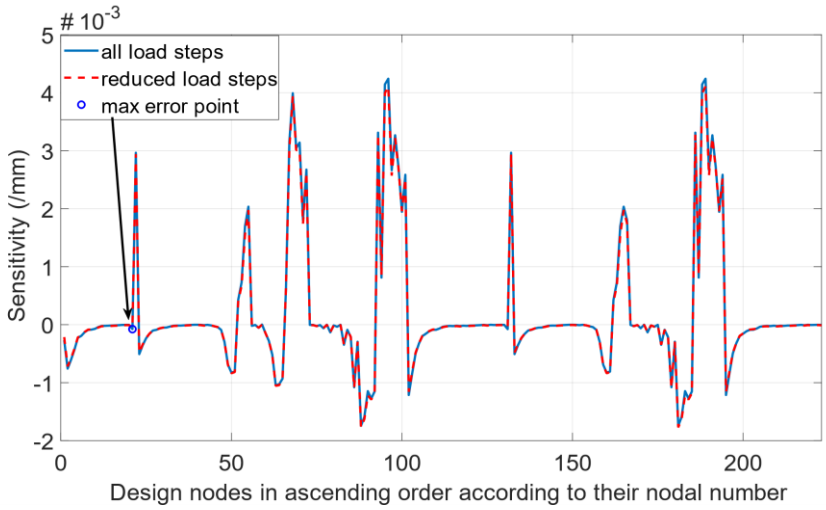

Figure 7-16. Sensitivity results of equivalent plastic strain response

It shows that the sensitivity analysis with reduced load steps matches well with results using all load steps. Excluding sensitivities whose absolute value is smaller than 1% of the largest value, the maximum percentage error is 41%, with an average error of only 3.6%. The point with the maximum percentage error is also identified in Figure 7-16. This figure illustrates that the large error is partially due to the small denominator in the calculation. Therefore, the applicability of the empirical rule to finite strain elastoplasticity with a kinematic hardening model is demonstrated.

8. Conclusion and outlook

In this dissertation, techniques for the efficient and accurate adjoint sensitivity analysis of nonlinear finite element systems, specifically for geometric nonlinearity and elastoplasticity, are investigated.

Based on the secant stiffness matrix of a geometric nonlinear system, the accuracy issue of semi-analytical adjoint sensitivity is discussed. The inaccuracy is shown to be dependent on the deformation form, primarily attributable to element rotation. An analytical expression for a correction term is formulated to address this issue while minimizing additional computational costs.

Numerical results under different conditions show that the correction term effectively eliminates errors. It improves the stability of sensitivity results with respect to the perturbation size in semi-analytical approximation. When applied to different system responses, including reaction force and stress, the approach yields a similar degree of accuracy. Examples also demonstrate that sensitivity accuracy after correction is independent of the degree of nonlinearity. Therefore, the presented correction term is applicable to problems with extremely severe geometric nonlinearity. The effectiveness of the presented sensitivity analysis is also demonstrated in typical geometric nonlinear optimization problems by integrating it into the TOSCA non-parametric shape optimization module.

Adjoint sensitivity analysis with simultaneous elastoplasticity and geometric nonlinearities is another focus of the study. The adjoint variables must be solved backwardly because of the path-dependency of the problem. Both computational and storage costs thus grow linearly with the total number of load steps. To improve efficiency, this thesis attempts to provide a thorough answer regarding when and which load steps could be reduced in the sensitivity analysis.

Firstly, several properties of adjoint variables are theoretically proven for the isotropic hardening model. Based on these properties, it is theoretically shown that, without loss of accuracy, intermediate elastic load steps can be skipped in the sensitivity analysis. In a monotonic loading stage, the former of two adjacent plastic steps can also be skipped. Following these findings, the

total number of load steps required in the sensitivity analysis could be significantly reduced. Both theoretical discussions and numerical examples on bar truss structures with typical load histories show that these strategies are exact for 1D elements. Multiple examples with tetrahedral elements are also presented under complex load histories. They demonstrate that, for general 3D elements, the load step reduction rules are both sufficient and necessary to obtain sensitivities with high efficiency and accuracy.

The proposed load step reduction rules are then extended to mixed-hardening and kinematic hardening models. Theoretical proofs and numerical examples demonstrate their applicability.

Last but not least, the discussion extends to large strain elastoplasticity, where logarithmic strain and the multiplicative decomposition of the deformation gradient are commonly adopted. The prerequisites for load step reduction in large strain cases are more stringent. Numerical examples demonstrate that if the incremental plastic flow aligns closely with the accumulated plastic flow, as expected, some plastic steps can still be reduced. Conversely, as anticipated, a counterexample illustrates that when the directions of plastic flow continue to change, the load steps should not be reduced in the sensitivity analysis.

As a direct extension of this work, the load step reduction for contact nonlinearity is worth investigating. How to integrate the developed procedure into commercial finite element codes, especially when state variables are not fully available, could be a challenging topic. In optimization applications, how the insignificant loss of sensitivity accuracy influences the optimization performance is an important topic. What's more, the application of the load step reduction to sensitivity analysis in topology optimization is also interesting.

Bibliography

[BB79] K. J. Bathe, S. Bolourchi, Large displacement analysis of three-dimensional beam structures, International Journal for Numerical Methods in Engineering, Vol. 14(7), pp.961-986, 1979.

[BCH88] B. Barthelemy, C.T. Chon, R.T. Haftka, Accuracy problems associated with semi-analytical derivatives of static response, Finite Elements in Analysis and Design, Vol. 4(3), pp.249–65, 1988.

[BFD08] K.-U. Bletzinger, M. Firl, F. Daoud, Approximation of derivatives in semi-analytical structural optimization, Computers & Structures, Vol. 86(13-14), pp.1404–16, 2008.

[BK97] H. de Boer, F. van Keulen, Error analysis of refined semi-analytical design sensitivities, Structural Optimization 14, pp.242-247, 1997.

[BK00] H. de Boer, F. van Keulen, Refined semi-analytical design sensitivities, International Journal of Solids and Structures, Vol. 37(46–47), pp.6961–80, 2000.

[Car05] J. Barradas Cardoso, Structural Design Sensitivity Analysis of Elasti-Plastic History-Dependent Response, 6th World Congress of Structural and Multidisciplinary Optimisation, Rio de Janeiro, 30 May-03 June 2005, Brazil.

[CD00] K.K. Choi, W. Duan , Design sensitivity analysis and shape optimization of structural components with hyperelastic material, Computer Methods in Applied Mechanics and Engineering, Vol.187(1-2), pp.219-243, 2000.

[CFC+03] S. H. Chung, L. Fourment, J. L. Chenot, S. M. Hwang, Adjoint state method for shape sensitivity analysis in non-steady forming applications, International Journal for Numerical Methods in Engineering, Vol.57(10), pp.1431–1444, 2003.

[CG95] A. Chattopadhyay, R. Guo, Structural design sensitivity analysis for composites undergoing elastoplastic deformation, Mathematical and Computer Modelling, Vol.22(2), pp.83-105, 1995.

[CG96] W. F. Chen, Y. Goto, Stability Design of Semi-Rigid Frames, Volume 1. New York: John Wiley & Sons, Inc., 1996.

[CK05a] K.K. Choi, N.H. Kim, Structrual Sensitivity Analysis and Optimization 1: Linear System, New York, Springer, 2005.

[CK05b] K.K. Choi, N.H. Kim, Structrual Sensitivity Analysis and Optimization 2: Nonlinear Systems and Applications, New York, Springer, 2005.

[CMB11] M.A.Caminero, F.J.Montáns and K.J.Bathe, Modeling large strain anisotropic elasto-plasticity with logarithmic strain and stress measures, Computers & Structures, Vol 89, pp.826-843, 2011.

[CO93] G. Cheng, N. Olhoff, Rigid body motion test against error in semi-analytical sensitivity analysis, Computers & Structures, Vol. 46(3), pp.515–27, 1993.

[Cr00] M. A.Crisfield, Non-linear finite element analysis of solids and structures Vol.1: Essentials, John Wiley & Sons Ltd, 2000.

[DPR94] E.N.Dvorkin, D.Pantuso and E.A.Repetto, A finite element formulation for finite strain elasto-plastic analysis based on mixed interpolation of tensorial components, Computer Methods in Applied Mechanics and Engineering, Vol. 114, pp.35-54, 1994.

[EB90] A.L.ETEROVIC and K.J.Bathe, A hyperelastic-based large strain elasto-plastic constitutive formulation with combined isotropic-kinematic hardening using the logarithmic stress and strain measures, International Journal for Numerical Methods in Engineering, Vol. 30, pp.1099-1114, 1990.

[Fi10] M. Firl, Optimal Shape Design of Shell Structures, PhD Dissertation, Lehrstuhl für Statik, Technischen Universität München, 2010.

[GB95] G.Gabriel and K.J.Bathe, Some computational issues in large strain elasto-plastic analysis, Computers & Structures, Vol.56, Iss.2/3, pp.249-267, 1995.

[GCE+09] Q. Gu, J.P. Conte, A. Elgamal, Z. Yang, Finite element response sensitivity analysis of multi-yield-surface J2 plasticity model by direct differentiation method, Computer Methods in Applied Mechanics and Engineering, Vol. 198(30-32), pp.2272-2285, 2009.

[HA89] R.T. Haftka, H.M. Adelman, Recent developments in structural sensitivity analysis, Structural Optimization, Vol. 1(3), pp.137-51, 1989.

[HM10] A. Habibi, H. Moharrami , Nonlinear sensitivity analysis of reinforced concrete frames, Finite Elements in Analysis and Design, Vol. 46(7), pp.571-585, 2010.

[Hi95] T. Hisada, Recent Progress in Sensitivity Nonlinear FEM-Based Sensitivity Analysis, JSME Intemationa Journal, SeriesA, VoL 38(3), 1995, pp. 301-310.

[Ho05] S. Holopainen, Parameter sensitivity of anisotropic elasto-plastic shell, 6th World Congress on Structural and Multidisciplinary Optimization, Rio de Janeiro, 2005, Brazil.

[HSM15] G.A. Haveroth, J. Stahlschmidt, P.A. Muñoz-Rojas, Application of the Complex Variable Semi-analytical Method for Improved Displacement Sensitivity Evaluation in Geometrically Nonlinear Truss Problems, Latin American Journal of Solids and Structures, Vol.12(5), pp. 980-1005, 2015.

[KAH+97] M. Kleiber, H. Antunez, T. D. Hien, P. Kowalczyk, Parameter Sensitivity in Nonlinear Mechanics, Theory and Finite Element Computations. Wiley: New York, 1997.

[Kam11] M. M. Kaminski, Structural sensitivity analysis in nonlinear and transient problems using the local response function technique, Structural and Multidisciplinary Optimization, Vol. 43, pp. 261—274, 2011.

[KB98] F. van Keulen, H. de Boer, Rigorous improvement of semi-analytical design sensitivities by exact differentiation of rigid body motions, International Journal for Numerical Methods in Engineering, Vol. 42(1), pp. 71–91, 1998.

[KCC00] N.H. Kim, K.K. Choi, J.S. Chen, Shape Design Sensitivity Analysis and Optimization of Elasto–Plasticity with Frictional Contact, AIAA Journal, Vol. 38(9), September 2000.

[KH98] P. Kolakowski, J. Holnicki-Szulc, Sensitivity Analysis of Truss Structures, International Journal for Numerical Methods in Engineering, Vol.43, pp.1085-1108, 1998.

[KHK05] F. van Keulen, R.T. Haftka, N.H. Kim, Review of options for structural design sensitivity analysis Part 1: Linear systems, Computer Methods in Applied Mechanics and Engineering, 194 (30-33), pp. 3213–43, 2005.

[KK96] M. Kleiber, P. Kowalczyk, Sensitivity analysis in plane stress elasto-plasticity and elasto-viscoplasticity, Computer Methods in Applied Mechanics and Engineering, Vol.137(3-4), pp.395-409, 1996.

[KK99] P. Kowalczyk, Michal Kleiber, Shape sensitivity in elasto-plastic computations, Computer Methods in Applied Mechanics and Engineering, Vol. 171, pp. 371-386, 1999.

[Köb15] J. Köbler, Adjungierte Sensitivitätsberechnung und Gestaltoptimierung von Materialien mit nicht-linearem und plastischem Verhalten, Master Thesis, Institut für Technische Mechanik, Karlsruhe Institut für Technology, 2015.

[KWH07] P. Kołakowski, M. Wiklo, J. Holnicki-Szulc, The virtual distortion method—a versatile reanalysis tool for structures and systems, Structural and Multidisciplinary Optimization, Vol. 36, pp. 217-234, 2008.

[Lee69] E. H. Lee, Elastic plastic deformation at finite strain, Journal of Applied Mechanics, Vo. 36, pp. 1-6, 1969.

[LL67] E. H. Lee and D. T. Liu, Finite strain elastic-plastic theory with application to plane-wave analysis, Journal of Applied Physics, Vol. 38, pp. 17-27, 1967.

[LYL04] T. H. Lee, J. H. Yoo and M. U. Lee, Refined Semi-analytical Design Sensitivity Analysis with Commercial Finite Element Package, 10th AIAA/ISSMO Multidisciplinary Analysis and Optimization Conference, Albany, New York, 2004.

[MB05] F. J. Montáns, K. J. Bathe, Computational issues in large strain elasto-plasticity: an algorithm for mixed hardening and plastic spin. International Journal for Numerical Methods in Engineering, Vol. 63(2), pp. 159–196, 2005.

[MFG+15] A. Montoya, R. Fielder, A. Gomez-Farias, H.Millwater, Finite-Element Sensitivity for Plasticity Using Complex Variable Methods, Journal of Engineering Mechanics, Vol.141(2), 2015.

[Mle92] H. P. Mlejnek, Accuracy of semi-analytical sensitivities and its improvement by the "natural method", Structural Optimization, Vol.4(2), pp. 128-131, 1992.

[MNF03] K. Maute, M. Nikbay, C. Farhat, Sensitivity analysis and design optimization of three-dimensional non-linear aeroelastic systems by the

adjoint method, International Journal for Numerical Methods in Engineering, Vol.56(6), pp. 911-933, 2003.

[MOM98] A. Morán, E. Oñate, J. Miquel, A general procedure for deriving symmetric expressions for the secant and tangent stiffness matrices in finite element analysis, International Journal for Numerical Methods in Engineering, Vol. 42, pp. 219-236, 1998.

[MSS05] R. Meske , J. Sauter, E. Schnack, Nonparametric gradient-less shape optimization for real-world applications, Structural and Multidisciplinary Optimization, Vol. 30(3), pp. 201-218, 2005.

[MTV94] P. Michaleris, D. A. Tortorelli, C.A. Vidal, Tangent operators and design sensitivity formulations for transient non-linear coupled problems with applications to elastoplasticity, International Journal for Numerical Methods in Engineering, Vol. 37(14), pp. 2471–2499, 1994.

[MWB+13] H. Millwater, D. Wagner, A. Baines and K. Lovelady, Improved WCTSE method for the generation of 2D weight functions through implementation into a commercial finite element code., Engineering Fracture Mechanics, Vol. 109, pp. 302-309, 2013.

[NEM16] Neff P, Eidel B, Martin R, Geometry of logarithmic strain measures in solid mechanics. Archive for Rational Mechanics and Analysis, Vol. 222, pp. 507-572, 2016.

[No12] Nonlinear Finite Element Methods (textbook), Department of Aerospace Engineering Sciences, University of Colorado at Boulder, 2012.

[NQR98] D.T. Nguyen, R. Qamar, H. Runesha, Automatic differentiation for design sensitivity analysis of structural systems using parallel-vector processors, Advances in Engineering Software, Vol.29(3–6), pp.375–382, 1998.

[OA94] M. Ohsaki, J. S. Arora, Design Sensitivity Analysis of Elastoplastic Structures, International Journal for Numerical Methods in Engineering, Vol. 37, pp. 737-762, 1994.

[Oñ91] E. Oñate, Formulation of a secant stiffness matrix for geometrically nonlinear finite element analysis, Nonlinear Engineering Computations, Swansea, U.K.: Pineridge Press, pp. 87–95, 1991.

[Oñ95] E. Oñate, On the derivation and possibilities of the secant stiffness matrix for nonlinear finite element analysis, Computational Mechanics, Vol. 15(6), pp. 572–593, 1995.

[OOM+86] E. Oñate, J. Oliver, J. Miquel, B. Suárez, A Finite element formulation for geometrically nonlinear problems using a secant matrix, Computational Mechanics, Tokyo: Springer-Verlag, pp. 563-570, 1986.

[ORL93] N. Olhoff, J. Rasmussen, E. Lund, A method of "exact" numerical differentiation for error elimination in finite-element-based semi-analytical shape sensitivity analyses, Mechanics of Structures and Machines, Vol. 21(1), pp. 1–66, 1993.

[PC99a] Y.H. Park and K.K. Choi, Shape design sensitivity analysis of eigenvalues using "exact" numerical differentiation of finite element matrices, Structural Optimization, Vol. 8, pp. 52-59, 1994.

[PC99b] Y.H. Park and K.K. Choi, Shape design sensitivity analysis of nonlinear 2-D solids with elasto-plastic material, Structural Optimization, Vol. 18, pp. 236-246, 1999.

[PCR89] P. Pedersen, G. Cheng, J. Rasmussen, On accuracy problems for semi-analytical sensitivity analysis, Mechanics of Structures and Machines, Vol. 17(3), pp. 373–84, 1989.

[Pe03a] C.B.W. Pedersen, Topology optimization of 2D-frame structures with path-dependent response, International Journal for Numerical Methods in Engineering, Vol. 57(10), pp. 1471-1501, 2003.

[Pe05] P. Pedersen, Analytical stiffness matrices with Green–Lagrange strain measure, International Journal for Numerical Methods in Engineering, Vol. 62(3), pp. 334–52, 2005.

[Pe06] P. Pedersen, Analytical stiffness matrices for tetrahedral elements, Computer Methods in Applied Mechanics and Engineering, Vol. 196(1-3), pp. 261–278, 2006.

[Pe08] P. Pedersen, The basic matrix approach for three simple finite elements (working print), 2008.

[PM06] J. M. Pajot, K. Maute, Analytical sensitivity analysis of geometrically nonlinear structures based on the co-rotational finite element method , Finite Elements in Analysis and Design, Vol. 42(10), pp. 900-913, 2006.

[PRA93] M. J. Poldneff, I. S. Rai, J.S. Arora, Implementation of Design Sensitivity Analysis for Nonlinear Elastic Structures, AIAA Journal, Vo. 31(11), pp. 2137–2142, 1993.

[QL10] G.Y. Qiu, X.S. Li, A note on the derivation of global stress constraints, Structural and Multidisciplinary Optimization, Vol. 40(1), pp. 625-628, 2010.

[RHW+85] Y.S. Ryu, M. Haririan, C.C. Wu and J.S Arora, Structural design sensitivity analysis of nonlinear response, Computers & Structures, Vol. 21, pp. 245-255, 1985.

[SC02] N. Stander, K.J. Craig, Response surface and sensitivity-based optimization in LS-OPT: a benchmark study, 7th International LS-DYNA Users Conference, Michigan, US, 2002.

[Sch01] S. Schwarz, Sensitivitätsanalyse und Optimierung bei nichtlinearem Strukturverhalten, Doktor Dissertation, Institut für Baustatik, Universität Stuttgart, 2001.

[SH98] J. C. Simot, TJ.R. Hughes, Computational Inelasticity, Springer-Verlag New York, 1998.

[SKD02] S. Stupkiewicz, J. Korelc, M. Dutko and T. Rodi, Shape sensitivity analysis of large deformation frictional contact problems, Computer Methods in Applied Mechanics and Engineering, Vol. 191, pp. 3555–3581, 2002.

[Sm03] D. E. Smith, Design sensitivity analysis and optimization for polymer sheet extrusion and mold filling processes, International Journal for Numerical Methods in Engineering, Vol. 57(10), pp. 1381-1411, 2003.

[SMR01] S. Schwarz, K. Maute, E. Ramm, Topology and shape optimization for elastoplastic structural response, Computer Methods in Applied Mechanics and Engineering, Vol. 190(15–17), pp. 2135–2155, 2001.

[SR01] S. Schwarz, E. Ramm, Sensitivity analysis and optimization for non-linear structural response, Engineering Computations, Vol. 18(3/4), pp. 610–641, 2001.

[ST94] C.O. Spivey, D. A. Tortorelli, Tangent operators, sensitivity expressions, and optimal design of non-linear elastica in contact with applications to beams, International Journal for Numerical Methods in Engineering, Vol. 37, pp. 49-73, 1994.

[TA90] J.J. Tsay, J.S. Arora, Nonlinear structural design sensitivity analysis for path dependent problems. Part 1: General theory, Computer Methods in Applied Mechanics and Engineering, Vol. 81(2), pp. 183-208, 1990.

[VH93] A.A. Vidal, R.B. Haber, Design sensitivity analysis for rate independent elastoplasticity. Computer Methods in Applied Mechanics and Engineering, Vol. 107, pp. 393-431, 1993.

[VLH91] C.A. Vidal, H.-S. Lee, R.B. Haber, The consistent tangent operator for design sensitivity analysis of history-dependent response, Computing Systems in Engineering, Vol. 2(5-6), pp. 509-523, 1991.

[WA87] C. Wu, J. S. Arora, Design sensitivity analysis and optimization of nonlinear structural response using incremental procedure, AIAA Journal, Vol. 25(8), pp. 1118-1125, 1987.

[WCB15] W. Wang, P.M. Clausen, K.-U. Bletzinger, Improved semi-analytical sensitivity analysis using a secant stiffness matrix for geometric nonlinear shape optimization, Computers & Structures, Vol. 146, pp. 143–151, 2015.

[WCB17] W. Wang, P.M. Clausen, K.-U. Bletzinger, Efficient adjoint sensitivity analysis of isotropic hardening elastoplasticity via load steps reduction approximation, Computers Methods in Applied Mechanics and Engineering, Vol. 325, pp. 612–44, 2017.

[WCB22] W. Wang, P.M. Clausen, K.-U. Bletzinger, Load step reduction for adjoint sensitivity analysis of finite strain elastoplasticity, Structural and Multidisciplinary Optimization, Vol. 65(1), 2022.

[We12] M. Werner, Master Thesis: Reduction models for stress sensitivities in industrial structural shape optimization, Department of Computational Engineering, TU Darmstadt, 2012.

[Wi02] K. J. Willam, Constitutive Models for Engineering Materials, Encyclopedia of Physical Science and Technology (Third Edition), Vol.3, University of Colorado at Boulder, pp.603-633, 2002.

[WKT03] K. Wisniewski, P. Kowalczyk, E. Turska, On the computation of design derivatives for Huber-Mises plasticity with non-linear hardening, International Journal for Numerical Methods in Engineering, Vol. 57(2), pp. 271–300, 2003.

[ZD99] W. H. Zhang and M. Domaszewski, Efficient sensitivity analysis and optimization of shell structures by the ABAQUS code, Structural Optimization, Vol. 18, pp. 173-182, 1999.

APPENDIX A. Analytical formulation of stiffness matrices for 3D 4-node tetrahedral element

In this section, analytical formulations of tangent and secant stiffness matrices for a 3D 4-node tetrahedral element under geometric nonlinearity are introduced. These formulations, as presented by Pederson [Pe06], provide closed-form expressions of stiffness matrices, offering a solid foundation for sensitivity studies. Particularly, they are useful in tracing the source of errors.

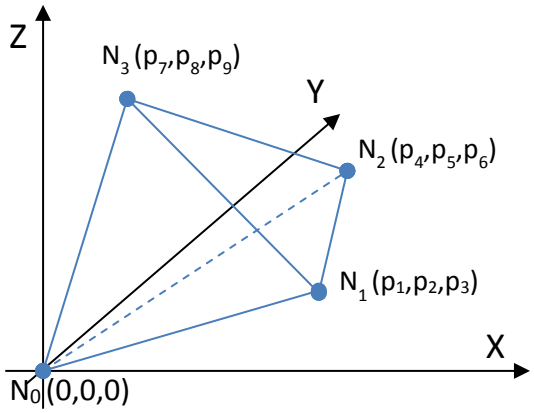

Figure A-1. Coordinate configuration of a 3D 4-node tetrahedral element

Figure A-1 depicts a 4-node linear tetrahedral element. Without loss of generality, Node 0 can be assumed to be located at the base point of a local Cartesian coordinate system. The local coordinates of nodes 1 to 3 are denoted by p1 to p9 and arranged in a matrix P, as shown in Eq.(A.1). In this matrix, the last three columns represent the coordinates of each node.

$$\boldsymbol{P} = \begin{bmatrix} 1 & 0 & 0 & 0 \\ 1 & p_1 & p_2 & p_3 \\ 1 & p_4 & p_5 & p_6 \\ 1 & p_7 & p_8 & p_9 \end{bmatrix} \tag{A.1}$$

In Eq.(A.2), several position parameters are defined for simplicity in subsequent deductions:

$$p_{5968} = p_5 p_9 - p_6 p_8 \tag{A.2}$$

$$p_{3829} = p_3 p_8 - p_2 p_9$$

$$p_{2635} = p_2 p_6 - p_3 p_5$$

$$p_{6749} = p_6 p_7 - p_4 p_9$$

$$p_{1937} = p_1 p_9 - p_3 p_7$$

$$p_{3416} = p_3 p_4 - p_1 p_6$$

$$p_{4857} = p_4 p_8 - p_5 p_7$$

$$p_{2718} = p_2 p_7 - p_1 p_8$$

$$p_{1524} = p_1 p_5 - p_2 p_4$$

$$q_x = p_{5968} + p_{3829} + p_{2635}$$

$$q_y = p_{6749} + p_{1937} + p_{3416}$$

$$q_z = p_{4857} + p_{2718} + p_{1524}$$

With these parameters, the volume of the element is

$$V = \frac{1}{6}\det|\boldsymbol{P}| = \frac{1}{6}(p_1 p_5 p_9 - p_1 p_6 p_8 + p_2 p_6 p_7 - p_2 p_4 p_9 + p_3 p_4 p_8 - p_3 p_5 p_7) \quad \text{(A.3)}$$

and the inverse of $\boldsymbol{P}$ is

$$\boldsymbol{P}^{-1} = \frac{1}{6V}\begin{bmatrix} 6V & 0 & 0 & 0 \\ -q_x & p_{5968} & p_{3829} & p_{2635} \\ -q_y & p_{6749} & p_{1937} & p_{3416} \\ -q_z & p_{4857} & p_{2718} & p_{1524} \end{bmatrix} \quad \text{(A.4)}$$

Given nodal displacements $\{u_{i\alpha}\}$ with respect to global Cartesian coordinates, where i=0,..,3 denote the node number, and α=x, y, z denote the component in global 3D space. Using linear shape functions for the tetrahedral element, displacement gradients can be calculated as:

$$\begin{bmatrix} u_{1\alpha} \\ u_{\alpha,x} \\ u_{\alpha,y} \\ u_{\alpha,z} \end{bmatrix} = \boldsymbol{P}^{-1}\begin{bmatrix} u_{1\alpha} \\ u_{2\alpha} \\ u_{3\alpha} \\ u_{4\alpha} \end{bmatrix} \quad \text{(A.5)}$$

To derive an analytical expression for the secant stiffness matrix, it is necessary to formulate both terms of $\boldsymbol{B}^{\mathrm{L}}$ and $\boldsymbol{U}^{\mathrm{T}}\boldsymbol{B}^{\mathrm{N}}$ in Eq.(2.4). To achieve

these two terms, the Green-Lagrange strains in Eq.(2.3) are expressed in detail as

$$\begin{aligned}
\varepsilon_{11} &= u_{x,x} + \frac{1}{2}\left({u_{x,x}}^2 + {u_{y,x}}^2 + {u_{z,x}}^2\right) \\
\varepsilon_{22} &= u_{y,y} + \frac{1}{2}\left({u_{x,y}}^2 + {u_{y,y}}^2 + {u_{z,y}}^2\right) \\
\varepsilon_{33} &= u_{z,z} + \frac{1}{2}\left({u_{x,z}}^2 + {u_{y,z}}^2 + {u_{z,z}}^2\right) \\
\varepsilon_{12} &= \frac{1}{2}\left(u_{x,y} + u_{y,x} + u_{x,x}u_{x,y} + u_{y,x}u_{y,y} + u_{z,x}u_{z,y}\right) \\
\varepsilon_{13} &= \frac{1}{2}\left(u_{x,z} + u_{z,x} + u_{x,x}u_{x,z} + u_{y,x}u_{y,z} + u_{z,x}u_{z,z}\right) \\
\varepsilon_{23} &= \frac{1}{2}\left(u_{y,z} + u_{z,y} + u_{x,y}u_{x,z} + u_{y,y}u_{y,z} + u_{z,y}u_{z,z}\right)
\end{aligned} \tag{A.6}$$

By substituting the matrix form expression of displacement gradients in Eq.(A.5) into Eq.(A.6), $\boldsymbol{B}^{\mathrm{L}}$ and $\boldsymbol{U}^{\mathrm{T}}\boldsymbol{B}^{\mathrm{N}}$ are obtained

$$\boldsymbol{B}^{\mathrm{L}} = \left[\boldsymbol{B}^{\mathrm{Lx}} \quad \boldsymbol{B}^{\mathrm{Ly}} \quad \boldsymbol{B}^{\mathrm{Lz}}\right] \tag{A.7}$$

where

$$\begin{aligned}
\boldsymbol{B}^{\mathrm{Lx}} &= \begin{bmatrix} 0 & 1 & 0 & 0 \\ 0 & 0 & 0 & 0 \\ 0 & 0 & 0 & 0 \\ 0 & 0 & 1 & 0 \\ 0 & 0 & 0 & 1 \\ 0 & 0 & 0 & 0 \end{bmatrix} \cdot \boldsymbol{P}^{-1} \\
\boldsymbol{B}^{\mathrm{Ly}} &= \begin{bmatrix} 0 & 0 & 0 & 0 \\ 0 & 0 & 1 & 0 \\ 0 & 0 & 0 & 0 \\ 0 & 1 & 0 & 0 \\ 0 & 0 & 0 & 0 \\ 0 & 0 & 0 & 1 \end{bmatrix} \cdot \boldsymbol{P}^{-1} \\
\boldsymbol{B}^{\mathrm{Lz}} &= \begin{bmatrix} 0 & 0 & 0 & 0 \\ 0 & 0 & 0 & 0 \\ 0 & 0 & 0 & 1 \\ 0 & 0 & 0 & 0 \\ 0 & 1 & 0 & 0 \\ 0 & 0 & 1 & 0 \end{bmatrix} \cdot \boldsymbol{P}^{-1}
\end{aligned} \tag{A.8}$$

And

$$\boldsymbol{U}^{\mathrm{T}}\boldsymbol{B}^{\mathrm{N}} = [\boldsymbol{U}^{\mathrm{T}}\boldsymbol{B}^{\mathrm{Nx}} \quad \boldsymbol{U}^{\mathrm{T}}\boldsymbol{B}^{\mathrm{Ny}} \quad \boldsymbol{U}^{\mathrm{T}}\boldsymbol{B}^{\mathrm{Nz}}] \tag{A.9}$$

where

$$\boldsymbol{U}^{\mathrm{T}}\boldsymbol{B}^{\mathrm{N}\alpha} = \begin{bmatrix} 0 & u_{\alpha,x} & 0 & 0 \\ 0 & 0 & u_{\alpha,y} & 0 \\ 0 & 0 & 0 & u_{\alpha,z} \\ 0 & u_{\alpha,y} & u_{\alpha,x} & 0 \\ 0 & u_{\alpha,z} & 0 & u_{\alpha,x} \\ 0 & 0 & u_{\alpha,z} & u_{\alpha,y} \end{bmatrix} \cdot \boldsymbol{P}^{-1} \tag{A.10}$$

Then, rearrange the sequences of rows and columns of $\boldsymbol{B}^{\mathrm{L}}$ and $\boldsymbol{U}^{\mathrm{T}}\boldsymbol{B}^{\mathrm{N}}$ to match the degrees of freedom in nodal displacement vector. As the integrals in Eqs.(2.12) and (2.13) are constant for the 4-node linear tetrahedral element, the stiffness matrices are:

$$\boldsymbol{K}_{\mathrm{S}}(\boldsymbol{U}) = \boldsymbol{B}^{\mathrm{T}}\boldsymbol{D}\bar{\boldsymbol{B}}V \tag{A.11}$$

$$\boldsymbol{K}_{\mathrm{T}}(\boldsymbol{U}) = \boldsymbol{B}^{\mathrm{T}}\boldsymbol{D}\boldsymbol{B}V + \boldsymbol{\nabla}_{\boldsymbol{U}}\boldsymbol{B}^{\mathrm{T}}\boldsymbol{\sigma}V \tag{A.12}$$

where $\boldsymbol{B}$ and $\bar{\boldsymbol{B}}$ are defined in Eqs.(2.8) and (2.10) via $\boldsymbol{B}^{\mathrm{L}}$ and $\boldsymbol{U}^{\mathrm{T}}\boldsymbol{B}^{\mathrm{N}}$.

The linear elastic constitutive matrix for the 3D type element is

$$\boldsymbol{D} = \frac{\mathrm{E}}{(1+\nu)(1-2\nu)} \begin{bmatrix} 1-\nu & \nu & \nu & & & \\ \nu & 1-\nu & \nu & & & \\ \nu & \nu & 1-\nu & & & \\ & & & \frac{1-2\nu}{2} & & \\ & & & & \frac{1-2\nu}{2} & \\ & & & & & \frac{1-2\nu}{2} \end{bmatrix} \tag{A.13}$$

APPENDIX B. Derivatives of residual force and dependent residual for finite strain elastoplasticity

The derivatives of the residual force and the dependent residual in finite strain elastoplasticity are presented in this appendix.

Following Eq.(7.26), it has

$$\frac{\partial {}^t\boldsymbol{R}}{\partial {}^t\boldsymbol{U}} = \int_{V^0} \frac{\partial {}^t\boldsymbol{B}}{\partial {}^t\boldsymbol{U}} {}^t\boldsymbol{\tau} dv + \int_{V^0} {}^t\boldsymbol{B} \frac{\partial {}^t\boldsymbol{R}^{\mathrm{e}}}{\partial {}^t\boldsymbol{U}} {}^t\bar{\boldsymbol{\tau}} {}^t\boldsymbol{R}^{\mathrm{e}\mathrm{T}} dv + \int_{V^0} {}^t\boldsymbol{B} {}^t\boldsymbol{R}^{\mathrm{e}} {}^t\bar{\boldsymbol{\tau}} \frac{\partial {}^t\boldsymbol{R}^{\mathrm{e}\mathrm{T}}}{\partial {}^t\boldsymbol{U}} dv \tag{B.1}$$

$$\frac{\partial {}^t\boldsymbol{R}}{\partial {}^t\boldsymbol{V}} = \left(\frac{\partial}{\partial {}^t\bar{\boldsymbol{\tau}}}, \frac{\partial}{\partial {}^t\varepsilon^{\mathrm{p}}_{\mathrm{eqv}}}, \frac{\partial}{\partial {}^t\boldsymbol{X}^{\mathrm{p}-1}} \right) {}^t\boldsymbol{R} = \left(-\int_{V^0} {}^t\boldsymbol{B} \frac{\partial {}^t\boldsymbol{R}^{\mathrm{e}} {}^t\bar{\boldsymbol{\tau}} {}^t\boldsymbol{R}^{\mathrm{e}\mathrm{T}}}{\partial {}^t\bar{\boldsymbol{\tau}}} dv, 0, 0 \right) \tag{B.2}$$

$$\frac{\partial {}^{t+1}\boldsymbol{R}}{\partial {}^t\boldsymbol{V}} = \left(\frac{\partial}{\partial {}^t\bar{\boldsymbol{\tau}}}, \frac{\partial}{\partial {}^t\varepsilon^{\mathrm{p}}_{\mathrm{eqv}}}, \frac{\partial}{\partial {}^t\boldsymbol{X}^{\mathrm{p}-1}} \right) {}^{t+1}\boldsymbol{R} = \left(0, 0, -\int_{V^0} {}^t\boldsymbol{B} \left(\frac{\partial {}^{t+1}\boldsymbol{R}^{\mathrm{e}}}{\partial {}^t\boldsymbol{X}^{\mathrm{p}-1}} {}^{t+1}\bar{\boldsymbol{\tau}} {}^{t+1}\boldsymbol{R}^{\mathrm{e}\mathrm{T}} + {}^{t+1}\boldsymbol{R}^{\mathrm{e}} {}^{t+1}\bar{\boldsymbol{\tau}} \frac{\partial {}^{t+1}\boldsymbol{R}^{\mathrm{e}\mathrm{T}}}{\partial {}^t\boldsymbol{X}^{\mathrm{p}-1}} \right) dv \right) \tag{B.3}$$

Following Eqs.(7.31), it has

$$\frac{\partial {}^t\boldsymbol{H}}{\partial {}^t\boldsymbol{U}} = \begin{pmatrix} -\boldsymbol{D}^{\mathrm{e}} \dfrac{\partial ln {}^t\boldsymbol{U}^{\mathrm{e}}_*}{\partial {}^t\boldsymbol{U}} \\ 0 \\ 0 \end{pmatrix} \tag{B.4}$$

If load step t is elastic, then

$${}^t\boldsymbol{H}({}^t\boldsymbol{U}, {}^t\boldsymbol{V}, {}^{t-1}\boldsymbol{V}, s) = \begin{pmatrix} {}^t\bar{\boldsymbol{\tau}} - \boldsymbol{D}^{\mathrm{e}} ln {}^t\boldsymbol{U}^{\mathrm{e}}_* \\ {}^t\varepsilon^{\mathrm{p}}_{\mathrm{eqv}} - {}^{t-1}\varepsilon^{\mathrm{p}}_{\mathrm{eqv}} \\ {}^t\boldsymbol{X}^{\mathrm{p}-1} - {}^{t-1}\boldsymbol{X}^{\mathrm{p}-1} \end{pmatrix} \equiv \boldsymbol{0} \tag{B.5}$$

Therefore

$$\frac{\partial {}^t\boldsymbol{H}}{\partial {}^t\boldsymbol{V}} = \left(\frac{\partial}{\partial {}^t\bar{\boldsymbol{\tau}}}, \frac{\partial}{\partial {}^t\varepsilon^{\mathrm{p}}_{\mathrm{eqv}}}, \frac{\partial}{\partial {}^t\boldsymbol{X}^{\mathrm{p}-1}} \right) {}^t\boldsymbol{H} = \boldsymbol{I} \tag{B.6}$$

$$\frac{\partial^t \boldsymbol{H}}{\partial^{t-1}\boldsymbol{V}} = \left(\frac{\partial}{\partial^{t-1}\bar{\boldsymbol{\tau}}}, \frac{\partial}{\partial^{t-1}\varepsilon^{\mathrm{p}}_{\mathrm{eqv}}}, \frac{\partial}{\partial^{t-1}\boldsymbol{X}^{\mathrm{p}-1}}\right)^t \boldsymbol{H} = \begin{bmatrix} \mathbf{0} & \mathbf{0} & -\boldsymbol{D}^{\mathrm{e}} \dfrac{\partial ln^t \boldsymbol{U}^{\mathrm{e}}_*}{\partial^{t-1}\boldsymbol{X}^{\mathrm{p}-1}} \\ \mathbf{0} & -1 & 0 \\ \mathbf{0} & \mathbf{0} & -\boldsymbol{I} \end{bmatrix} \tag{B.7}$$

Following Eqs.(7.31), if load step t is plastic, then

$${}^t\boldsymbol{H}({}^t\boldsymbol{U}, {}^t\boldsymbol{V}, {}^{t-1}\boldsymbol{V}, s) = \begin{pmatrix} {}^t\bar{\boldsymbol{\tau}} - \boldsymbol{D}^{\mathrm{e}} ln^t \boldsymbol{U}^{\mathrm{e}}_* + \boldsymbol{D}^{\mathrm{e}} \cdot {}^t\Delta\boldsymbol{\varepsilon}^{\mathrm{p}} \\ |{}^t\bar{\boldsymbol{\tau}}|_{\mathrm{eqv}} - \sigma_{\mathrm{Y}}({}^t\varepsilon^{\mathrm{p}}_{\mathrm{eqv}}) \\ {}^t\boldsymbol{X}^{\mathrm{p}-1} - {}^{t-1}\boldsymbol{X}^{\mathrm{p}-1} \cdot e^{-{}^t\Delta\boldsymbol{\varepsilon}^{\mathrm{p}}} \end{pmatrix} \equiv \mathbf{0} \tag{B.8}$$

It follows

$$\frac{\partial^t \boldsymbol{H}}{\partial^t \boldsymbol{V}} = \left(\frac{\partial}{\partial^t\bar{\boldsymbol{\tau}}}, \frac{\partial}{\partial^t\varepsilon^{\mathrm{p}}_{\mathrm{eqv}}}, \frac{\partial}{\partial^t\boldsymbol{X}^{\mathrm{p}-1}}\right)^t \boldsymbol{H} = \begin{bmatrix} \boldsymbol{Q} & D^{\mathrm{e}}{}^t\mathbf{a} & \mathbf{0} \\ {}^t\mathbf{a}^{\mathrm{T}} & -E^{\mathrm{p}} & \mathbf{0} \\ -{}^{t-1}\boldsymbol{X}^{\mathrm{p}-1} \dfrac{\partial e^{-{}^t\Delta\varepsilon^{\mathrm{p}}_{\mathrm{eqv}}{}^t\mathbf{a}}}{\partial^t\bar{\boldsymbol{\tau}}} & {}^t\boldsymbol{X}^{\mathrm{p}-1}{}^t\mathbf{a} & \boldsymbol{I} \end{bmatrix} \tag{B.9}$$

$$\frac{\partial^t \boldsymbol{H}^{-1}}{\partial^t \boldsymbol{V}} = \begin{bmatrix} \boldsymbol{D}^{\mathrm{ep}}\boldsymbol{D}^{\mathrm{e}-1} & \dfrac{\boldsymbol{D}^{\mathrm{ep}}{}^t\mathbf{a}}{E^{\mathrm{p}}} & \mathbf{0} \\ \dfrac{{}^t\mathbf{a}^{\mathrm{T}}}{E^p}\boldsymbol{D}^{\mathrm{ep}}\boldsymbol{D}^{\mathrm{e}-1} & {}^t\mathbf{a}^{\mathrm{T}}\dfrac{\boldsymbol{D}^{\mathrm{ep}}{}^t\mathbf{a}}{E^{\mathrm{p}2}} - \dfrac{1}{E^{\mathrm{p}}} & \mathbf{0} \\ -{}^t\boldsymbol{X}^{\mathrm{p}-1}\left({}^t\Delta\varepsilon^{\mathrm{p}}_{\mathrm{eqv}}\dfrac{\partial^t\mathbf{a}}{\partial^t\bar{\boldsymbol{\tau}}} + \dfrac{{}^t\mathbf{a}{}^t\mathbf{a}^{\mathrm{T}}}{E^{\mathrm{p}}}\right)\boldsymbol{D}^{\mathrm{ep}}\boldsymbol{D}^{\mathrm{e}-1} & -{}^t\boldsymbol{X}^{\mathrm{p}-1}\left({}^t\Delta\varepsilon^{\mathrm{p}}_{\mathrm{eqv}}{}^t\mathbf{a} + \dfrac{{}^t\mathbf{a}{}^t\mathbf{a}^{\mathrm{T}}}{E^{\mathrm{p}}}\right)\dfrac{\boldsymbol{D}^{\mathrm{ep}}{}^t\mathbf{a}}{E^{\mathrm{p}}} + \dfrac{{}^t\boldsymbol{X}^{\mathrm{p}-1}{}^t\mathbf{a}}{E^{\mathrm{p}}} & \boldsymbol{I} \end{bmatrix} \tag{B.10}$$

$$\frac{\partial^t \boldsymbol{H}}{\partial^{t-1}\boldsymbol{V}} = \left(\frac{\partial}{\partial^{t-1}\bar{\boldsymbol{\tau}}}, \frac{\partial}{\partial^{t-1}\varepsilon^{\mathrm{p}}_{\mathrm{eqv}}}, \frac{\partial}{\partial^{t-1}\boldsymbol{X}^{\mathrm{p}-1}}\right)^t \boldsymbol{H} = \begin{bmatrix} \mathbf{0} & -D^{\mathrm{e}}{}^t\mathbf{a} & -D^{\mathrm{e}}\dfrac{\partial ln^t \boldsymbol{U}^{\mathrm{e}}_*}{\partial^{t-1}\boldsymbol{X}^{\mathrm{p}-1}} \\ \mathbf{0} & 0 & \mathbf{0} \\ \mathbf{0} & -{}^t\boldsymbol{X}^{\mathrm{p}-1}{}^t\mathbf{a} & -e^{-{}^t\Delta\varepsilon^{\mathrm{p}}_{\mathrm{eqv}}{}^t\mathbf{a}} \end{bmatrix} \tag{B.11}$$

where $\boldsymbol{Q}$ and $\boldsymbol{D}^{\mathrm{ep}}$ follow Eqs.(2.27) and (2.28).

Bisherige Titel der Schriftenreihe

Band	Titel
1	Frank Koschnick, *Geometrische Lockingeffekte bei Finiten Elementen und ein allgemeines Konzept zu ihrer Vermeidung*, 2004.
2	Natalia Camprubi, *Design and Analysis in Shape Optimization of Shells*, 2004.
3	Bernhard Thomee, *Physikalisch nichtlineare Berechnung von Stahlfaserbetonkonstruktionen*, 2005.
4	Fernaß Daoud, *Formoptimierung von Freiformschalen - Mathematische Algorithmen und Filtertechniken*, 2005.
5	Manfred Bischoff, *Models and Finite Elements for Thin-walled Structures*, 2005.
6	Alexander Hörmann, *Ermittlung optimierter Stabwerkmodelle auf Basis des Kraftflusses als Anwendung plattformunabhängiger Prozesskopplung*, 2006.
7	Roland Wüchner, *Mechanik und Numerik der Formfindung und Fluid-Struktur-Interaktion von Membrantragwerken*, 2006.
8	Florian Jurecka, *Robust Design Optimization Based on Metamodeling Techniques*, 2007.
9	Johannes Linhard, *Numerisch-mechanische Betrachtung des Entwurfsprozesses von Membrantragwerken*, 2009.
10	Alexander Kupzok, *Modeling the Interaction of Wind and Membrane Structures by Numerical Simulation*, 2009.
11	Bin Yang, *Modified Particle Swarm Optimizers and their Application to Robust Design and Structural Optimization*, 2009.
12	Michael Fleischer, *Absicherung der virtuellen Prozesskette für Folgeoperationen in der Umformtechnik*, 2009.
13	Amphon Jrusjrungkiat, *Nonlinear Analysis of Pneumatic Membranes - From Subgrid to Interface*, 2009.
14	Alexander Michalski, *Simulation leichter Flächentragwerke in einer numerisch generierten atmosphärischen Grenzschicht*, 2010.
15	Matthias Firl, *Optimal Shape Design of Shell Structures*, 2010.
16	Thomas Gallinger, *Effiziente Algorithmen zur partitionierten Lösung stark gekoppelter Probleme der Fluid-Struktur-Wechselwirkung*, 2011.
17	Josef Kiendl, *Isogeometric Analysis and Shape Optimal Design of Shell Structures*, 2011.
18	Joseph Jordan, *Effiziente Simulation großer Mauerwerksstrukturen mit diskreten Rissmodellen*, 2011.
19	Albrecht von Boetticher, *Flexible Hangmurenbarrieren: Eine numerische Modellierung des Tragwerks, der Hangmure und der Fluid-Struktur-Interaktion*, 2012.

Band	Titel
20	Robert Schmidt, *Trimming, Mapping, and Optimization in Isogeometric Analysis of Shell Structures*, 2013.
21	Michael Fischer, *Finite Element Based Simulation, Design and Control of Piezoelectric and Lightweight Smart Structures*, 2013.
22	Falko Hartmut Dieringer, *Numerical Methods for the Design and Analysis for Tensile Structures*, 2014.
23	Rupert Fisch, *Code Verification of Partitioned FSI Environments for Lightweight Structures*, 2014.
24	Stefan Sicklinger, *Stabilized Co-Simulation of Coupled Problems Including Fields and Signals*, 2014.
25	Madjid Hojjat, *Node-based parametrization for shape optimal design*, 2015.
26	Ute Israel, *Optimierung in der Fluid-Struktur-Interaktion – Sensitivitätsanalyse für die Formoptimierung auf Grundlage des partitionierten Verfahrens*, 2015.
27	Electra Stavropoulou, *Sensitivity analysis and regularization for shape optimization of coupled problems*, 2015.
28	Daniel Markus, *Numerical and Experimental Modeling for Shape Optimization of Offshore Structures*, 2015.
29	Pablo Suárez, *Design Process for the Shape Optimization of Pressurized Bulkheads as Components of Aircraft Structures*, 2015.
30	Armin Widhammer, *Variation of Reference Strategy - Generation of Optimized Cutting Patterns for Textile Fabrics*, 2015.
31	Helmut Masching, *Parameter Free Optimization of Shape Adaptive Shell Structures*, 2016.
32	Hao Zhang, *A General Approach for Solving Inverse Problems in Geophysical Systems by Applying Finite Element Method and Metamodel Techniques*, 2016.
33	Tianyang Wang, *Development of Co-Simulation Environment and Mapping Algorithms*, 2016.
34	Michael Breitenberger, *CAD-integrated Design and Analysis of Shell Structures*, 2016.
35	Önay Can, *Functional Adaptation with Hyperkinematics using Natural Element Method: Application for Articular Cartilage*, 2016.
36	Benedikt Philipp, *Methodological Treatment of Non-linear Structural Behavior in the Design, Analysis and Verification of Lightweight Structures*, 2017.
37	Michael Andre, *Aeroelastic Modeling and Simulation for the Assessment of Wind Effects on a Parabolic Trough Solar Collector*, 2018.
38	Andreas Apostolatos, *Isogeometric Analysis of Thin-Walled Structures on Multipatch Surfaces in Fluid-Structure Interaction*, 2018.

Band	Titel
39	Altuğ Emiroğlu, *Multiphysics Simulation and CAD-Integrated Shape Optimization in Fluid-Structure Interaction*, 2019.
40	Mehran Saeedi, *Multi-Fidelity Aeroelastic Analysis of Flexible Membrane Wind Turbine Blades*, 2017.
41	Reza Najian Asl, *Shape optimization and sensitivity analysis of fluids, structures, and their interaction using Vertex Morphing Parametrization*, 2019.
42	Ahmed Abodonya, *Verification Methodology for Computational Wind Engineering Prediction of Wind Loads on Structures*, 2020.
43	Anna Maria Bauer, *CAD-integrated Isogeometric Analysis and Design of Lightweight Structures*, 2020.
44	Andreas Winterstein, *Modeling and Simulation of Wind Structure Interaction of Slender Civil Engineering Structures Including Vibration Systems*, 2020.
45	Franz-Josef Ertl, *Vertex Morphing for Constrained Shape Optimization of Three-dimensional Solid Structures*, 2020.
46	Daniel Baumgärtner, *On the Grid-based Shape Optimization of Structures with Internal Flow and the Feedback of Shape Changes into a CAD Model*, 2020.
47	Mohamed Khalil, *Combining Physics-based models and machine learning for an Enhanced Structural Health Monitoring*,2021.
48	Long Chen, *Gradient Descent Akin Method*, 2021.
49	Aditya Ghantasala, *Coupling Procedures for Fluid-Fluid and Fluid-Structure Interaction Problems Based on Domain Decomposition Methods*, 2021.
50	Ann-Kathrin Goldbach, *The CAD-Integrated Design Cycle for Structural Membranes*, 2022.
51	Iñigo Pablo López Canalejo, *A Finite-Element Transonic Potential Flow Solver with an Embedded Wake Approach for Aircraft Conceptual Design*, 2022.
52	Mayu Sakuma, *An Application of Multi-Fidelity Uncertainty Quantification for Computational Wind Engineering*, 2022.
53	Suneth Warnakulasuriya, *Development of methods for Finite Element-based sensitivity analysis and goal-directed mesh refinement using the adjoint approach for steady and transient flows*, 2022.
54	Klaus Bernd Sautter, *Modeling and Simulation of Flexible Protective Structures by Coupling Particle and Finite Element Methods*, 2022.
55	Efthymios Papoutsis, *On the incorporation of industrial constraints in node-based optimization for car body design*, 2023.
56	Thomas Josef Oberbichler, *A modular and efficient implementation of isogeometric analysis for the interactive CAD-integrated design of lightweight structures*, 2023.
57	Tobias Christoph Teschemacher, *CAD-integrated constitutive modelling, analysis, and design of masonry structures*, 2023.

Band	Titel
58	Shahrokh Shayegan, *Enhanced Algorithms for Fluid-Structure Interaction Simulations – Accurate Temporal Discretization and Robust Convergence Acceleration*, 2023.
59	Ihar Antonau, *Enhanced computational design methods for large industrial node-based shape optimization problems*, 2023.
60	Rishith Ellath Meethal, *Hybrid modelling and simulation approaches for the solution of forward and inverse problems in engineering by combining finite element methods and neural networks*, 2023.
61	Máté Péntek, *Method Development for the Numerical Wind Tunnel in Applied Structural Engineering*, 2023.
62	Anoop Kodakkal, *High Fidelity Modeling and Simulations for Uncertainty Quantification and Risk-averse Optimization of Structures Under Natural Wind Conditions*, 2024.
63	Philipp Bucher, *CoSimulation and Mapping for large scale engineering applications*, 2024.
64	Martin Fußeder, *Methodological and Application-Oriented Advances in Sensitivity Analysis with a Focus on Structural Engineering*, 2024.
65	Wenjia Wang, *Adjoint Sensitivity Analysis for Non-parametric Shape Optimization with Geometric Nonlinearity and Elastoplasticity*, 2024